Antenne Multifonction pour Radar et Communication

Samir Ouedraogo

université PARIS-SACLAY

NNT: 2018SACLC010

CentraleSupélec

Multifunction Antenna for Radar and Communication

Thèse de doctorat de l'Université Paris-Saclay
préparée à CentraleSupélec

École doctorale n°575 electrical, optical, bio: physics and engineering (EOBE)
Spécialité de doctorat : électronique et optoélectronique, nano- et microtechnologies

Thèse présentée et soutenue à Gif-sur-Yvette, le 09 janvier 2018, par

Samir Ouedraogo

Composition du Jury :

Elodie Richalot Professeur des universités, Université Paris-Est Marne-La-Vallée	Président
Marc Hélier Professeur des universités, Université Pierre et Marie Curie	Rapporteur
Thierry Monédière Professeur des universités, Université de Limoges	Rapporteur
Mohammed Serhir Professeur adjoint, CentraleSupélec	Examinateur
Israel Hinostroza Professeur assistant, CentraleSupelec	Encadrant de thèse
Régis Guinvarc'h Professeur, CentraleSupelec	Directeur de thèse
Raphaël Gillard Professeur des universités, INSA de Rennes	Invité

Thèse de doctorat

REMERCIEMENT

Je tiens tout d'abord à remercier Israel Hinostroza, mon encadrant de thèse, avec qui j'ai aimé travailler. Je lui exprime toute ma reconnaissance pour le temps qu'il m'a consacré et pour ses précieux conseils. Il a su tout au long de ces trois années faire preuve d'une grande écoute et d'une grande compréhension. J'espère bien qu'on aura encore l'occasion dans un futur proche de travailler ensemble sur de nouvelles thématiques.

Je remercie Régis Guinvarc'h, mon directeur de thèse et Raphaël Gillard, mon co-endrant pour leur aide très précieuse. À travers leurs expertises scientifiques et leur professionnalisme, ils ont contribué énormément à la qualité de cette thèse. Ils ont su être disponibles malgré un emploi du temps assez chargé pour répondre à mes multiples questions. Enfin, j'ai beaucoup apprécié les réunions organisées à Rennes où on discutait pendant des heures sur mes travaux. Ces moments étaient très important pour moi car je pouvais tirer profit de leurs expertises et expériences et je sortais le plus souvent de ces réunions avec de nouvelles idées. J'espère pouvoir profiter aussi longtemps que possible de votre expertise à travers des collaborations afin d'enrichir ma carrière professionnelle.

Je remercie également Sylvain Azarian, directeur du laboratoire SONDRA et Jérôme Sol, assistant ingénieur à l'INSA de Rennes pour le temps qu'ils ont consacré respectivement à la réalisation de la maquette et aux mesures.

Je remercie tous ceux sans qui cette thèse ne serait pas ce qu'elle est : aussi bien par les discussions que j'ai eu la chance d'avoir avec eux, leurs suggestions ou contributions. Je pense ici en particulier à l'ensemble du personnel du laboratoire SONDRA. J'exprime ma profonde reconnaissance pour leur accueil, leur aide, leur gentillesse et pour la bonne ambiance qui règne au laboratoire.

Pour finir, j'adresse un remerciement particulier à ma famille, notamment à ma fiancée pour l'encouragement et le soutien qu'ils m'ont apportés tout au long de la thèse. Ils ont tous cru en moi du début à la fin. Merci à vous tous…

RÉSUMÉ ÉTENDU

Introduction

Afin de répondre à la demande croissante de nouveaux services, les objets que nous utilisons au quotidien (tels que les smartphones, les voitures, les avions, etc.) tendent à intégrer de plus en plus de systèmes radio tandis que l'espace disponible pour l'intégration de ces éléments est de plus en plus réduit. Ces systèmes radio nécessitent l'utilisation de plusieurs antennes devant répondre à des critères de compacité, d'isolation, de coût, etc. À titre d'illustration, un smartphone contient plusieurs antennes pour assurer des fonctions telles que la téléphonie, la navigation, la connexion à internet par WiFi, les liaisons Bluetooth, la technologie NFC (Near-Field Communications) et ce nombre tend à s'accroitre considérablement avec l'émergence de nouveaux services. Le même phénomène se retrouve également au niveau des plateformes aéroportées où des fonctions telles que la communication, la navigation, le radar, etc. sont utilisées. Cela conduit donc à la nécessité de réduire le nombre d'antennes en regroupant par exemple plusieurs fonctions au sein d'une même et unique antenne. Cependant, regrouper les fonctionnalités de plusieurs systèmes radio au sein du même élément rayonnant présente un réel défi. Dans de précédents travaux de recherches, J. Euzière a démontré la possibilité de combiner une fonction radar et une seconde fonction (ici de communication) en utilisant un réseau de 16 monopoles initialement dédié au seul radar, grâce au Time Modulated Array (TMA). De cette façon, les deux fonctions utilisaient la même fréquence et étaient alimentées par une seule source. L'objectif principal de cette thèse est de proposer une solution d'antenne multifonction pour radar et communication encore plus compacte (constituée d'une seule antenne). L'idée est de partir d'une solution antennaire déjà existante et d'y apporter les modifications nécessaires à l'ajout d'une seconde fonction, sans pour autant augmenter la surface de l'antenne ni la complexité du système. Pour les besoins du radar, le choix s'est porté sur une antenne directive, à savoir une antenne cornet. L'objectif est donc d'étudier la possibilité de modifier le diagramme de rayonnement de l'antenne cornet à travers l'ajout d'éléments contrôlables (des fentes) afin de transmettre un signal de communication modulé directement au niveau de l'antenne. La diversité de polarisation étant un moyen attractif d'assurer une meilleure isolation entre les deux fonctions, cet aspect sera pris en compte dans la conception de l'antenne.

1.1. Classification des antennes multifonctions

Afin de faciliter la compréhension du principe de fonctionnement et de conception des antennes multifonctions, on se propose d'en faire une classification en se basant sur les solutions présentées dans cette thèse (cf. Figure 1). On s'intéressera ici uniquement aux solutions offrant un fonctionnement simultané des fonctions et se basant sur la modification de l'élément rayonnant. Ainsi, en fonction du type d'applications considérées, les fonctions peuvent être réalisées dans la même direction ou dans des directions différentes. Dans le cas où celles-ci sont

réalisées dans la même direction, les diversités de polarisation et de fréquence peuvent être utilisées pour améliorer l'isolation entre les fonctions. Il faut noter que ces deux techniques peuvent également être combinées pour les antennes multifaisceaux (dans des directions différentes), cf. Tableau 1. Pour les applications réalisées dans des directions différentes, le choix de la direction offre un degré de liberté additionnel dans la réduction du couplage entre les différentes fonctions considérées. En ce qui concerne les antennes multifaisceaux, elles peuvent être alimentées à travers un seul ou plusieurs ports d'accès. Les avantages de l'utilisation d'un port unique sont entre autres la réduction de la surface totale et la possibilité de réaliser la modulation directe qui ne nécessite pas l'utilisation d'une électronique complexe (cf. Tableau 1).

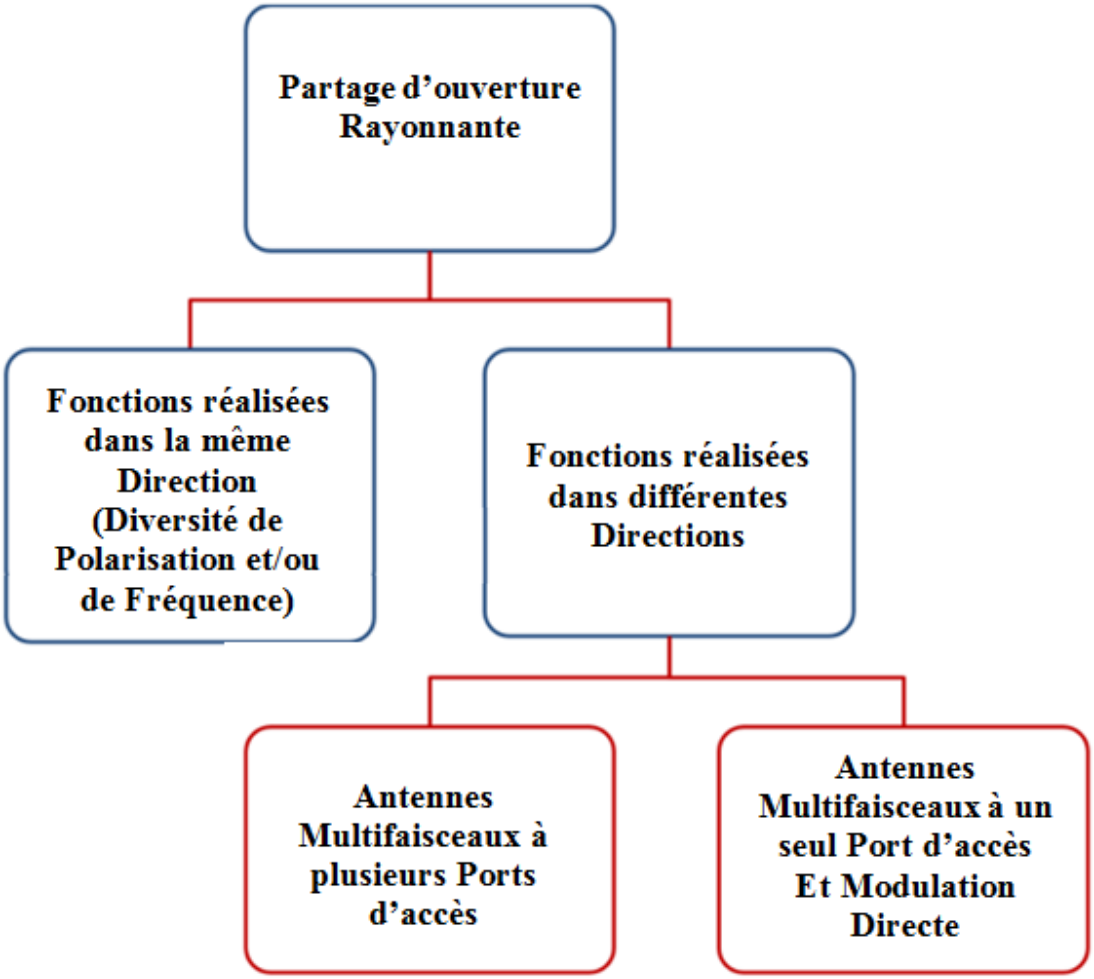

Figure 1: classification des antennes multifonctions

Pour la suite, on se focalisera sur le principe du partage d'ouverture rayonnante pour concevoir l'antenne multifonction. La possibilité d'utiliser la modulation directe pour générer un lien de communication discret sera également étudiée. Contrairement aux travaux de J. Euzière, on utilisera cette fois-ci une seule antenne. Généralement, pour les applications multifonctions, des antennes différentes sont considérées à l'émission et à la réception afin d'éviter que les différents signaux ne se perturbent. L'antenne proposée pour cette thèse fonctionnera uniquement en mode émission.

	Multifaisceau	**Diversité**	**Nombre de ports**	**Modulation Directe**
Réseau de Patch Carré [5- chap.1]	Non	Polarisation	2	Non
Réseau empilé de patch circulaire et résonateur à anneau rectangulaire [19 - chap.1]	Oui	Polarisation et frequence	4	Non
Réseau de Vivaldi [9 - chap.1]	Oui	Polarisation	2	Non
Réseau ALTSA [11 - chap.1]	Oui	Non	4	Non
Guide à fentes [6 - chap.1]	Oui	Polarisation et frequence	2	Non
Réseau de Monopole [7 - chap.1]	Oui	Non	1	Oui

Tableau 1: Résumé des antennes multifonctions utilisant la technique du partage d'ouverture

1.2. Validation expérimentale de l'antenne Multifonction

1.2.1. Principe de fonctionnement

On rappelle que pour les besoins du radar, le système est composé d'un cornet standard alimenté par un guide d'onde et rayonnant un faisceau directif dans la direction *x* (cf. Figure 2). Le principe de la solution proposée est de prélever une faible quantité de l'énergie se propageant dans le guide avant qu'elle ne soit rayonnée par le cornet et de l'utiliser pour transmettre de l'information. Il faut noter que cette caractéristique additionnelle de communication ne doit pas perturber le fonctionnement du radar, c'est-à-dire pas de modifications dans lobe principal du cornet. De plus, le système doit être le plus simple possible afin de ne pas accroitre la complexité de l'ensemble.

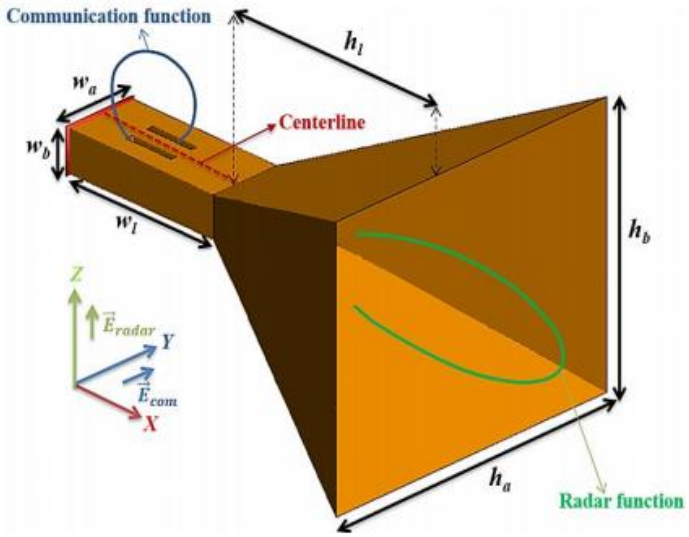

Figure 2: L'antenne cornet et son guide d'alimentation (w_a = 20.1 mm, w_b = 10.3 mm, w_l = 62.3 mm, h_l =73.8 mm, h_b = 68.6 mm, h_a = 88.2 mm)

Pour ce faire, deux fentes seront réalisées dans la face supérieure du guide d'onde d'alimentation. Ainsi, en utilisant un mécanisme de commutation pour activer une des fentes à un instant *t* donné, une partie de l'énergie dans le guide sera rayonnée à travers la fente active, offrant ainsi un lien de communication dans la direction *z*. Comme on le verra, grâce au mécanisme de commutation (à base de diode PIN, HSMP-381Z) entre les fentes, une modulation de type BPSK sera générée dans la direction de communication.

1.2.2. Conception de l'antenne

Comme il a été mentionné précédemment, on considère un cornet standard rayonnant un faisceau directif polarisé linéairement suivant l'axe *z* dans la direction ($\theta = 90°$; $\phi = 0°$), cf. Figure 2. Deux fentes identiques (de dimensions L = 29 mm et l = 1.5 mm placées à D = 12.5 mm du centre du guide d'onde, cf. Figure 3) sont réalisées dans la face supérieure du guide d'onde avec pour

objectif de rayonner une fraction de l'énergie se propageant dans le guide dans la direction (θ = 0° ; ϕ = 0°). Étant donné que les fentes sont placées longitudinalement à l'axe du guide d'onde, le champ rayonné résultant est polarisé suivant l'axe *y*. Ceci implique que la fonction radar et la fonction communication seront réalisées dans des directions et polarisations orthogonales pour plus d'isolation entre les fonctions.
De plus, les fentes étant placées de façon symétrique au centre du guide d'onde (cf. Figure 2), un déphasage de 180° du champ rayonné est obtenu à chaque fois que l'on commute entre les deux fentes [6 – chap. 2]. Ceci nous amène à définir deux configurations complémentaires pour notre étude (cf. Figure 3). La configuration 1 correspond au cas où la diode 1 est à l'état OFF (la fente 1 rayonne) et la diode 2 à l'état ON (la fente 2 ne rayonne pas). La configuration 2 n'est rien d'autre que l'inverse de la précédente.

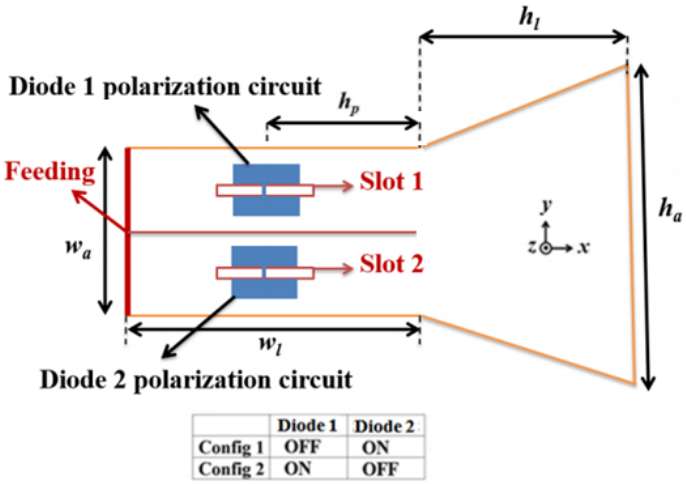

	Diode 1	Diode 2
Config 1	OFF	ON
Config 2	ON	OFF

Figure 3: Configuration de l'antenne (L = 29 mm, l = 1.5 mm, D =12.5 mm, hp = 38.6 mm)

1.2.3. Résultats de mesures de l'antenne multifonction

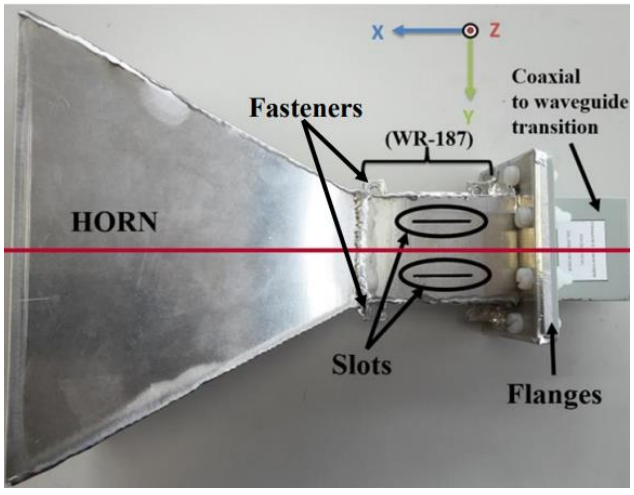

Figure 4: Prototype de l'antenne multifunction

Le prototype de l'antenne réalisé en aluminium AG3 d'épaisseur de 2 mm est présenté sur la Figure 4. Ainsi, le guide WR-187 de dimensions (47.55 x 22.15 mm^2) fonctionnant de 3.95 GHz à 5.85 GHz sera utilisé pour alimenter l'antenne.

L'ensemble des mesures ont été réalisées dans la base SATIMO STARGATE de l'INSA de Rennes fonctionnant entre 800 MHz et 6 GHz (cf. Figure 5).

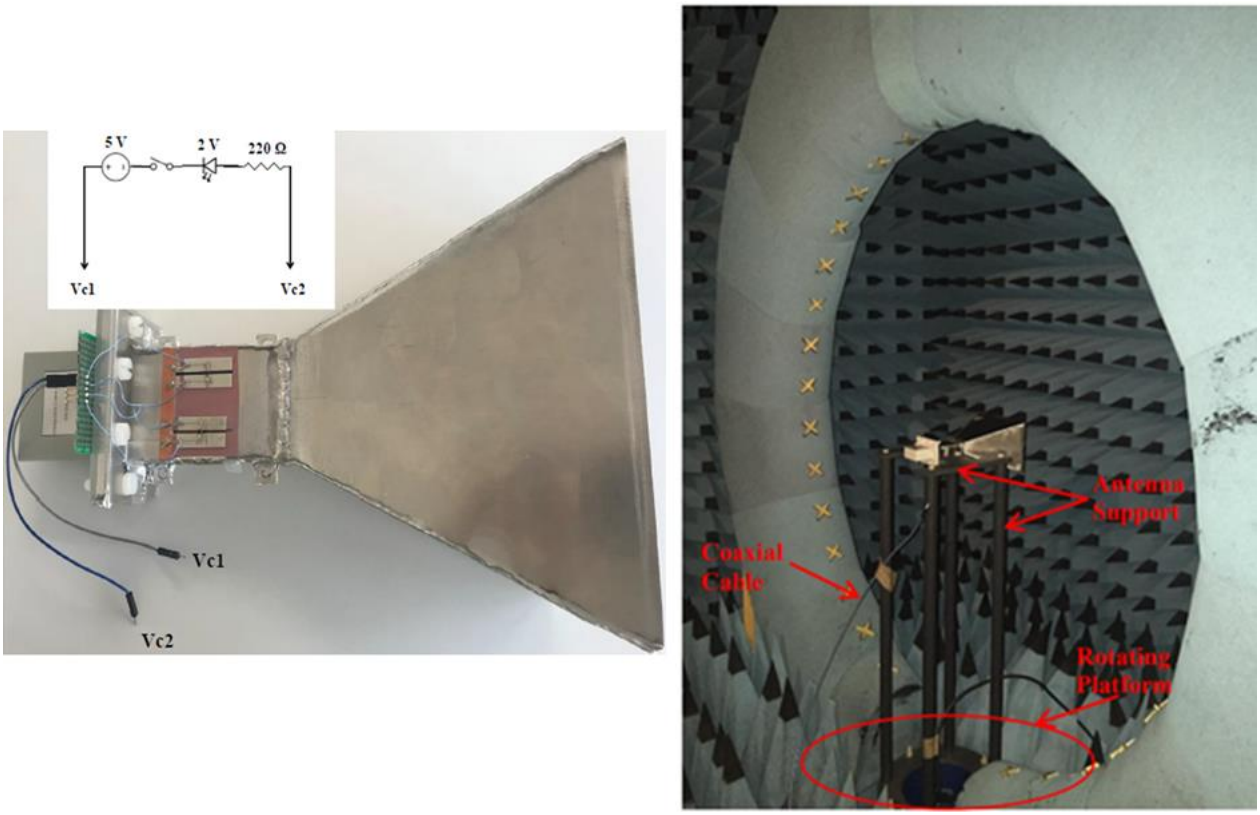

Figure 5: (a) Schéma et (b) photo de la SATIMO STARGATE de l'INSA de Rennes

Les Figure 6 et Figure 7 présentent les résultats de mesure et de simulation de la configuration 1 de l'antenne multifonction à 4 GHz dans les plans xOz et xOy respectivement. On note un accord acceptable entre mesure et simulation.

On observe dans le plan xOz, à $\theta = 0°$, une chute de gain de 3.51 dB dans le gain suivant ϕ (fonction communication) entre mesure et simulation. Cette différence peut être attribuée aux pertes liées au circuit de commande des diodes, aux éléments parasites de la diode utilisée mais aussi aux incertitudes dans la réalisation du prototype.

Ces figures font également ressortir l'isolation entre les deux fonctions. Deux paramètres sont alors définis pour évaluer cette isolation:

- La réjection de la communication correspondant à la réjection de la polarisation suivant ϕ (due la fonction communication) dans la direction du radar ($\theta = 90°$; $\phi = 0°$).

❖ La réjection du radar correspondant à la réjection de la polarisation suivant θ (due à la fonction radar) dans la direction de communication ($\theta = 0°$; $\phi = 0°$).

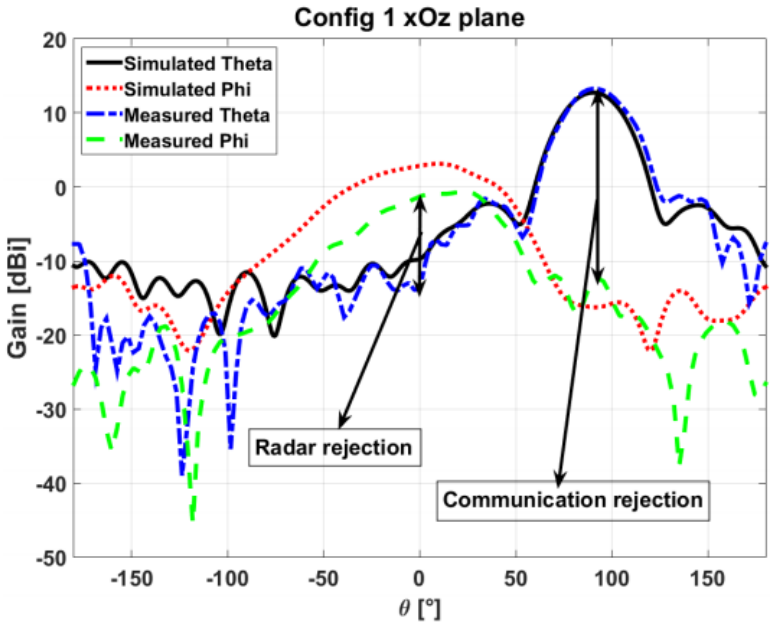

Figure 6: Diagramme de rayonnement de la configuration à 4 GHz dans le plan xOz

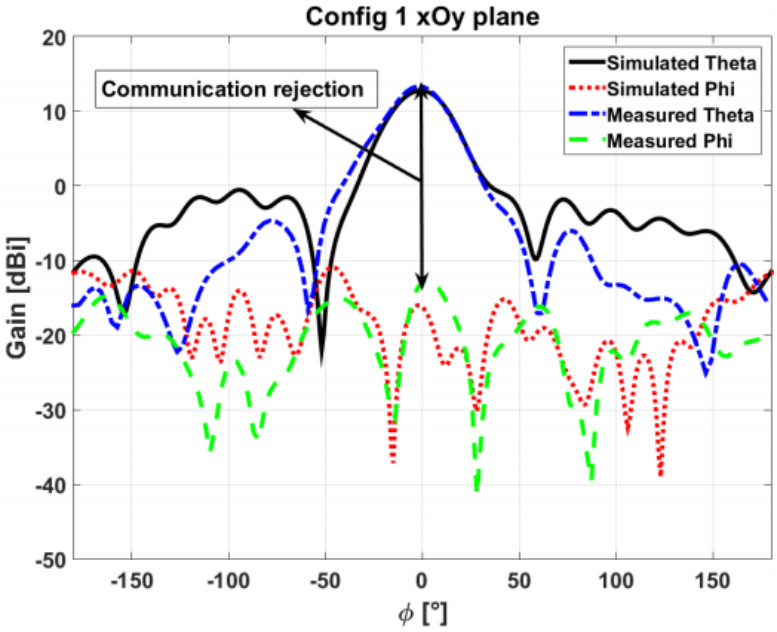

Figure 7: Diagramme de rayonnement de la configuration à 4 GHz dans le plan xOy

En mesure, la réjection du radar est de 12.47 dB et celle de la communication de 26.1 dB, assurant l'isolation entre les deux fonctions.

Les deux configurations étant identiques, on retrouve les mêmes résultats pour la configuration 2. Ainsi, en commutant entre les deux configurations, un déphasage de 180° est généré à θ =

0° (direction de communication, gain suivant ϕ) sans affecter la fonction radar (gain suivant θ) à θ = 90°. Ceci nous permet de valider le principe de l'antenne multifonction.

Après avoir validé expérimentalement le fonctionnement de l'antenne multifonction, nous verrons dans la partie suivante comment transposer le concept en une technologie planaire, facile à réaliser et peu encombrante par rapport aux cornets standards.

1.3. Antenne Multifonction en Technologie SIW

La technologie SIW (Substrate Integrated Waveguide) a été proposée au cours des dernières décennies [1 – chap. 5] [2 – chap. 5] comme un nouveau concept de circuits intégrés pour les générations futures. Le but de cette technologie est de faciliter l'intégration du guide d'onde rectangulaire avec les circuits planaires. En raison de sa structure planaire, de sa simplicité de réalisation et de son intégration facile avec d'autres circuits planaires, le SIW attire beaucoup l'attention des chercheurs [7 – chap. 5] [10 – chap. 5]. Dans sa forme la plus simple, il est composé de deux rangées périodiques de trous métallisés traversant un substrat diélectrique et reliant deux plaques métalliques parallèles (cf. Figure 8).

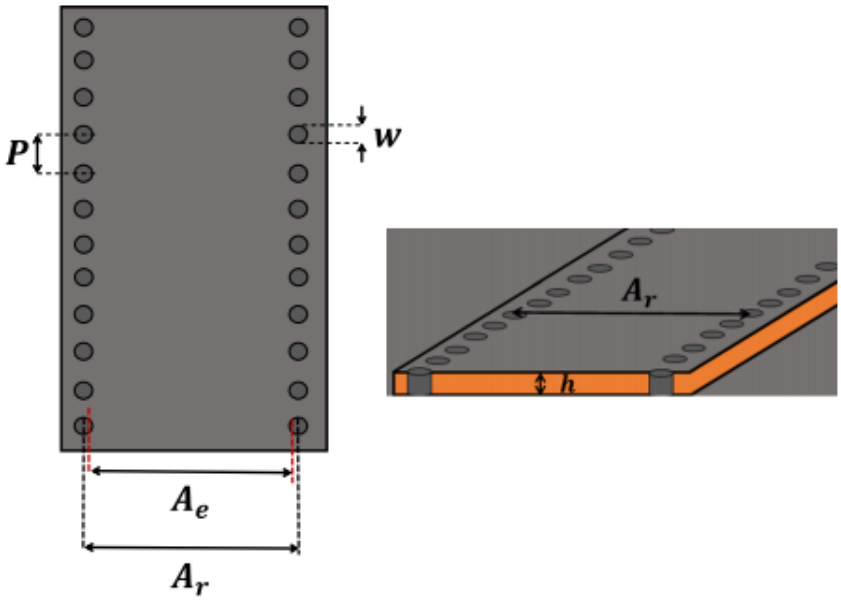

Figure 8: Le SIW

Comme il a déjà été mentionné, l'objectif est de transposer le concept de l'antenne multifonction en technologie SIW. Ainsi nous optons pour les cornets SIW. L'antenne cornet SIW a été proposée dans [17 - chap. 5] [18 - chap. 5] en raison de sa structure plane, de sa fabrication simple et de son intégration facile avec d'autres circuits planaires. Cependant, la faible épaisseur du substrat conduit à un diagramme de rayonnement large, très peu directif et l'adaptation de l'impédance est très critique. Ainsi, nous travaillerons à améliorer les performances du cornet SIW pour des applications ne nécessitant pas de rayonnement très directif telles que la communication et la navigation par exemple.

1.3.1. L'antenne multifonction utilisant un cornet SIW

Le principe de fonctionnement est toujours le même que celui présenté précédemment à savoir prélever de l'énergie à travers des fentes placées dans le SIW d'alimentation pour la modulation BPSK avant qu'elle ne soit rayonnée par le cornet.

Comme il a été mentionné précédemment, la faible épaisseur du substrat affecte les performances du cornet SIW. Ainsi, pour améliorer les caractéristiques de rayonnement et d'adaptation d'impédance du cornet SIW, il est nécessaire d'augmenter l'épaisseur du substrat tout en garantissant la faisabilité des trous métallisés. Pour cela, nous décidons de travailler en haute fréquence pour gagner en épaisseur électrique. Pour cette étude nous choisissons arbitrairement la bande Ka (20 GHz - 30 GHz).

- **Conception de l'antenne**

Pour réaliser le cornet SIW épais, nous commençons par déterminer les dimensions du SIW d'alimentation telles que présentées sur la Figure 8. Pour un SIW fonctionnant en bande Ka, le guide rectangulaire WR-28 (A = 7.11 mm et B = 3.56 mm) sera utilisé pour synthétiser le SIW. Un substrat de permittivité ε_r = 2.33, tan δ = 0.0013 (choisi arbitrairement) et d'épaisseur h = 3 mm sera utilisé pour cette étude. L'ensemble de ces données nous conduisent aux dimensions telles que présentées dans le Tableau 2. (cf. le chapitre 5 de la thèse pour plus de détails).

A_r	5.4 mm
A_e	4.7 mm
P	1 mm
w	0.8 mm

Tableau 2: Les dimensions du SIW fonctionnant en bande Ka

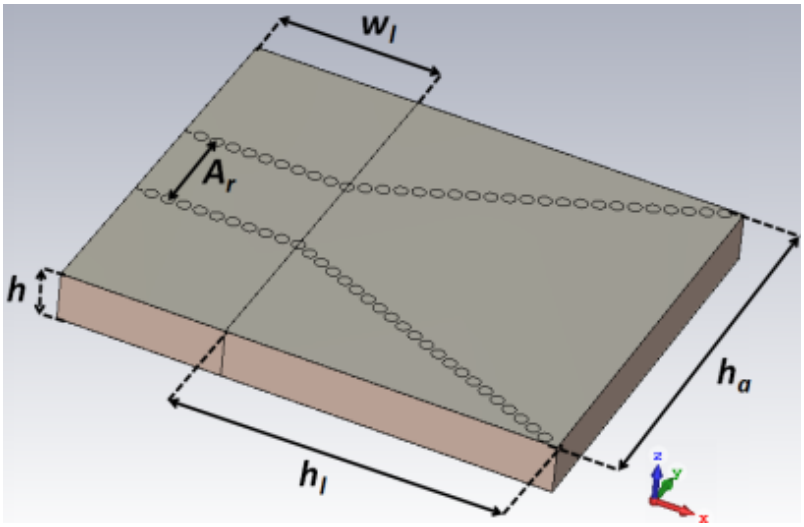

Figure 9: Cornet SIW épais (h = 3 mm, A_r = 6.3 mm, w_l = 10 mm, h_a = 25 mm, h_l = 20 mm)

Cependant, pour s'assurer que le second mode supérieur (dans ce cas le TE01) ne perturbe pas le mode fondamental, le paramètre A_r a été affiné à 6,3 mm, permettant ainsi de maintenir un rapport de 2.1 entre la largeur et l'épaisseur du SIW (h = 3 mm) comme c'est le cas pour les guides d'onde rectangulaires. Ceci nous donne une fréquence de coupure théorique du mode TE10 du SIW de f_c = 15,6 GHz.

La Figure 9 nous présente le cornet SIW qui sera utilisé pour la suite de l'étude. Dans cette figure, h_a et h_l sont respectivement les dimensions de l'ouverture du cornet dans le plan xOy et la longueur du cornet. Elles sont choisies afin de contrôler le diagramme de rayonnement dans ce plan [17 – chap. 5].

- **Les performances du SIW**

Dans cette partie, nous analysons les performances du cornet SIW épais. Les configurations qui seront étudiées sont celles présentées sur la Figure 10 avec des fentes de dimensions L = 3.8 mm et l = 0.2 mm placée à D =1.2 mm du centre du SIW et à une distance H_p = 5.5 mm de l'ouverture du cornet. Ces dimensions ont été choisies pour une résonnance à 28.5 GHz.

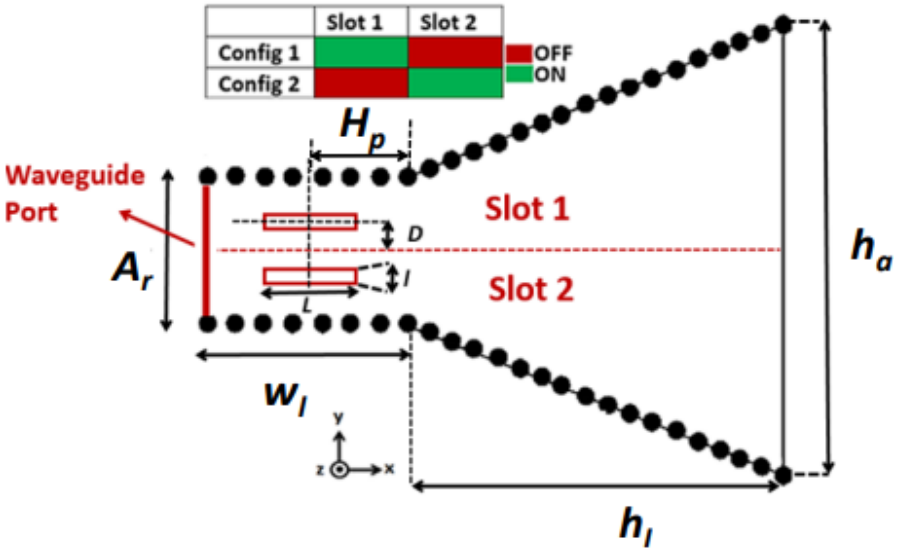

Figure 10: Les configurations de l'antenne

Afin d'améliorer les caractéristiques d'adaptation et de rayonnement du cornet SIW, une extension du substrat diélectrique de longueur 18.5 mm est effectuée au niveau de l'ouverture du cornet.

Le Tableau 3 résume l'ensemble des performances obtenues avec le cornet SIW quand on ajoute l'extension diélectrique et une des fentes (configuration 1 de l'antenne).

Comme on peut le voir dans le Tableau 3, l'utilisation de l'extension diélectrique permet d'améliorer considérablement la bande d'adaptation d'impédance du cornet SIW. De plus, cela nous permet de rendre plus directif le rayonnement du cornet dans le plan xOz.

	Impedance Bandwidth	Horn Gain	HPBW xOz plane	HPBW xOy plane
	460 MHz	6.15 dBi	132°	84°
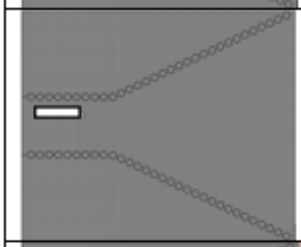	1.20 GHz	-0.31 dBi	137°	78°
	1.45 GHz	10.69 dBi	37.3°	47.15°
	3.55 GHz	7.9 dBi	37°	41°

Tableau 3: Performances du cornet SIW épais

On s'intéresse maintenant aux diagrammes de rayonnement à 28.5 GHz des deux configurations utilisant l'extension diélectrique.

Les Figure 11 et Figure 12 présentent respectivement les résultats de simulation des deux configurations (gain suivant θ et ϕ) dans le plan xOz respectivement xOy.

Comme on pouvait s'y attendre, dans le plan xOz, du fait de la symétrie entre les deux configurations, nous obtenons exactement les mêmes diagrammes pour les deux configurations, ce qui implique que les deux fonctions ne sont pas affectées par la commutation entre les fentes. Le gain maximum dans la direction principale du cornet est de 7.9 dBi (gain suivant θ à θ = 90°) et celui des fentes 2.73 dBi (gain suivant ϕ à θ = 0°).

Dans, le plan xOy, on note une dissymétrie entre les deux configurations. Cette dissymétrie est plus prononcée dans le cas présent car les fentes rayonnent plus d'énergie (comparativement au cas précédent utilisant le cornet standard) afin que leur rayonnement ne soit pas noyé dans les

lobes secondaires du cornet. Dans la direction principale du cornet (ϕ = 0°), les deux configurations sont identiques avec un gain de 7.9 dBi.

Il a été démontré dans la thèse que cette dissymétrie dans le plan xOy pouvait être réduite en utilisant un réseau de fente (trois) dans le SIW.

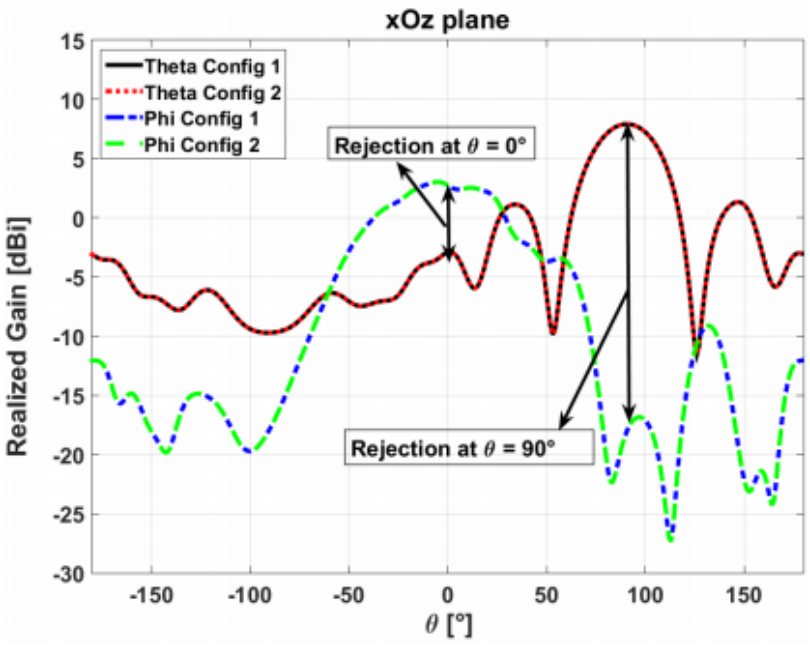

Figure 11: Diagramme de rayonnement de l'antenne multifonction à 28.5 GHz dans le plan xOz

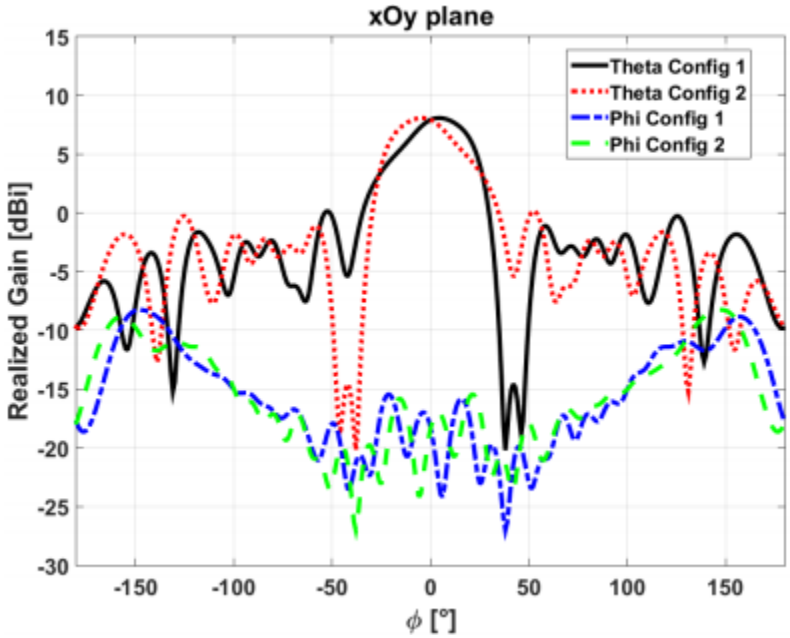

Figure 12: Diagramme de rayonnement de l'antenne multifonction à 28.5 GHz dans le plan xOy

Le Tableau 4 résume les performances obtenues pour la modulation BPSK à θ = 0°.

Directions	Config	Phase (°)	Amp. (dBi)
$\theta = 0°$	1	0	2.73
	2	180	2.73

Tableau 4: Modulation BPSK à 28.5 GHz

En ce qui concerne les rejections telles que définies sur la Figure 11, à 28.5 GHz, nous avons une réjection à θ = 0° de 5.6 dB, relativement faible (comparée à celle qu'on pourrait obtenir avec le cornet standard). En ce qui concerne la réjection à $\theta = 90°$, elle de 26 dB assurant une meilleure isolation entre les deux fonctions dans cette direction.

Il a également été démontré dans la thèse que la réjection à θ = 0° pouvait être améliorée en utilisant un réseau de fente dans le SIW (cf. Tableau 5).

	Impedance bandwidth	**Horn Gain**	**Slot Gain**	**Rejection at $\theta = 0°$**	**Rejection at $\theta = 90°$**
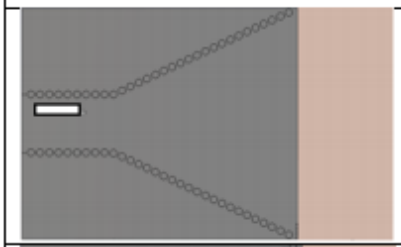	3.55 GHz	7.9 dBi	2.73 dBi	5.6 dB	26.19 dB
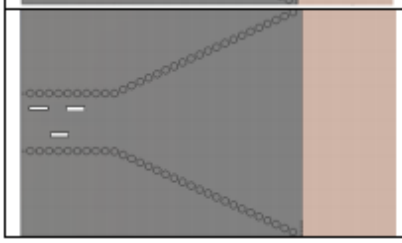	2.64 GHz	8.28 dBi	5.26 dBi	8.62 dB	32 dB

Tableau 5: Comparaison des performances du SIW avec le réseau de fente (27.6 GHz) et de l'antenne avec une fente (28.5 GHz)

Cette étude nous a permis de transposer le concept de l'antenne multifonction avec modulation BPSK en une technologie planaire (SIW) simple à fabriquer et peu encombrante. Compte tenu de la faible épaisseur du substrat, le rayonnement du cornet SIW est large, empêchant ainsi l'utilisation de cette antenne pour des applications radar. Toutefois, les performances de l'antenne ont été améliorées, ce qui permettrait d'envisager des applications de type communication ou navigation ne nécessitant pas un fort gain. Le niveau de réjection reste faible à $\theta = 0°$ (5.6 dB), ce qui n'est pas suffisant pour assurer l'isolation entre les deux fonctions dans cette direction. Toutefois, l'utilisation d'un réseau de trois fentes nous permet d'améliorer la réjection dans cette direction de 3 dB.

Afin de pouvoir utiliser cette solution pour des applications de type radar, il conviendrait de travailler à améliorer les caractéristiques de rayonnement du cornet SIW. Une solution serait de le remplacer par exemple par un réseau de fentes évasées comme dans [25 – chap. 5].

1.4. Conclusion générale et perspectives

Cette thèse a été consacrée au développement d'une antenne multifonction compacte pour les applications de type radar et communication. L'étude s'est basée sur une antenne à cornet standard (pour le radar), qui a été modifiée pour ajouter une fonction secondaire de communication à travers le rayonnement d'une fente (ou réseau de fente) dans le guide d'alimentation. Les fentes sont conçues de sorte que les deux fonctions utilisent des polarisations et des directions orthogonales. En utilisant un mécanisme de commutation pour activer l'une des fentes à un instant donné, une fraction de la puissance dans le guide d'alimentation est ensuite rayonnée à travers la fente active, fournissant ainsi un lien de communication discret avec une modulation BPSK.

Pour valider le concept, une caractérisation complète de l'antenne multifonction a été réalisée. Afin de contrôler dynamiquement le rayonnement des fentes et donc la modulation BPSK, un circuit de commande à base de diodes PIN a été étudié et monté sur le prototype. La différence de gain obtenue entre le mode OFF et ON de la diode est de 15.18 dB à 4 GHz validant ainsi le principe de commutation. Les réjections obtenues pour ce nouveau système sont de 12.47 dB pour le radar et de 26.1 dB pour la communication assurant l'isolation entre les deux fonctions.

Pour finir, le concept de l'antenne multifonction avec la modulation directe BPSK a été transposé en technologie planaire (SIW), facile à réaliser et peu encombrante. Cependant, en raison de la faible épaisseur du substrat, le rayonnement du cornet SIW est peu directif, empêchant l'utilisation de cette antenne pour des applications radar. Par conséquent, les performances de l'antenne ont été améliorées pour d'autres applications de type communication ou navigation ne nécessitant pas un fort gain. La réjection obtenue à $\theta = 0°$ reste trop faible (5.6 dB) pour assurer l'isolation entre les deux fonctions dans cette direction. En utilisant donc un réseau de fente (trois) dans le SIW, on parvient à améliorer la réjection de 3 dB dans cette direction pour une meilleure isolation. La réjection à $\theta = 90°$ reste importante (au moins 26 dB), assurant une meilleure isolation dans cette direction.

Perspectives

Comme nous l'avons vu dans cette thèse, l'antenne multifonction développée nous permet d'assurer simultanément des fonctions radar et communication mais dans des directions figées. Il serait alors intéressant de modifier les caractéristiques de cette antenne, afin de contrôler le balayage des différents faisceaux. Cela offrira plus de flexibilité à notre système. Afin de conserver la compacité de l'antenne sans pour autant augmenter la complexité, plusieurs pistes peuvent être envisagées:

- Concernant le rayonnement du cornet dédié à la fonction radar, la direction du faisceau pourrait être reconfigurée en considérant par exemple des métamatériaux à l'intérieur du cornet. De cette façon, les caractéristiques de rayonnement du cornet pourront être améliorées, sans augmenter la surface de l'antenne ni compromettre le poids et le coût de la solution.

- En ce qui concerne la fonction communication, les fentes dans le guide pourraient servir de sources d'alimentation à un réseau d'éléments de façon à former une sorte de cavité de Fabry-Pérot. Ainsi, il serait possible de placer un réseau d'éléments contrôlables juste au-dessus des fentes pour contrôler le faisceau rayonné pour la fonction de communication.

On pourrait également envisager comme application d'utiliser l'antenne pour des drones. En effet, les bras métallisés des drones peuvent servir de guide d'onde où viendrait se loger les fentes. Cependant, cela ajoutera des contraintes mécaniques qui devront être prises en compte dans la conception système. Ainsi, nous pourrions envisager un scénario où les fentes dans les bras pourraient être utilisées pour transmettre de l'information vers la terre tandis que le cornet pourrait être utilisé pour détecter des drones voisins ou même transmettre de l'information.

En ce qui concerne le cornet SIW, nous avons vu que la faible épaisseur du substrat affecte les performances de l'antenne. Cette antenne pourrait être améliorée pour les applications radar en remplaçant le cornet SIW par un réseau de fentes évasées qui est déjà une solution d'antenne SIW. De cette manière, les fentes seront toujours réalisées dans le SIW d'alimentation pour la fonction secondaire.

Table des matières

Introduction

In order to respond to the increasingly demand of new services, the objects we use on a daily basis (such as mobile phones, cars, airplanes etc.), tend to integrate more and more radio systems while the space available is limited. These radio systems require the use of many antennas that must meet multiple requirements such as compactness, isolation, costs, etc. A smart-phone, for example, contains several antennas for global navigation satellite system (GNSS), WiFi, TV, FM radio, Bluetooth, near-field communications (NFC) and the number is expected to increase as new systems are added. Another example is in airborne platforms where multiple functions such as communication, navigation, radar, electronic warfare are used. This leads to the need of reducing the number of associated antennas by regrouping several radio functions into a single antenna. However, combining the functionality of several antennas into one shared radiating element while maintaining the functionality of the various radio systems presents a great challenge. During its Ph.D, J. Euzière demonstrated the possibility to combine a radar function and a secondary function from a 16-monopole array originally dedicated to radar operation by using Time Modulated Array (TMA) technique. By this way, the two functions were operating at the same frequency and the system was powered by a single source.

The main objective of this thesis is to propose a more compact antenna (a single antenna) dedicated to radar and communication operations instead of using antenna array as J. Euzière did it. The idea is to start from an existing antenna solution and make the necessary modifications to add a second function without adding additional surface and complexity. As we are interested in radar applications, we will choose a directive antenna: a horn antenna. The goal is then to study the possibility to modify the radiation pattern of the horn antenna through controllable elements (slots) and to transmit a direct modulated signal at the antenna level for the communication function. Furthermore, polarization diversity is an attractive way to increase the isolation between two applications. Thus, this aspect will be taken into account in the design of the antenna solution.

The thesis is divided into 5 chapters:

Chapter 1 begins with a short overview of recent developments in multifunction antennas and presents the techniques most used to accomplish multifunctionnality. Several solutions of multifunction antennas found in the literature are investigated. For each case, their advantages and their drawbacks are highlighted. This study led to a general classification of multifunction antennas according to several criteria such as: number of radiating elements, radiation characteristics and feeding structure.

Chapter 2 is dedicated to the multifunction antenna solution concept developed in this PhD. The antenna system is composed of a horn antenna fed by a single waveguide port (for the radar purposes), thus offering extreme simplicity and direct compatibility with many existing systems. Through slots milled in the input waveguide and a switching mechanism, a fraction of the power in the feeding waveguide is then radiated through the activated slot for the communication purposes. The possibility to transmit a direct BPSK modulation (in a fixed direction) thanks to this switching mechanism is investigated. A study of large slots in the horn walls is conducted in order to find an alternative to corrugated horns in order to reduce the horn side lobes.

Chapter 3 is entirely dedicated to expanding the previous solution. Multiple communication directions and QPSK modulation are investigated. In addition, the possibility of increasing the directivity of the communication function while keeping the performance of the antenna system is studied.

Chapter 4 presents the technical characteristics of the prototype that has been built to provide experimental validations of the antenna system. It consists of the validation of the antenna system with direct BPSK modulation (in a single fixed direction) presented in chapter 2 and the switching mechanism to control the communication function. Measured results are compared to simulations to validate the antenna concept.

Chapter 5 deals with the possibility to extend the former solution presented in chapter 2 into planar technology. Indeed, the basic horn antenna suffers from its bulky size. This disadvantage can be overcome by using SIW horn antenna which is more compact. Hence, the performance of the SIW horn will be enhanced for the multifunction purposes.

Chapter 1: State of the Art on Multifunction Antenna

1.1. Introduction

The proliferation of advanced radio systems aboard airborne platform, mobile phones, cars etc. has led to an increasingly number of associated antennas. These antennas have to coexist in environments with severe space constraints. To address the problem of integrating antennas in tight environments, different radio functions can be regrouped to reduce the number of antennas. This leads to multifunction antennas, which offer the possibility of sharing the radiating elements in order to achieve multiple applications. However, combining the functions of several systems into one antenna while maintaining the required capabilities for each system presents a great challenge. In some cases, the functions grouping can be done by sharing more than the antenna (the radio frequency (RF) front-end) [1] - [4] whereas other solutions focus rather on the antenna architecture [5] - [15]. The main goal of this thesis is to address the space constraints by proposing a much more compact antenna solution able to perform simultaneously radar and communication functions. Hence, for this thesis we will focus on solutions consisting in modifying the antenna characteristics to achieve multifunction capabilities.

In section 1.2 we describe the most intuitive solution to radiate several different signals. In section 1.3 a short overview of recent developments in multifunction antennas is given. We begin by introducing the concept of multifunction antennas, more precisely by describing the techniques most used to accomplish multifunctionnality. The investigation of multifunction antennas based on antenna architecture found in literature led to a general classification of multifunction antennas that will be presented in section 1.4.

1.2. Separated radiators

In order to realize multiple functions, the intuitive solution is to juxtapose several antennas, each optimized and working independently for a specific function [12] - [15]. In general, the considered radiators work in different frequencies, share the same support but are fed separately. This solution will be called separated radiators in this chapter. However, taking into account directivity constraints for one or more functions will straightforwardly cause significant increase in the space occupied by the antennas. Thus, the trend is to place the antennas as close as possible to reduce the space they occupy. In this case, it would be necessary to take into account the eventual mutual coupling between the antennas.

As an example, Figure 1.1 depicts an integrated vehicular antenna for global positioning system (GPS), remote keyless entry system (RKES) and personal communication system (PCS) [14]. As can be seen, the two antennas share the same substrate each with its own feeding port. The isolation obtained between the two ports is at least 20 dB from 0.2 GHz to 2.2 GHz. However, as already explained, for applications requiring more directivity it would be necessary to increase the size of the antennas and therefore that of the support. Moreover, the use of separated radiators requires different feeding ports to route the signals, reducing the system compactness.

The next section will deal with multifunction antennas techniques.

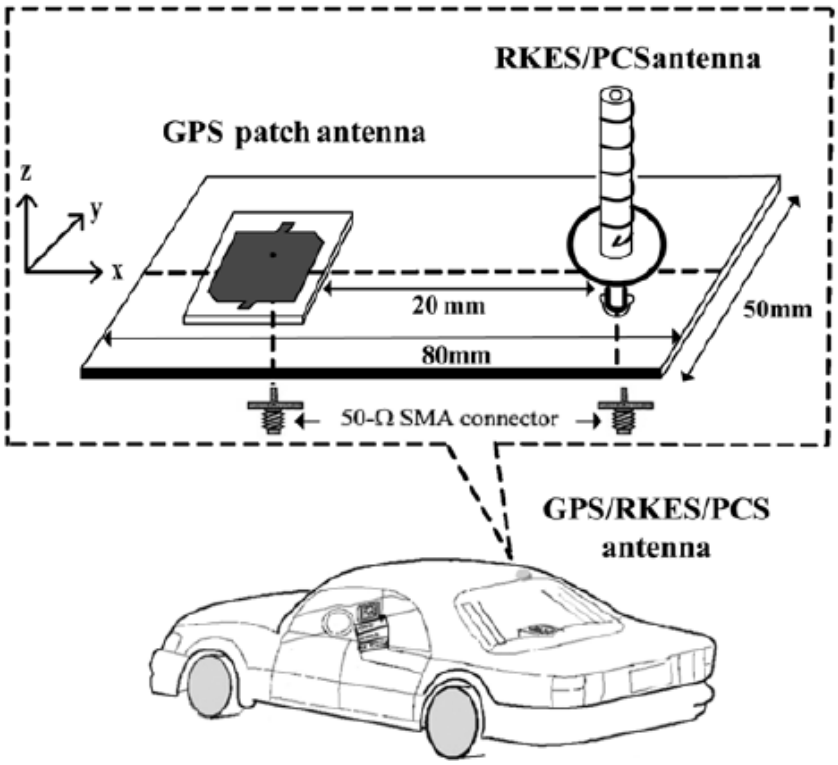

Figure 1. 1: Integrated GPS and RKES/PCS antenna [14]

1.3. Multifunction techniques

Traditionally, there are two approaches to achieve multifunctionality: time sharing [2] (time domain or time multiplexing), and aperture sharing [2] (space domain or aperture segmentation). This section presents the principle of the two approaches and some examples.

1.3.1. Time sharing

Time sharing technique, compatible with any type of antenna, consists in sharing the antenna resources alternatively with different systems at distinct time slots. Figure 1.2 depicts the use of this technique for *n* functions. As can be seen from this figure, when function 1 is needed, the switch allows the use of its modem, while others are completely disabled and so on for each function. Moreover, this solution requires at least two feeding networks (according to the number of functions sharing the antenna) resulting in bulky system.
Since the applications are accomplished sequentially, in the case of radar and communication applications, the radar performance is affected each time a communication is needed [2]. Thus, the time sharing technique is not that good for radar and communication integration.

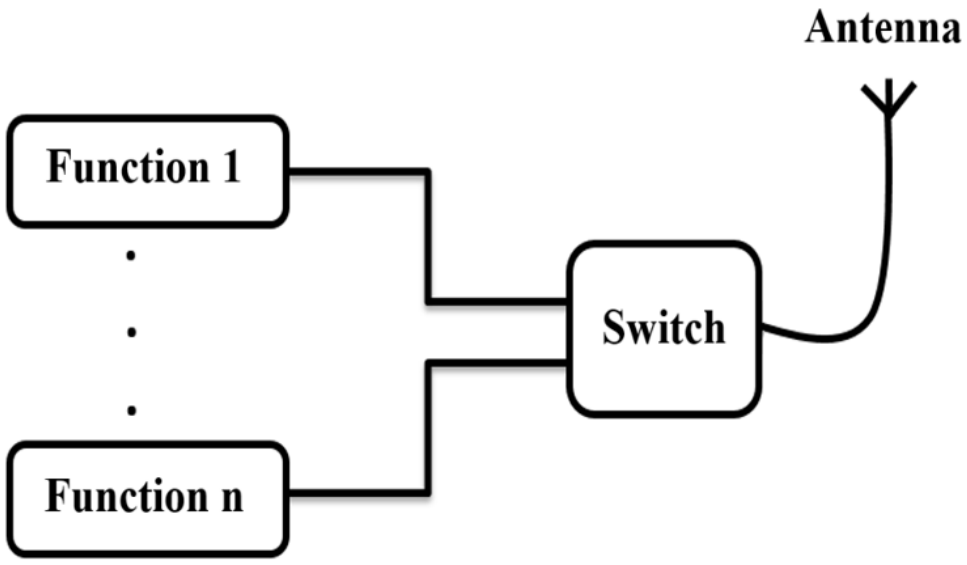

Figure 1. 2: Time sharing technique

With the recent technological developments, the current trend on this type of solution is to try to go even further by sharing more than the antenna (the RF front-end) [1]-[4]. Hence, the antenna, transmitter and receiver are reused by different radio systems. As already explained, for this thesis we will focus on solution consisting in modifying the antenna characteristics to achieve multiple functions.

In the next section, the shared aperture technique used to achieve multifunction capabilities will be presented.

1.3.2. Shared aperture

Shared aperture antennas are new type of antennas that regroup the functionality of several antennas into one aperture [8] [9] [10]. Then, the antenna aperture can be shared amongst many different radio applications such as communications, electronic warfare, or radar systems. As already explained, since the space available for the integration of antennas is limited in mobile phones, cars, residential access gateways, etc., the radiators must be carefully selected and designed to take into account this constraint.
According to the radiation characteristics of the shared aperture antenna, more precisely the directions considered (radiation pattern main beam) for the different RF applications, this solution can be divided in two categories: either the applications are realized in the same direction or they use different directions.

In the sections to come, we will present the particularities of each of the cases presented by giving some examples.

1.3.2.1. Same direction

In the present case, the applications are realized in the same direction. In order to ensure a good isolation between the different required applications, polarization diversity or frequency diversity are usually used [16].

- **Polarization diversity**

The polarization diversity approach consists of assigning to an antenna system the possibility to use orthogonal polarizations without physical separations in the antenna. The concept is based on the fact that in scattering environment, two orthogonal polarizations provide uncorrelated signals.

In [5], polarization diversity is used to achieve 45 dB isolation over a 20% band for a LFM radar with communication capabilities (cf. Figure 1.3). The used antenna is a microstrip pacth antenna working in S-band. The horizontal polarization is used for the communication function while the vertical polarization is dedicated to radar operation. To achieve the multifunction capabilities, the antenna uses two different feeding ports to route the different signals to the antenna reducing the compactness of the system. However, to improve the directivity, 1x4 antenna array is used, increasing the overall size of the antenna.

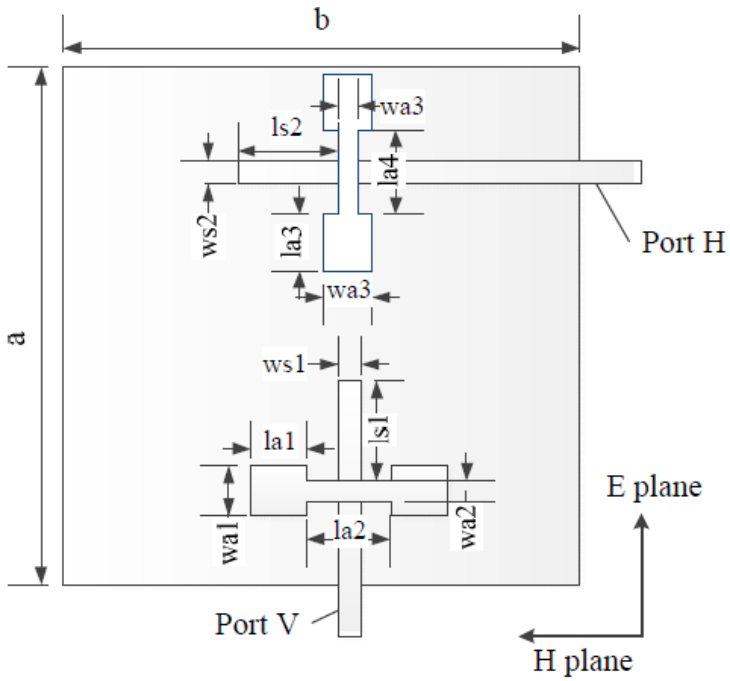

Figure 1. 3: Integrated radar and communication applications using patch antenna [5]

- **Frequency diversity**

The frequency diversity technique, often employed in microwave line of sight links, consists in transmitting or receiving simultaneously an information signal on two or more independently carrier frequencies (channels).
With the rapid development of wireless communication technology, this technique is more and more used [13] [17] [18]. This is frequently encountered in modern mobile communication systems where wideband radiating elements are used allowing to subdivide the total bandwidth into sub-bands used for each function [17] [18]. Hence, several applications such as GSM 900/1800 working between (824 MHz- 960 MHz) and (1.71 GHz – 1.92 GHz), 3G and 4G operating respectively between (1.8 GHz – 2.17 GHz) and (2.3 GHz – 2.69 GHz) can coexist.

In literature, many antenna systems combine frequency and polarization diversity [8] [19] for enhanced isolation between the various radio applications. In [19] for example, a stacked array structure providing continuous operation in S and X bands is designed. The array is a combination of a large rectangular ring-resonator antenna for S-band (2 elements) and circular patches for X-band (32 elements) and is dedicated to wireless communication, radar, remote sensing, and surveillance applications. Each of the arrays is fed by two ports to obtained horizontal and vertical polarizations. Hence the overall antenna is feed through four ports. The isolation between X and S bands are better than 25 dB.

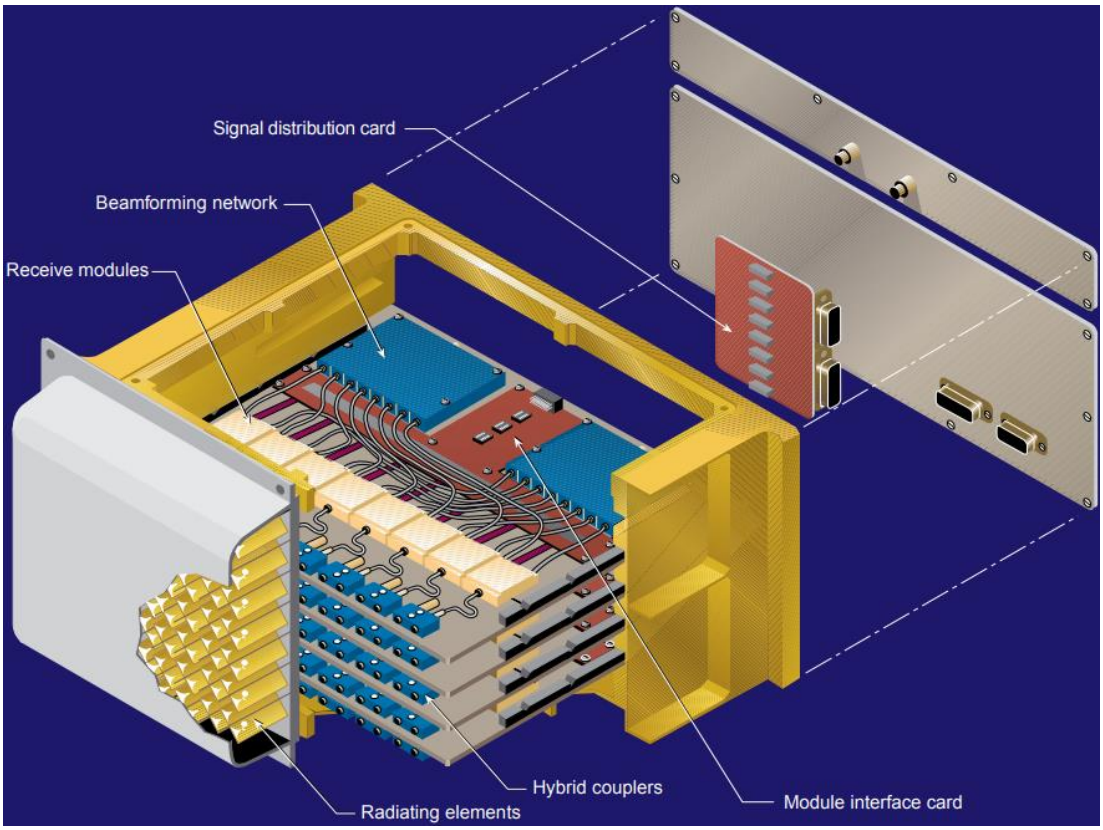

Figure 1. 4: Dual beam receive array [9]

1.3.2.2. Different directions

In this part we investigate the possibility to realize the applications in different directions. Indeed, the use of different directions to achieve a multifunction antenna leads to the concept of multibeam antennas. A multibeam antenna is usually an array where the *N* elements are combined in several different ways, so as to produce *M* radiations [7] [8] [9] [11]. Considering the number of ports (input or ouput) of the antenna, the multibeam antennas can be divided into two categories: standard multibeam antennas using multiple ports [8] [9] [11] and multibeam antenna using a single port [7].

- **Multibeam antenna with multiple ports**

An example of multibeam antenna with multiple ports is depicted in Figure 1.4. This antenna is used in receive mode and can receive communication signals from two different directions through the use of two beamforming networks and two reception ports [9]. The array is composed of 8x8 dual polarized elements (Vivaldi) and works between 7 GHz and 10 GHz.

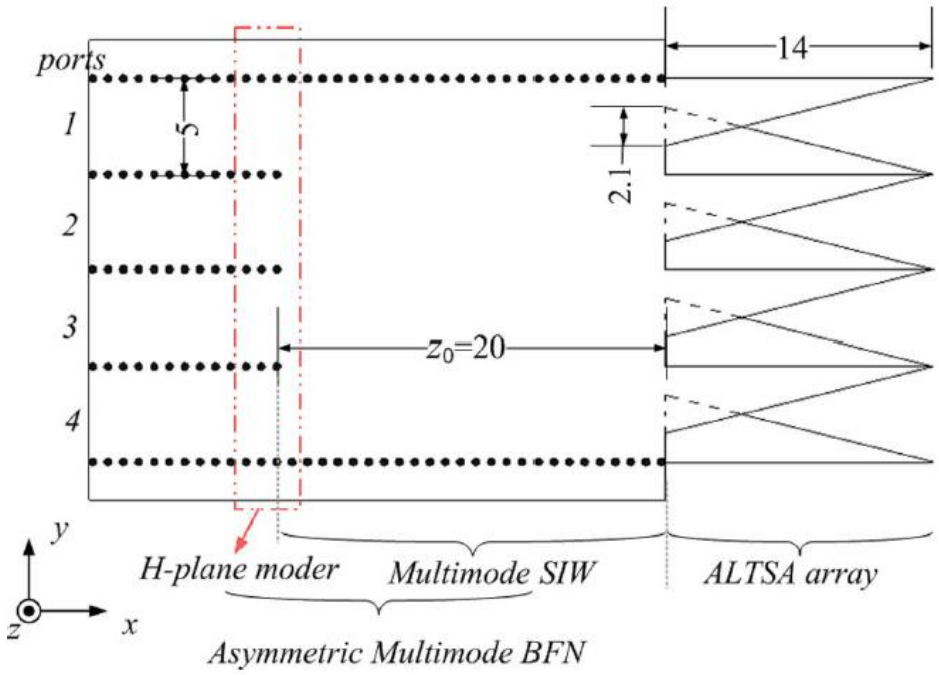

Figure 1. 5: SIW multibeam antenna [11]

In Figure 1.5, a substrate integrated waveguide (SIW) is used as a beamforming network, with four input ports and one output port, directly connected to the radiator [11]. Hence, four different beams can be obtained in different directions. The antenna works from 31 GHz to 36 GHz

Multibeam antennas can also take the advantages of polarization and frequency diversitiy techniques (presented in section 1.2.3.1), depending on the targeted applications. In [6], a slotted

waveguide with slots milled into opposite walls is used to provide a high-gain solution for two signals with orthogonal polarizations and working at two different frequencies (S-band for radar and C-band for communication).

However, as already explained, the use of multiple ports to route the different function signals to the radiating structure, may be seen as a drawback regarding the overall compactness. The next point will deal with the possibility of using a single feeding port with the aim of reducing the compactness of the system.

- **Multibeam antenna with single port**

The use of a single access port for a multibeam antenna is intended to make the antenna more compact. However, when applied to multifunction antennas, it is necessary to be able to modify the signal initially dedicated to one of the functions so that to include the signal of the other functions. This then introduces the notion of direct antenna modulation [21]-[24].
Direct antenna modulation is an attractive solution to generate RF data modulation for information transmission (or phased array beamforming) from a transmitting (receiving) antenna driven by a single unmodulated carrier. The unmodulated signal is transmitted in one direction while a part of this signal is modulated and transmitted in another direction. In contrast to conventional modulation, direct antenna modulation does not need a conventional modulator or variable RF phase shifter devices. Furthermore, as the phase and magnitude of the modulated fields are radiated coherently in desired directions only, this can provide a very discrete communication link, which is highly relevant when combined with a radar application.

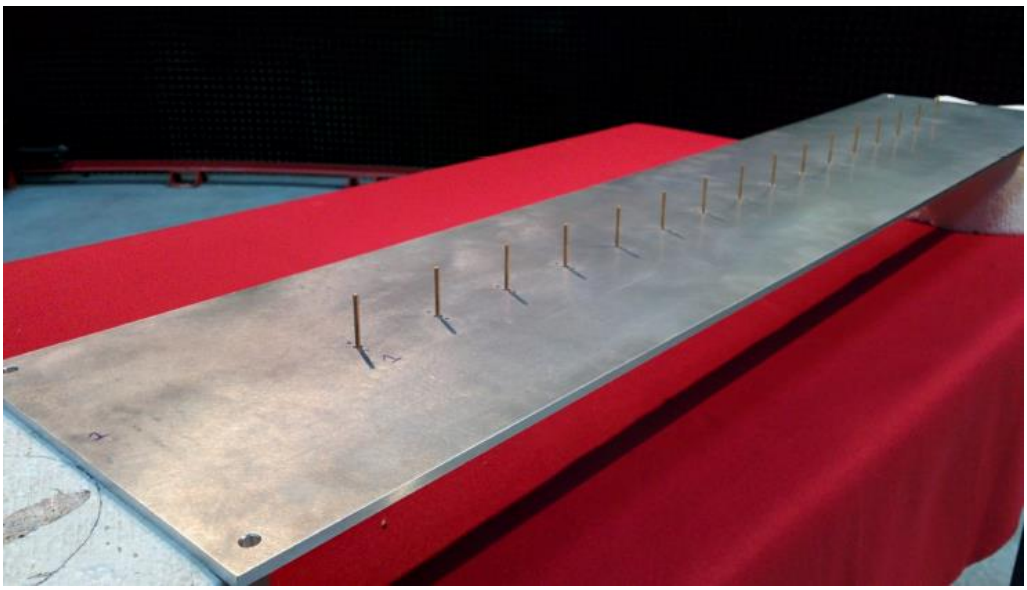

Figure 1. 6: 16 elements array for TMA [7]

In [7], J. Euzière took benefit of the Time Modulated Array (TMA) technique [25] and direct antenna modulation to combine a radar function and a secondary communication function. The used antenna is a 16-monopole array originally dedicated to radar operation (cf. Figure 1.6). The possibility to vary instantaneously the sidelobes of the radiation pattern is used to transmit additional information in another direction. Hence, by conveniently switching the active dipoles while keeping the main lobe unchanged (preserving the radar function), a low data-rate communication could be established in desired directions.

After presenting the different multifunction antennas used in literature, in the next section, a classification of the set solutions presented in is chapter will be done.

1.4. Multifunction antennas classification

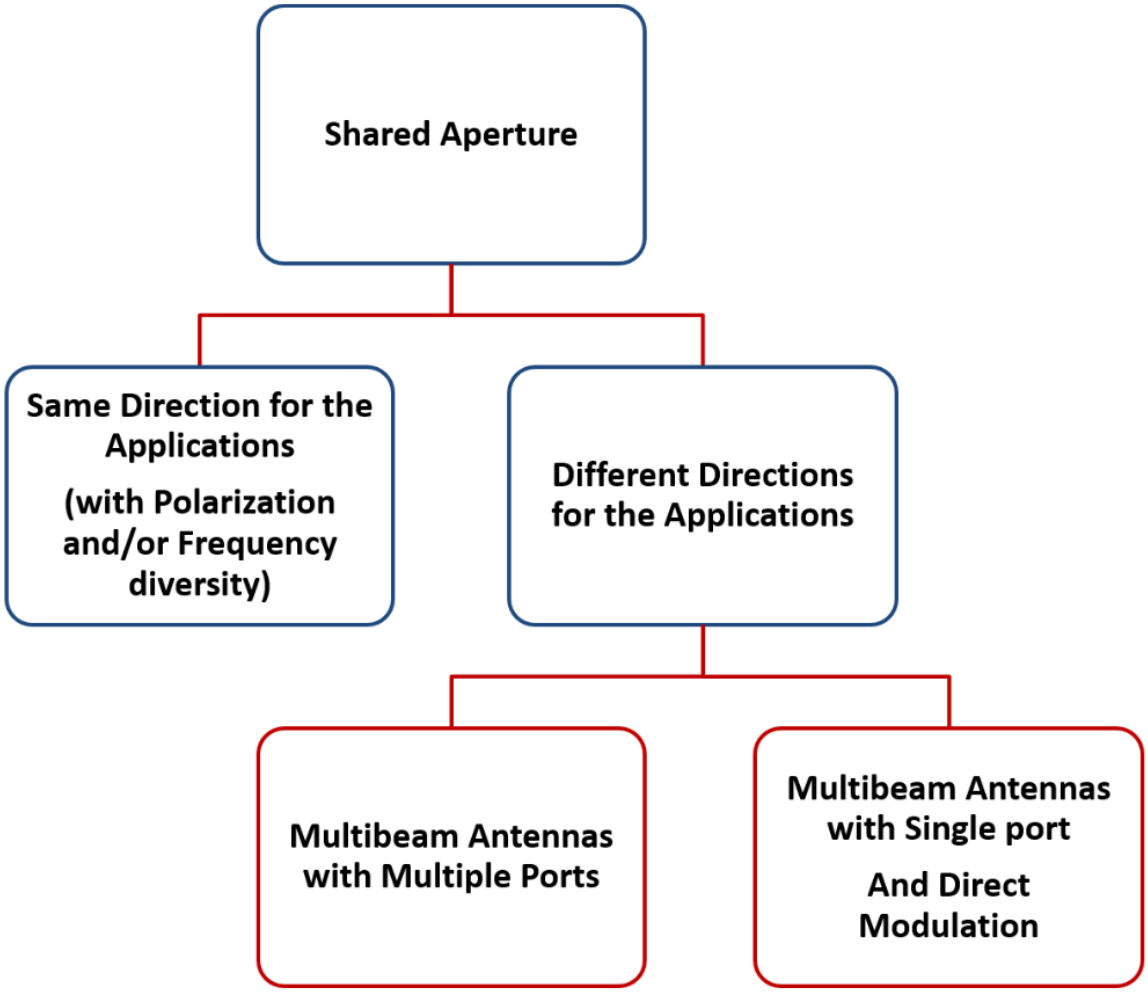

Figure 1. 7: proposed multifunction antennas (based on antenna architecture) classification

To facilitate the understanding of the operating principle of multifunction antennas and how they are designed, we propose a classification of the solutions (based on antenna architecture) presented in this chapter.

Figure 1.7 depicts the classification of the multifunction antennas solution. As presented before, in the present context, we will focus on solution offering simultaneous operation and based on antenna architecture. Hence, shared aperture takes advantage of time sharing. After the choice of the antenna structure (here shared aperture), now comes the choice of the directions in which we want to perform the set of functions. As presented before, this choice depends on the type of applications considered. Hence, in the case where the applications are needed in the same directions, polarization and frequency diversity can be used to enhance the isolation between the functions. Note that it is also possible to combine the polarization and frequency diversity techniques to multibeam antennas (different directions), cf. Table 1.1. However, for the applications performed in different directions, the space diversity offers an additional degree of freedom to reduce the mutual coupling between the considered functions. Concerning the multibeam antenna systems, they can be either powered by a single port or by multiple ports. The advantage of using a single port is the reduction of the size of the overall system. Furthermore, this offers the possibility to perform a direct antenna modulation without the need of complex electronic as for conventional modulation systems (cf. Table 1.1).

1.5. Conclusion of chapter 1

In this first chapter, a brief state of the art on multifunction antennas techniques has been presented. Based on the techniques presented in this chapter, two categories are distinguished: time sharing and aperture sharing. For integrated radar and communication applications, the downside in the former technique is that the functions are accomplished sequentially. The later approach makes it possible to perform the functions simultaneously, but also to control independently the radiation pattern (direction, polarization, frequency, etc.) required for each of the functions by focusing on the antenna architecture. Moreover, the compactness of the system can be further reduced by using a single input port and by realizing a direct modulation at the antenna level.

The first objective of this thesis being to take into account the space constraints of multifunction antennas, we will consider aperture sharing technique, using a single aperture, allowing to perform the functions simultaneously and to control the radiation pattern at antenna level. Furthermore, the possibility to integrate a direct modulation for the communication at the antenna level will be considered, offering a discrete communication link and reducing the compactness of the overall system by the use of a single feeding port. Hence, contrary to the work of J. Euzière [7] based on antenna array, this thesis will focus on the study of a single antenna that will be presented in the next chapter. Generally, for multifunction antennas, separated antennas are considered in transmission and reception. Thus, the proposed antenna system will only work in transmit mode.

	Multibeam	**Diversity**	**Number of ports**	**Direct modulation**
Square Patch array [5]	No	Polarization	2	No
Stacked array of circular patch and rectangular ring resonator [19]	Yes	Polarization and frequency	4	No
Vivaldi array [9]	Yes	Polarization	2	No
ALTSA array [11]	Yes	No	4	No
Slotted waveguide [6]	Yes	Polarization and frequency	2	No
Monopole array [7]	Yes	No	1	Yes

Table 1. 1: Summary of multifunction antennas based on shared aperture presented in the chapter

[1] M. Alansi, I. Elshafiey, A. M. Al-Sanie, and M. A. Hossain, “Multi-user detection for radar and communication multifunction system,” Journal of Circuits, Systems, and Computers, vol. 24, no. 3, 2015.

[2] S. J. Quan, W. P. Qian, and J. H. Guo, “Radar-Communication Integration: An Overview,” Advanced Infocomm Technology (ICATT), 2014, pp.98-103.

[3] J. Zhao, K. Huo and X. Li, “A Chaos-Based Phase-Coded OFDM Signal for Joint Radar-Communication Systems,” in Proc. 12th ICSP, Hangzhou, China, Oct. 19-23, 2014.

[4] Liang Han, Ke Wu, “Joint wireless communication and radar sensing systems – state of the art and future prospects,” IET Microwaves, Antennas and Propagation, Aug. 2013, pp. 876-885.

[5] Y. Yue, J. Zhou, “A Wideband Dual-Polarized Antenna Array for Multifunction Radar,” in Proc. 5th APCAP, Kaohsiung, Taiwan, Jul. 26- 29, 2016.

[6] Arismar Cerqueira S. Jr., I.F. da Costa, S. Pinna, S. Melo, F. Laghezza, F. Scotti, P. Ghelfi, D. H. Spadoti and A. Bogoni, "A Novel Dual-polarization and Dual-band Slotted Waveguide Antenna Array for Dual-use Radars", in Proc. 10th EuCAP, Davos, Switzerland, Apr. 10- 15, 2016.

[7] J. Euziere, “Multifunction Array for Radar Applications,” PhD dissertation, Supélec, 2015.

[8] C. Hemmi, T. Dover, F. German, and A. Vespa, “Multifunction wide-band array design,” IEEE Trans. Antennas Propagat., vol. 47, pp. 425–431, Mar. 1999.
[9] T. A. Axness, R. V. Coffmann, B. A. Kopp, and K. W. O’Haver, “Shared aperture technology development,” Johns Hopkins APL Tech. Dig., vol. 17, no. 3, pp. 285–294, 1996.

[10] C. I. Coman, I. E. Lager, and L. P. Ligthart, “The design of shared aperture antennas consisting of differently sized elements,” IEEE Trans. Antennas Propag., vol. 54, no. 2, pp. 376–383, Feb. 2006.

[11] Y. J. Cheng and Y. Fan, “Millimeter-wave miniaturized substrate integrated multibeam antenna,” IEEE Trans. Antennas Propag., vol. 59, no. 12, pp. 4840–4844, Dec. 2011.

[12] S. Y. Lin and K. C. Huang, “A Compact Microstrip Antenna for GPS and DCS Application,” IEEE Transactions on Antennas and Propagation, AP-53, 3, March 2005, pp. 1227-1229.

[13] Lei Chang, Jian-qiang Zhang, Yu-feng Wang, Bao-ming Li, “Design of Compact Multifunction Antennas in a Common Aperture,” 2014 3rd Asia-Pacific Conference on Antennas and Propagation, Harbin, China, Jul. 26-29, 2014.

[14] K. Oh, B. Kim, and J. Choi, “Novel integrated GPS/RKES/PCS antenna for vehicular application,” IEEE Microw. Wireless Comp. Lett., vol. 15, no. 4, pp. 244–246, Apr. 2005.

[15] Victor Rabinovich, Dmitri Rabinovich, “Three Port Compact Multifunction Printed Antenna System for Automotive Application,” 2010 IEEE Antennas and Propagation Society International Symposium, Toronto, ON, Canada, Jul. 10-17, 2010.

[16] W. L. Van Rossum, J. J. M. De Wit, M. P. G. Otten, et al. SMRF architecture concepts. IEEE Electronic Systems Magazine, 2011(5):12-17.

[17] A. Diallo, C. Luxey, P. Le Thuc, R. Staraj, and G. Kossiavas, “An efficient two-port antenna-system for GSM/DCS/UMTS multi-mode mobile phones,” Electron. Lett., vol. 43, no. 7, pp. 369–370, Mar. 29th, 2007.

[18] G. Villemaud, C. Decroze, F. Torres, T. Monediire, B. Jecko, "Multi-Band Antenna for Mobile Cominiinicatioii Standards", Intern. Con/: on Antenna Technologv and Applied Eledroniugnefics, Montreal, August 2002.

[19] S.-H. Hsu, Y.-J. Ren, and K. Chang, “A dual-polarized planar-array antenna for S-band and X-band airborne applications,” IEEE Antennas Propag. Mag., vol. 51, no. 4, pp. 70–78, Aug. 2009.

[20] B. Uhl, “Direct Spatial Antenna Modulation for Phased-Array Applications,” in Proc. Int Telemetering Conference, Las Vegas, Nevada, Oct 2009.

[21] A. Babakani, David. B. Rutledge and A. Hajimiri, “Near-Field Direct Antenna Modulation,” IEEE microwave magazine, Feb. 2009, pp 36- 46.

[22] A. H. Chang, A. Babakhani, and A. Hajimiri, “Near-field direct antenna modulation (NFDAM) transmitter at 2.4 GHz,” in Proc. IEEE Int. Symp., Antennas Propagat. Soc. (APSURSI ’09), 2009, pp. 1–4.

[23] W. Yao and Y. Wang, “An integrated antenna for pulse modulation and radiation,” in Proc. IEEE Radio Wireless Conf., 2004, pp. 427–429.

[24] S.D. Keller, W.D. Palmer, and W.T. Joines, “Direct Modulation of an L-band Microstrip Patch Antenna Using Integrated PIN Diodes”, Conf. Rec. 2006 Allerton Antenna Applications Symposium, pp. 132-140.

[25] H. E. Shanks and R. W. Bickmore, “Four-dimensional electromagnetic radiators,” Canadian Journal of Physics, vol. 37, pp. 263-275, 1959.

Chapter 2: The Multifunction Antenna System

2.1. Introduction

This chapter presents the general structure that will be studied in this thesis, namely a horn antenna on which modifications will be made. These adjustments will aim globally to act on the side lobes of the horn antenna.

In section 2.2, we will study the possibility of reducing the side lobe level (SLL) by using slots in the horn antenna. We will then show in section 2.3 that it is more judicious to make the slots in the feeding waveguide if we want to dynamically control the horn SLL. Finally, in section 2. 4, we will exploit this dynamic control of the SLL in order to perform a communication function in addition to the radar function for the multifunction purposes.

2.2. Reduction of SLL

In this section, the possibility of reducing the horn antenna SLL by using slots in the horn is studied. The impact of such a structure on the horn antenna radiation pattern will be investigated.

The standard horn antenna and its feeding waveguide that will be used for this study are presented in Figure 2.1. This antenna operates at 10 GHz and radiates a directive beam with linear vertical polarization along *z*-axis. Such an antenna is often used in radar applications [1] - [5] and is designed following the procedure presented in [6].

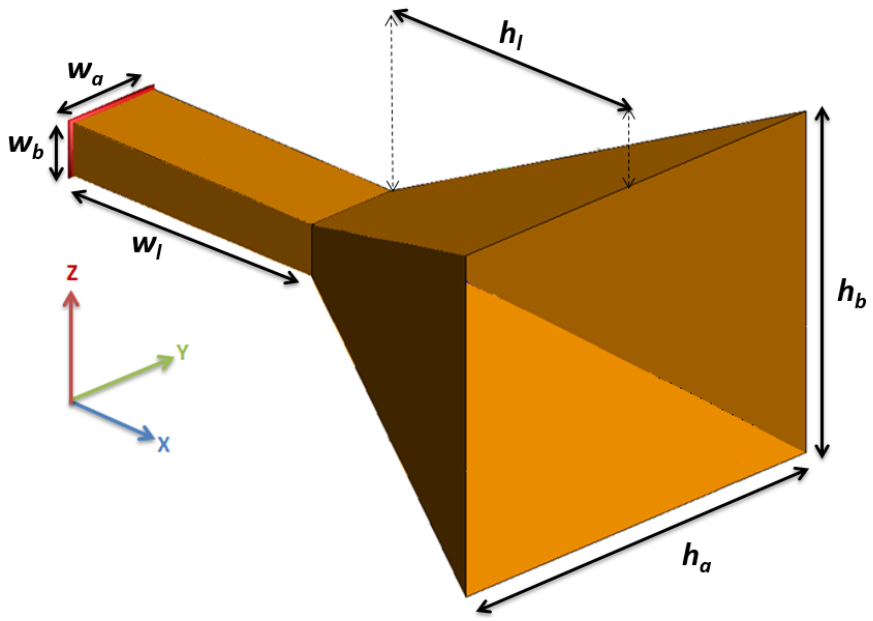

Figure 2. 1: Horn antenna and its feeding waveguide (w_a = 20.7 mm, w_b = 10.3 mm, w_l = 62.3 mm, h_l = 73.8 mm, h_b = 68.6 mm, h_a = 88.2 mm)

Generally, the modification of the radiation pattern of a horn antenna can be obtained by using a corrugation [7] [8], whose goal is to reduce the side lobes or dielectric lens [2] [3] [9] [10] in the aperture to provide more gain to the horn (cf. Figure 2.2). However, the use of these techniques is costly and may be complicated to achieve, in particular the realization of the corrugations.
It is therefore proposed here to reduce the cost and the manufacturing complexity of the corrugation by using a slot antenna, which can be etched on whatever surface, in order to reduce the horn SLL.

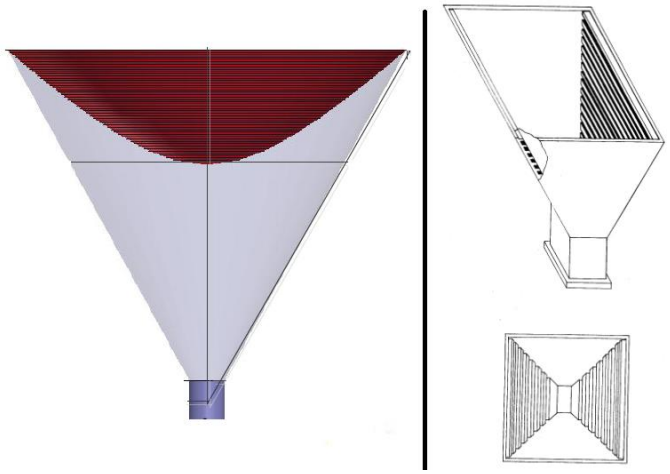

(a) (b)

Figure 2. 2: (a) dielectric lens in the horn aperture [2] and (b) corrugated horn [7]

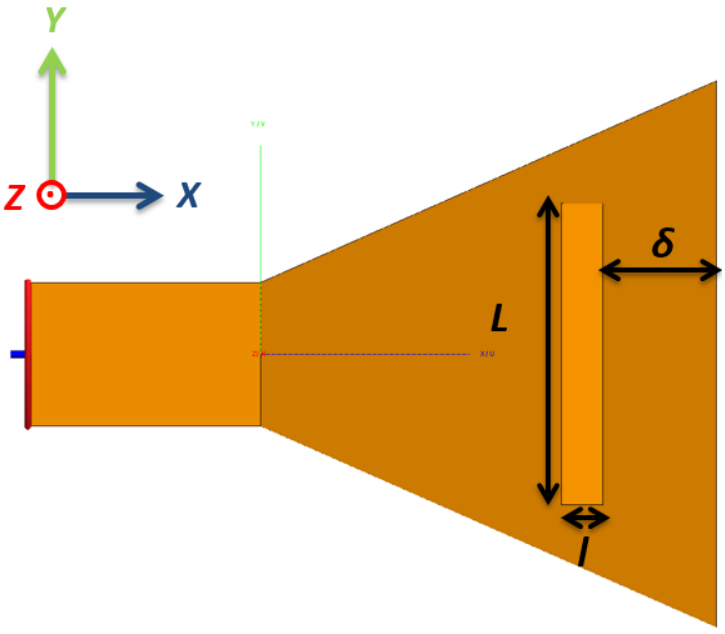

Figure 2. 3: Slot etched close to the Horn aperture

The role of the slot in the present case is to disrupt the field distribution (amplitude and phase) in the horn aperture in order to modify the radiation pattern of the horn antenna (more precisely the side lobes) while keeping the main lobe of the horn unchanged.

The study will be limited to rectangular slots for the simplicity of design. Figure 2.3 depicts the slot configuration (length L and width l) that we will be considered for this study. In this figure, δ is the slot position from the horn aperture.

2.2.1. Slot design

In this section, the slot design and the impact of this antenna on the horn side lobes are investigated. In order to simplify the study and better understand the results, as a first step we will only consider one slot in the horn.

Generally, slots are designed to be half wavelength long at the operating frequency ($L \approx \lambda_0/2$) and are typically thin ($l \leq \lambda_0/10$). In this case, at 10 GHz, L = 15 mm and $l \leq 3$ mm.

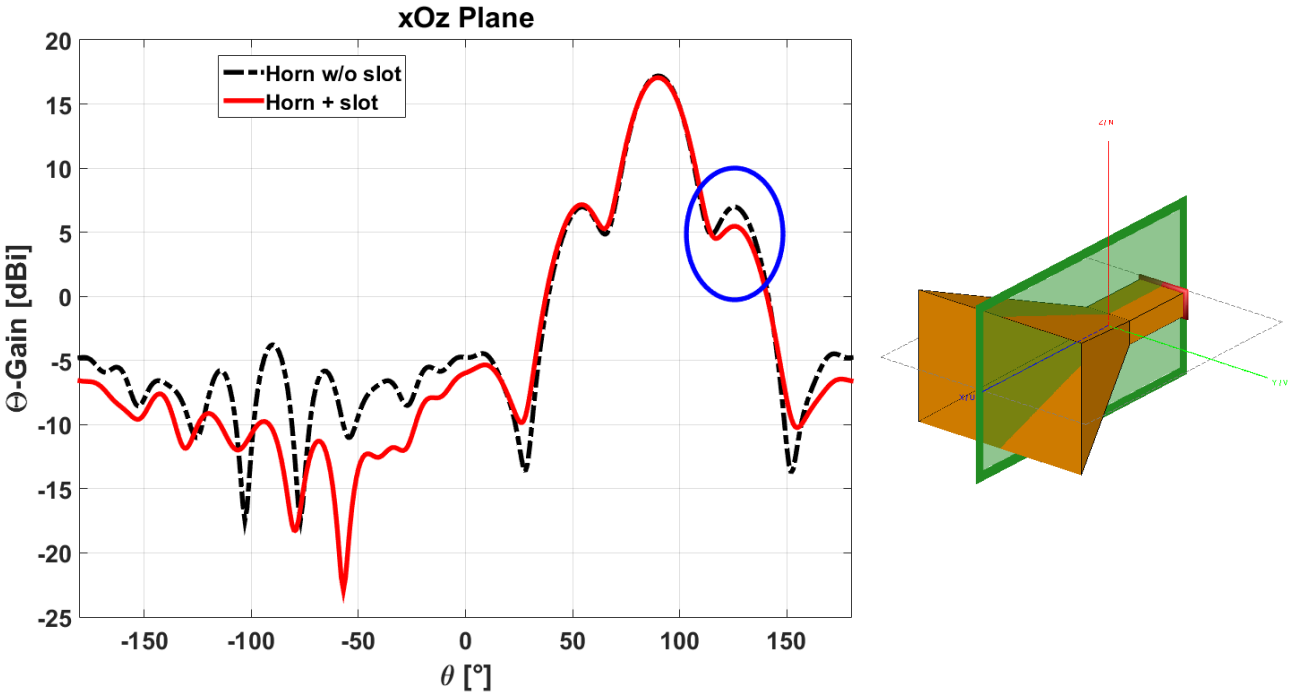

Figure 2. 4: Theta Gain in xOz plane at 10 GHz of the Reference horn in comparison to slotted Horn

We first study the impact of this slot antenna on the horn radiation pattern at 10 GHz. Figure 2.4 and Figure 2.5 present the horn radiation patterns in respectively xOz and xOy plane for a slot of width l = 3 mm and placed arbitrarily at δ = 10 mm from the aperture. In comparison to the same horn antenna without slot, the side lobes have been modified in the two planes. Moreover, the front to back ratio (FTBR) was increased by 6.66 dB. These results are obtained without modifying the main lobe of the horn antenna.

We remark that in xOz plane (cf. Figure 2.4), the slot affects the first SLL in only one side (at θ =126°). In fact, this is due to the use of one slot in the horn (cf. Figure 2.3). As we will see later, a second slot in the opposite wall of the horn will lead to symmetrical modification in the radiation pattern.

Because of the slot position in the horn, the main lobe of the horn in xOy plane is not affected except in the backward directions (cf. Figure 2.5).

In order to better control and increase the side lobes modification in xOz plane, a parametric study is then necessary to find the appropriate dimensions of the slot and position from the horn aperture. Hence, in the next section, the impact in xOz plane of the slot dimensions and position on the horn antenna SLL will be carried out.

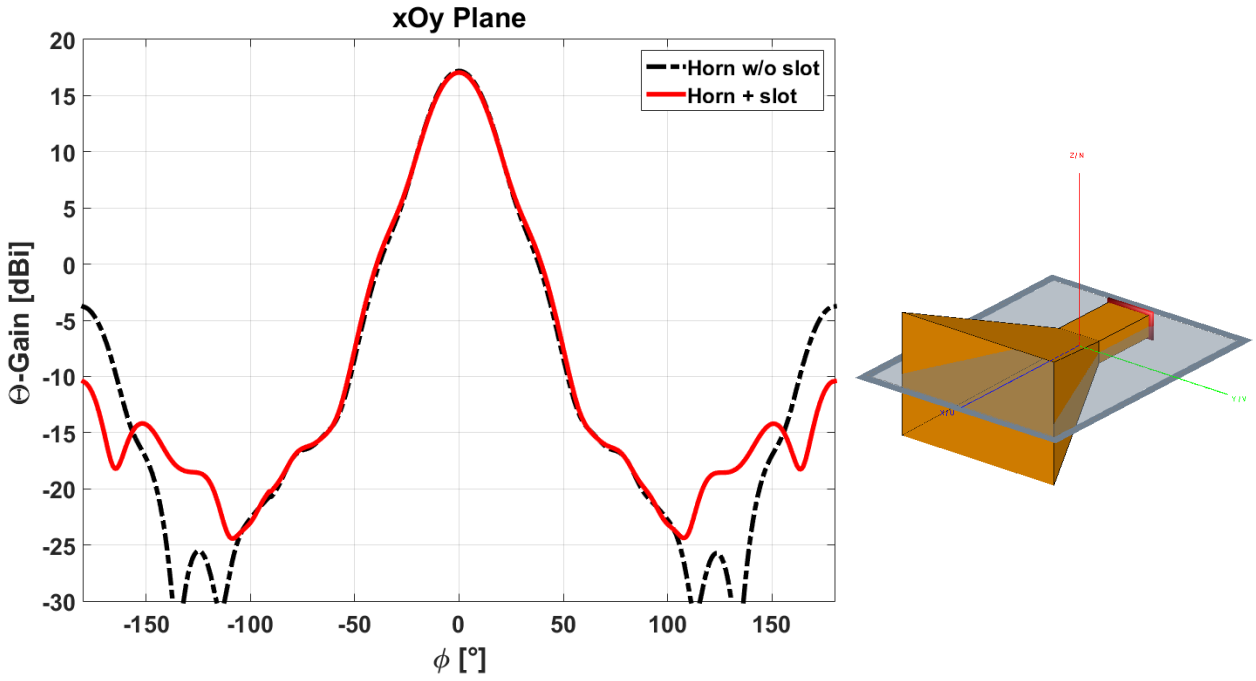

Figure 2. 5: Theta Gain in xOy plane at 10 GHz of the Reference horn in comparison to slotted Horn

2.2.1.1. Parametric study on slot dimensions and position

In this section, the impact of slot dimensions and position in the SLL is investigated.

Taking into account the dimensions of the horn antenna (cf. Figure 2.1), in this section, the study is limited to slots of dimensions $L \leq 50$ mm and $l \leq 10$ mm, physically achievable in the horn walls.

- **Slot length *L***

We first study the impact of the slot length on the horn SLL. For this study, the width and the distance to aperture are set respectively at $l = 4$ mm and $\delta = 10$ mm. Figure 2.6 (a) depicts the SLL as a function of the slot dimension L at 10 GHz. As can be seen, the SLL decreases slightly with the length L in comparison to the horn without slot. For $L = 50$ mm, the SLL is equal to -11 dB. Hence, the SLL has been reduced by 0.78 dB in comparison to the horn without slot.
Concerning the gain in the main direction of the horn (cf. Figure 2.6 (b)), the maximum variation is 0.16 dB
For the remainder of the study the slot length is set at $L = 50$ mm.

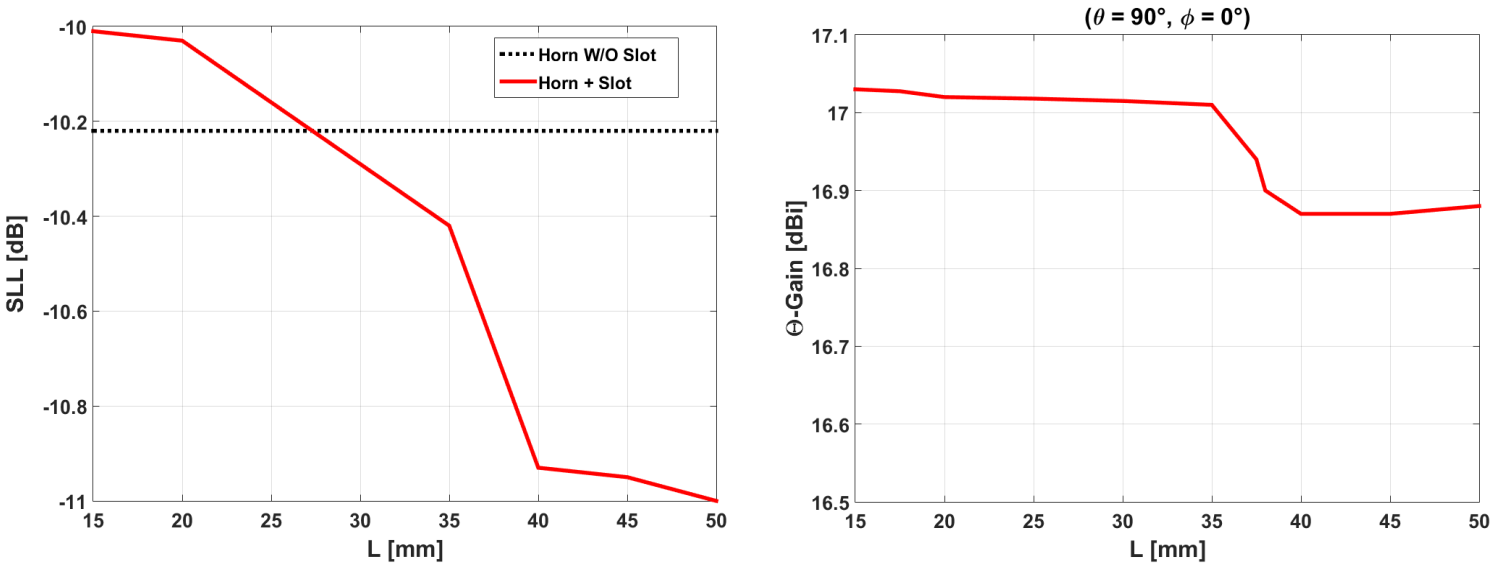

(a) (b)

Figure 2. 6: SLL (a) and the gain in the main direction of the horn (b) at 10 GHz for l = 4 mm versus slot length L

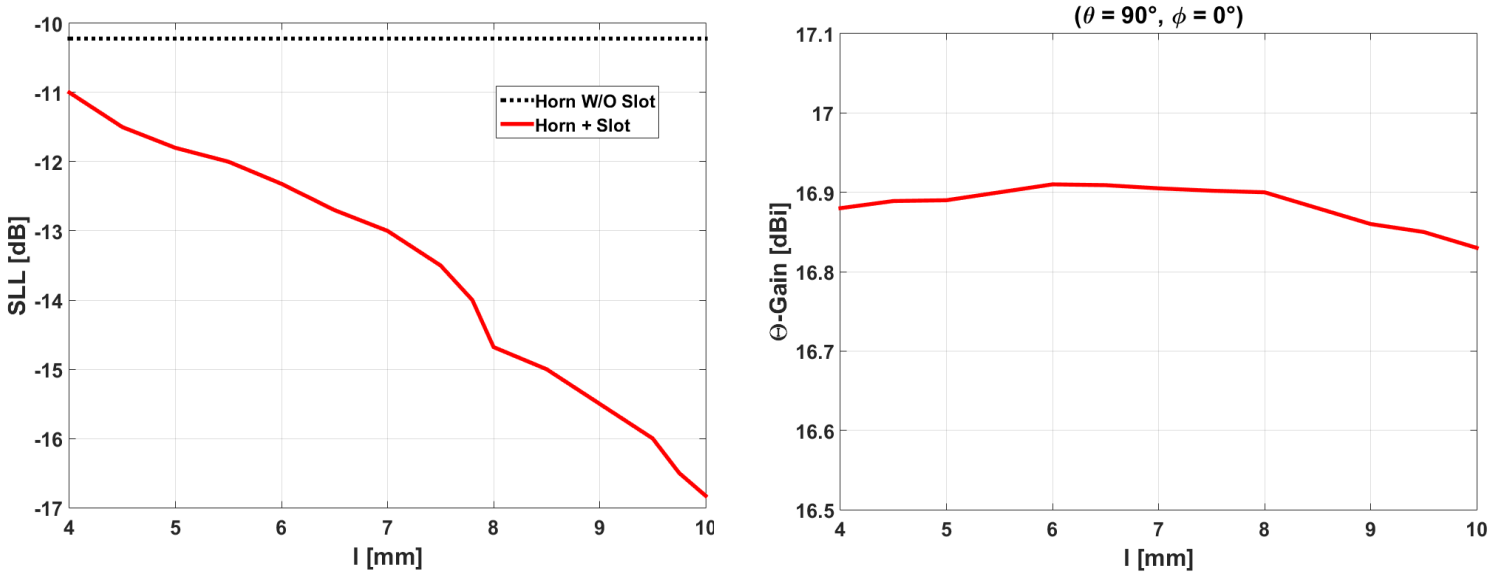

(a) (b)

Figure 2. 7: SLL (a) and the gain in the main direction of the horn (b) at 10 GHz for L = 50 mm versus slot width l

- **Slot width *l***

By varying this time the slot width l while keeping δ = 10 mm (cf. Figure 2.7 (a)), we observe as before, a decrease in the SLL with the width. For example, l = 10 mm gives a SLL of -16.83 dB. In comparison to the horn without slot, the SLL has been reduced by 6.6 dB.
In this case, the gain variation in the horn main beam is less than 0.1 dB (cf. Figure 2.7 (b)).

Then, the slot width is set at l = 10 mm for the remainder of the study.

The analysis of these first results shows that the horn side lobes modification requires the use of large size slots (L = 1.6* λ_0 (50 mm) and l = 0.3* λ_0 (10 mm)). As already explained, these dimensions correspond to the maximum size of the slot physically achievable in the horn walls. Now, in order to refine the results we need to find the proper distance δ between the slot and the horn aperture.

- **Slot position from the horn aperture δ**

We now investigate the impact of the slot position on the horn SLL. Figure 2.8 depicts the SLL as a function of δ. As can be seen from this figure, the SLL decreases to -16.98 dB at 10.8 mm corresponding to 1.5* λ_g.

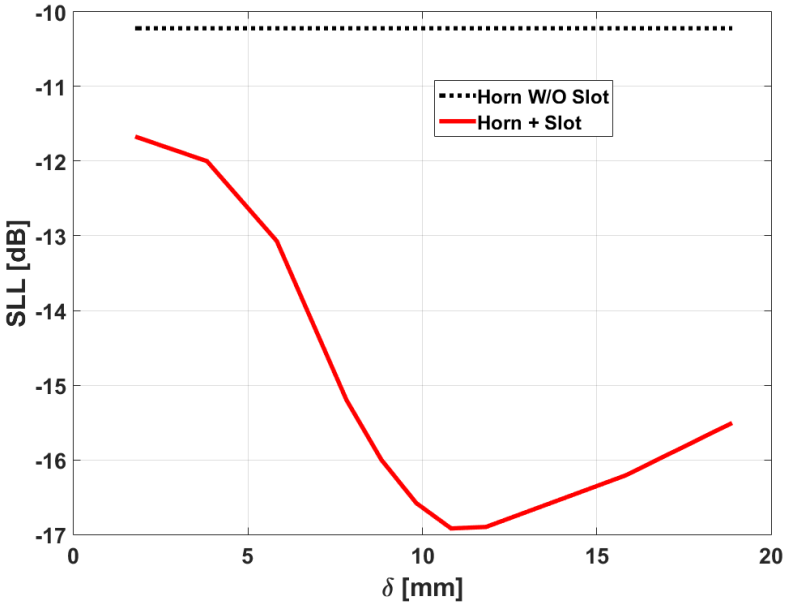

Figure 2. 8: SLL at 10 GHz for L = 50 mm; l = 10 mm versus the slot position to aperture

All these results show that the use of very large slots (L = 50 mm and l = 10 mm) placed at δ = 10.8 mm from the horn aperture leads to an important reduction in the side lobes level (-16.98 dB) in comparison to a horn without slots. However, this result is obtained 10 GHz. It would be interesting to consider the impact of this large slot on the radiation pattern of the horn antenna over a larger frequency range in order to draw relevant conclusions.

2.2.2. Impact of the large slot on the horn radiation over the studied band

In the following section, the impact of the large slot on the entire studied band (8 GHz – 12 GHz) is investigated. Figure 2.9 (a) and Figure 2.9 (b) present respectively the gain in the main direction of the horn and the SLL versus frequency. In comparison to the horn without slot, as expected, we can see a quasi-constant gain drop in the main direction of the horn (Figure 2.9 (a)) due to the

power dissipated by the slot, meaning that the slot is very wideband (use of wide slot). This is not a concern provided the main beam is not modified.
Concerning the SLL shown in Figure 2.9 (b), as expected it is much lower with slots over the entire band. The main improvement is obtained close to 9 GHz and reaches 8 dB. At 11.5 GHz, the situation is not so good but the improvement is still better than 1.5 dB.

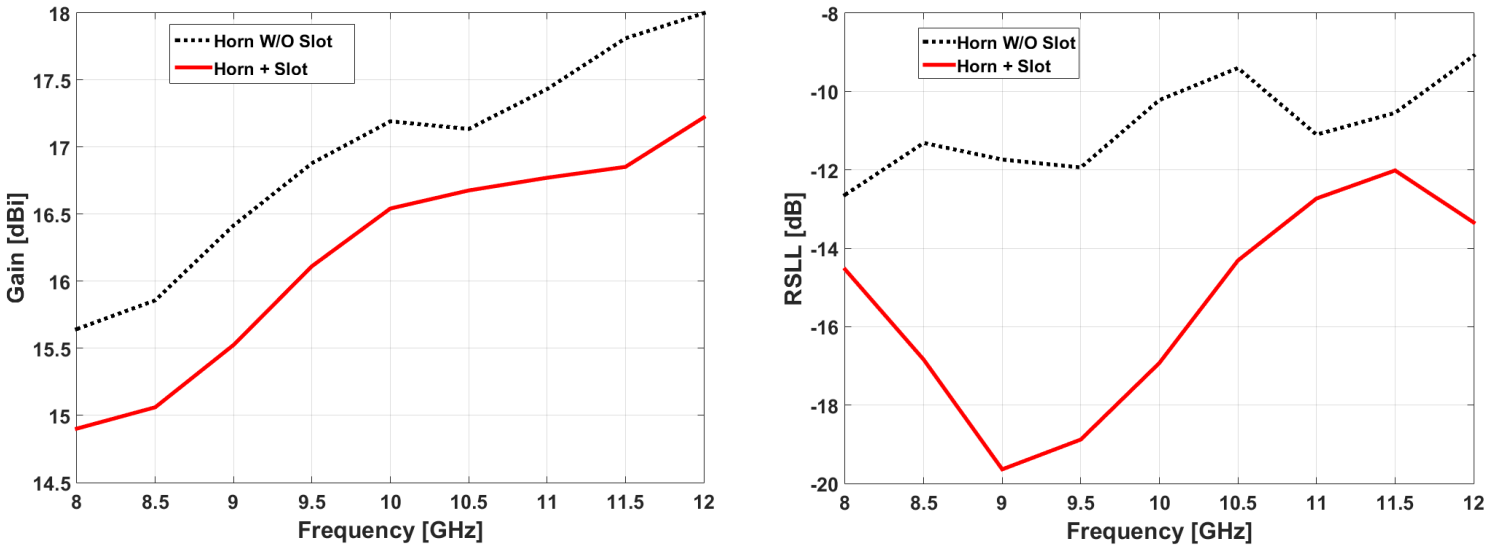

(a) (b)

Figure 2. 9: (a) Gain in the main direction of the Horn and (b) SLL versus frequency

By analyzing the results more closely, we note that this technique could allow us to reduce considerably at no cost the SLL of a standard horn antenna by placing a second identical slot on the opposite face (bottom wall).

To validate this assumption, the results for L = 50 mm, l = 10 mm and δ = 10.8 mm at different frequencies are depicted in Figure 2.10, 2.11 and 2.12. As expected, the side lobes have been reduced on all the patterns in xOz planes. On the other hand, it reduces the gain in the main lobe of the horn by 0.95 dB in the worst case due to power dissipated in the slots. Furthermore, the horn beamwidth was slightly increased by 5.26° (in the worst case) in comparison to the horn without slots.

Nevertheless, etching large slots in the horn walls is another way of decreasing SLL. This solution, simple to implement and inexpensive, offers an alternative to the use of corrugated horns to reduce the SLL.

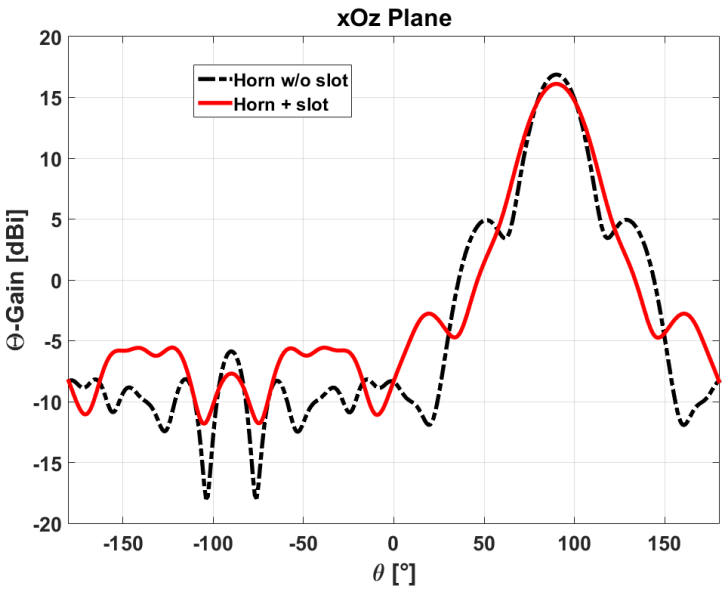

(a)

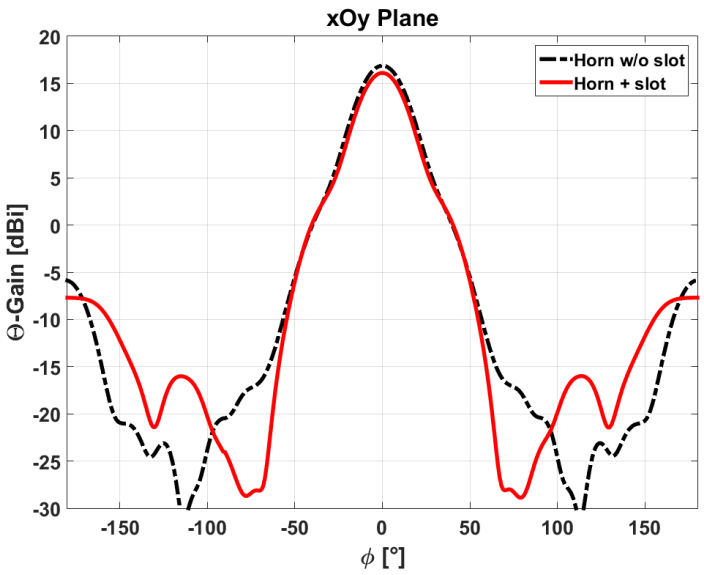

(b)

Figure 2. 10: Horn radiation patterns: at 9.5 GHz (a) in XOZ plane, (b) XOY plane

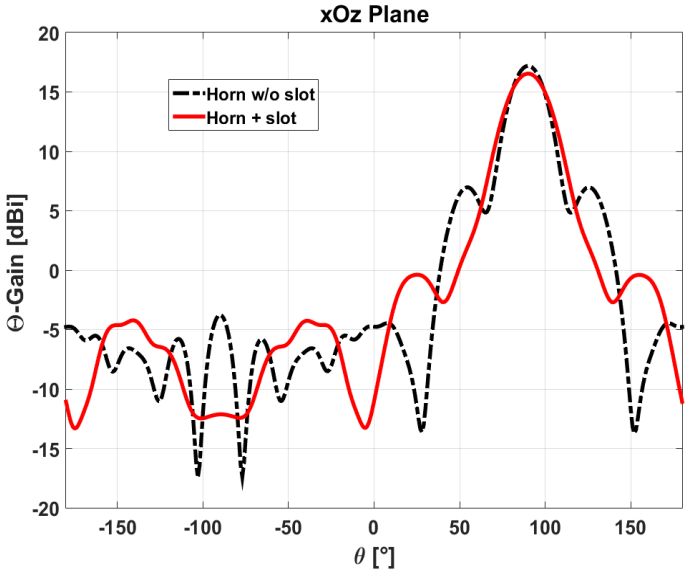

(a)

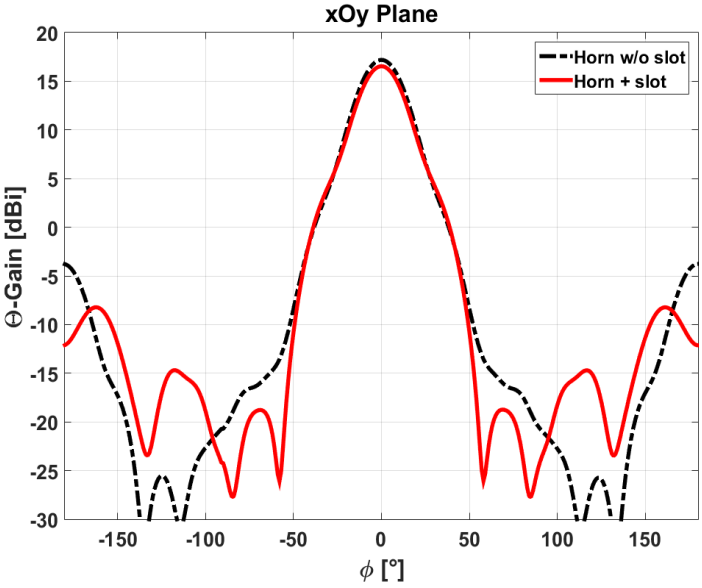

(b)

Figure 2. 11: Horn radiation patterns at 10 GHz: (a) in XOZ plane and (b) XOY plane

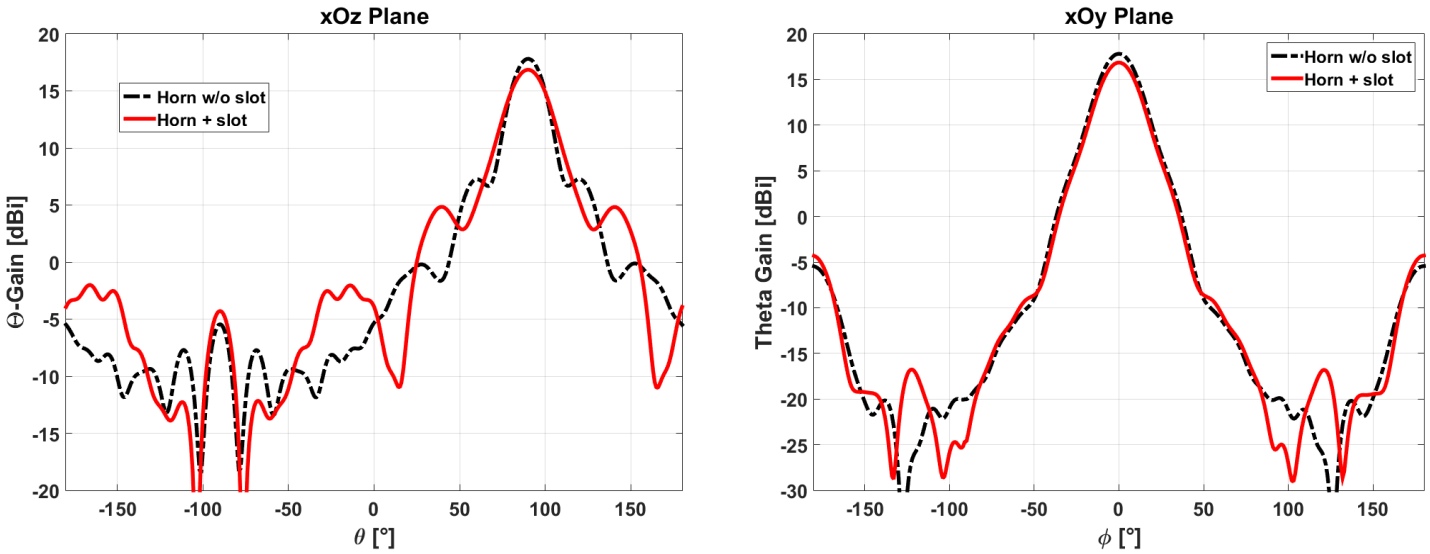

(a) (b)

Figure 2. 12: Horn radiation patterns at 11.5 GHz: (a) in XOZ plane and (b) XOY plane

In the next section, we will try to dynamically control the SLL of the horn antenna. This is similar to what J. Euzière did in [11] with TMA.

2.2.3. Slot short circuit

In this section, the goal is to dynamically control the horn SLL through the slot etched in the horn to transmit information as in [11]. The slot will then act as a controllable element. To do so, a switching mechanism as the one presented in [12], consisting of diodes connected to slots will be considered to control the slot. In a first step, to simplify the study, the slots will be short-circuited using a metal ribbon in the middle of the slots (cf. Figure 2.13), as an intermediate step before the use of conventional switching mechanisms. Thus, the impact of the metallic ribbon on the horn radiation will be investigated. For this study, previous structure of the horn antenna will be considered.

The results obtained by short-circuiting the slot using metallic ribbon are shown in Figure 2.14. For comparison purposes the gain of the horn without slot is also given. As can be seen from this figure, the SLL is the same with and without the metal ribbon. Indeed, given the large dimensions of the slot (L = 50 mm and l = 10 mm), the short-circuit has no effect on it and it is therefore impossible to recover the initial state of the horn radiation pattern (without slot). Consequently, the SLL cannot be controlled dynamically with a single metal ribbon. Indeed, it would be necessary to use several metallic ribbons to switch off the large slot. However, the objective being to replace the metallic ribbons with diodes, this could introduce several parasitic elements that will disrupt the horn radiation. In addition, the use of several diodes could complicate the design of the antenna. In order to simplify the design and limit the parasitic elements, it is therefore preferable to move towards simple solutions such as slotted waveguide [12] [13] [14] [15].

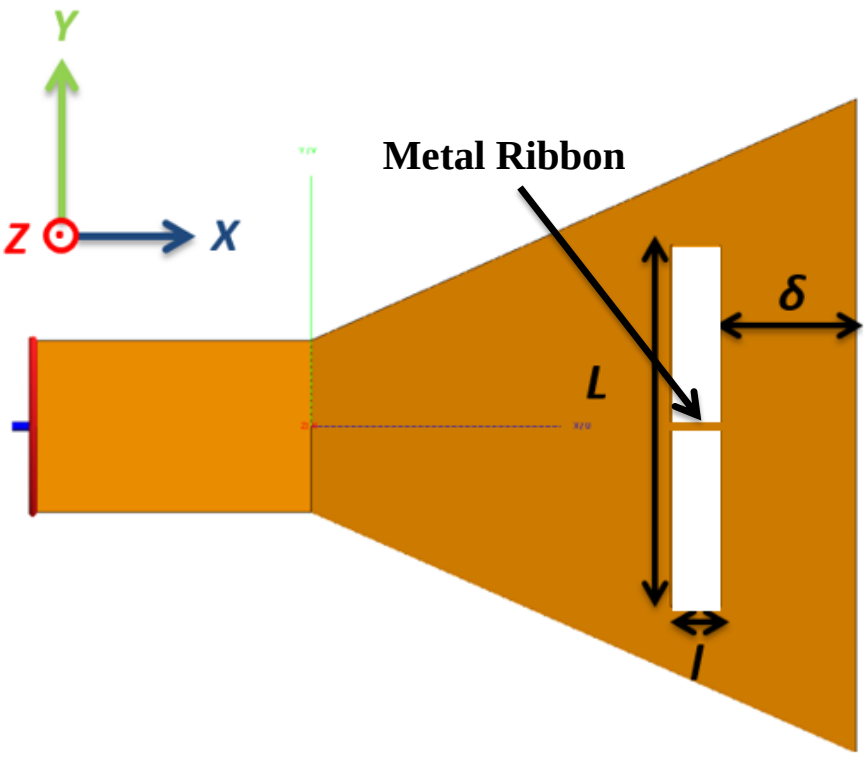

Figure 2. 13: Slot short-circuited by metallic ribbon

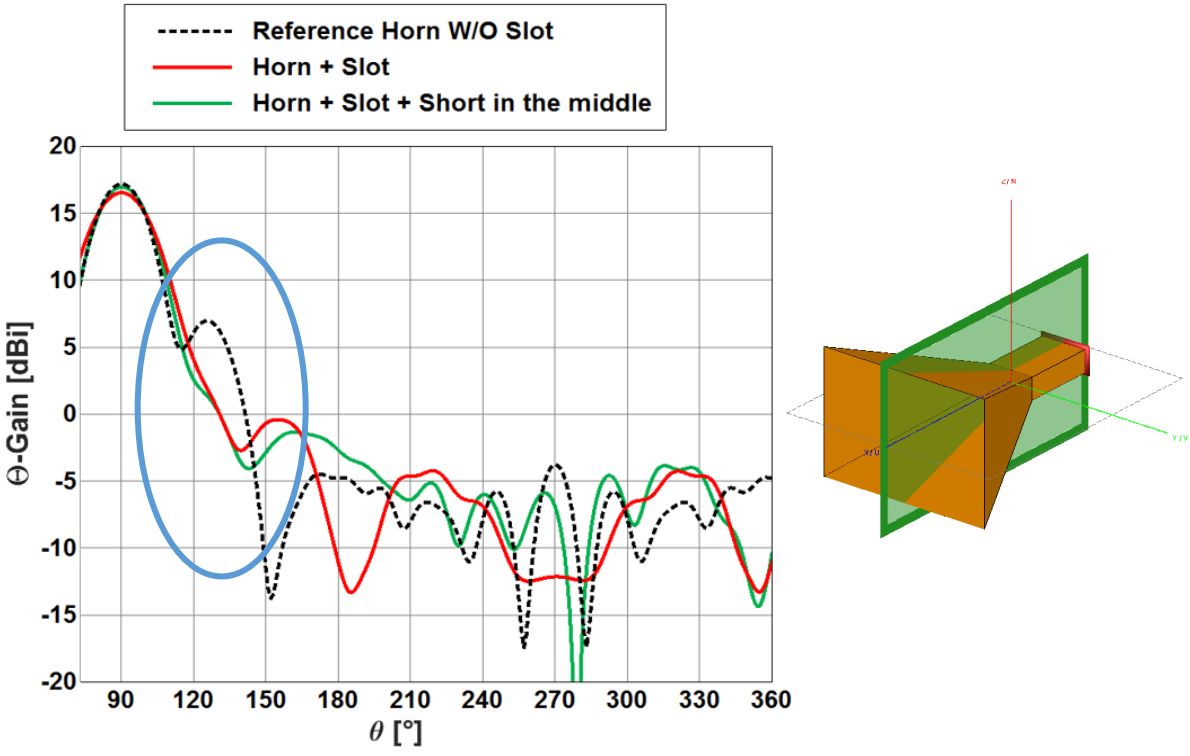

Figure 2. 14: Effect of metal ribbon on the SLL

2.2.4. Conclusion

In the previous parts, we have seen that the slots placed close to the horn aperture (δ = 10.8 mm) allow to reduce the SLL (at least 4 dB) from 8.3 GHz to 10.2 GHz in comparison to a standard horn without slot. This solution using wide slots, simple to implement and inexpensive is an alternative to corrugated horns for SLL reduction. However, due to their large size (L = 50 mm, l = 10 mm) it is impossible to dynamically control the SLL by using conventional switching mechanism.
To address this issue, we then investigate in the next section the possibility to etch slots in the feeding waveguide and to control them using the switching mechanism presented in [12].

2.3. Slotted waveguide (Travelling wave mode)

It is proposed in this section to study the possibility to etch slots in the feeding waveguide and to control their radiation for the multifunction purposes. Indeed, the slot antenna is very popular because it can be etched on whatever surface and have an omnidirectional radiation patterns and linear polarization. Adjusting the slot dimensions (size and shape) offers several degrees of freedom to control the resonant frequency, the bandwidth and the cross-polarization.
As a first step, to simplify the study of the slotted waveguide, we replace the horn by a matched load to ensure a travelling wave mode. Taking into account the frequency range of the available measurement chamber (800 MHz - 6 GHz), in this section, the study will be done at 5 GHz.

2.3.1. General overview

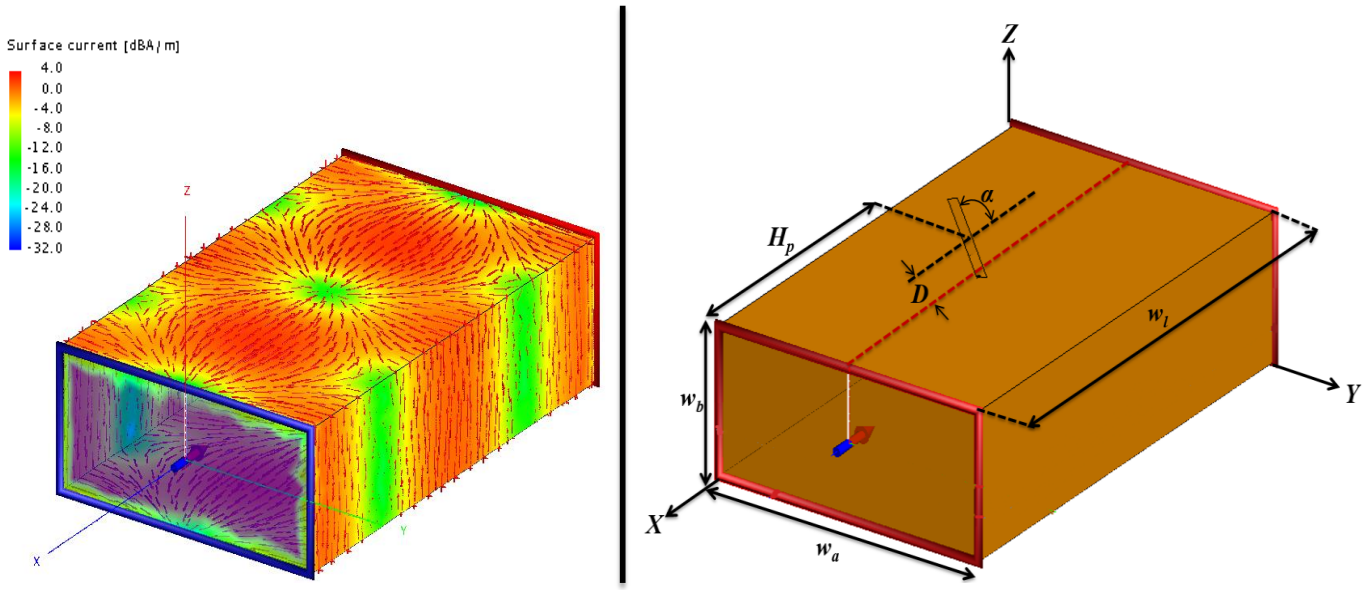

(a) (b)

Figure 2. 15: (a) Current distribution in the waveguide and (b) slot configuration in the waveguide (w_a = 47.55 mm, w_b = 22.15 mm, w_l = 77.2 mm, H_p = 38.6 mm)

Slot arrays on waveguide are commonly used for radar, navigation and many other applications operating at high frequencies. This is due in part to its simplicity of design, low losses and also the advantages in terms of weight, volume and radiation characteristics [13] [14] [15]. The slots are placed in the waveguide (either on the broad or narrow walls) to couple the fields in the waveguide to have a desired radiated field (amplitude and phase). For that reason, it is important to see how the slots affect the field distribution in the waveguide. Figure 2.15 (a) and Figure 2.15 (b) present respectively the current distribution of the rectangular waveguide ended by a matched load (simulating the horn) and a basic geometry of a slotted waveguide antenna. In Figure 14 (b) are presented the slot parameters used for the study. The dominant mode for a rectangular waveguide is the TE10 mode. In our case, using the geometry of Figure 2.15 (b), it is defined so that the broad wall of the waveguide (w_a) is along y-axis and the narrow wall (w_b) along z-axis, which gives us the following cut-off frequency:

$$f_{c_{mn}} = \frac{c}{2}\sqrt{\left(\frac{m}{w_a}\right)^2 + \left(\frac{n}{w_b}\right)^2}$$

The fields that propagate in the waveguide are given by [6]:

$$H_x = \frac{jE_0}{2w_a f\mu}\cos\left(\frac{\pi y}{w_a}\right)e^{-j\beta x} \quad (1)$$

$$H_y = \frac{-E_0}{2\pi f\mu}\sqrt{k^2 - \left(\frac{\pi}{w_a}\right)^2}\sin\left(\frac{\pi y}{w_a}\right)e^{-j\beta x} \quad (2)$$

$$E_z = E_0 \sin(\frac{\pi y}{w_a})e^{-j\beta x} \quad (3)$$

Also, on the top wall of the waveguide, where the slots are located, the induced currents ($\boldsymbol{j} = \hat{\boldsymbol{n}}\,\mathbf{X}\,\boldsymbol{H}$) are given by:

$$J_x = \frac{-E_0}{2\pi f\mu}\sqrt{k^2 - \left(\frac{\pi}{w_a}\right)^2}\sin(\frac{\pi y}{w_a})e^{-j\beta x} \quad (4)$$

$$J_y = -\frac{jE_0}{2w_a f\mu}\cos\left(\frac{\pi y}{w_a}\right)e^{-j\beta x} \quad (5)$$

2.3.2. Slots in waveguide broad wall

In Figure 2.16 are depicted the impact of slots position on the current distribution in the waveguide. A longitudinal slot (along x-axis) on the waveguide broad wall, placed at the center of the waveguide ($w_a/2$) does not disturb the current flowing on the waveguide (Figure 2.16 (a)). Since the slot is thin, the current along the x-axis is slightly perturbed. In this case, only the current along the y-axis is responsible for radiation. If we have a look to the analytical expression of this current on the waveguide for a constant z (5), it is clear that the current density in the y direction becomes zero at $y = w_a/2$ position. Such a slot orientation, on the waveguide, does not produce any radiation. However, by moving the slot in the y direction, the y directed current will not be zero causing a disruption of the current in the waveguide and then resulting in a radiation of the slot (Figure 2.16 (c) shows the slot at D = 12.5 mm). Then, increasing D increases the power radiated by the slot.

On the other hand, rotating the slot to α = 30° for example while keeping the slot to the center of the waveguide as shown in Figure 2.16 (b) disrupts the current flow and causes radiation. For α = 90°, (a transversal slot in the waveguide) as shown in Figure 2.16 (d), the slot will only disturb the *x* component of the current for the same reason than before that the slot is thin. This slot will then radiate. Then, the power radiated by the slot is a function of α. In the latter two cases, the possibility to displace the slot away from the waveguide centerline provides an additional degree of freedom to control the power radiated by the slot.

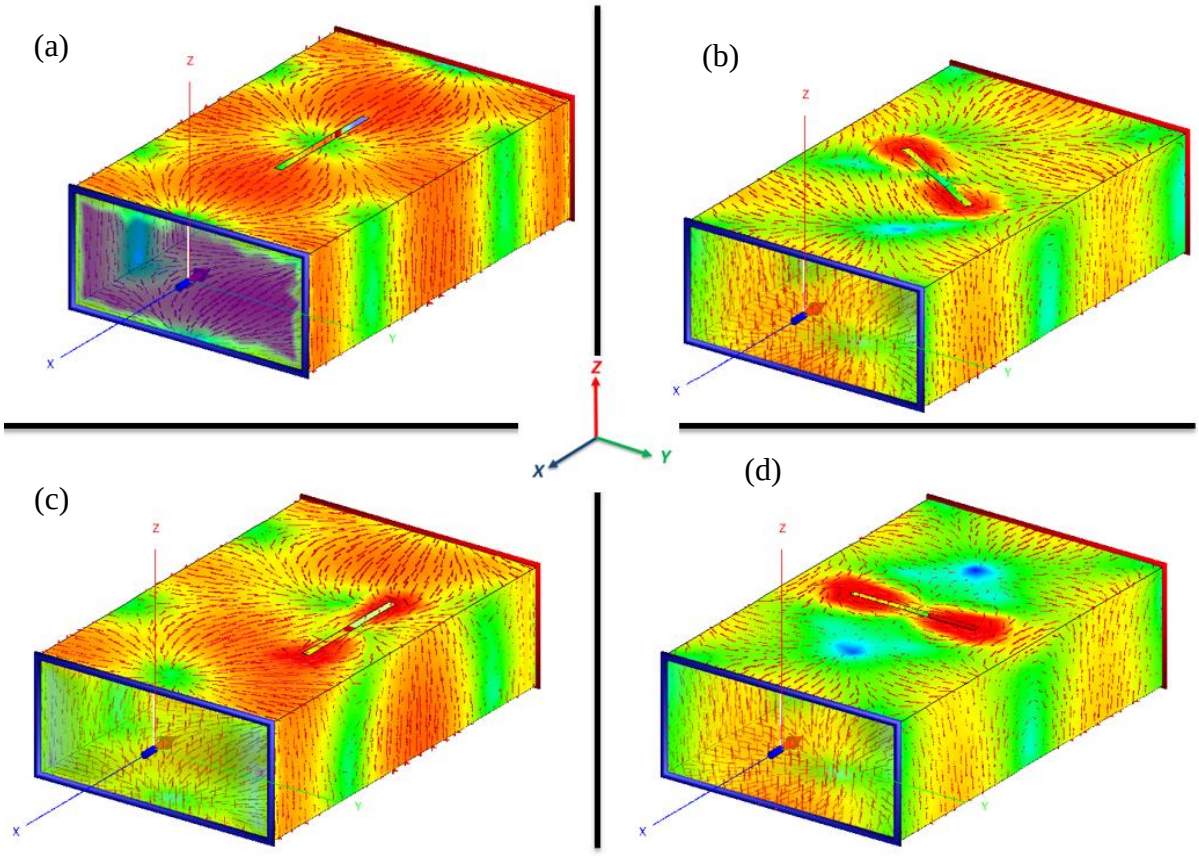

Figure 2. 16: Impact of the slot on current flowing in the waveguide

By the same way, slots can also interrupt the currents flowing on the narrow wall of the waveguide, but these cases will not be studied here.

By analyzing the E-field distribution in each of the cases presented in Figure 2.16, one can observe that the slots are either linearly polarized along *x*-axis (cf. Figure 2.16 (d)), *y*-axis (cf. Figure 2.16 (c)) or obliquely polarized (contribution of both *x* and *y* components, cf. Figure 2.16 (b)). Contrary to these results, the horn studied in the previous section 2.2 is linearly polarized along *z*-axis. This means that the horn and the slot in the feeding waveguide work in orthogonal polarization. This characteristic will be discussed in section 2.4.

2.3.2.1. Slot design in the waveguide

Slot's dimensions (length, position, inclination and width) control the electrical behavior in terms of radiation and bandwidth [6]. More precisely, the length L permits to set the operating frequency while the width l controls the slot bandwidth and the level of cross-polarization. The impedance of a slot is function of its displacement from the centerline (D) and its tilt (α). Furthermore, as shown in Figure 2.16, the power radiated by the slot can be controlled by adjusting these two parameters.

For this study, we will focus on the design of longitudinal slots along x-axis ($\alpha = 0°$) placed in the upper face of the waveguide (positive z-axis), cf. Figure 2.15 (b). The slot is located at $H_P = 38.6$ mm from the matched load. The considered waveguide has a length of $w_l = 77.2$ mm.

- **Slot length *L***

In order to find the resonant length of the slot at 5 GHz, a parametric study is necessary. Figure 2.17 presents the slot radiation (ϕ-gain) versus frequency for $L = 25.3$ mm, $l = 1.5$ mm and positioned at $D = 12.5$ mm from the waveguide centerline. As can be seen from this figure, the peak gain is obtained at 5 GHz. We recall that this gain (0 dB) is the result of a non-directive radiating element (a single slot) placed at $D = 12.5$ mm along a waveguide terminated by matched load. On the other hand, this gain drops when moving in frequency. The -3 dB gain bandwidth of this slot is 664 MHz.
In the present case, the slot length L is inferior to $\lambda_0/2$ because of the readjustment taking into account the offset D.
L is set to 25.3 mm for the remainder of the study.

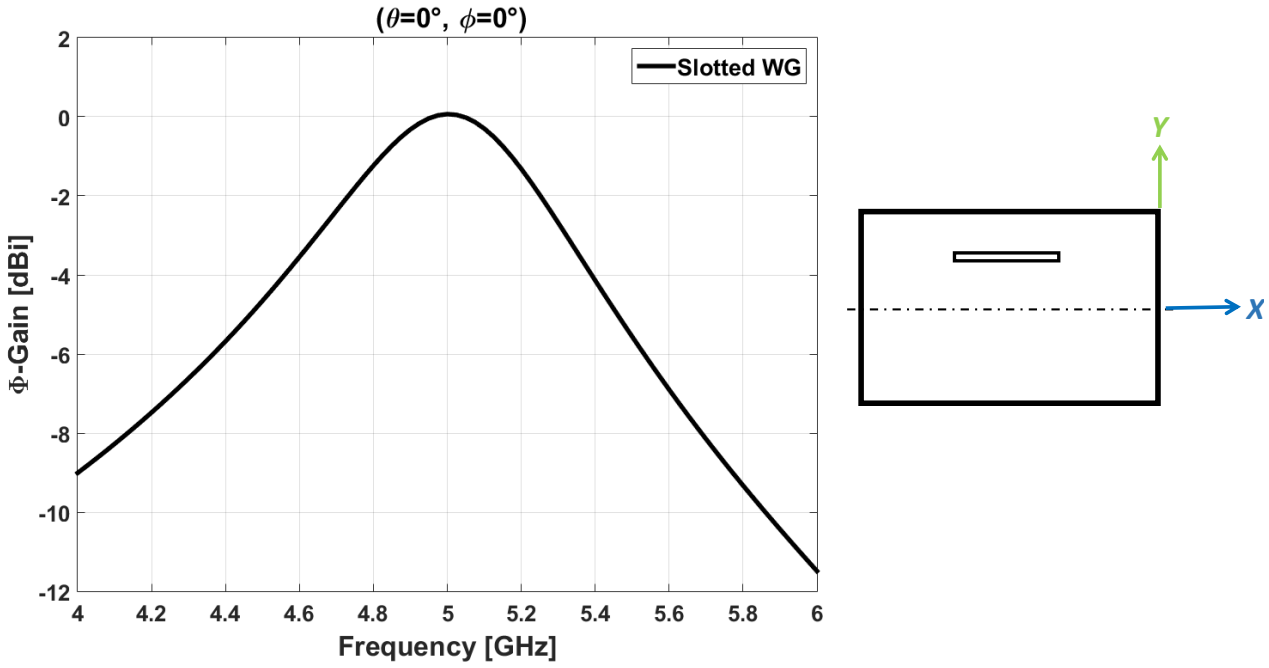

Figure 2. 17: Slot radiation (ϕ-gain) versus frequency at ($\theta = 0°$, $\phi = 0°$)

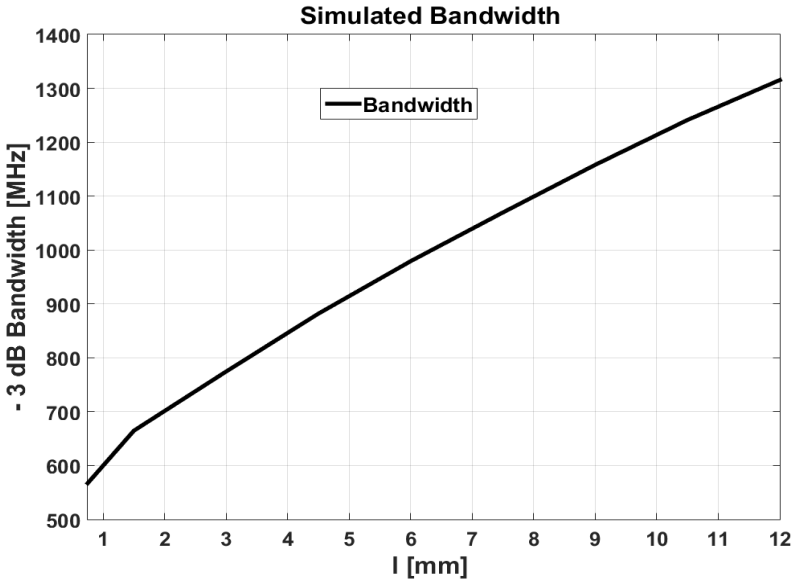

Figure 2. 18: The -3dB bandwidth at 5 GHz of the slot of length L = 25.3 mm

- **Slot width *l***

As with the dipole antenna, increasing the slot width increases the slot bandwidth. Many others techniques using complex slot shapes to increase the bandwidth are used [16], but as mentioned in section 2.1, the study will be limited to rectangular slots because they are simple to implement.

The slot -3dB bandwidth at 5 GHz is shown in Figure 2.18 as a function of the width *l*. As expected the bandwidth increases with the slot width and reaches up to 1.3 GHz for *l* = 12 mm.
It is also important to note that the expense of a very wide slot is a higher level of cross-polarization.

The objective being subsequently to use this waveguide to feed the horn antenna, as already explained the slot will act as a parasitic element to control the horn radiation pattern. Thus, as in the section 2.2, it will be necessary to switch off the slot. However, the results of section 2.2.3 have shown that it is difficult to short-circuit a large slot. We are then limited in our case to technological constraints.

This time, we investigate the possibility to short-circuit the slot in the waveguide. As a first step, we will try to switch off the slot by using a metallic strip of width *w* = 2 mm in the middle of the slot, cf. Figure 2.19. As can be seen from this figure, the gain difference between a radiating slot (slot ON) and a short-circuited slot (slot OFF) decreases with the slot width. At 1.5 mm the difference reaches 20 dB.

The overall results show that the slot width *l* has to be defined as a trade-off between the desired bandwidth and finally the technology to be used to dynamically control the slot. For all these reasons, the remainder of the study is done by considering slots of width *l* = 1.5 mm in order to maximize the impact of the short-circuit.

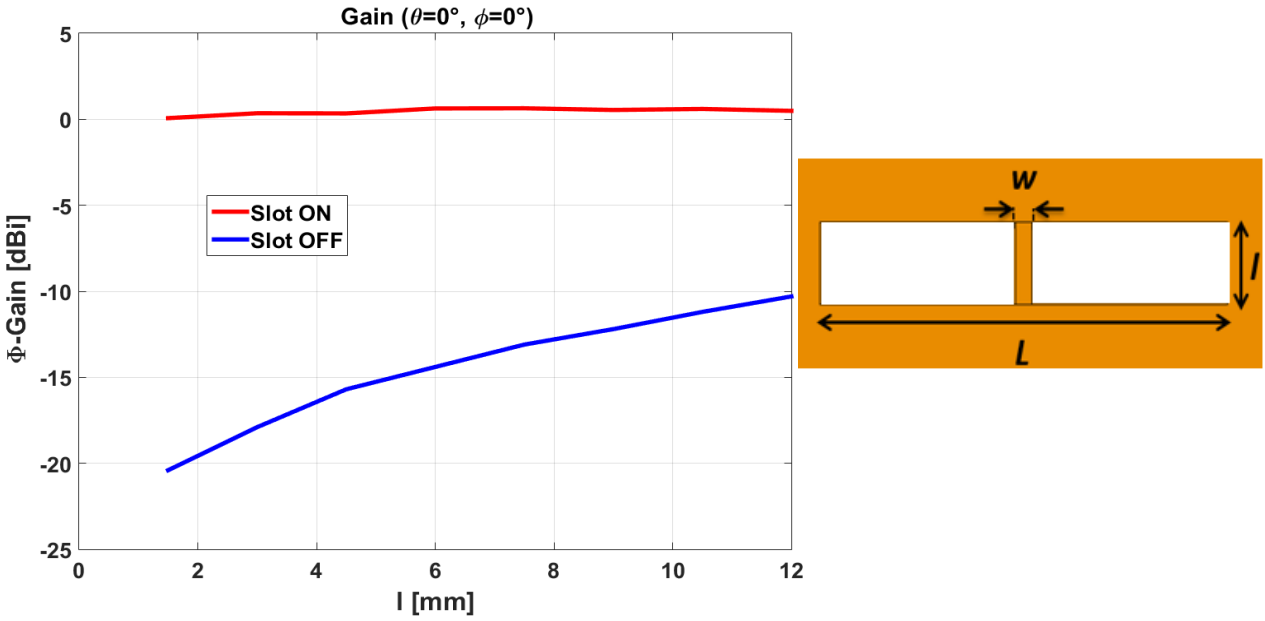

Figure 2. 19: Slot radiation with and without metal strip at 5 GHz versus the width l

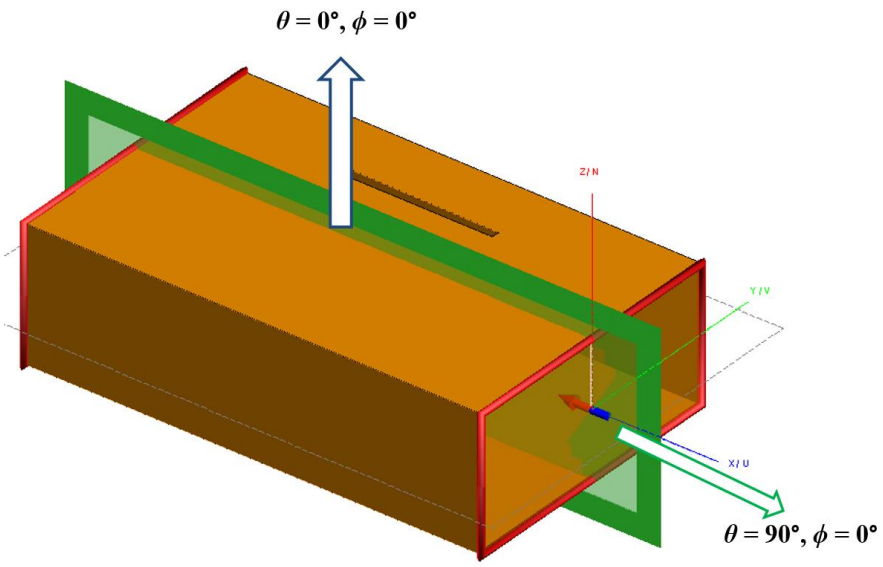

Figure 2. 20: Two directions of interest

- **Slot offset *D***

To control the power radiated by the slot, it is important to study the impact of the parameter *D* (slot offset). The ultimate goal being to use the slot to transmit information, without disturbing the horn radiation (dedicated to the radar function), two main directions will be considered for this study: the slot radiation direction (θ = 0°, ϕ = 0°) and the main direction of the horn (θ = 90°, ϕ = 0°), cf. Figure 2.20. As already explained, the longitudinal slot along *x*-axis is linearly polarized

along *y*-axis whereas the horn is linearly polarized along *z* axis. Hence, the slot contribution will be analyzed through ϕ-gain while the horn contribution will be analyzed through θ-gain. We recall that in the present case, to simply the study, the horn is replaced by a matched load.

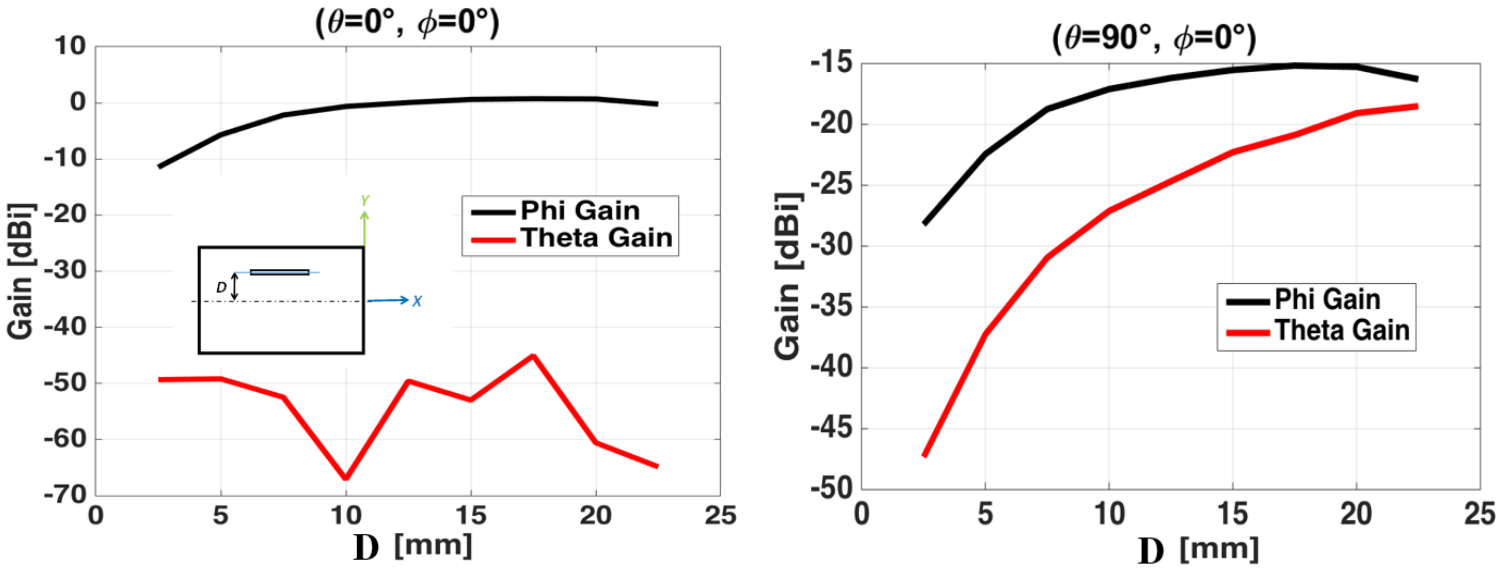

(a) (b)

Figure 2. 21: Gains versus the offset D at 5 GHz: (a) at (θ = 0°, ϕ = 0°) and (b) at (θ = 90°, ϕ = 0°)

We now analysis the results obtained by varying the parameter *D*. Figure 2.21 presents the gains in the two directions versus the offset *D*. As expected, at (θ = 0°, ϕ = 0°), the ϕ-gain increases with the offset, but from 15 mm the level becomes constant due to edge effects (slot near the waveguide extremity). Moreover, θ-gain is 48 dB below ϕ-gain in the worst case (*D* = 2.5 mm) because the slot is polarized along *y*-axis. This ensures that the slot does not disturb θ-component in this direction.
For (θ = 90°; ϕ = 0°), both θ and ϕ gains increase with the offset, but the levels are below -15 dBi. Unlike the previous case, the slot affects θ-component. However, the gain levels of the two components are low compared to a standard horn (17.23 dBi at 5 GHz). Hence, the impact of this result on the final application will be studied in section 2.4.

All these results show that increasing the offset *D* increases the total radiated power but, depending on the direction either θ or ϕ gain increases, offering possibilities for the final application as will be seen in the section 2.4.

2.3.3. Conclusion

In this part, we have seen how to design a longitudinal slot in a waveguide. By adjusting the parameters *L*, *1* and *D*, it is possible to fix respectively the resonance frequency, the bandwidth and the power radiated by the slot. Unlike section 2.2, the slots used in the waveguide are of standard size, thus making it possible to short-circuit them in the middle by using a metallic strip. Moreover,

by wisely orienting the slot in the waveguide, it is possible to generate radiation with orthogonal polarization to that of the horn offering added freedom degree for the multifunction antenna.

In the next section, we propose to feed the horn antenna by using the previous slotted waveguide, and thus draw conclusions of this feeding technique.

2.4. The multifunction antenna

After replacing the horn by a matched load, this time it is proposed to study the real case of the waveguide feeding the horn for the multifunction antenna purposes.

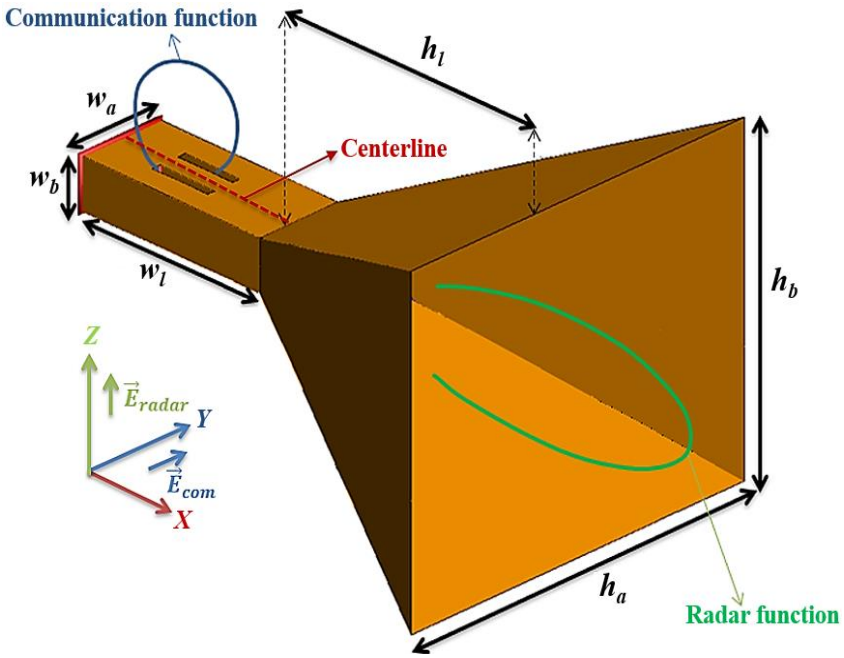

Figure 2. 22: Horn antenna fed by slotted waveguide (WR 187): w_a = 47.55 mm, w_b = 22.15 mm, w_l = 77.2 mm, h_l = 151.34 mm, h_a = 180.95 mm, h_b = 125.81 mm, H_p = 38.6 mm

2.4.1. Antenna system

We recall that for the radar function, the system is composed of a horn antenna fed through a single waveguide port and radiating a directive beam in the *x*-direction cf. Figure 2.22. The principle of the proposed system is to pick up a small amount of the propagating power in the feeding waveguide before it is radiated by the horn and to use it to transmit information. Note that this additional communication feature should not disturb the radar operation, which means the main lobe of the horn must not be modified except a small gain drop in the main direction of the horn, proportional to the picked-up energy for the communication. In the meantime, the antenna system should be as simple as possible so that the overall complexity does not increase.
To do so, a couple of slots is milled in the top face of the feeding waveguide. By using a switching mechanism to activate one of the slots at a given time, a fraction of the power in the feeding

waveguide is then radiated through the activated slot thus providing a communication link in the z-direction. As we will see later, BPSK direct modulation can be achieved thanks to this switching mechanism.

2.4.2. Antenna design

We consider a standard horn antenna operating at 5 GHz and radiating directive beam with linear z-polarization at (θ = 90°; ϕ = 0°), well-suited for a high-gain radar application (cf. Figure 2.22). Two identical slots are milled in the upper wall of the feeding waveguide with the objective to radiate a fraction of the incident power in (θ = 0°; ϕ = 0°) direction. This leakage mechanism aims at creating a communication link in addition to the main radar function. As the slots are longitudinal to the waveguide axis, the associated radiated field is *y*-polarized (cf. section 2.3.2), which means radar and communication functions involve both orthogonal polarizations and directions for enhanced isolation.

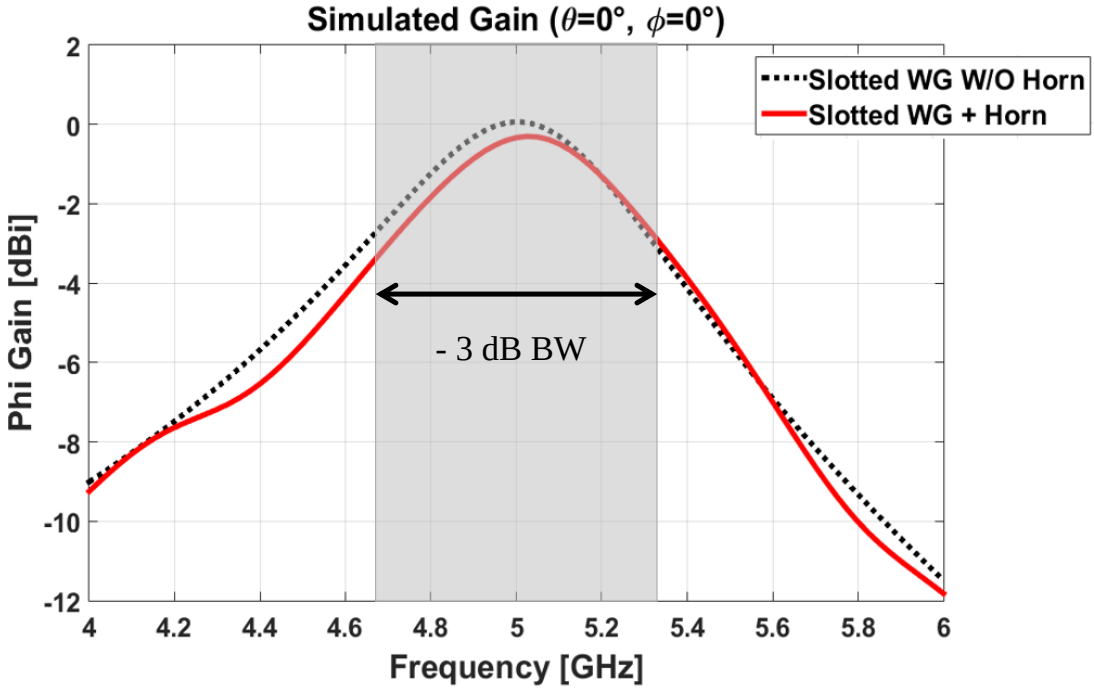

Figure 2. 23: Slot radiation versus frequency

2.4.2.1. Slot design

To take into account the effect of the horn antenna, the slot length was adjusted to be resonant at 5 GHz. Figure 2.23 shows the slot radiation (ϕ-gain) in (θ = 0°; ϕ = 0°) direction for L = 25.6 mm and l = 1.5 mm placed at D = 12.5 mm versus frequency in presence of the horn antenna. As can be seen from this figure, the maximum gain (-0.3 dBi) is obtained at 5 GHz. This gain is low because only one slot placed at D = 12.5 mm is used in waveguide. Then, the slot length is now L = 25.6 mm (instead of 25.3 mm, previously).

However, as can be seen in Figure 2.23, the gain level drops sharply when moving in frequency. For example, at 5.25 GHz it is -1.9 dBi (1.6 dB gain drop, compared to the peak gain), demonstrating that the slot is not broadband. The -3 dB bandwidth of this slot is about 681 MHz.

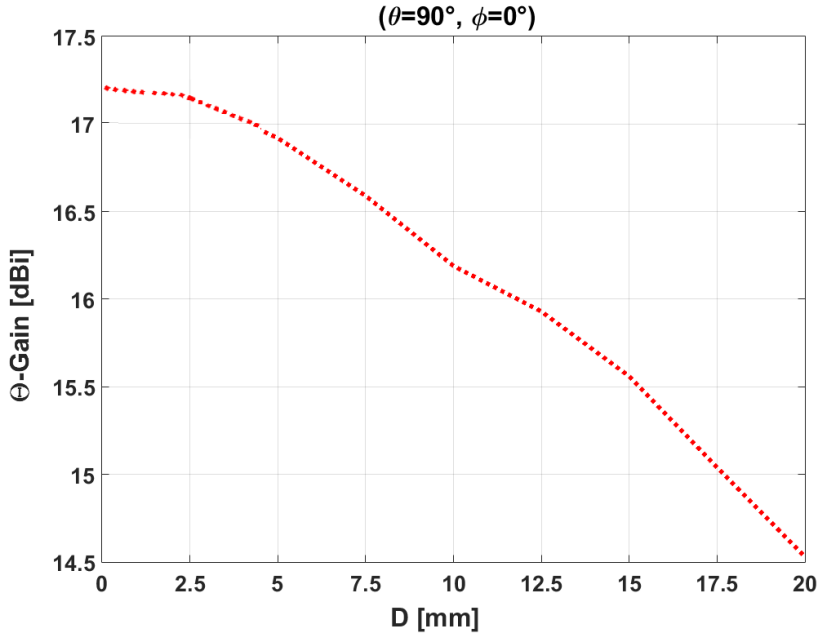

Figure 2. 24: Simulated Theta gain (radar function) versus offset D for one active slot (θ = 90°, ϕ = 0°, f =5 GHz)

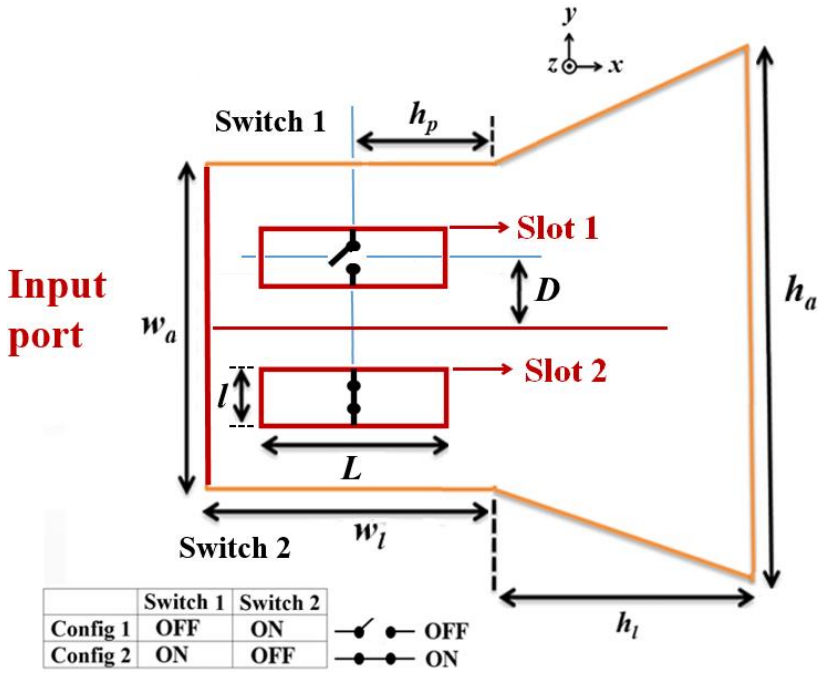

Figure 2. 25: Configurations of slots for the communication function (L = 25.6 mm, l = 1.5mm, D = 12.5 mm, h_p = 38.6 mm)

As mentioned in section 2.3.2.1, the offset *D*, is used to control the leakage from the slot and thus the amount of incident power devoted to the communication function. Subsequently, it also defines the associated loss for the radar function. As an illustration, Figure 2.24 depicts the decrease of the horn gain versus *D*. In practice, *D* has to be defined as a trade-off between radar loss and communication gain and thus depends on the target application. In the present design, *D* is arbitrary set to 12.5 mm, which corresponds to a 1.3 dB gain drop for the horn antenna.

2.4.2.2. BPSK direct modulation

In the present design, the communication function consists in a direct BPSK modulation of the *y*-polarized field in (θ = 0°; ϕ = 0°) direction. It is obtained by activating only one of the two slots. Indeed, as these slots are placed symmetrically with regards to the waveguide centerline, a 180° phase jump in the radiated field is achieved each time the activated slot is changed [6]. This defines two complementary configurations (cf. Figure 2.25). In configuration 1, only slot 1 radiates while slot 2 is closed. Configuration 2 corresponds to the reverse situation. At this stage, as mentioned in previous sections, we did not implement a real switching mechanism but the one presented in [12] could be used quite straightforwardly. For the sake of simplicity, only the activated slot is present in simulations (the other one being completely closed with PEC).

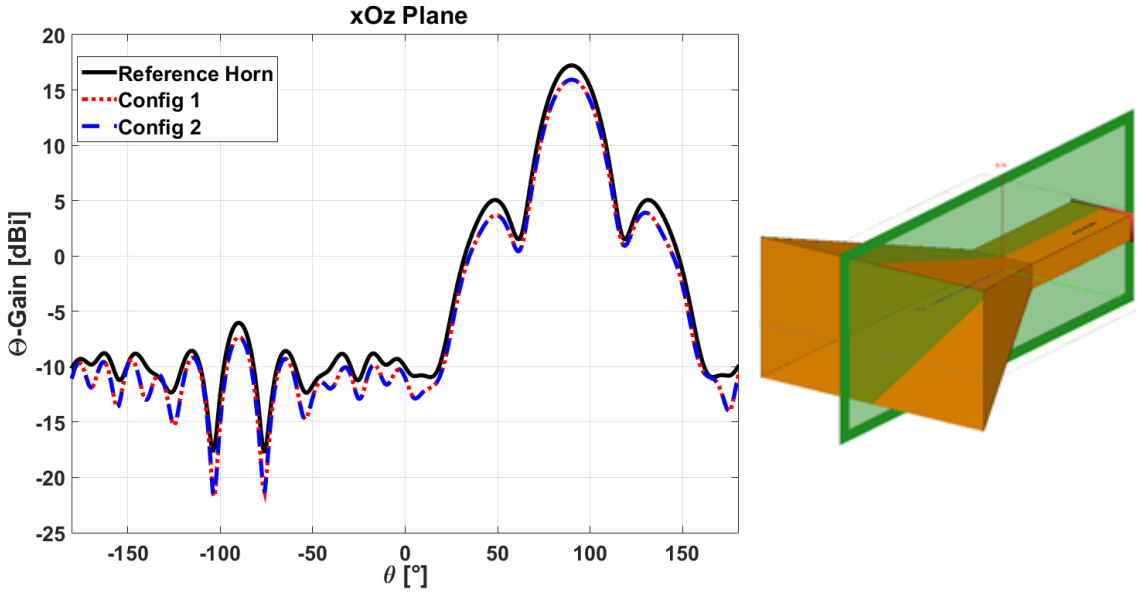

Figure 2. 26: Comparison of Simulated Theta Gains (radar function) in xOz plane at 5 GHz

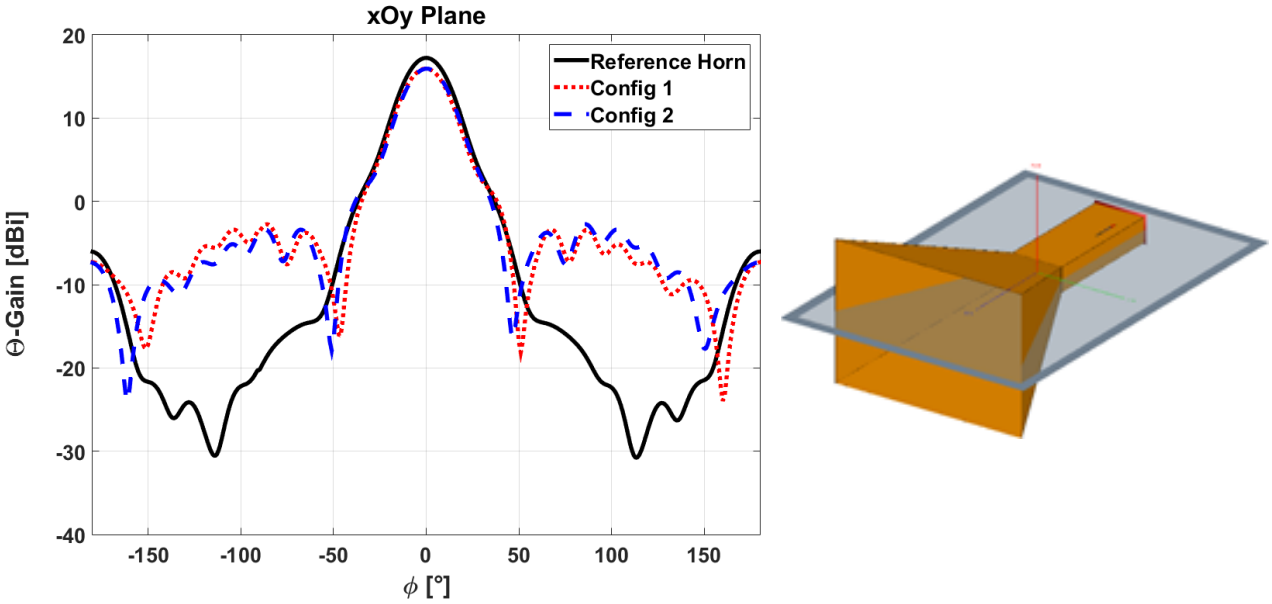

Figure 2. 27: Comparison of Simulated Theta Gains (radar function) in xOy plane at 5 GHz

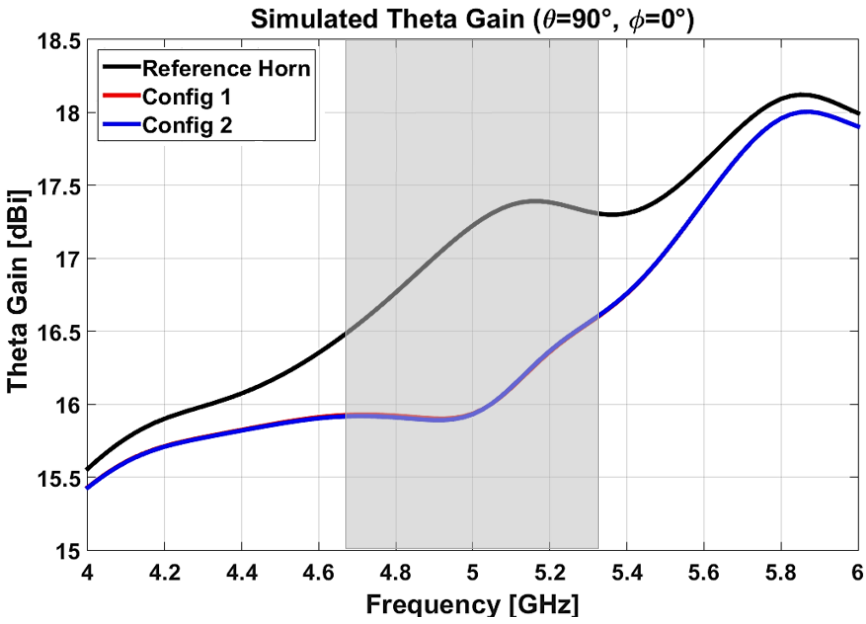

Figure 2. 28: Horn radiation in the main direction versus frequency

2.4.3. Antenna performances

2.4.3.1. The main radar function

In this part of the report, the simulated performance of the radar antenna (horn) is discussed. More precisely, the modification of the horn radiation due to the slots is investigated to make sure that the communication function does not disturb the radar one.

Figure 2.26 and Figure 2.27 present θ-gains in xOz and xOy plane respectively at 5 GHz for configurations 1 and configuration 2. For comparison purposes, the gain of the horn antenna without slots is also given.

In xOz plane, due to symmetry, both configurations 1 and 2 give exactly the same patterns, which guarantees the radar radiation is not affected when switching the slots. The maximum gain is 15.93 dBi at $\theta = 90°$. As already discussed in section 2.4.2.1, this is 1.3 dB less than for the horn antenna without any slot. Apart from this expected and controlled gain drop, the patterns are not disturbed compared to that of the reference antenna.

However, in xOy plane, the slots are responsible for an increase in side lobe level (in comparison to the horn without slot). Indeed, in these directions the slots contribute to *z*-polarization and then contribute to horn radiation. This characteristic will be a subject of an in-depth study in chapter 3. Nevertheless, SLL remains lower than -18.66 dB, which is acceptable for many radar applications. Moreover, this SLL could easily be reduced further by using a smaller offset *D* (nonetheless at the expanse of a lower power available for communication).

Figure 2.28 depicts θ-gain in the main directions of the horn versus frequency for the two configurations in comparison to that of the horn without slot. As expected, the slot activation on the waveguide causes a gain drop in the main direction of the horn. Indeed, at 4 GHz and 6 GHz the gain drop is low (0.1 dB) because at these frequencies the slot does not radiate and then the picked-up energy in the waveguide is negligible. However, at 5 GHz corresponding to the resonance frequency of the slot the gain drop is significant (1.3 dB).

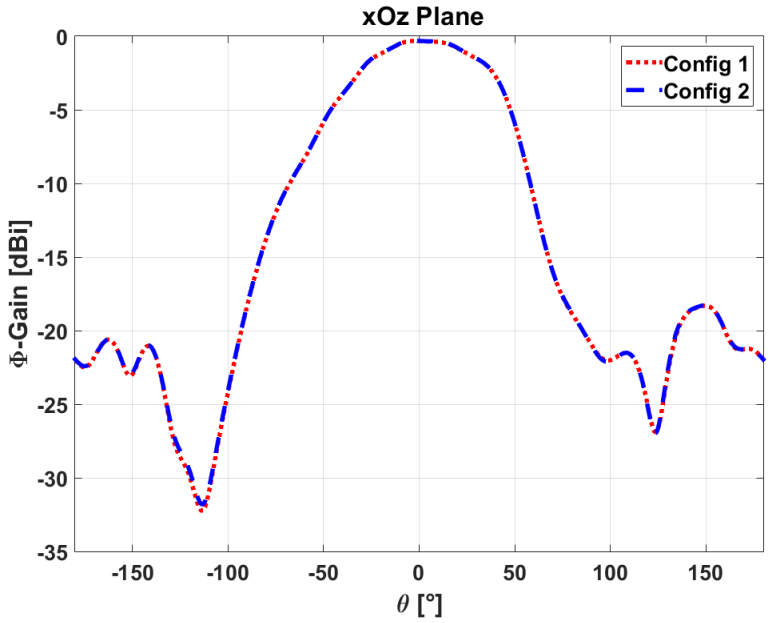

Figure 2. 29: Comparison of Simulated Phi Gains (communication function) in xOz plane at 5 GHz

2.4.3.2. Communication function

In this section, the performance of the communication antenna (slot) is analyzed.

Figure 2.29 presents the ϕ-gain in xOz plane for configurations 1 and 2. This radiation, with orthogonal polarization and direction compared to that in the previous section, corresponds to the communication function. As could be expected, the gain is identical for both configurations and the maximum gain is reached at $\theta = 0°$. As stated before, the quite low value (-0.3 dBi) results from both the use of a non-directive radiating element (a single slot) and the small amount of power dedicated to communication in this design. As already explained, a different trade-off could be used when selecting D in order to foster communication radiation. The number of longitudinal slots could also be increased to improve the associated directivity (cf. chapter 3) but also to steer the beam if needed [6].

Table I summarizes the characteristics obtained for BPSK communication at $\theta = 0°$.

Directions	Config	Phase (°)	Amp. (dBi)
$\theta = 0°$	1	0	-0.3
	2	180	-0.3

Table 1. 2: Direct BPSK modulation at 5 GHz

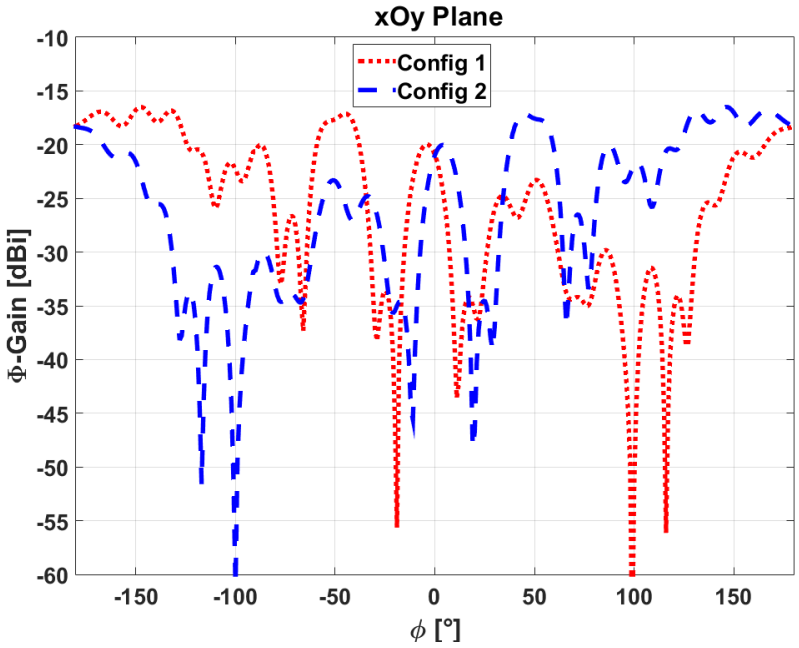

Figure 2. 30: Simulated Phi Gains (communication function) in xOz plane at 5 GHz

In xOy plane (cf. Figure 2.30), the ϕ-gain of the two configurations is low (below -16 dBi). Indeed, in this plane, as already explained, the slot contributes to the horn radiation but in the side lobes directions (cf. Figure 2.27).

Hence the direct BPSK modulated signal will be only transmitted in $\theta = 0°$ direction.

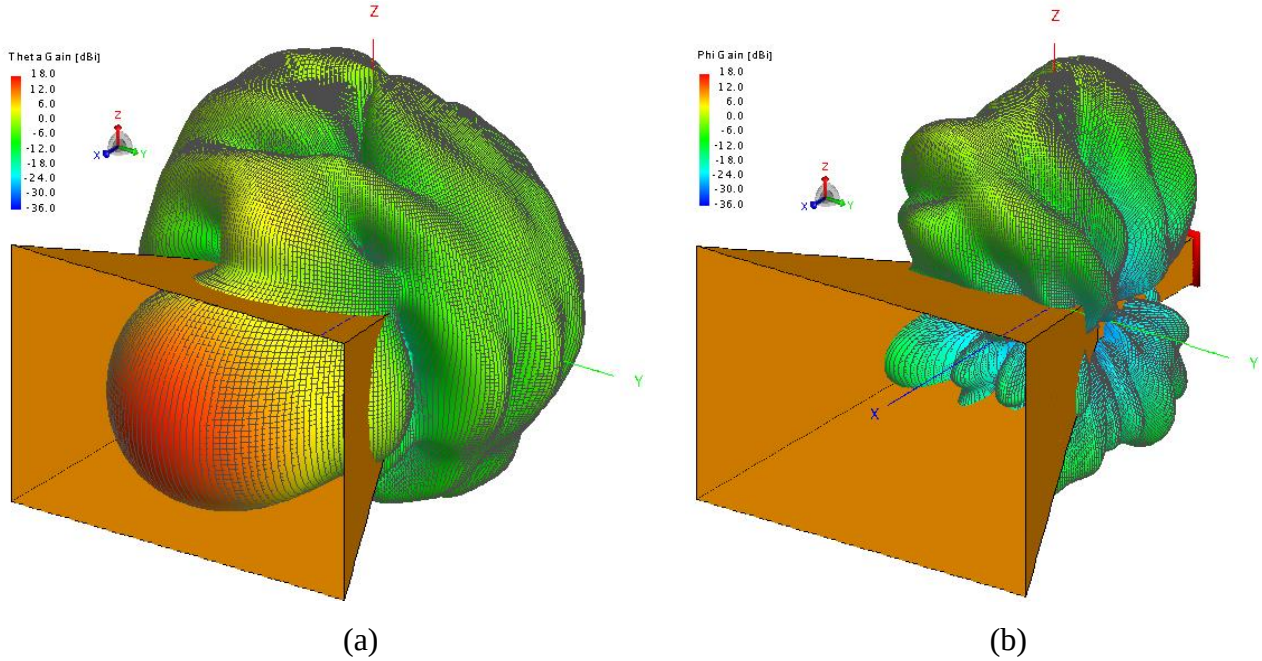

(a) (b)

Figure 2. 31: 3D radiation patterns of the multifunction antenna configuration 1 at 5 GHz (a) theta gain and (b) phi gain

Figure 2.31 depicts a 3D view of the radiated fields from both horn and slot antenna. As can be seen, θ-gain is more focused in the horn direction while ϕ-gain is focused at the slot broadside.

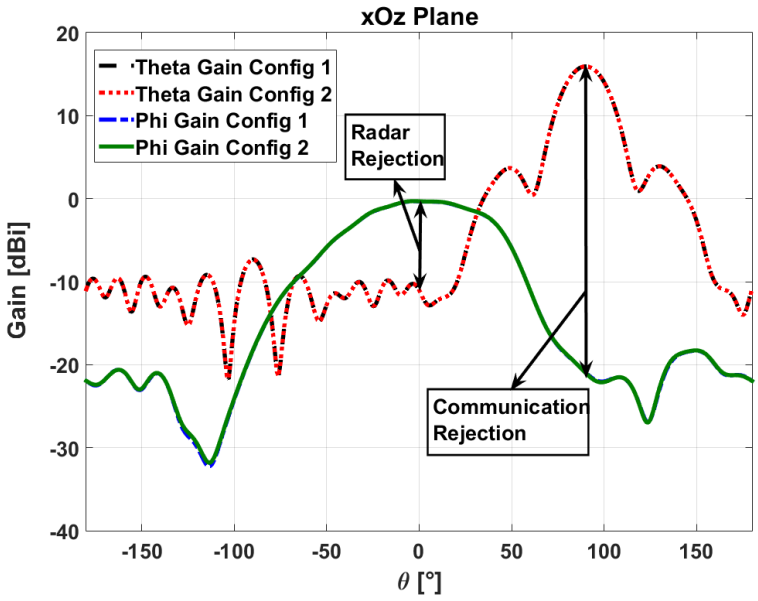

Figure 2. 32: Simulated Results of the Multifunction Antenna at 5 GHz in xOz plane

2.4.3.3. Study of radar and communications isolation

In this section, the radar and communication rejections are studied from 4 GHz to 6 GHz in order to evaluate the robustness of the proposed multifunction antenna system.

Figure 2.32 superimposes the θ and ϕ gains in xOz plane. It better highlights the achieved isolation between radar and communication functions. Two quantities can be defined to assess this isolation:

- The communication rejection corresponds to the rejection of ϕ polarization (due to communication function) in the radar direction ($\theta = 90°$, $\phi = 0°$).
- The radar rejection corresponds to the rejection of θ polarization (due to radar function) in the communication direction ($\theta = 0°$).

As can be observed, at 5 GHz, the radar rejection is 11 dB while the communication rejection is 37 dB. This confirms that the radar function is not disturbed by the added communication system while this last one could be used for moderate budget links.

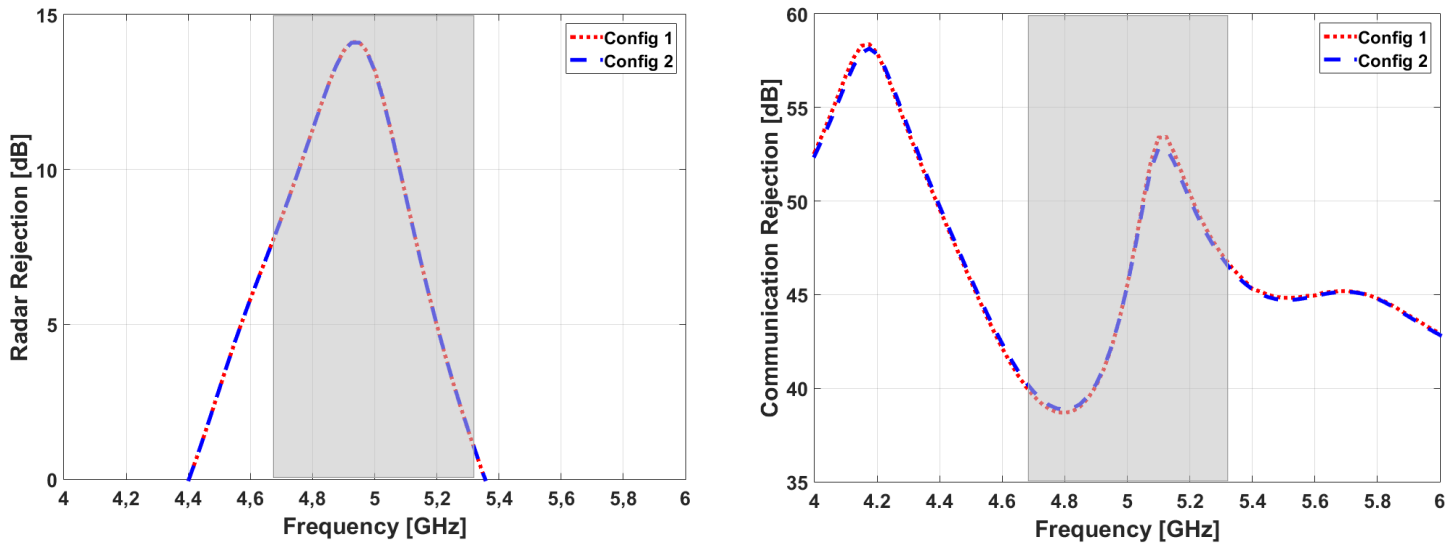

(a) (b)

Figure 2. 33: (a) radar rejection and (b) communication rejection versus frequency

Figure 2.33 (a) compares the simulated radar rejection of the two configurations versus frequency. It is 14.1 dB in the best case at 4.95 GHz. However, when going away from the center frequency, the value decreases, reducing the operating bandwidth. In order to ensure at least 10 dB of rejection, the antenna system bandwidth reduces to 325 MHz (instead of 681 MHz). This could be improved by using, for example a corrugated horn, which presents much lower side lobes than the standard horn or broadband slots.
Concerning the communication rejection ($\theta = 90°$, $\phi = 0°$), cf. Figure 2.33 (b), it is greater than 25 dB on the entire studied band, ensuring the isolation of radar and communication functions in this direction.

The reflection coefficients of the antenna system are depict in Figure 2.34 and are below -14 dB from 4 to 6 GHz.

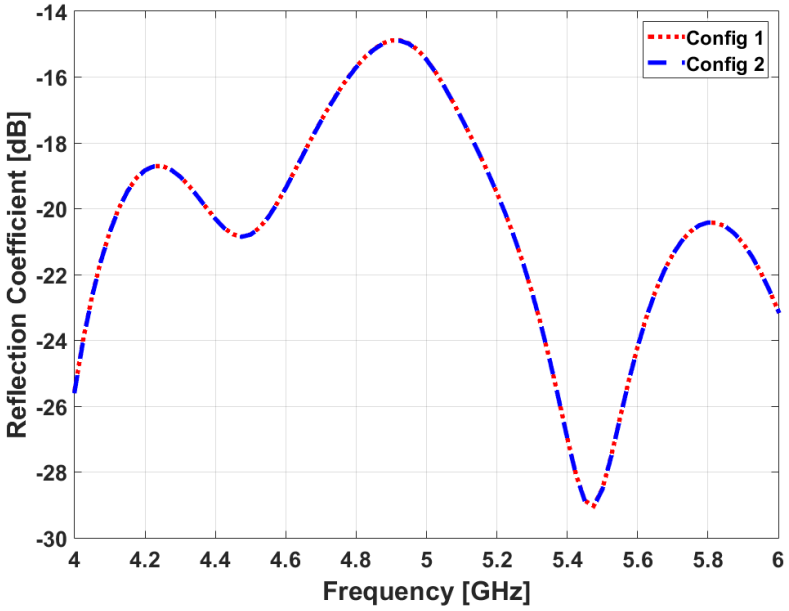

Figure 2. 34: Reflection coefficient

2.5. Conclusion of chapter 2

In this chapter we have seen that by etching slots of large size close to the horn aperture we are able to reduce the side lobes of a standard horn by 7 dB at 10 GHz. With this technique it is impossible to control the side lobes by using a switching mechanism. Nevertheless, this solution, simple to implement and inexpensive is an alternative to corrugated horn.

A solution to realize a multifunction antenna providing simultaneously a radar and communication functions by using a horn antenna and slot as a controllable element has been studied. The system is composed of a horn antenna for radar purposes and a slotted waveguide for communication function. The system is designed so that the slots do not affect the operation of the main radar function. The slot picks up 1.3 dB of the radar gain to provide the communication link. This gain value can be controled by adjusting the slot offset. By using orthogonal polarizations and directions, the two functions operate simultaneously and do not interfere. At 5 GHz, the radar rejection is 11 dB in the communication direction and the communication rejection is $\geq$ 25 dB in the radar direction. A direct BPSK modulation is achieved by switching between the two slots on the waveguide. The antenna system is capable to work over 325 MHz bandwidth while ensuring at least a rejection of 10 dB.

This initial solution does not offer many degrees of freedom for the communication function, because one can only communicate in one direction. In the next chapter, the possibility to transmit communication in several directions will be studied as well as the possibility to use another type of modulation such as QPSK.

[1] Y. J. Ren and C. P. Lai, “Wideband Antennas for Modern Radar,” Advanced A&M Technologies, Inc. USA, 2010.

[2] X. Yan, Y. Fang and Z. Lu, “Design of a Broadband Ku-Band Lens Horn Antenna for SAR Applications,” in Proc. 3rd Asia-Pacific Conference on Antennas and Propagation, Harbin, China, jul. 16-29, 2014.

[3] A. Kuriyama, H. Nagaishi, H. Kuroda and K. Takano, “A High Efficiency Antenna with Horn and Lens for 77 GHz Aytomotive Long Range Radar,” in Proc. 46th EuMC, London, England, Oct. 3-7, 2016.

[4] N. Smitha, S. Vipula and S. N. Sridhara, “Pyramidal Horn Antenna for Ground Penetrating Radar Application,” in Proc. IEEE Annual India Conference, Bangalore, India, Dec. 16-18, 2016.

[5] X. Wan, L. Zhang, S. L. Jia, J. Y. Yin, and T. J. Cui, “Horn Antenna with Reconfigurable Beam-Refraction and Polarization Based on Anisotropic Huygens Metasurface,” IEEE Trans. Antennas Propag., vol. 65, no. 9, pp. 4427-4434, Sep. 2017.

[6] Robert E. Collin, “Aperture-Type Antenna,” in Antennas and Radiowave Propagation, USA: McGraw-Hill.

[7] R. E. Lawrie and L. P. Jr, “Corrugated horn antenna,” U. S. patent 3 631502, Oct. 21, 1965.

[8] C. Granet and G. L. James, “Design of Corrugated Horns: A Primer,” IEE Antennas and Propagation Magazine, Vol. 47, No. 2, April 2005.

[9] X. Chen and Y. Ge, “Enhancing the Radiation Performance of a Pyramidal Horn Antenna by Loading a Subwavelength Metasurface,” IEEE Acces, Sep. 2017.

[10] S. Shahcheraghi and A. Yahaghi, “Design of a pyramidal horn antenna with low E-plane sidelobes using transformation optics,” Progress in Electromagnetics Research M, vol. 44, pp.109-118, Oct.2015.

[11] J. Euziere, R. Guinvarc’h, R. Gillard and B. Uguen, “Optimization of Sparse Time-Modulated Array by Genetic Algorithm for Radar Applications,” IEEE Antennas and Wireless Propagation letters, vol.13, 2014, pp 161-164.

[12] H. Kubo, M. Takamatsu, T. Yamamoto and A. Sanada, “Waveguide-Type Discrete Beam-Scan Antenna with Switching Diodes,” in Proc. EuMC, Paris, France, Sept. 7-10, 2015, pp. 1479-1482.

[13] S. S. Sekretarov and D. M. Vavriv, “A wideband slotted waveguide antenna array for sar systems,” Progress in electromagnetics research M, vol. 11, pp. 165 – 176, 2010.

[14] S. Liao, J. Wang, Y. Chen, W. Tang, J. Wei, J.Xu and Z. Zhao and D. M. Vavriv, “Synthesis, simulation and experiment of unequally spaced resonant slotted-waveguide antenna arrays

based on the infinite wavelength propagation property of composite right/left-handed waveguide," IEEE Transactions on antennas and propagation, vol. 60, pp. 3182 – 3194, July 2012.

[15] Robert S. Elliot, L. A. Kurtz, "The design of small slot arrays," IEEE Trans. Antennas Propagation, vol. AP-26, pp. 214-219, Mar. 1978.

[16] A. J. N. Maritz, "Investigation and Design of a Slotted Waveguide Antenna with Low 3D Sidelobes", Master Thesis, Stellenbosch University, 2010.

Chapter 3: Extensions of the Multifunction Antenna Concept

3.1. Introduction

In the previous chapter, a multifunction antenna system was developed using a horn antenna and a slotted waveguide as a feeding system. With this solution, the secondary communication function is fixed to a single direction (θ = 0°) with a wide beamwidth (79°). It was also shown that a direct BPSK modulation can be achieved in the communication direction thanks to a switching mechanism applied to the slots. In the present chapter, it is proposed to improve significantly the possibilities on the secondary communication function of this initial solution without increasing too much complexity accordingly by a strategic addition of slots. We will also discuss the impact of these enhanced solutions on the antenna system (gain, directions, radar and communication rejections).

First, in section 3.2 we will study the possibility of having multiple directions (four) by doubling the number of slots and switches in the waveguide. In section 3.3, a slot array in the waveguide will be studied to see the impact on the antenna system. To finish, in section 3.4 the possibility to use another type of modulation such as QPSK will be investigated.
As in previous chapter, we did not implement a real switching mechanism, only the activated slot is present in simulations (the others being completely closed with PEC).

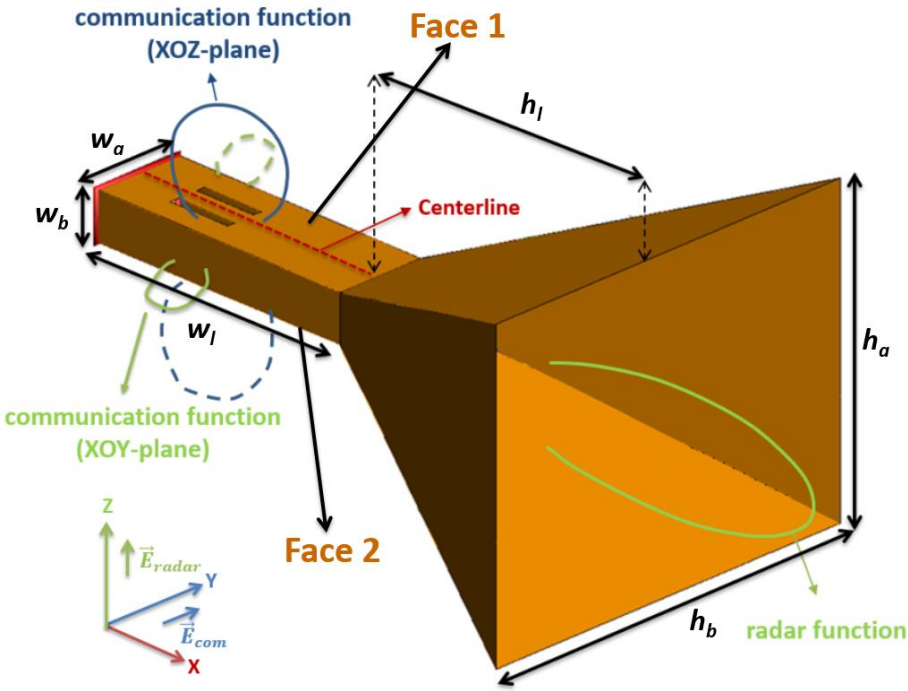

Figure 3. 1: Antenna system and its physical characteristics (w_a = 47.55 mm, w_b = 22.15 mm, w_l = 135.2 mm, h_l = 151.34 mm, h_b =125.8 mm and h_a = 180.95 mm)

3.2. Multifunction antenna with four communication directions

In this section, the goal is to improve the initial solution in particular the communication function through the possibility of transmitting information in several directions. Indeed, the proposed solution presented in the previous chapter allows only a single and fixed direction. The possibility to modify the initial solution in order to establish communication links in several directions without increasing the complexity accordingly will be discuss in this section. This could be of real interest for many communication applications. As we will see in this section, considering the rectangular shape of the feeding waveguide it would be wise to transmit information in four directions (up, down and sideways).

3.2.1. Antenna system

The same principle as the one presented in chapter 2 will be used, except that this time four identical slots (each equipped with a switching mechanism) are milled in the waveguide. As in previous chapter, the first two slots are located in the top face of the input waveguide (Face 1) and placed symmetrically to the waveguide centerline to establish the direct BPSK communication link in $\theta = 0°$ direction. The two others in the bottom face (Face 2) are also placed symmetrically to the centerline for radiation at $\theta = 180°$ offering one more communication direction (cf. Figure 3.1). Straightforwardly, the BPSK direct modulation is achieved in this direction ($\theta = 180°$) by switching between the two slots on Face 2.

We have seen in chapter 2 that the slots contribute to *z*-polarization at ($\theta = 90°$, $\phi = 90°$) and ($\theta = 90°$, $\phi = -90°$), resulting in the modification of the horn side lobes in these directions. As we will see later, BPSK direct modulation can be achieved in these two additional directions by switching between the slots in Face 1 and Face 2.

3.2.2. Antenna design

For an optimal radiation at 5 GHz, we consider the same slots as in chapter 2: length $L = 25.6$ mm, width $l = 1.5$ mm placed at $D = 12.5$ mm from the waveguide centerline (cf. Figure 3.2). In this figure, H_p is the slots position in Face 1 from the horn antenna.

- BPSK modulation at $\theta = 0°$ and $\theta = 180°$

The communication function consists in a direct BPSK modulation of the *y*-polarized field at $\theta = 0°$ (respectively $\theta = 180°$) which is obtained by activating only one of the four slots in Face 1 (respectively in Face 2) of the waveguide. As for the BPSK modulation in $\theta = 0°$ direction (presented in chapter 2), the slots in Face 2 are placed symmetrically to the waveguide centerline, so that to generate a 180° phase jump in the radiated field each time the activated slot is changed. This defines four configurations (cf. Figure 3.2).
For BSPK modulation at $\theta = 0°$, the two complementary configurations defined (involving slots in Face 1) are: in configuration 1, only slot 1 radiates while the three others are closed, in configuration 2 only slot 2 radiates while the three others are also closed.

For BSPK modulation at $\theta = 180°$, the two complementary configurations defined (involving slots in Face 2) are: in configuration 3, only slot 3 radiates while the three others are closed and in configuration 4 only slot 4 radiates while the three others are also closed.

- BPSK at ($\theta = 90°$, $\phi = 90°$) and ($\theta = 90°$, $\phi = -90°$)

In the present design, the communication function consists in a direct BPSK modulation of the *z*-polarized field in ($\theta = 90°$, $\phi = 90°$) and ($\theta = 90°$, $\phi = -90°$) directions. It is also obtained by activating only one of the four slots. Hence, the four configurations used in this case are the same as before. Contrary to the previous case, we will consider a pair of slots in opposite faces: configurations 1 and 3 (respectively configurations 2 and 4). A displacement of $d = 35.1$ mm $\approx \lambda_g/2$ (along *x* axis) is needed between the pair of slots in opposite faces (cf. Figure 3.2) in order to generate a 180° shift in the radiated field each time the activated slot is changed. More precisely, the BPSK modulated signal will be transmitted at ($\theta = 90°$, $\phi = 90°$) by switching between configuration 1 and 3 and at ($\theta = 90°$, $\phi = -90°$) by switching between configuration 2 and 4.

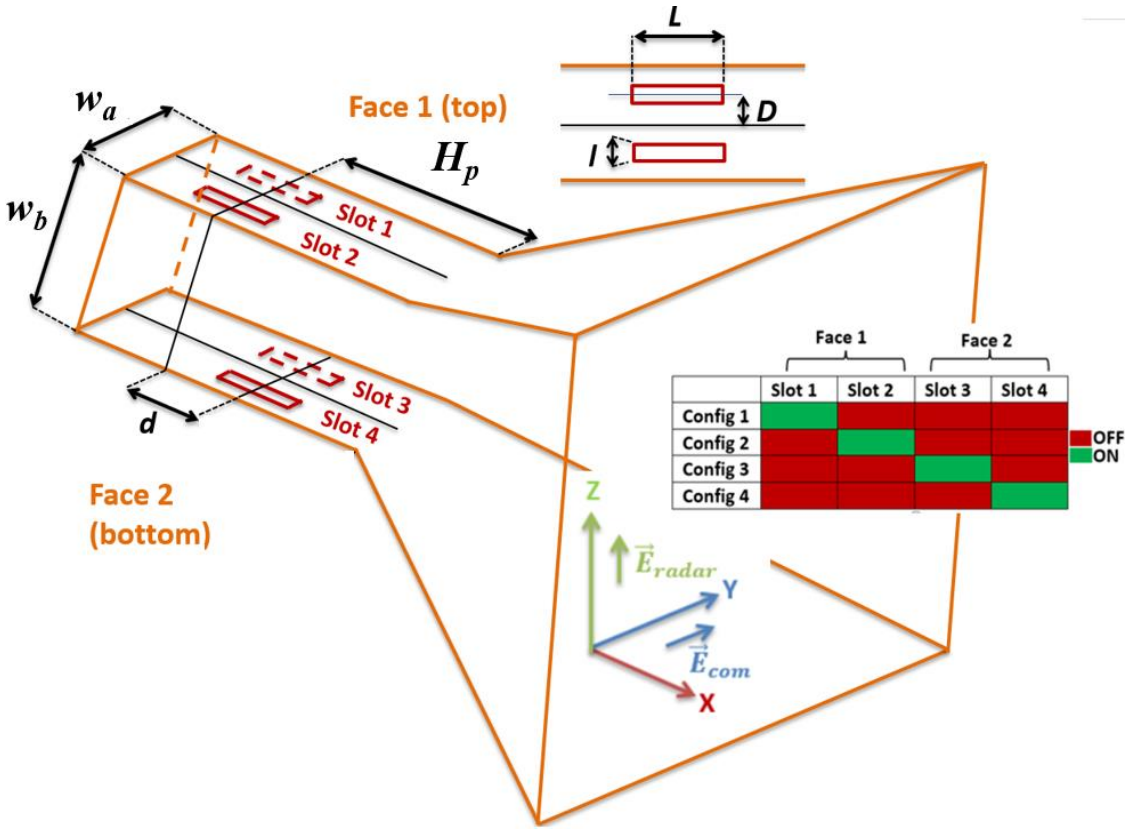

Figure 3. 2: Configurations of the antenna system (w_a = 47.55 mm, w_b = 22.15 mm, H_p = 77.2 mm, d = 38.6 mm)

3.2.3. Antenna performances

In this section, the simulated performance of the radar antenna (horn) and communication antenna (slots) of this new solution are discussed. More precisely, we investigate the impact of the four slots on the antenna system.

3.2.3.1. The main radar function

We now investigate the modification of the horn radiation due to the slots to make sure that the main radar function is not affected.

Figure 3.3 and Figure 3.4 present θ-gain in xOz and xOy plane respectively at 5 GHz for the four configurations. The gain of the horn antenna without slots is also given for comparison purposes.

As expected, the main beam of the horn, used for radar function, is identical for all the configurations with a maximum gain of 16 dBi in the two cut planes. This ensures that the radar pattern does not change when switching between the four configurations. As already explained in chapter 2, this gain is 1.23 dB less than for the horn antenna without slot.

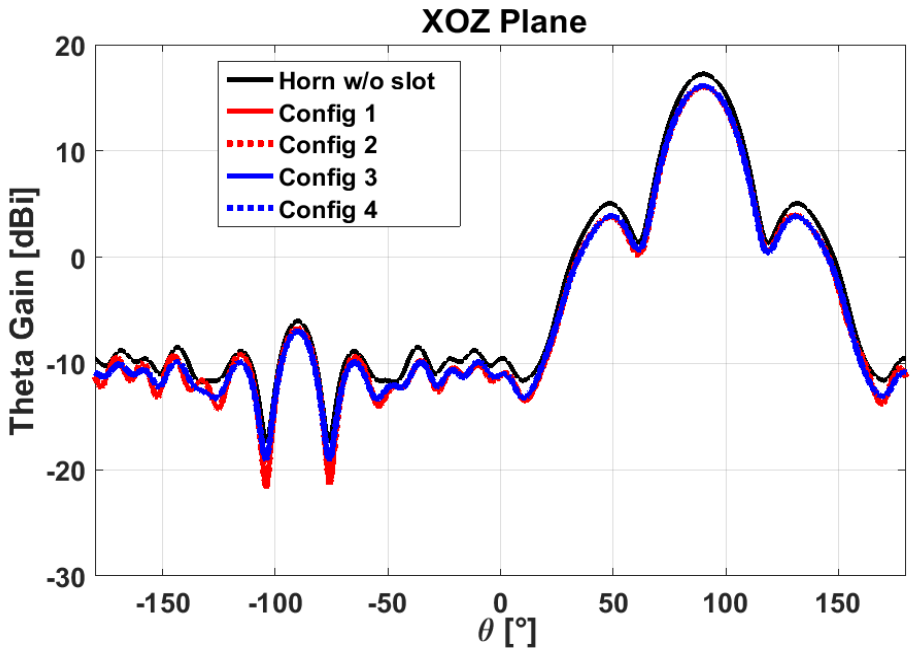

Figure 3. 3: Radiation pattern (θ-gain) in XOZ plane of the four configurations and horn without slot at 5 GHz

However, as it has been shown in previous chapter, in xOy plane, the slots are responsible for an increase in the horn side lobes because in these directions the radiated field from slots contributes to *z*-polarization. In this plane, due to the symmetry, configurations 1 and 3 (respectively 2 and 4) give exactly the same patterns. The possibility to use this characteristic to transmit additional information will be studied in section 3.2.3.2.

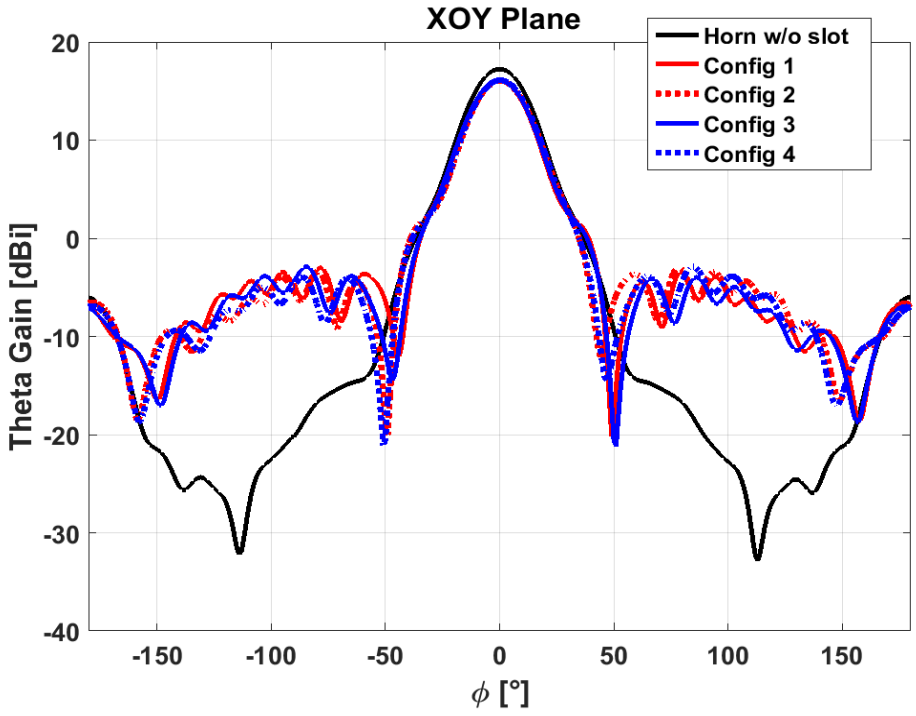

Figure 3. 4: Radiation pattern (θ-gain) in XOY plane of the four configurations and horn without slot at 5 GHz

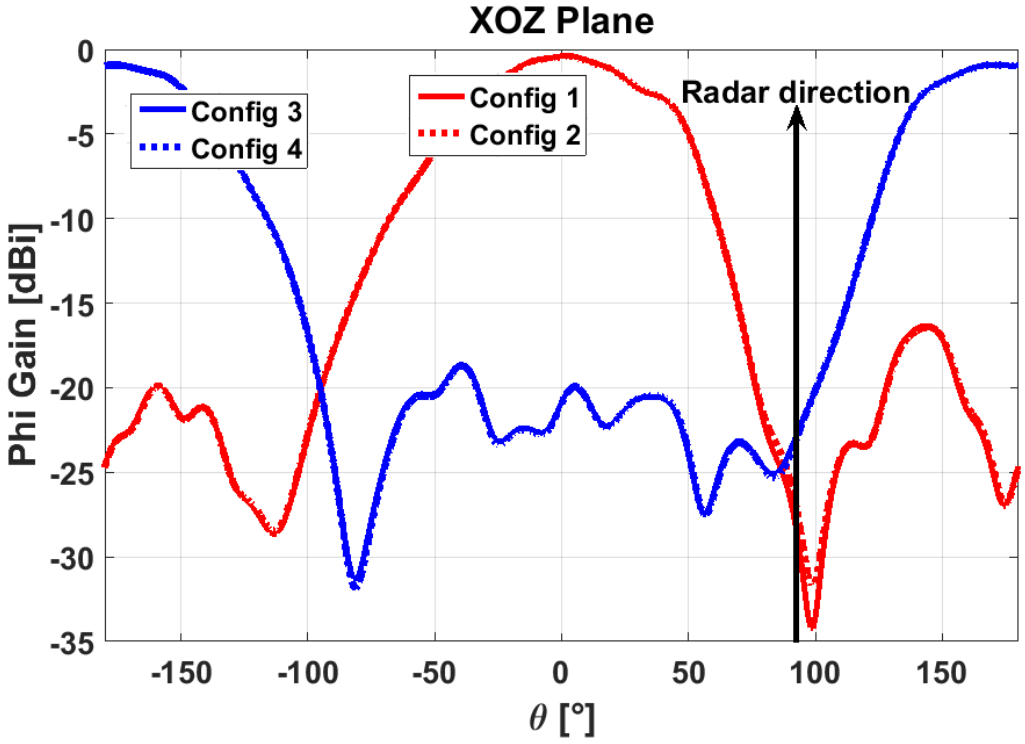

Figure 3. 5: Radiation pattern (ϕ-gain) in XOZ plane of the four configurations at 5 GHz

3.2.3.2. BPSK communication

In this section, the performance of communication antenna is analyzed.

- BPSK communication at $\theta = 0°$ and $\theta = 180°$

Figure 3.5 presents the ϕ-gain in xOz plane at 5 GHz for all the configurations. These radiation with orthogonal polarizations and directions to horn correspond to communication function. As could be expected, the maximum gain is now obtained at $\theta = 0°$ for configurations using slots on Face 1 (configurations 1 and 2) and at $\theta = 180°$ for slots on Face 2 (configurations 3 and 4).

Table 3.1 summarizes the characteristics obtained for the BPSK communication at $\theta = 0°$ and $\theta = 180°$. As already explained the gains are low due to the use of a single slot and the small amount of power dedicated to the communication in the design. We can also note a 0.55 dB gain drop between the slots on Face 1 (configuration 1 and 2) and Face 2 (configurations 3 and 4). This slight difference can be explained by the use of different spacing between the pair of slots and the horn aperture (parameter *d*, cf. Figure 3.2) but does not affect the antenna operation because in each direction the pair of slots considered has the same gain.

Directions	Config	Phase (°)	Amp. (dBi)
$\theta = 0°$	1	0	-0.4
	2	180	-0.4
$\theta = 180°$	3	0	-0.95
	4	180	-0.95

Table 3. 1: BPSK modulation at 5 GHz at $\theta = 0°$ and $\theta = 180°$

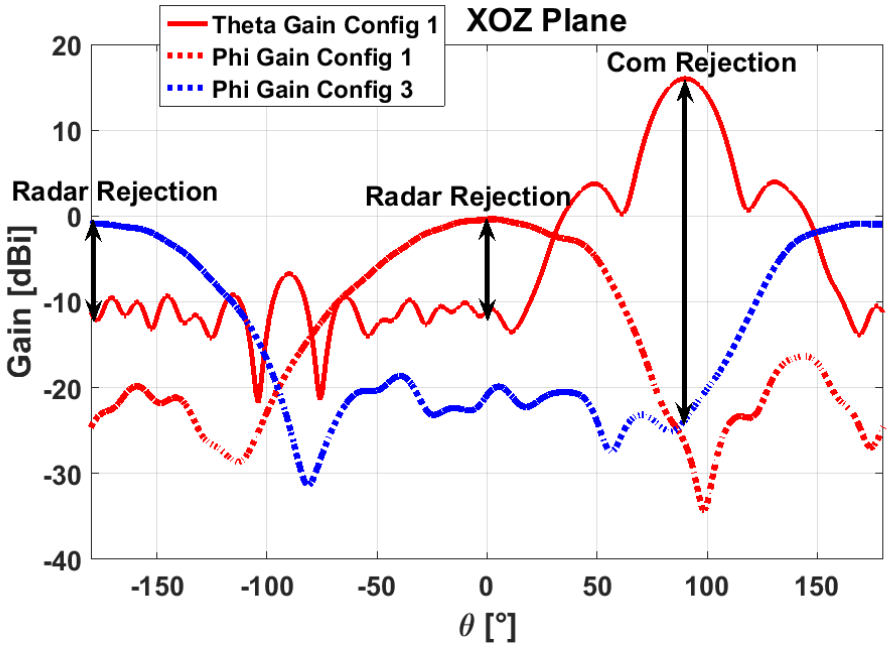

Figure 3. 6: Radiation characteristics of the antenna system at 5 GHz for communication at $\theta = 0°$ and $\theta = 180°$

Figure 3.6 summarizes the radiation properties of the proposed antenna for configurations 1 and 3 (configurations 2 and 4 would lead to similar conclusions). As can be seen, configuration 1 corresponds to a prominent radiation in *z*-polarization at θ = 90° (radar function, θ-gain) and a secondary radiation in *y*-polarization at θ = 0° (communication function, ϕ-gain). The same radar function is achieved for configuration 3 but communication now occurs at θ =180°.
The rejections, as defined in previous chapter and Figure 3.6 are 10 dB for radar rejection and 40 dB for communication rejection at 5 GHz. This ensures the isolation between the two functions and validates the possibility to transmit BPSK modulation at θ = 0° and at θ =180°.

A solution to further increase the communication directivity by using slot array [1] will be discussed in section 3.3 for communication at θ = 0°.

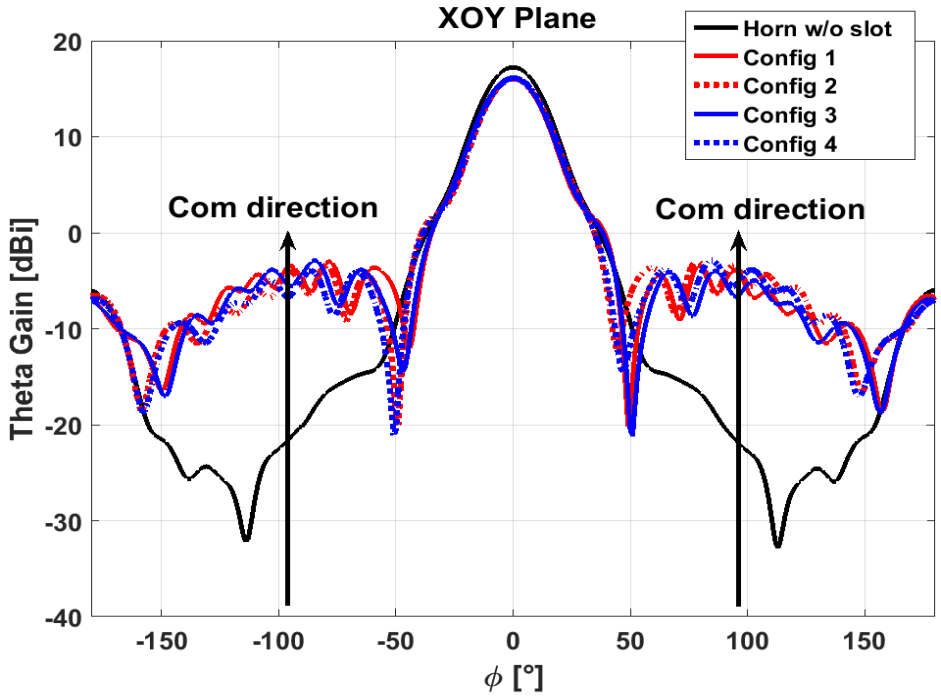

Figure 3. 7: Radiation characteristics of the antenna system at 5 GHz for communication at (θ = 90°, ϕ = 90°) and (θ = 90°, ϕ = -90°)

- BPSK communication at (θ = 90°, ϕ = 90°) and (θ = 90°, ϕ = -90°)

We now investigate the possibility to also transmit a BPSK modulated signal at (θ = 90°, ϕ = 90°) and (θ = 90°, ϕ = -90°) using the same switching mechanism. Quite straightforwardly, this can be achieved by switching from configuration 1 to configuration 3 (respectively configuration 2 to 4) taking into account the offset *d* (≈λg/2) between the two considered configurations and consequently the 180° phase shift generated by the switching. Once again, the two considered slots lead to opposite radiated fields in the direction of interest. However, the situation is quite different from the one we had previously. Indeed, at (θ = 90°, ϕ = 90°) and (θ = 90°, ϕ = -90°), the field radiated by the slots is *z*-polarized, which means the communication and radar functions now use the same polarization but orthogonal directions, as shown in Figure 3.7. More precisely, the

communication signal is now produced by the phase-modulation of the horn side lobes (much lower than the main lobe of the horn, SLL lower than -18.66 dB) when switching occurs.

Table 3.2 summarizes the characteristics obtained for the BPSK communication at (θ = 90°, ϕ = 90°) and (θ = 90°, ϕ = -90°). As already explained in chapter 2, the gain levels can be increased (resulting in lower power available for the radar) by using a large offset *D*. Although the gains are low (at least 4 dB less than the slot radiation at θ = 0° and 180°), the possibility to communicate in these two directions offers additional flexibility at no cost.
As previously, the gain difference (0.45 dB) between the pair of slots considered is the result of the spacing between the slots and the horn aperture (parameter *d*, cf. Figure 3.2).

Directions	Config	Phase (°)	Amp. (dBi)
ϕ = 90°	1	0	-5.34
	3	180	-4.89
ϕ = -90°	2	0	-4.9
	4	180	-5.35

Table 3. 2: BPSK modulation at 5 GHz at (θ = 90°, ϕ = 90°) and (θ = 90°, ϕ = -90°)

To evaluate the impact of this gain difference in the communication function, we calculate the error vector magnitude (EVM) [2] [3]. EVM is used to determine the quality of a communication and expresses the difference between the expected symbol and the value of the actual symbol. This parameter is useful in our case because it contains information about both amplitude and phase errors in the signal [4], [5]. EVM is calculated by using the formula below [2]:

$$EVM(\%) = \frac{\sqrt{\frac{1}{N}\sum_{n=0}^{N-1}(I_{ideal}(n) - I_{meas}(n))^2 + (Q_{Ideal}(n) - Q_{meas}(n))^2}}{|P_0|} * 100\% \quad (1)$$

where N is the number of symbols, $I_{ideal\ or\ meas}$ and $Q_{ideal\ or\ meas}$ are the normalized ideal (or measured) inphase and quadrature components. P_0 is the EVM normalization reference corresponding to the maximum magnitude of the ideal constellation.

It is important to point out that the smaller percentage values represent the best error modulation results [6]. Moreover, in literature, the EVM limit for a BPSK modulation is - 7 dB [7].

Hence using (1), in our case, the EVM is 6.92 % (corresponding to -23.2 dB) at ϕ = ± 90° ensuring that the amplitude difference between the two configurations does not affects the communication link. For more details on the EVM calculation for BPSK modulation cf. Appendix 1.

We now investigate the reflection coefficients of the four configurations (cf. Figure 3.8). As can be seen from this figure, the reflection coefficients are below -13 dB from 4 GHz to 6 GHz for all the configurations.

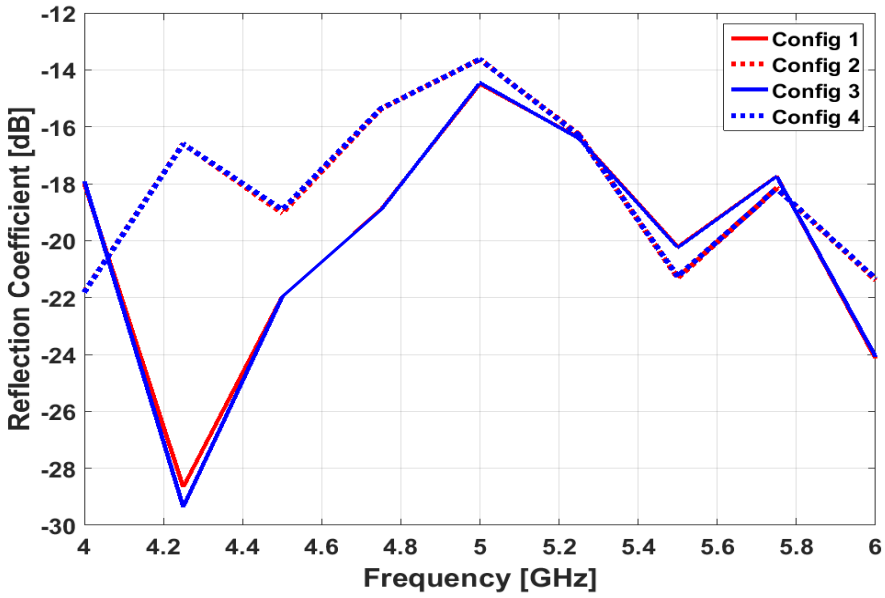

Figure 3. 8: Reflection coefficient of the four configurations

3.2.4. Conclusion

The two additional slots and the associated switches in Face 2 make it possible to select three other possible directions for the transmission of the BPSK directly-modulated signal. The EVM computation gives -23.2 dB which is acceptable for applications using BPSK modulation. We then obtain four different possible communication directions (isolated from the radar function), which largely extends the capabilities of the initial system. This does not lead to too much added complexity. This new structure combines two different concepts: either the communication signal is transmitted in the cross-polarization of the radar system (as in the previous version, at $\theta = 0°$ and 180°) or through phase-modulation of the horn side lobes (SLL lower than -18.66 dB) at (θ =90°, $\phi = 90°$) and ($\theta = 90°$, $\phi = -90°$). The radar and communication rejections obtained at 5 GHz are respectively 10 dB and 40 dB ensuring that the two functions do not interfere.

In the next section, we investigate the possibility to reduce the beamwidth of the communication antenna (by using slot array in the waveguide) while maintaining the BPSK modulation capabilities.

3.2. Slot array in the waveguide

In this section the goal is to study the impact of a slot array on the radar and communication function. In doing so the directivity (and then the gain) of the communication function will be improved which might be of interest for some applications. As we will see using a slot array gives us one more degree of freedom to control the power available for the radar. Additionally, the impact of this array on the rejections will be discussed.

3.2.1. Antenna Design

For this study, we go back to the configuration allowing to transmit the communication signal in only one direction (θ = 0°). The same slots dimensions (L = 25.6 mm and l = 1.5 mm) as in the previous section are considered.

In order to reduce the beamwidth of the communication function at θ = 0°, the array is here arbitrarily composed of five slots milled in the top face of the waveguide (array 1, cf. Figure 3.9). To have consecutive elements in phase, the slots are spaced $\lambda_g/2$ and offset on opposite sides of the centerline by D [1]. In the present case, taking into account the number of slots and to maintain in the main beam of the horn a gain level of at least 15.93 dBi as in chapter 2, the offset has been reduced to D = 3 mm (instead of 12.5 mm in chapter 2).

As already explained, the communication function consists in a direct BPSK modulation of the *y*-polarized field in θ = 0° direction. For that reason, a second array of five slots is placed symmetrically to the waveguide centerline (array 2, cf. Figure 3.9) so that to generate a 180° phase jump in the radiated field each time the activated array is changed. This defines two complementary configurations (cf. Figure 3.9). In configuration 1, only the slots forming the array 1 radiate while the other are closed. Configuration 2 corresponds to reverse situation.

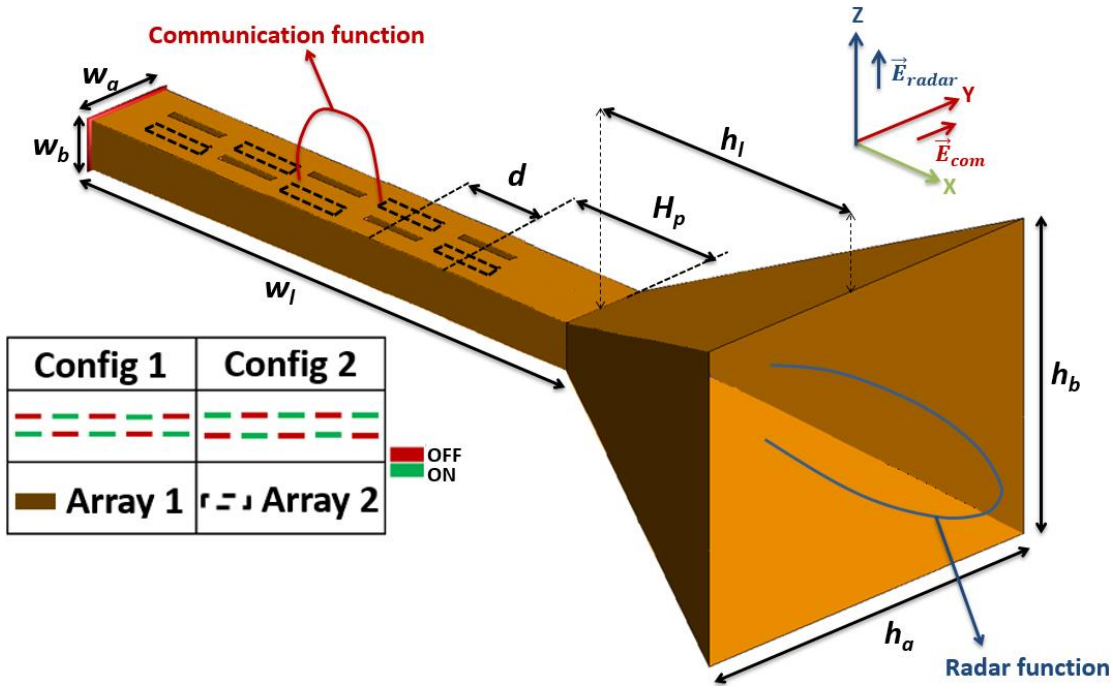

Figure 3. 9: Antenna array configurations and physical characteristics (w_a = 47.55 mm, w_b = 22.15 mm, w_l = 231.7 mm, h_l = 151.34 mm, h_b =125.8 mm and h_a = 180.95 mm, d = H_p =38.6 mm)

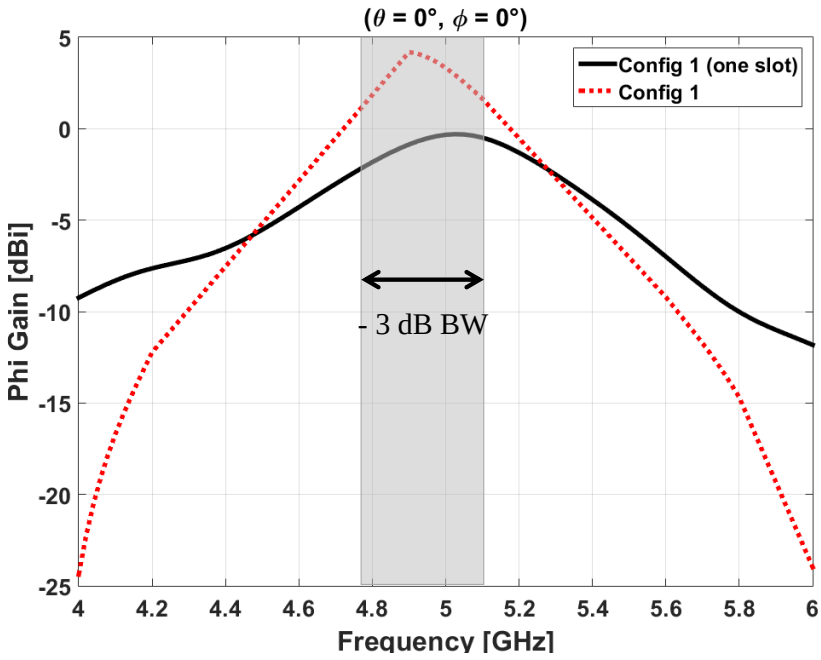

Figure 3. 10: Slots radiation (ϕ-gain) at θ =0° versus frequency

3.2.2. Antenna performance

We are now interested in the resonance frequency of the slot array. Figure 3.10 shows the ϕ-gain versus frequency of the array 1 (configuration 1). For comparison purposes, the gain of the horn with one slot is also given. We can see that at 5 GHz the gain of the array 1 increased by 3.63 dB compared to the case with one slot. As already explained, the slots offset *D* have been reduced to 3 mm, (reducing then the power radiated by the slots) in order to have at least 15.93 dBi gain for the horn. We can also note that the interaction between the slots causes a slight frequency shift and the maximum gain (4.18 dBi) is obtained at 4.9 GHz.
The -3 dB gain bandwidth of the slot array is 348.68 MHz (from 4.77 GH to 5.12 GHz). In this frequency range, the ϕ-gain is at least 1.16 dBi, which is 1.46 dB higher than the case presented in chapter using one slot in the waveguide.

3.2.2.1. The main radar function

We now study the impact of this slot array on the radar antenna (horn).

Figure 3.11 and Figure 3.12 show θ-gain of the two configurations in respectively xOz and xOy plane at 5 GHz. For comparison purposes, the gain of the horn with one slot (presented in chapter 2 is also given).

In xOz plane, as expected, due to symmetry both configurations 1 and 2 give the same patterns, which guarantees the radar operation is not affected when switching the arrays. The maximum gain in the main direction of the horn is 16.17 dBi. We also notice a slight increase in the horn beamwidth (3.85°) due to the slot array.

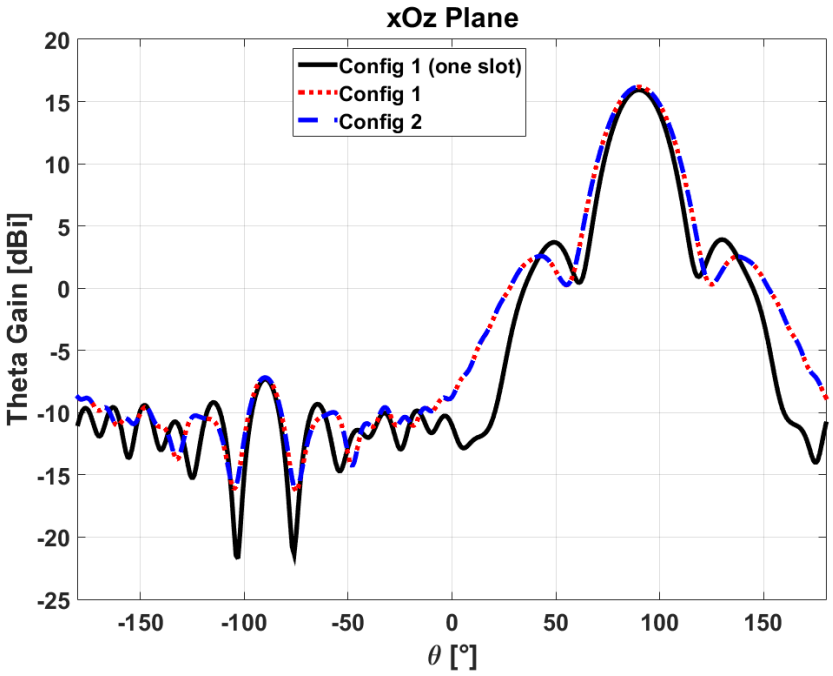

Figure 3. 11: Radiation pattern (θ-gain) in XOZ plane of the two array configurations at 5 GHz

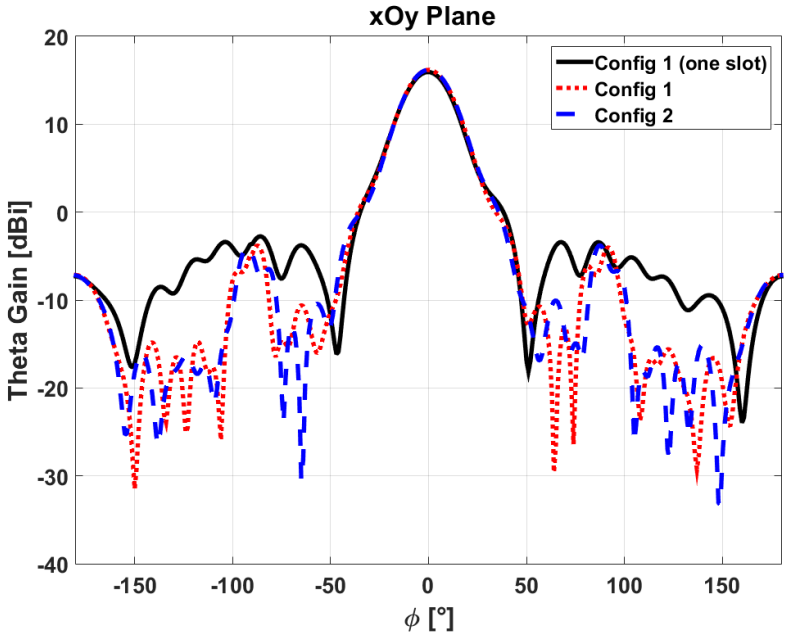

Figure 3. 12: Radiation pattern (θ-gain) in XOY plane of the two array configurations at 5 GHz

Concerning the xOy plane, the main lobe of the horn is not affected by the array in comparison to the horn with one slot. Moreover, as with one slot, the slot array leads to an increase in the horn side lobes. This time, the modifications in side lobes are more located at $\phi = \pm 90°$ (cf. Figure 3.12). As we will see in the next section, this is the result of the communication function directivity improvement, reducing the zone of impact of the slots radiation in the horn side lobes.

Nevertheless, the SLL remains lower than -18.66 dB, which is acceptable for many radar applications.

Figure 3.13 depicts θ-gain in the main direction of the horn versus frequency for the two configurations in comparison to that of the horn without slot. As expected, the slot activation in the waveguide causes a gain drop in the main direction of the horn. At 5 GHz the gain drop is 0.45 dB.

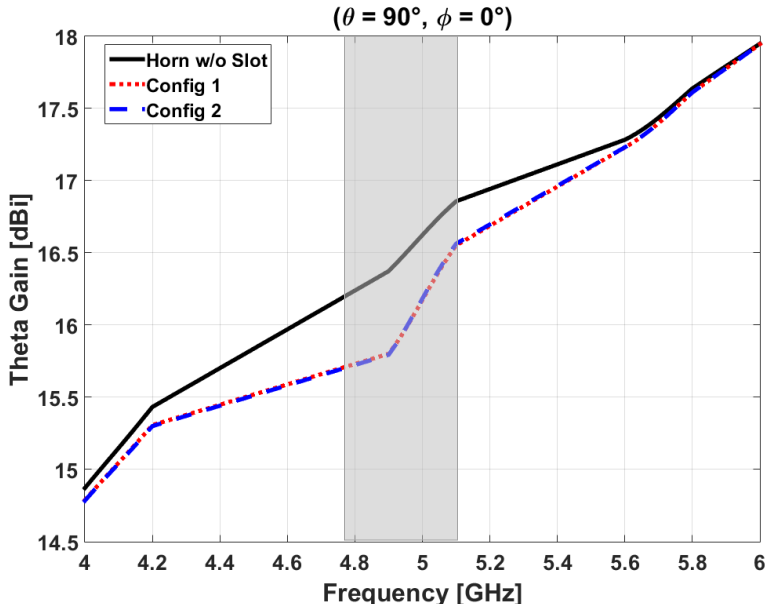

Figure 3. 13: θ-gain (horn radiation) at versus frequency

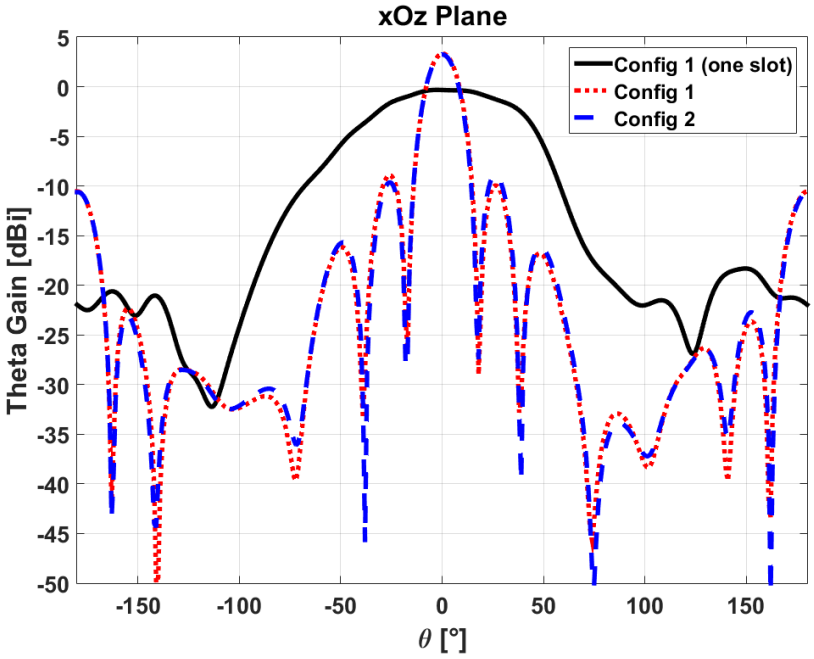

Figure 3. 14: Radiation pattern (ϕ-gain) in XOZ plane of the two array configurations at 5 GHz

3.2.2.2. Communication function

In this section, the performance of the communication antenna (slot array) is analyzed.

Figure 3.14 shows the ϕ-gain in xOz plane of the two configurations at 5 GHz and as expected, the slot radiation is more directive.

Table 3.3 summarizes the results obtained for the BPSK communication at $\theta = 0°$.

Directions	Config	Phase (°)	Amp. (dBi)
$\theta = 0°$	1	0	3.33
	2	180	3.33

Table 3. 3: BPSK communication at 5 GHz

The rejections obtained at 5 GHz are presented in Figure 3.15. As can be seen, the increase in ϕ-gain at $\theta = 0°$ leads to an increase of the radar rejection which is now 12.1 dB. The communication rejection is still high (48.4 dB).

Table 3.4 compares the performances of the antennas configuration 1 with one slot and five slots. As already explained in chapter 2, the communication gain and radar losses are linked to the slot offset *D*. Hence, by using a large *D* the communication gain can be increased (without reducing the beamwidth) at the expense of a lower power available for the radar. However, in comparison to the horn with one slot, the use of the slot array allows at the same time to reduce the slot beamwidth by 63.42° (and then increase the gain by 3.63 dB). Furthermore, the radar rejection has been increased by 1.1 dB, improving the isolation between the two functions in this direction.

	1 slot	**5 slots array**
Horn Gain	15.93 dBi	16.17 dBi
Slot Gain	-0.3	3.33 dBi
Slot beamwidth	79°	15.58°
Radar rejection	11 dB	12.1 dB
Communication rejection	37 dB	49.6 dB

Table 3. 4: Comparison of configuration 1 with one slot and five slots array at 5 GHz

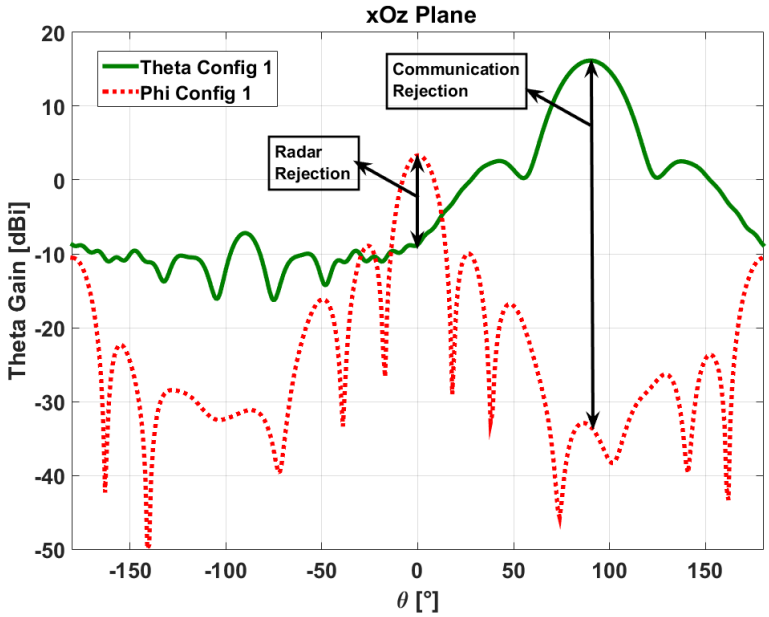

Figure 3. 15: Radar and communications rejections at 5 GHz

In the next section, we will study the isolation of radar and communication functions.

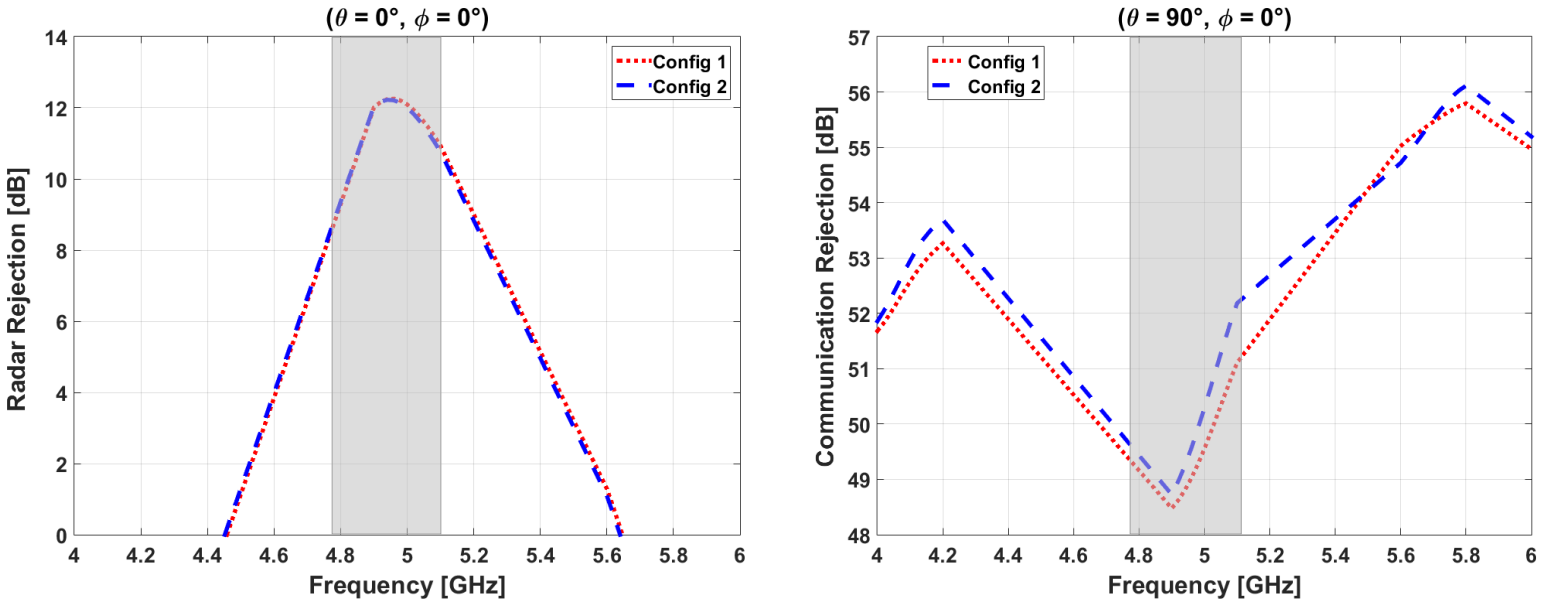

(a) (b)

Figure 3. 16: (a) radar rejection and (b) communication rejection versus frequency

3.2.2.3. Study of radar and communication isolation

In this section the radar and communication rejections are studied to evaluate the robustness of the antenna system.

Figure 3.16 (a) and (b) present the variation of respectively radar and communication rejections versus frequency.
Always considering the -3 dB gain bandwidth of the slot array, a radar rejection between 8.49 dB and 12.25 dB is ensured for the antenna at $\theta = 0°$. As explained in chapter 2, this could be improved by replacing the standard horn by a corrugated horn [8], which presents much lower side lobes.

Concerning the communication rejection, it is at least 48 dB in the same bandwidth.

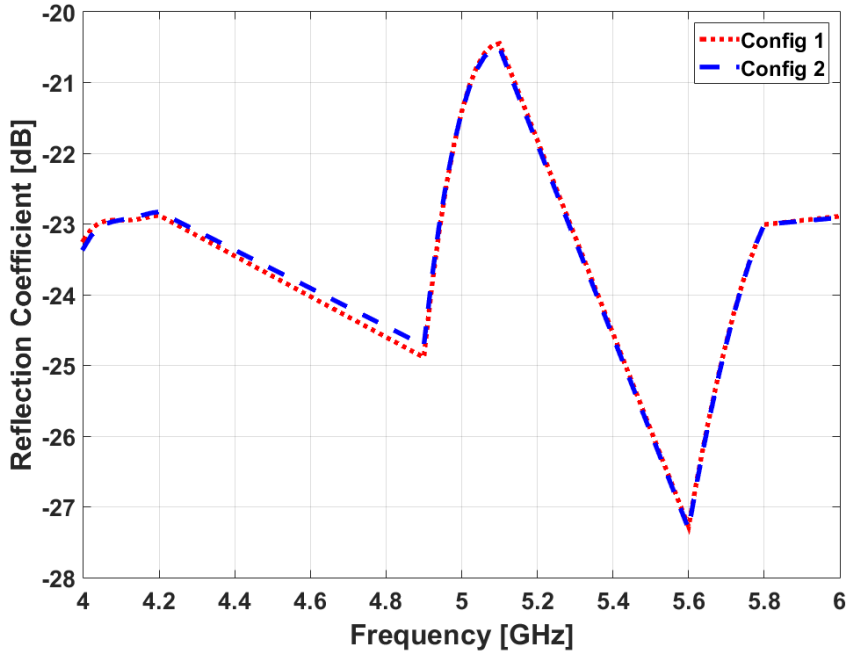

Figure 3. 17: Reflection coefficient

As for the reflection coefficients of the two configurations, they are depicted in Figure 3.17. As can be seen, the reflection coefficients are below -20 dB from 4 GHz to 6 GHz.

3.2.3. Conclusion

The slots array allowed to improve the communication radiation in term of directivity at $\theta = 0°$. The communication gain was increased by 3.63 dB at 5 GHz in comparison to the horn with one slot. Furthermore, the radar and communication rejections have been increased by 1.1 dB and 12.6 dB respectively, which ensures more isolation between the two functions at 5 GHz. This is achieved while ensuring 16.17 dBi gain for the radar function.

The frequency study over the -3 dB gain bandwidth shows at least 1.16 dBi gain at $\theta = 0°$ for the communication function. Moreover, in this bandwidth, the radar and communication rejections are respectively 8.49 dB and 48 dB in the worst cases providing more isolation between radar and communication functions. In return these results were obtained using a much larger feeding waveguide, 96.5 mm larger than the case using one slot.

After discussing the possibility of using slots array to provide more directivity to the communication function, in the next section, a solution to perform a direct QPSK modulation will be studied.

3.3. QPSK modulation

The goal in this section is to propose an alternative to the BPSK modulation presented in previous sections. For that reason, we study the possibility to achieve a QPSK modulation for the communication function (which could be of interest for some communication applications) and the impact of this type of modulation on the main radar function. As in previous sections slots of length L = 25.6 mm, width l = 1.5 mm placed at D = 12.5 mm from the waveguide centerline will be considered for this study.

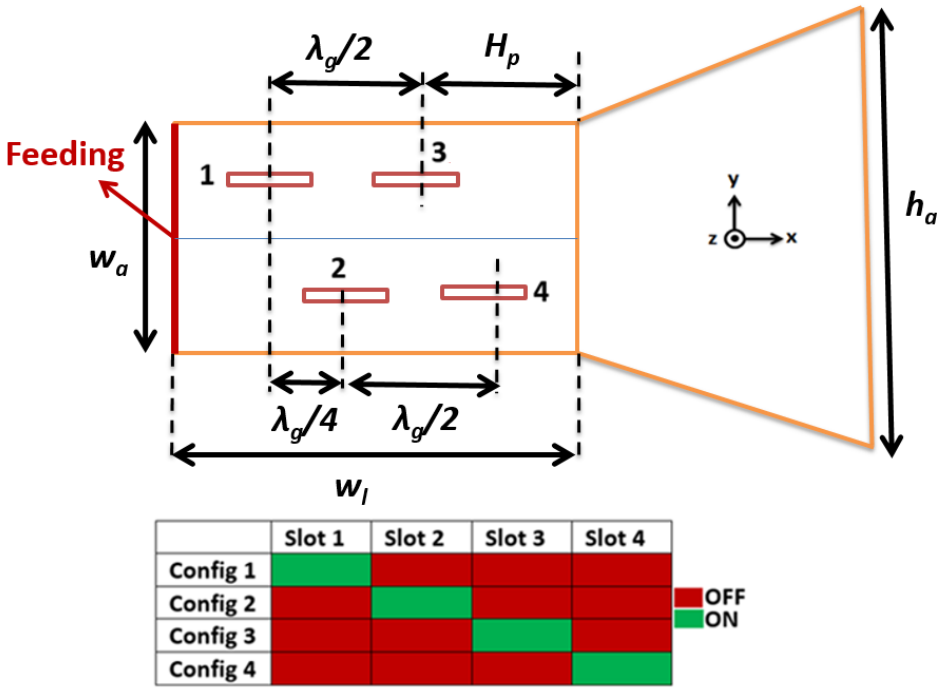

Figure 3. 18: Antenna system configurations and physical characteristics (w_a = 47.55 mm, w_b = 22.15 mm, w_l = 135.2 mm, h_l = 135.2 mm, h_b =125.8 mm and h_a = 180.95 mm, $d = H_p$ =38.6 mm)

3.3.1. Antenna design

In the present design, the communication function consists in a direct QPSK modulation at $\theta = 0°$.

Examining the equations of the propagating fields in the waveguide for the dominant TE10 mode, presented in chapter 2, a QPSK modulation could be achieved by milled four identical slots in the feeding waveguide, each spaced by $\lambda_g/4$ (19.31 mm at 5 GHz) to generate 90° phase shift each time the activated slot is changed. For that reason, the antenna architecture (slots arrangements in the feeding waveguide) as the one presented in Figure 3.18 will be used.

Starting from the feeding point to the horn aperture (Figure 3.18), one goes from slot 1 to slot 4. In the present case, only the activated slot radiates the other being completely closed with PEC. This defines four configurations: in configuration 1, only slot 1 radiates while the others are closed, in configuration 2 only slot 2 radiates while the others are closed and so on for the two other configurations.

In the next section, the performance of such a modulation on the antenna system will be investigated.

3.3.2. Antenna performance

3.3.2.1. The main radar function

We first study the modification of the horn radiation (dedicated to radar function) due to the slots. For comparison purposes, the gain of the horn antenna without slots is also given.

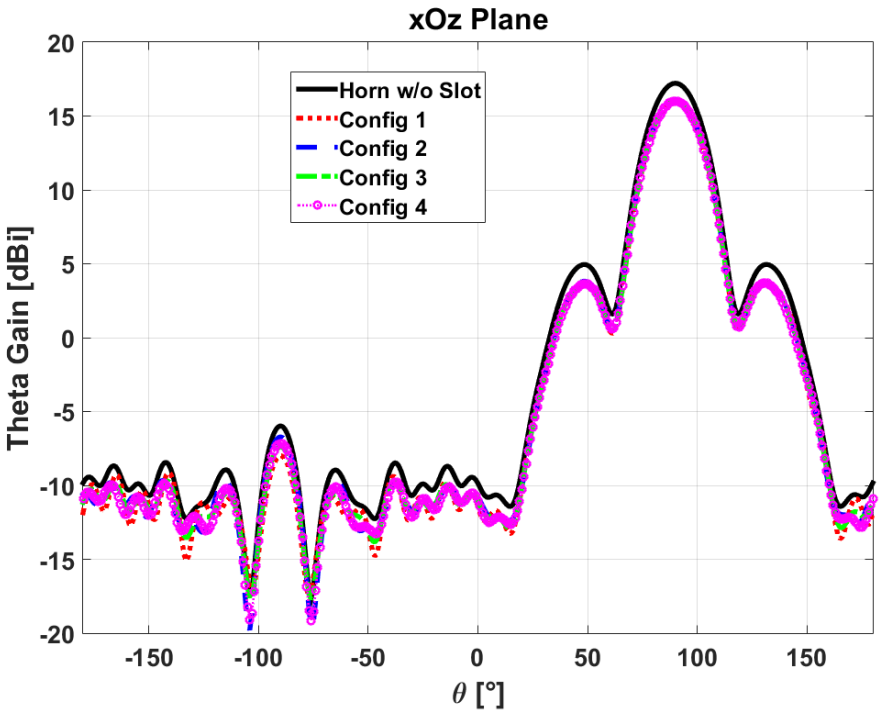

Figure 3. 19: Radiation pattern (θ-gain) in xOz plane of the four configurations at 5 GHz

Figure 3.19 and Figure 3.20 show θ-gain of the four configurations in respectively xOz and xOy plane at 5 GHz.

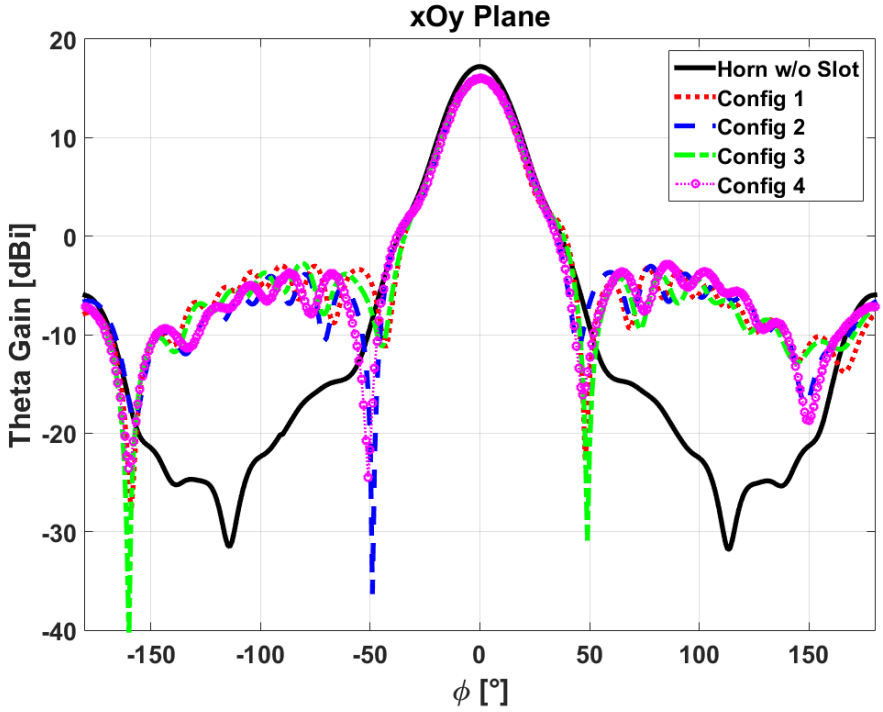

Figure 3. 20: Radiation pattern (θ-gain) in xOy plane of the four configurations at 5 GHz

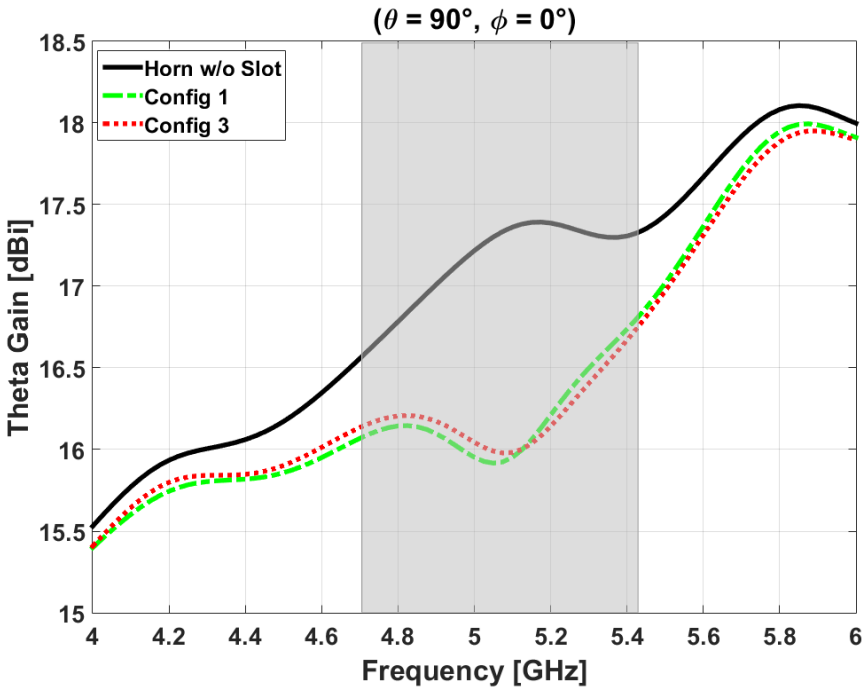

Figure 3. 21: Horn radiation in the main direction of the horn versus frequency

In xOz plane, the main beam of the horn, used for radar function are exactly the same for all the configurations. This ensures that the radar pattern does not change when switching between the configurations. The maximum gain is 15.94 dBi at θ = 90° and this corresponds to 1.27 dB gain drop due to the power picked up by the slot for communication function.

In xOy plane, as in the previous cases, the horn side lobes are affected by the slot radiation because in these directions the radiated field from slots contributes to *z*-polarization. The SLL remains lower than -18.83 dB which is acceptable for many radar applications.

Concerning the horn gain, Figure 3.21 depicts θ-gain in the main direction of the horn versus frequency for configurations 1 and 3 in comparison to that of the horn without slot. As expected, the slot activation in the waveguide causes a gain drop in the main direction of the horn. At 5 GHz, corresponding to the resonance frequency of the slot the gain drop is 1.27 dB.

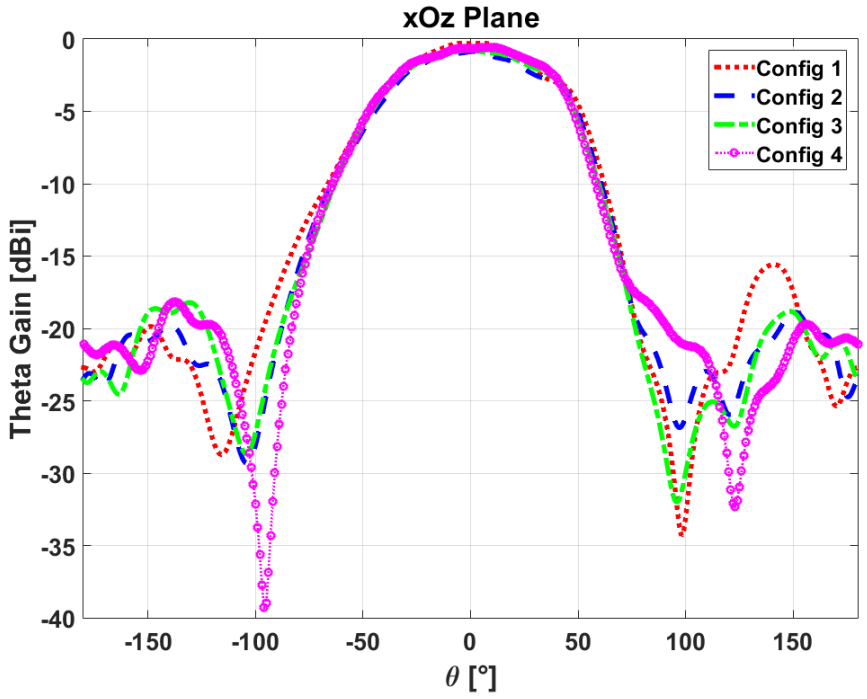

Figure 3. 22: Radiation pattern (ϕ-gain) in XOZ plane of the four configurations at 5 GHz

Directions	Config	Theoretical Phase (°)	Simulation Phase (°)	Phase Error (°)	Amp. (dBi)
$\theta = 0°$	1	0	0	0	-0.3
	2	270	269.9	0.1	-0.87
	3	180	174.7	5.3	-0.79
	4	90	91.35	1.35	-0.63

Table 3. 5: QPSK modulation at 5 GHz at $\theta = 0°$

3.3.2.2. Communication function

In this section, the performance of the communication function is analyzed.

Figure 3.22 presents the ϕ-gain in xOz plane at 5 GHz for the four configurations. As could be expected, the maximum gain is obtained at $\theta = 0°$ for all the configurations with similar levels.

Table 3.5 summarizes the characteristics obtained for the QPSK communication at $\theta = 0°$. Note that the phases presented in this table are calculated by considering configuration 1 as reference.

As can be seen in this table, the maximum gain difference between the configurations is 0.57 dB in the worst case. This variation results from the position of the slots with respect to the horn aperture and feeding point, which is not equal for all the four slots. Moreover, the phase error between theory and simulations is 5.3° in the worst case. A possible solution to reduce the phase error would be to readjust the slots spacing in the waveguide.

To evaluate the impact of these variations on the communication function, as in section 3.2.3.2, we compute the EVM using equation (1). In the present case for the simulated QPSK the EVM is 10% corresponding to -20 dB (cf. Appendix 1 for more details on the EVM calculation for QPSK modulation). In [8] for example, the EVM limit for applications using QPSK modulation is 17.5%. This ensures that the communication link is not affected by the amplitude variation and phase errors.

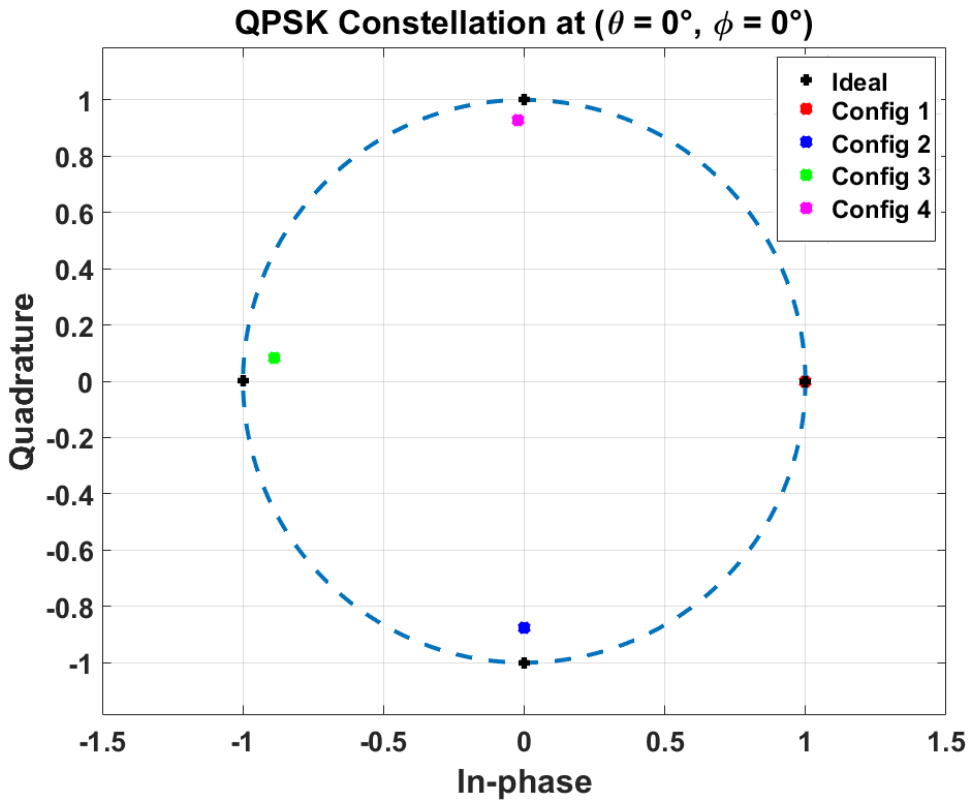

Figure 3. 23: QPSK constellation in the communication direction (θ =0°) at 5 GHz

The constellation obtained for the QPSK modulation is presented in Figure 3.23. For comparison purposes the ideal QPSK constellation is also given. As shown in this figure, although the gain variation between the configurations is 0.57 dB and the phase error can reach 5.3°, the possibility to transmit QPSK modulation at $\theta = 0°$ direction offers added flexibility.

After discussing the possibility to transmit QPSK communication, in the next section, the robustness of this solution will be studied.

3.3.2.3. Study of radar and Communication rejections

Is this section, we study the isolation between the two functions (radar and communication) through the analysis of radar rejection and com rejection.

Figure 3.24 summarizes the radiation properties of the proposed antenna for configurations 1 (configurations 2, 3 and 4 would lead to similar conclusions) at 5 GHz. As can be seen, configuration 1 corresponds to a prominent radiation in *z*-polarization at $\theta = 90°$ (radar function) and a secondary radiation in *y*-polarization at $\theta = 0°$ (communication function).

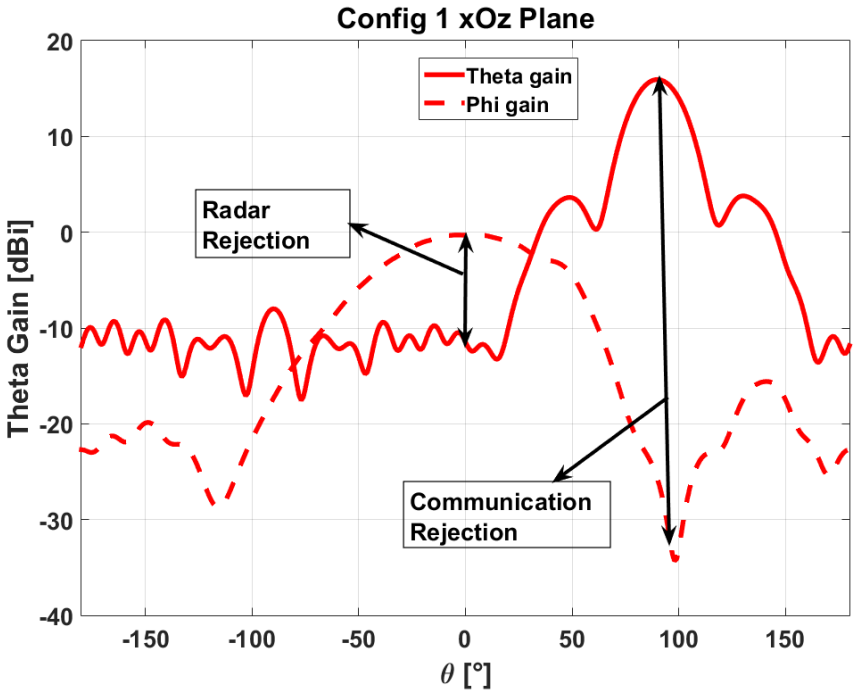

Figure 3. 24: Radiation characteristics of the antenna system at 5 GHz

The rejections at 5 GHz, as defined in this figure, are presented in Table 3.6 for all the configurations. As can be seen in this table, in the worst case, the radar rejection is 9.94 dB for configuration 2, but can reach 11.14 dB for configuration 1. Indeed, the variation in radar rejection between the 4 configurations is linked to the gain variation between the configurations ϕ-gain as presented in Table 3.5. As already explained, the rejection at $\theta = 0°$ could be increased by reducing the horn side lobes through the use of corrugated horn which presents low side lobes [9].

Config	Communication Rejection (dB)	Radar Rejection (dB)
1	11.14	41.7
2	9.94	39.64
3	10.25	44.32
4	10.38	35.61

Table 3. 6: rejections of the four configurations at 5 GHz

As for the communication rejection it is 35.61 dB in the worst case ensuring a good isolation between the two functions in this direction.

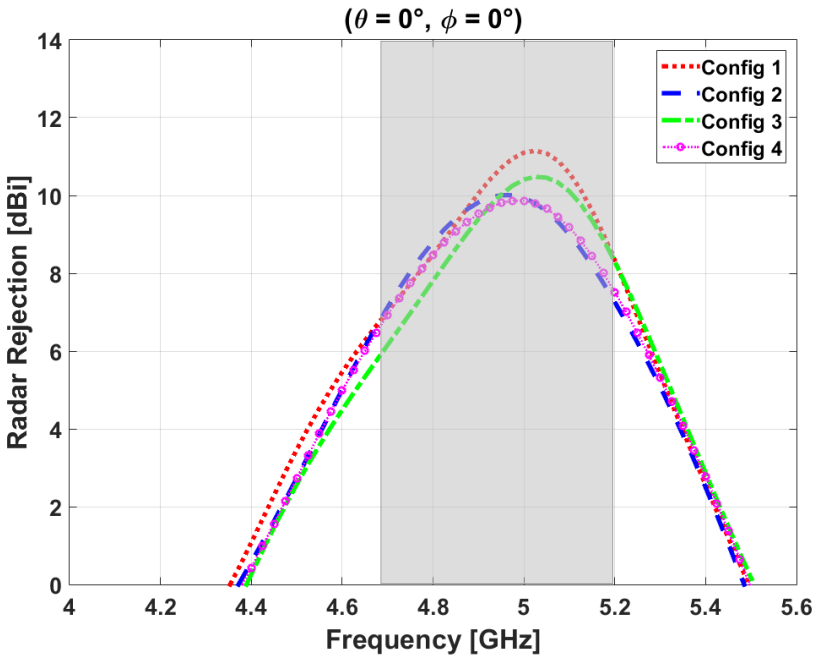

Figure 3. 25: Radar rejection in the communication direction (θ =0°)

Figure 3.25 and Figure 3.26 depict respectively radar and communication rejections versus frequency. As can be seen, in the -3 dB bandwidth of the slot, the radar rejection is 2.13 dB in the worst case, limiting the operating bandwidth of the antenna system.

Concerning the communication rejection, it is at least 35 dB from 4 to 6 GHz.

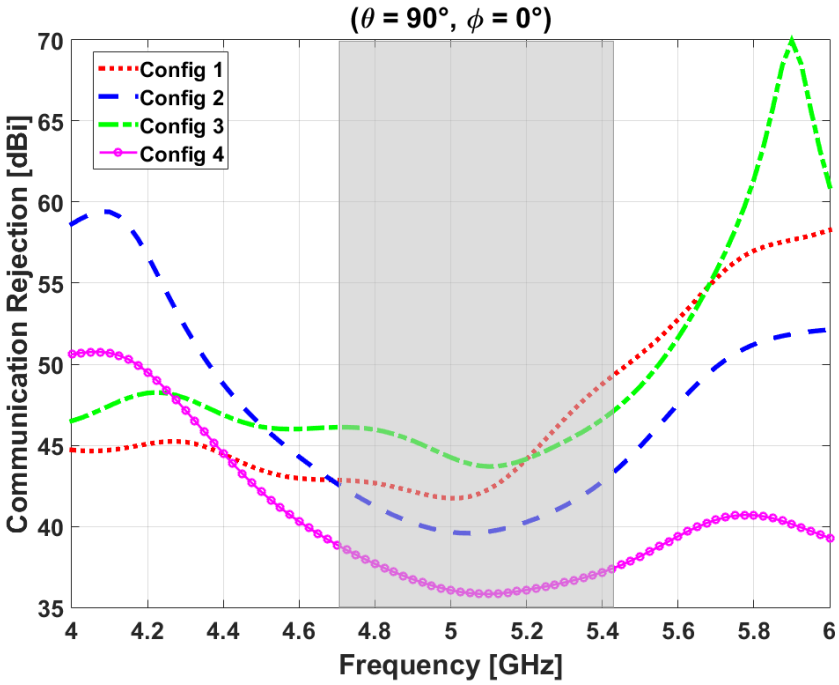

Figure 3. 26: Communication rejection in the radar direction (θ = 90°, ϕ = 0°)

The reflection coefficient of the four configurations are depicted in Figure 3.27 and as can be seen it is below -14 dB from 4 GHz to 6 GHz.

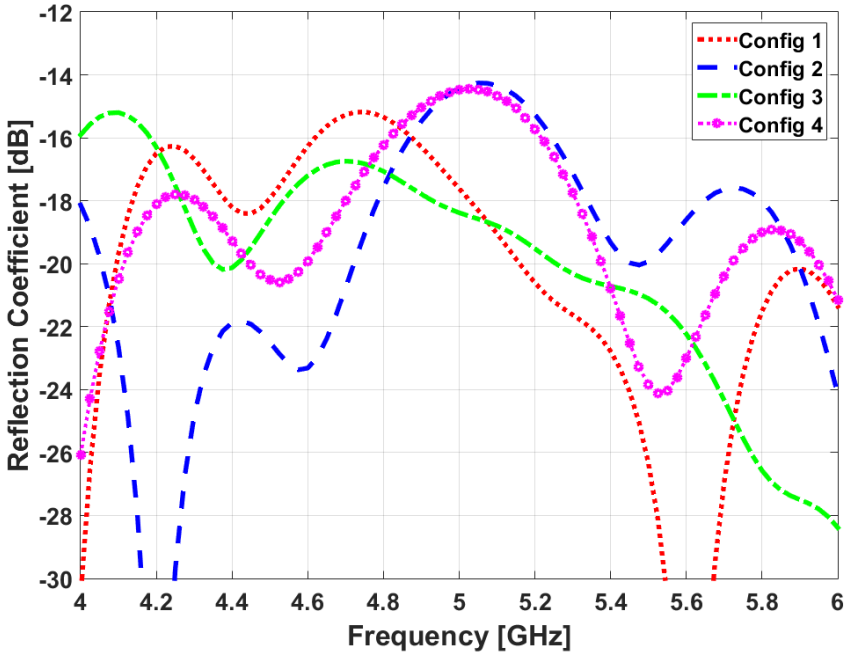

Figure 3. 27: Reflection coefficient of the four configurations

3.3.3. Conclusion

This section allowed us to study the possibility to use another modulation (QPSK) for the antenna system. By spacing the slot by $\lambda_g/4$ we are able to generate a 90° phase shift between the four configurations defined for this study. However, the phase error reaches 5.3° and the gain variation is 0.57 dB in the worst case. By computing the EVM taking into account the constellation, we obtain 10%, which is acceptable for applications using QPSK modulation. The radar rejection obtained at 5 GHz for this antenna system is 9.94 dB in the worst case at θ = 0°. This rejection could be further increased by using a corrugated horn which presents low side lobes. Concerning the communication rejection, it is at least 35 dB in the worst case ensuring a good isolation at (θ = 90°,ϕ = *0*). The study on the slot -3 dB gain bandwidth shows a radar rejection of 2.13 dB in the worst case limiting the operating bandwidth of the antenna system.

3.4. Conclusion of chapter 3

The possibility to add more flexibility to the communication function of the antenna system consisting of a horn antenna fed by a slotted waveguide has been studied in simulations. Compared to the previous version of this antenna, the number of slots has been doubled resulting in the capability to transmit the communication signal in four different directions with direct BPSK modulation. The EVM computation gives -23.2 dB which is acceptable for applications using BPSK modulation. The new structure combines two different concepts: either the communication signal is transmitted in orthogonal polarization and direction to the radar system (as in the previous version, θ = 0° and 180°) or it uses phase-modulation of the radar side lobes at (θ = 90°, ϕ = 90°) and (θ = 90°, ϕ = -90°)). By this way, the two functions do not interfere. The radar and communication rejection are 10 dB and 40 dB respectively.
In order to increase the slot directivity (communication function) while keeping the BPSK capabilities, 5 slots-array was used in the waveguide increasing the gain by 3.63 dB compared to the case with one slot. The study on the slot array -3 dB gain bandwidth demonstrates that the system is stable over 348.68 MHz with at least 1.16 dBi gain for the communication function at θ = 0°. Additionally, the rejections of radar and communication functions in the same bandwidth are respectively 8.49 dB and 48 dB in the worst case, ensuring a good isolation between the two functions.
A QPSK modulation was also performed by changing the slots arrangement in the feeding waveguide. The constellation obtained in simulations is close to theory with 5.3° phase error. The EVM calculation gives 10%, which is acceptable for applications using QPSK modulation. This phase error could be corrected by adjusting the slot spacing in the waveguide. Concerning the radar rejection, it is 9.94 dB in the worst case and could be increased by using corrugated horn.
To finish, the set of solutions presented in this chapter can be directly integrated to existing radar systems using a horn by only replacing the feeding waveguide.

[1] Robert E. Collin, “Aperture-Type Antenna,” in Antennas and Radiowave Propagation, USA: McGraw-Hill, 1985, pp. 265-273.

[2] Michael D. McKinley, Kate A. Remley, Maciej Mylinski, J. Stevenson Kenney, Dominique Schreurs, and Bart Nauwelaers. “EVM Calculation for Broadband Modulated Signals”. Technical Report, 2005. Work of United States Government.

[3] Apostolos Georgiadis, Christos Kalialakis, “Evaluation of Error Vector Magnitude due to Combined IQ Imbalances and Phase Noise” IET Circuits, Devices & Systems, vol.8, issue: 6, pp. 421-426, Dec. 2014.

[4] IEEE Standard for Wireless LAN Medium Access Control (MAC) and Physical Layer (PHY) Specifications: High-Speed Physical Layer in the 5 GHz Band, IEEE Standard 802.11aTM-1999.

[5] IEEE Standard for Wireless LAN Medium Access Control (MAC) and Physical Layer (PHY) Specifications: Higher-Speed Physical Layer Extension in the 2.4 GHz Band, IEEE Standard 802.11b- 1999.

[6] Lou Frenzel, “Understanding Error Vector Magnitude”, Electronic design, pp. 42-46, Jul. 2013.

[7] Sarra Rebhi, Rim Barrak and Mourad Menif, “A Multistandard and Multiservice Radio over Fiber System for Next Generation Networks” 5th International Conference on Multimedia Computing and Systems (ICMCS), Marrakech, Morocco, 29 Sep - 01 Oct, 2016.

[8] Sandeep Kowlgi, Paul Mattheijssen, Corinne Berland and Tim Ridgers, “EVM Considerations for Convergent Multi-Standard Cellular Base-Station Transmitters” IEEE 22nd International Symposium on Personal, Indoor and Mobile Radio Communications, Toronto, Canada, 11-14 Sep. 2011.

[9] R. E. Lawrie and L. P. Jr, “Corrugated horn antenna,” U. S. patent 3 631502, Oct. 21, 1965.

Chapter 4: Experimental Validation of the Multifunction Antenna System

4.1. Introduction

In this chapter, it is proposed to validate the multifunction antenna concept presented in chapter 2 through a full characterization supported by experimental measurements. Hence, the performance of the antenna system in terms of radiation and rejections between the two functions will be investigated to evaluate the robustness of the proposed system.

First, in section 4.2, a description of the antenna prototype and the measurement chamber is carried out. In section 4.3, comparison between simulated and measurement results is done in order to validate the concept. To finish, in section 4.4, a switching mechanism consisting of PIN diodes is realized in order to dynamically control the communication function of the proposed antenna system. The impact of such equipment on the antenna system is also investigated.

4.2. Antenna prototype and measurement chamber

This section details the antenna prototype that has been built as well as the near field chamber and the measurements configurations.

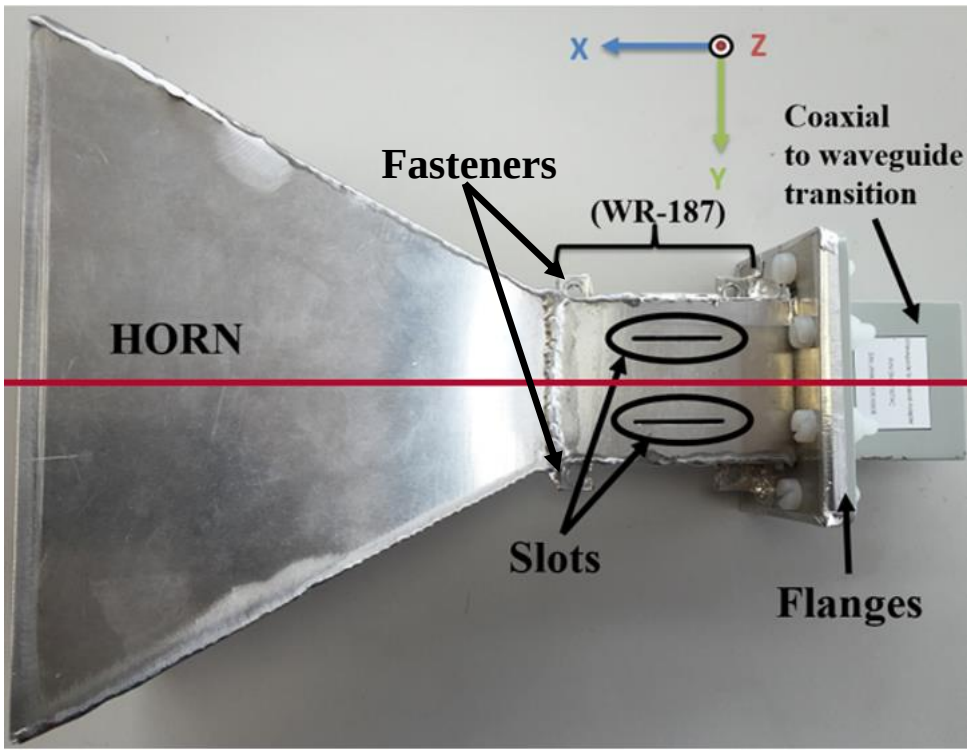

Figure 4. 1: The multifunction antenna: prototype

4.2.1 Antenna prototype

The prototype of the fabricated antenna is shown in Figure 4.1. We recall that the considered system is composed of a horn antenna fed through a single waveguide. The horn antenna is used to radiate a directive beam in the *x*-direction for radar purposes. Here, a couple of slots is milled in the top face of the input waveguide. For the direct BPSK modulation, a switching mechanism will be used in the last section to activate one of the slots at a given time. A fraction of the power in the feeding waveguide is then radiated through the activated slot thus providing a communication link in the *z*-direction.

The fabricated antenna is made of AG3 with a thickness of 2 mm. The WR-187 (cf. Appendix 2) waveguide (47.55 x 21.15 mm^2) operating from 3.95 GHz to 5.85 GHz is used to feed the antenna system. Thus, the slot length was readjusted to be resonant at 5 GHz while taking into account the real thickness of the metal but also the flanges of the transition. Indeed, as already explained, in the previous chapters all simulations have been carried out with FEKO assuming zero thickness for the metallic walls.

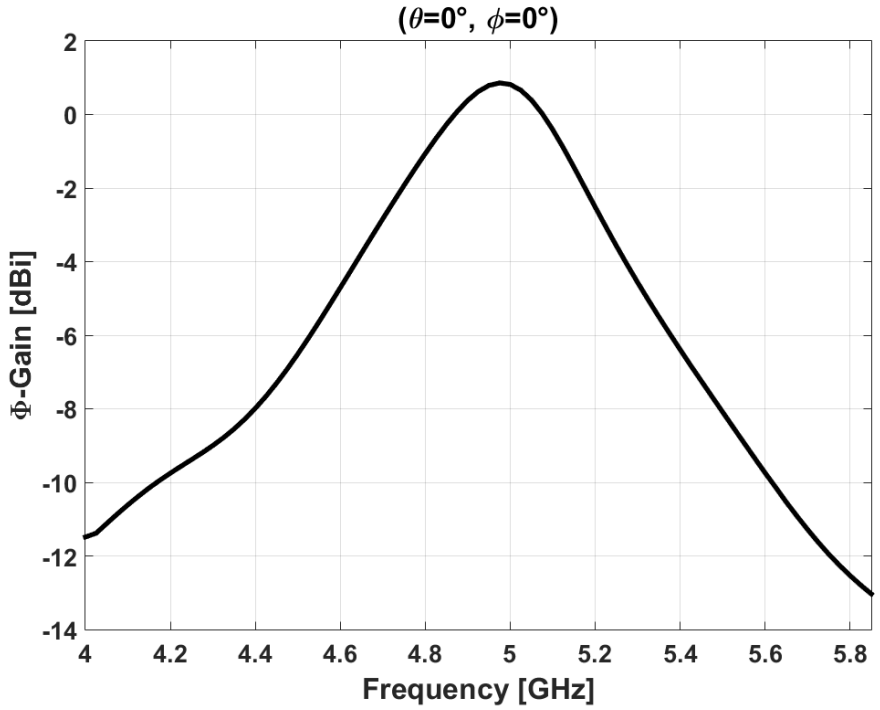

Figure 4. 2: ϕ-gain (one slot radiation) versus frequency

Figure 4.2 depicts one slot radiation (ϕ-gain) versus frequency for a slot of length L = 29 mm l = 1.5 mm placed at D = 12.5 mm from the waveguide centerline. As can be seen, a maximum radiation (0.66 dBi) is obtained at 5 GHz. Hence, for the remainder of the study, L = 29 mm (instead of 25.6 mm in previous chapters).

In order to fix the antenna to the measuring support, four fasteners are placed on the lateral sides of the waveguide as shown in Figure 4.1.

In the next section the measurement environment will be presented.

4.2.2. Measurement chamber

All the measurements of the antenna have been realized in the near field chamber, SATIMO STARGATE (working from 800 MHz to 6 GHz) at INSA Rennes. A scheme and a picture of this chamber are given in Figure 4.3.

The antenna under test is placed in the center of the arch thanks to a support made of PVC positioned on a rotating platform. The platform rotates from 0° to 180° in the azimuth plane. Thanks to crossed probes placed on the arch and each spaced by 10.59°, we are able to measure the different polarizations of the antenna under test from 0° to 360° in elevation plane. As a result, the radiated field is obtained over a spherical scan.

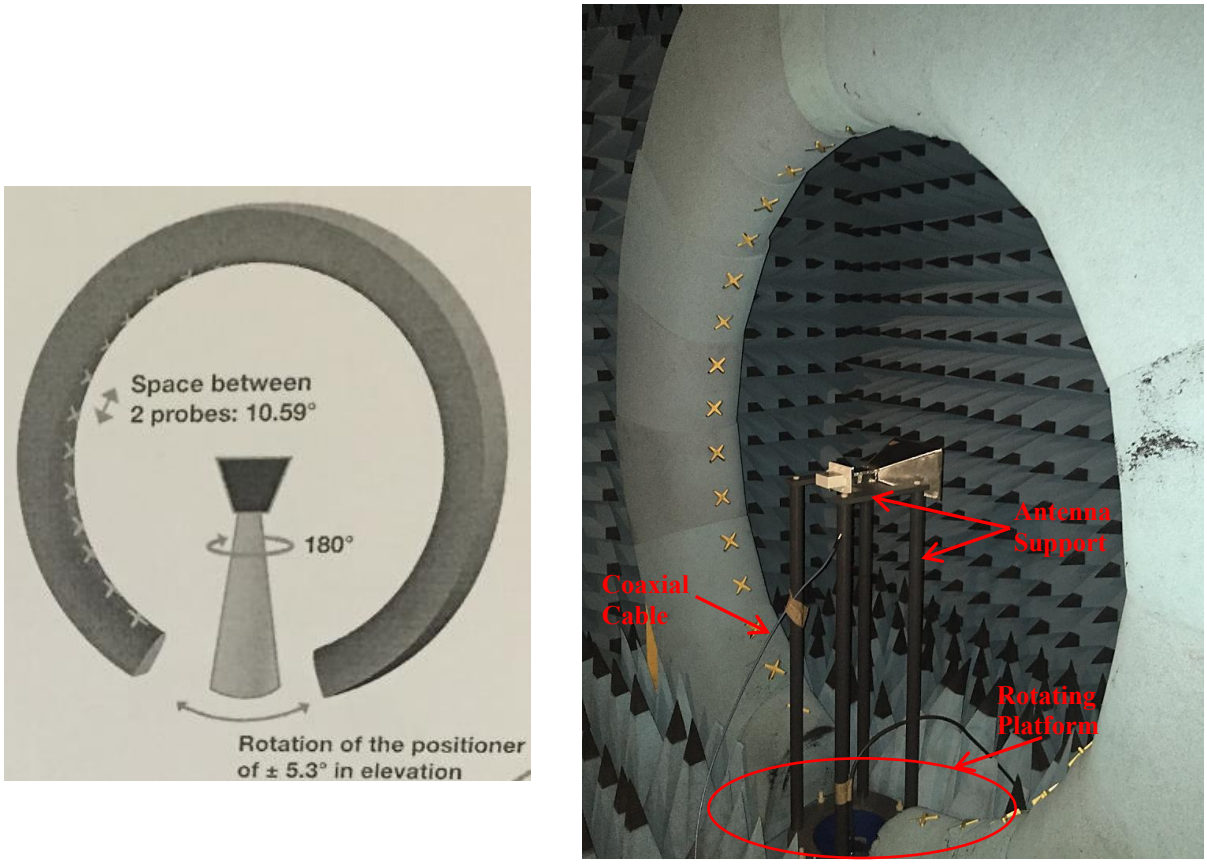

(a) (b)

Figure 4. 3: (a) scheme and (b) picture of the SATIMO STARGATE near field chamber at INSA Rennes

After presenting the antenna prototype and the measurement environment, in the next section the measurement results will be compared to those of simulations to validate the multifunction antenna system.

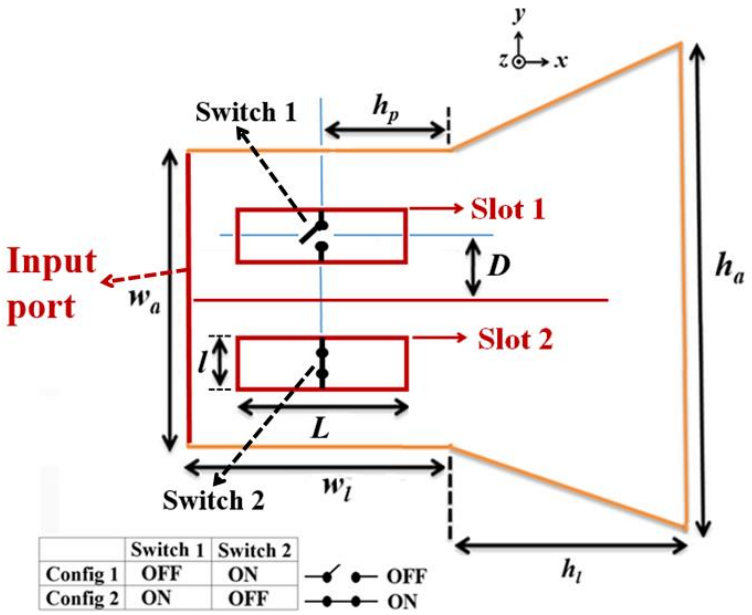

Figure 4. 4: Antenna configurations

4.3. Comparison of simulated and measured results

In this part of the chapter, a comparison of measured results and simulated results (considering the metal thickness) is made to validate the proposed solution. Since the resonance frequency of the slot is 5 GHz, the measurements are performed from 4 GHz to 5.85 GHz. We recall that the recommended operating bandwidth of the feeding WR-187 waveguide is 3.95 GHz to 5.85 GHz.

As in previous chapters, in the present case, we did not implement a real switching mechanism, only the activated slot is present, the others being completely closed with PEC in simulations and metal ribbon for measurement. This defines two complementary configurations (cf. Figure 4.4).

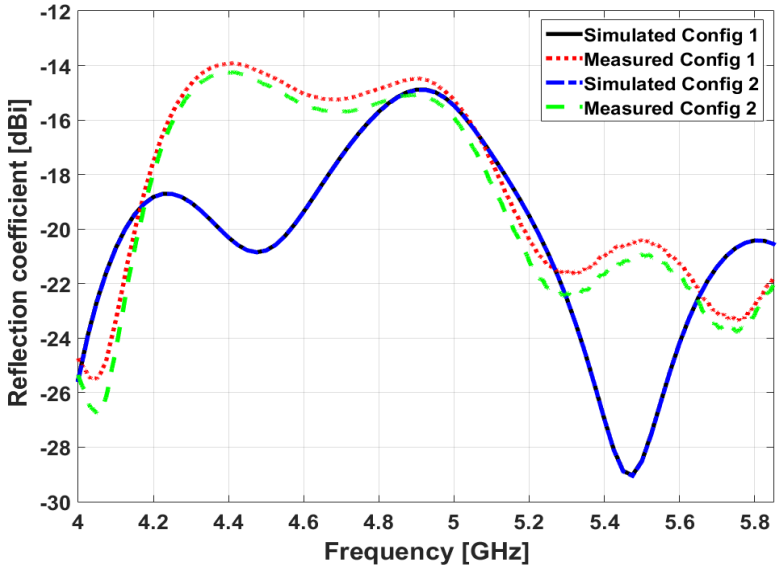

Figure 4. 5: Comparison of measured and simulated reflection coefficient of the two configurations

4.3.1. Reflection coefficient

We first investigate the reflection coefficient of the antenna system. Figure 4.5 shows a comparison of simulated and measured reflection coefficients of the two configurations. As can be seen, the measured and simulated results are in good agreement at 5 GHz (operating frequency of the antenna). However, between (4.2 GHz - 4.8 GHz) and (5.3 GHz - 5.85 GHz) there are some differences due to manufacturing uncertainties. Nevertheless, for all the studied configurations, the measured and simulated reflection coefficient is below -14 dB from 4 to 5.85 GHz.

4.3.2. Radiation characteristics

4.3.2.1. Configuration 1

We now investigate the radiation patterns of configuration 1. The simulated and measured gains at 5 GHz for configuration 1, in respectively xOz and xOy planes are plotted in Figure 4.6 and Figure 4.7. It can be observed that θ-gains in simulation and measurement are in good agreement in the two planes. However, maximum θ-gain is 14.96 dBi for measurement and 15.9 dBi for simulation (0.94 dB variation). Furthermore, in xOz plane, there is the appearance of oscillations in the side lobes region (θ-gain). These modifications in comparison to simulation may be due to the measurement environment and the manufacturing uncertainties.

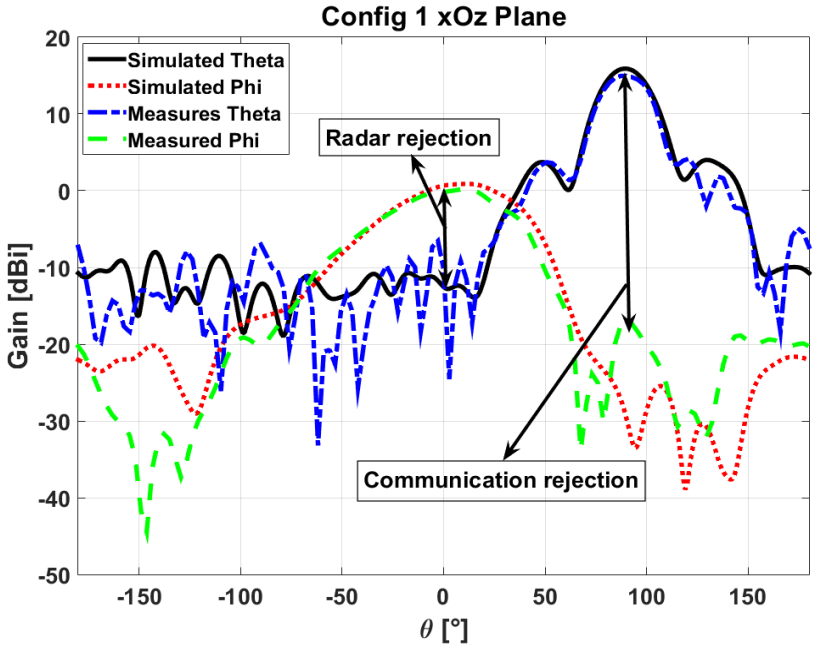

Figure 4. 6: Measured and simulated radiation patterns at 5 GHz of configuration 1 in xOz plane

In order to find the origin of these oscillations, this time the simulations take into account the antenna support (in PVC), the coaxial cable and the rotating platform (cf. Figure 4.3 (b)).

Figure 4.8 depicts the radiation patterns at 5 GHz in xOz plane of configurations 1. In fact, we can see that the oscillations are strongly related to the reflection of the wave on the rotating platform (in metal) although it was covered with absorber. Figure 4.9 depicts the position and dimensions of the rotating platform used for the simulation.
The antenna support and the coaxial cable add some marginal modifications.

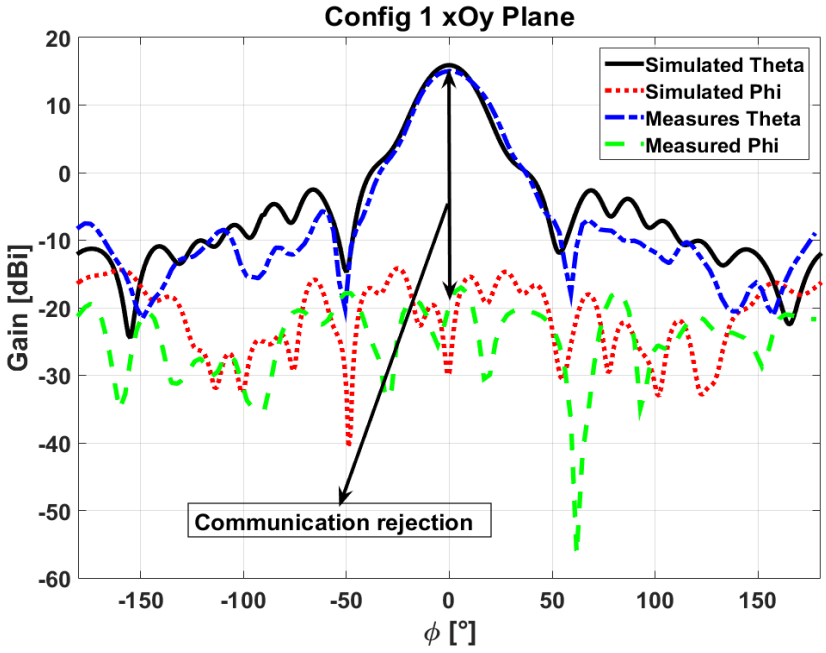

Figure 4. 7: Measured and simulated radiation patterns at 5 GHz of configuration 1 in xOy plane

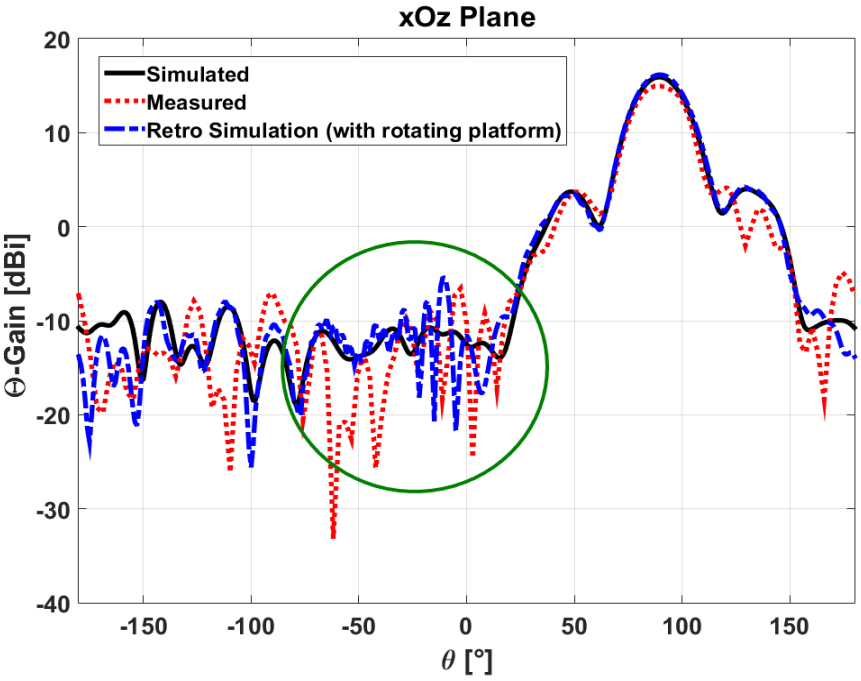

Figure 4. 8: Measured results of configuration 1 and simulated results of the measurement environment

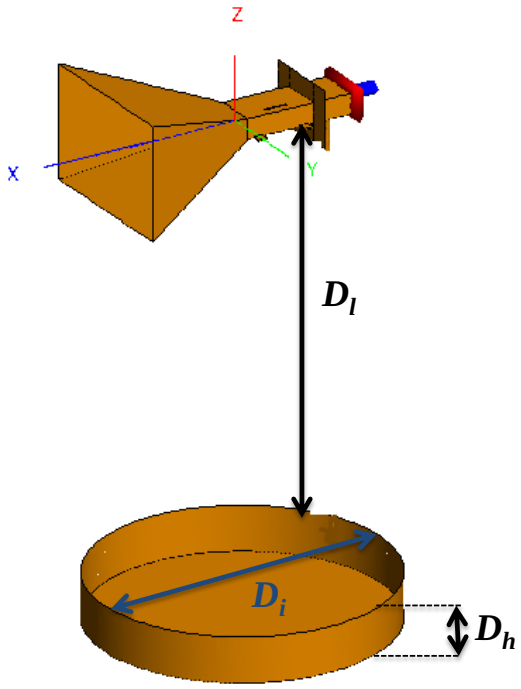

Figure 4. 9: Retro simulation with rotating platform: D_l = 858 mm, D_i = 323 mm, D_h = 50 mm

Concerning the ϕ-gains, in xOz plane (cf. Figure 4.6), simulated and measured results present the same behavior for θ = [-50°, 50°] (corresponding to the ϕ-gain main lobe). However, as could be expected, due to the appearance of oscillations in the side lobes region, the radar rejection at θ = 0° (corresponding to communication direction) has been reduced by 3.5 dB compared to simulation (cf. Table 4.1). Nevertheless, at θ = 90° (radar direction) the communication rejection is still high (32 dB), cf. Table 4.1.

	Simulations		Measures	
	Rejection at θ = 0°	Rejection at θ = 90°	Rejection at θ = 0°	Rejection at θ = 90°
Configuration 1	13 dB	45 dB	9.5 dB	32 dB

Table 4. 1: Simulated and measured radar and communication rejections of configurations 1 at 5 GHz

The good isolation between radar and communication at θ = 90° is confirmed by the low level of ϕ-gain in xOy plane (Figure 4.7).

4.3.2.2. Configuration 2

This time the radiation patterns of configuration 2 is studied. Figure 4.10 and Figure 4.11 present the results of configuration 2 in respectively xOz and xOy plane at 5 GHz. Due to the symmetry between the two configurations, the same results as configuration 1 are expected. However, in the

main direction of the horn dedicated to the radar function the gain variation in comparison to simulation is 0.82 dB (0.12 dB lower than configuration 1). This slight variation is due to manufacturing uncertainties.

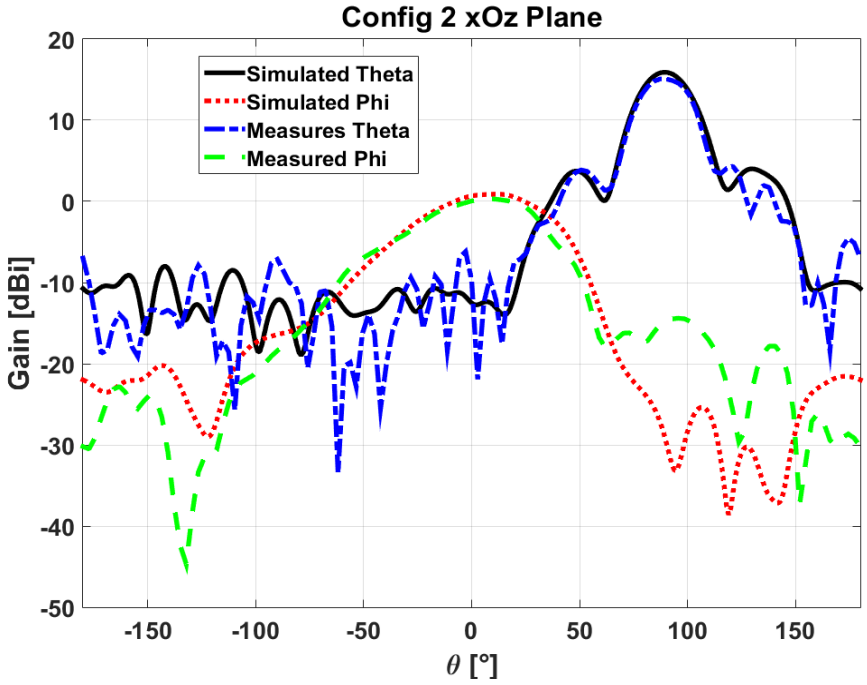

Figure 4. 10: Measured and simulated radiation patterns at 5 GHz of configuration 2 in xOz plane

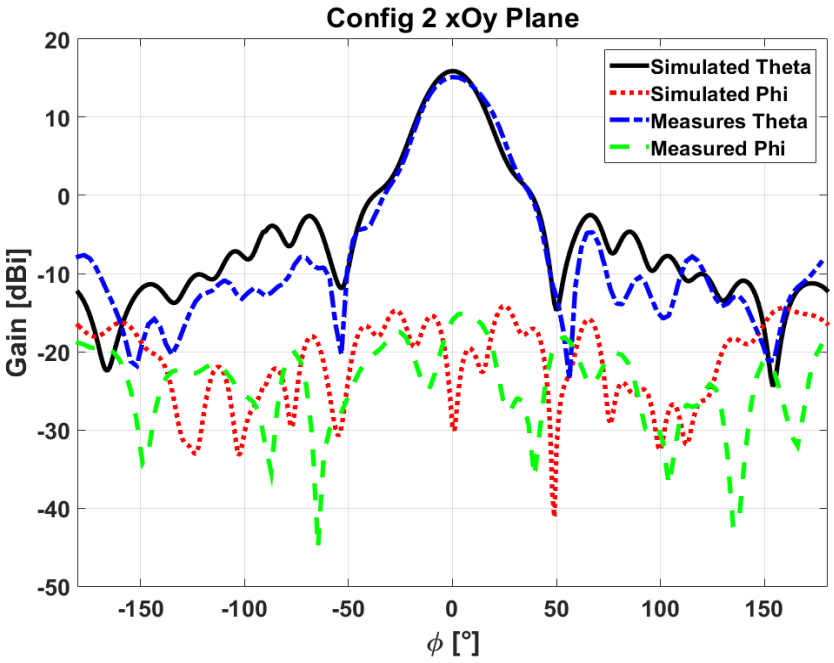

Figure 4. 11: Measured and simulated radiation patterns at 5 GHz of configuration 2 in xOy plane

As already explained, in xOz plane, the oscillations in side lobes region (θ-gain) are also due to the measurement environment. As for configuration 1 these oscillations result in a degradation of the rejection at $\theta = 0°$ in comparison to simulations (cf. Table 4.2).

	Simulations		Measures	
	Rejection at $\theta = 0°$	Rejection at $\theta = 90°$	Rejection at $\theta = 0°$	Rejection at $\theta = 90°$
Configuration 2	13 dB	45 dB	9. 1 dB	30 dB

Table 4. 2: Simulated and measured radar and communication rejections of configurations 2 at 5 GHz

These first results on the two configurations show that measurements and simulations are in quite good agreement. However, there are some modifications due to measurement environment that affect the radiation patterns in particular the side lobes region in xOz plane where some oscillations can be observed. This leads to a degradation of the radar rejection at $\theta = 0°$ (reduction of 3.9 dB in comparison to simulation in the worst case). Nevertheless, the communication rejection at $\theta = 90°$ is at least 30 dB in measurement at 5 GHz.

In the next section we investigate the measured results of the two configurations for the multifunction antenna purposes.

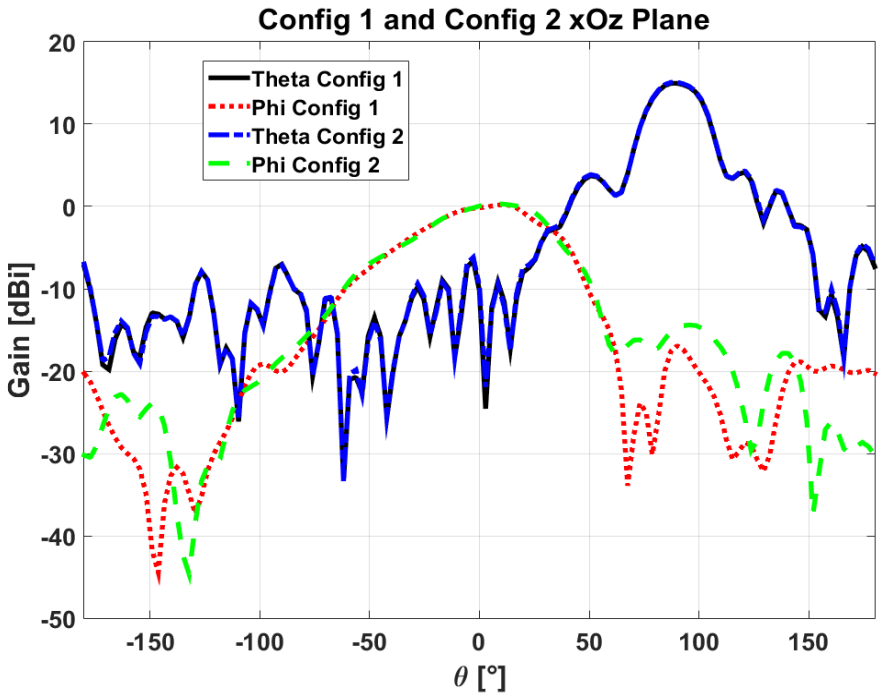

Figure 4. 12: Measured θ and ϕ-gains at 5 GHz of the two configurations in xOz plane

4.3.3. The multifunction antenna

In order to perform the multifunction antenna providing simultaneously the radar function and direct BPSK communication, it is important for us to compare the results of the two configurations to ensure that when switching occurs, we keep the same performances. In this section, only measured parameters of the two configurations are investigated.

Figure 4.12 and Figure 4.13 present the measured results of the two configurations in respectively xOz and xOy plane at 5 GHz. The main beam of the horn antenna (θ-gain), used for radar function is identical for the two configurations in the two planes, which guarantees the radar radiation is not affected when switching the configurations. This criterion is very important for the radar application.

In xOy plane, as already explained in previous chapters, the slots contribute to z-polarization resulting in the modification of the side lobes level. Nevertheless, the SLL remains lower than -19 dB, which is acceptable for many radar applications. We can also note that the two curves present a mirror symmetry at $\phi = 0°$ due to the activation of one slot.

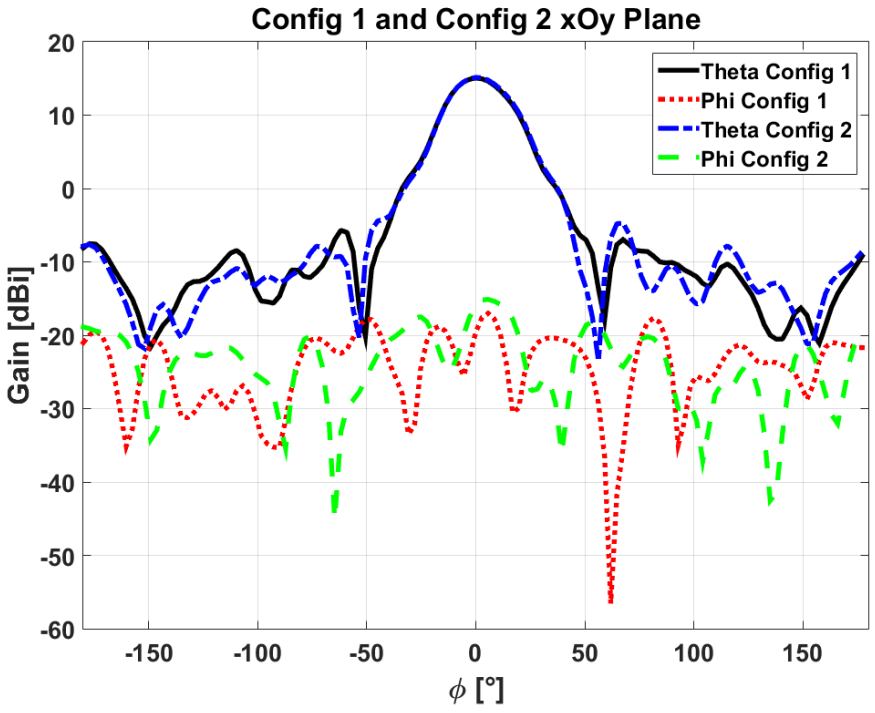

Figure 4. 13: Measured θ and ϕ-gains at 5 GHz of the two configurations in xOy plane

Figure 4.14 presents the measured θ-gains at ($\theta = 90°$, $\phi = 0°$) corresponding to the main direction of the horn versus frequency. As expected the two configurations present the same behavior. At 5 GHz corresponding to the resonant frequency of the slot, the gain decreases due to the leakage in the slot for the communication function.

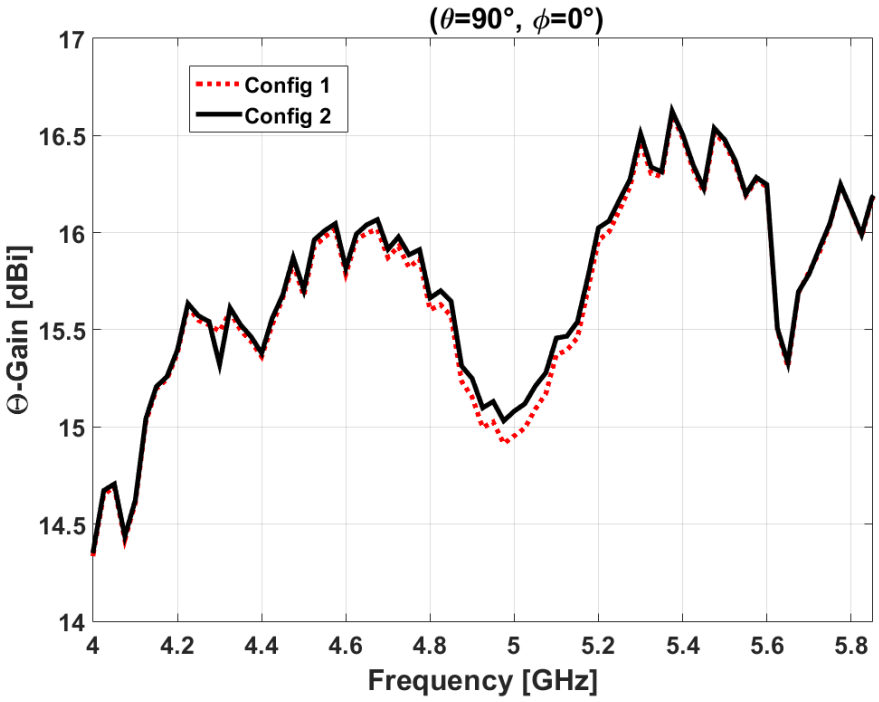

Figure 4. 14: Measured θ-gain of the two configurations in the main direction of the horn versus frequency

Concerning the communication radiation (ϕ-gain), as expected, in xOz plane (cf. Figure 4.12) the two curves are identical in the slot main lobe. This characteristic allows us to transmit information at $\theta = 0°$.

Table 4.3 depicts the characteristics of the direct BPSK modulation at 5 GHz in $\theta = 0°$ direction. To see the impact of the slight gain difference between the configurations (0.06 dB), as in chapter 3, we calculate the EVM. In this case, using the information in Table 4.3, the EVM is 3.53% (-29.04 dB), cf. Appendix 1 for EVM calculation. In literature, the EVM limit for BPSK modulation is - 7 dB [1], showing that the gain difference between the configurations does not affect the antenna operation.

Directions	Config	Phase (°)	Amp. (dBi)
$\theta = 0°$	1	0	-0.22
	2	180	-0.16

Table 4. 3: Measured BPSK modulation at 5 GHz

Figure 4.15 presents the measured ϕ-gains at $\theta = 0°$ (corresponding to the communication direction) of the two configurations versus frequency. The -3 dB bandwidth of the communication function is 440 MHz (from 4.77 GHz to 5.21 GHz). In this frequency range the difference between the ϕ-gains

is 0.3 dB in this worst case. As already explained, this is due to measurement environment and manufacturing uncertainties.

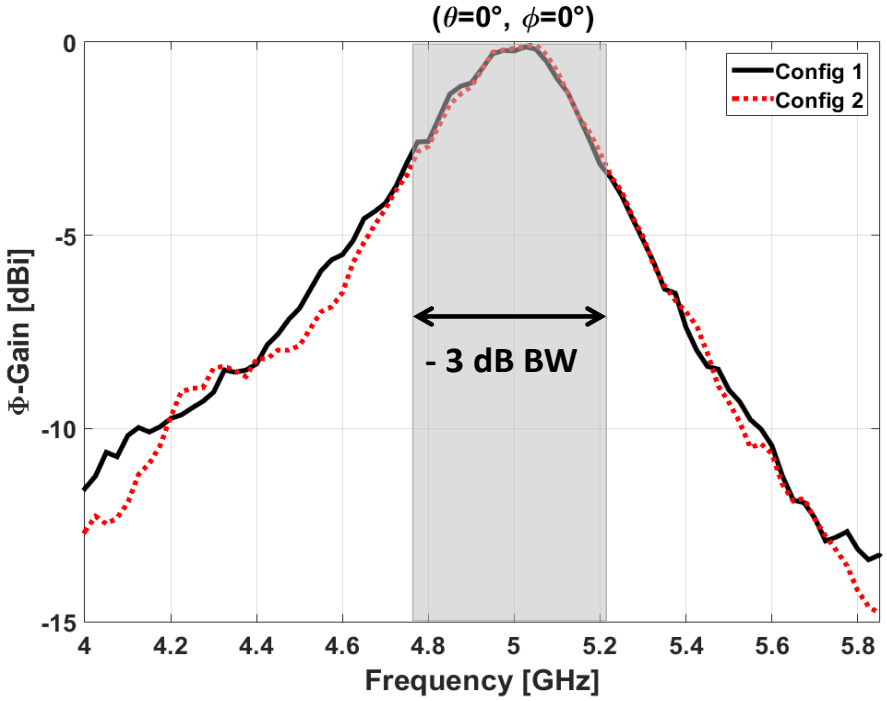

Figure 4. 15: Measured ϕ-gains of the two configurations in the communication direction versus frequency

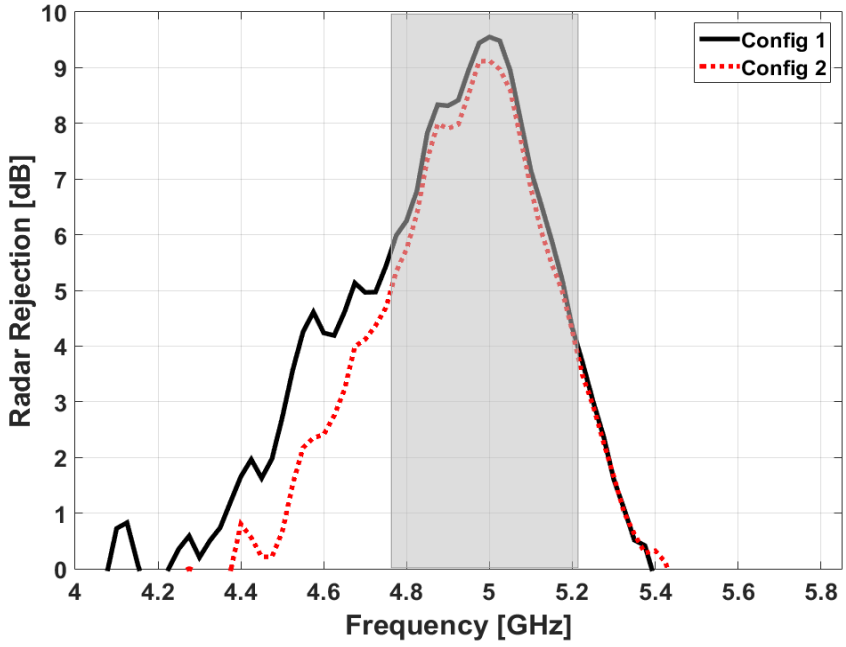

Figure 4. 16: Radar rejection at θ = 0°

In order to evaluate the robustness of the antenna system, radar and communication rejections are studied from 4 GHz to 5.85 GHz.

We first investigate the rejection in the communication direction. Figure 4.16 compares the measured radar rejection of the two configurations. At 5 GHz, it is 9.1 dB in the worst case. However, when going away from the center frequency, the value decreases, reducing the operating bandwidth of the antenna system. As already explained in previous chapters, this could be improved by using for example a corrugated horn, which presents much lower side lobes than the standard horn.

Concerning now the communication rejection at (θ = 90°, ϕ = 0°), cf. Figure 4.17, always considering the same bandwidth, it is greater than 25 dB, ensuring the isolation of the two functions in this direction.

The comparison between the simulated results of the two configurations allowed us to verify that when switching the activated slot, both configurations 1 and configuration 2 give the same radiation patterns. This is essential for the multifunction antenna system to work properly. However, due to measurement environment and manufacturing uncertainties, the rejections between the two functions have been reduced, in particular at θ = 0° (3.9 dB in comparison to simulation). At θ = 90° the rejection is still high (30 dB) to ensure the isolation between the two functions in this direction.

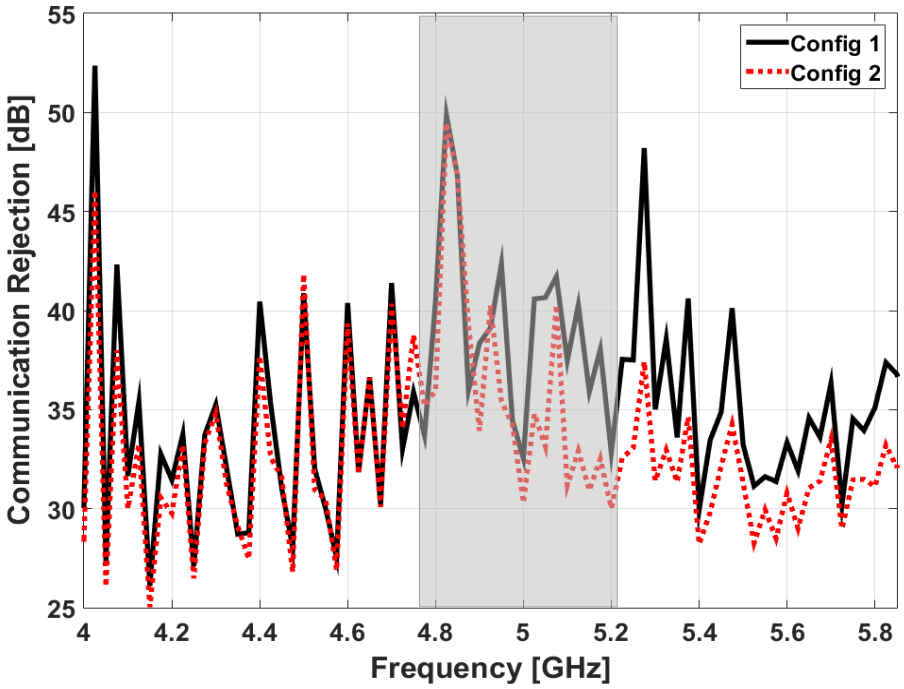

Figure 4. 17: Communication rejection at θ = 90°

4.3.4. Conclusion

This first part allowed us to experimentally validate the multifunction antenna system providing simultaneously a radar function and a direct BPSK modulation consisting of a horn antenna whose feeding waveguide is loaded with slots. Moreover, the results show that measurements and simulations are in good agreement. However, the measurement environment affects the radiation patterns, in particular the side lobes region where some oscillations can be observed, reducing the radar rejection at $\theta = 0°$ by 3.9 dB in comparison to simulation. As already explained, the rejection in this direction can be further increased by using a corrugated horn which presents low side lobes. Nevertheless, when switching the activated slot, the two configurations give the same radiation patterns, ensuring that the two functions are not affected.

In order to dynamically control the slot activation and the BPSK modulation, in the next section we study the impact of a switching mechanism on the antenna system.

4.4. Switching mechanism concept

In order to dynamically control the slots radiation and then the communication function, it is proposed in this section to design a switching mechanism using PIN diode as in [2] [3] to validate the antenna concept.
In general, a switching mechanism consisting of PIN diode may be designed by using either a single series or shunt connected PIN diode [2]. In our case we will focus on the design of series connected diode because it is simple to implement and presents a minimum insertion loss over a broad frequency range [2]. As we will see in the next paragraphs, two kinds of diodes will be considered for this study: beam lead PIN diodes and packaged PIN diodes. All the loading diodes are simulated using CST.

4.4.1. Beam lead diode

In this section we investigate the possibility to use a beam lead PIN diode to control the slots radiation. In fact, beam lead devices offer low parasitic elements, small size and work up to 20 GHz. In this study, the DSM8100-000 Mesa beam lead PIN diode (0.89 mm long and 0.28 mm wide) will be considered because of its low capacitance and low resistance (cf. Appendix 3). From the manufacturer's data sheet, this diode can be modeled as a 3.5 Ω resistance when forward biased and as a 0.025 pF capacitor when reverse biased.

4.4.1.1. Ideal switches

We now investigate the impact of these resistance and capacitor on the antenna radiation. In a first step, to simplify the study, the switching is performed by loading the slots with the beam lead PIN diode (without polarization circuit). More precisely, the slots will be only loaded by the beam lead PIN diode resistance of 3.5 Ω in forward bias to short circuit the slots (ON mode) and by its 0.025 pF capacitor in reverse bias for radiating slots (OFF mode).

In order to better understand the impact of this elements on the antenna, we will first consider the ideal configuration 1 of the antenna system as shown in Figure 4.4 where slot 2 is closed with PEC. Slot 1 will be successively loaded by the beam lead PIN diode capacitor and resistance.

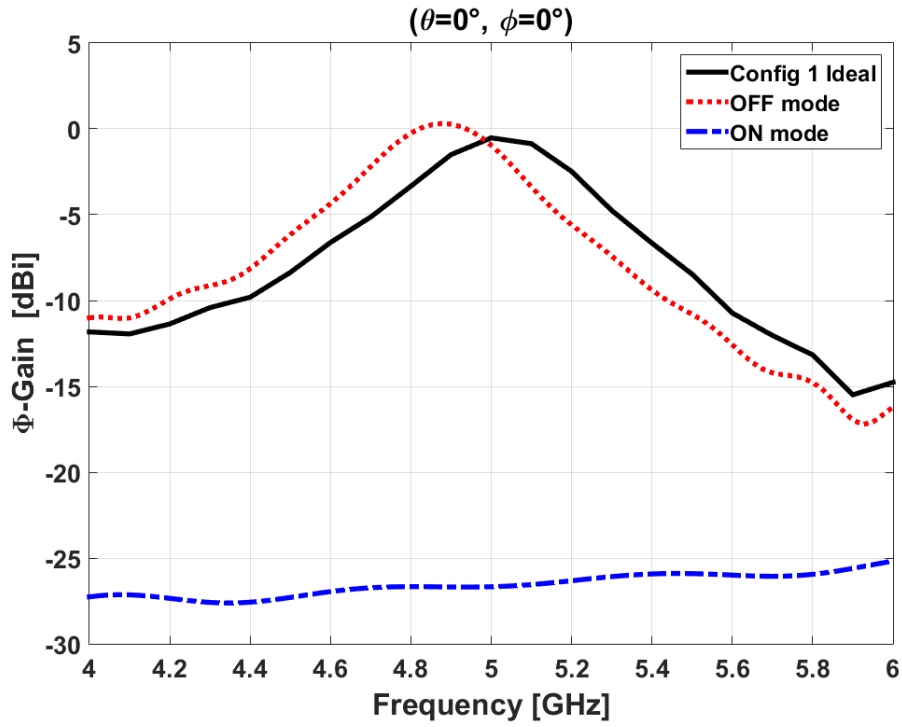

Figure 4. 18: Comparison between ideal configuration 1 (ϕ-gain) and ON and OFF mode at (θ = 0°, ϕ = 0°) versus frequency

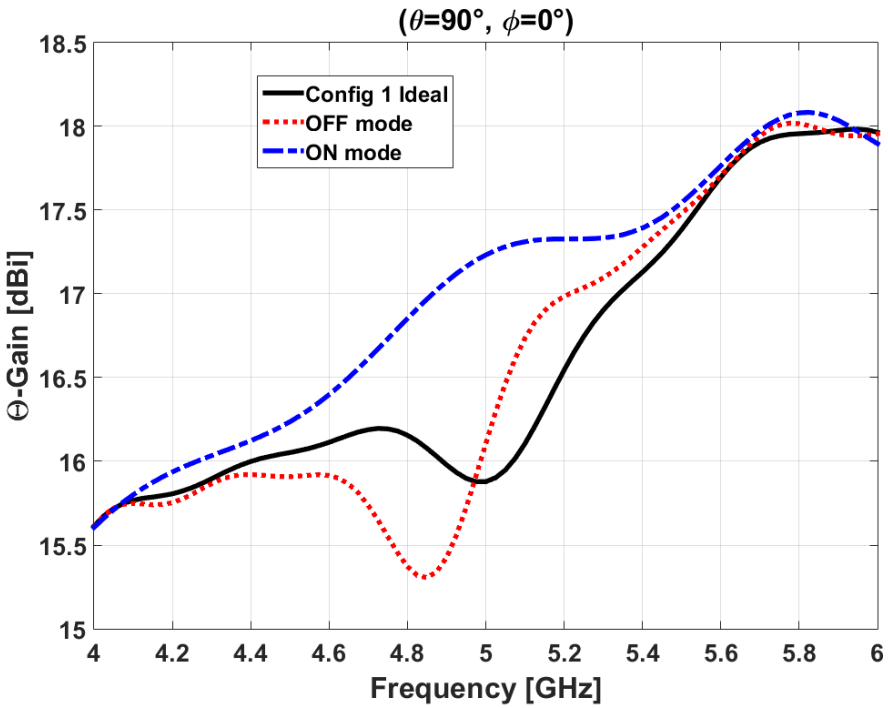

Figure 4. 19: Comparison between ideal configuration 1 (θ-gain) and ON and OFF mode at (θ = 90°, ϕ = 0°) versus frequency

Figure 4.18 depicts the slot gain (ϕ-gain) at (θ = 0°, ϕ = 0°) versus frequency when slot 1 is loaded with the diode characteristics. For comparison purposes the gain of configuration 1 without loaded elements (configuration 1 ideal) is also given. As expected, with the capacitor (OFF mode) we find the same characteristics as for a radiating slot. However, we note that the resonance frequency of the slot is shifted to 4.87 GHz due to this capacitor.
Concerning the gain of the slot loaded with the diode resistance (ON mode), it is very low as expected (below -25 dB). In fact, the major part of the current in the vicinity of the slot flows in the resistance (3.5 Ω), then short-circuiting the slot. The gain difference between OFF and ON modes is 27 dB at 4.87 GHz.

We now investigate the gain in the main direction of the horn (cf. Figure 4.19). As expected, due to the diode capacitor, the gain drop in the horn (due to the power radiated by the slot) is also shifted in frequency whereas with the loaded resistance there is no gain drop because the slot does not radiate.

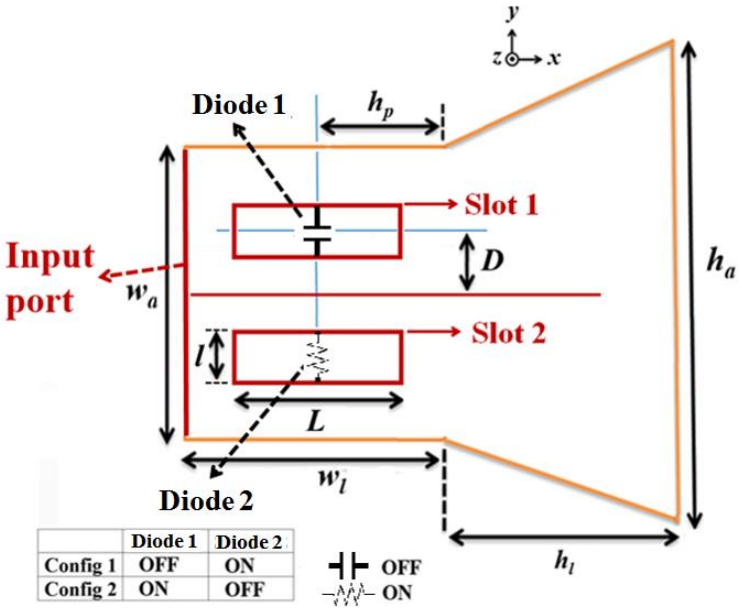

Figure 4. 20: Configurations of the antenna system when loaded with the beam lead PIN diode capacitor and resistance

In order to draw relevant conclusions for this first study, we now consider the case where one slot is loaded by the diode capacitor and the second one by the diode resistance. As in previous chapter, this leads to two opposite configurations (cf. Figure 4.20). In configuration 1 only slot 1 (loaded by the diode capacitor, OFF mode) radiates while slot 2 (loaded with the diode resistance, ON mode) does not radiate. Configuration 2 corresponds to the reverse situation.

Figure 4.21 and Figure 4.22 depict respectively the slot gain at (θ = 0°, ϕ = 0°) and the horn gain at (θ = 90°, ϕ = 0°) versus frequency for the two configurations. As expected, due to the symmetry in xOz plane (cf. Figure 4.20) the two configurations give exactly the same gain.

This first study on the beam lead diode shows that it is possible, by loading diode resistance and capacitor to the slot to control its radiation. However, in radiating mode (OFF mode of the diode), the resonance frequency of the slot is shifted to 4.87 GHz due to the diode capacitor. At the new

resonance frequency, the gain difference between OFF and ON modes is 27 dB. In the next section, to dynamically control the slots radiation we will investigate the diode polarization circuit.

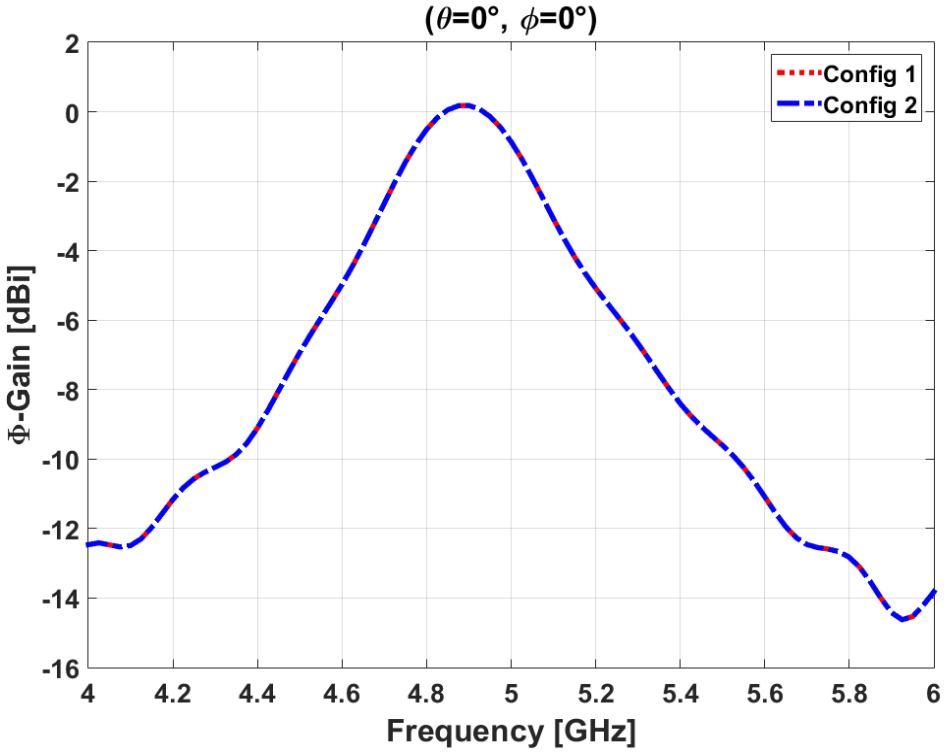

Figure 4. 21: Slot radiation (ϕ-gain) of the two configurations at (θ = 0°, ϕ = 0°) versus frequency

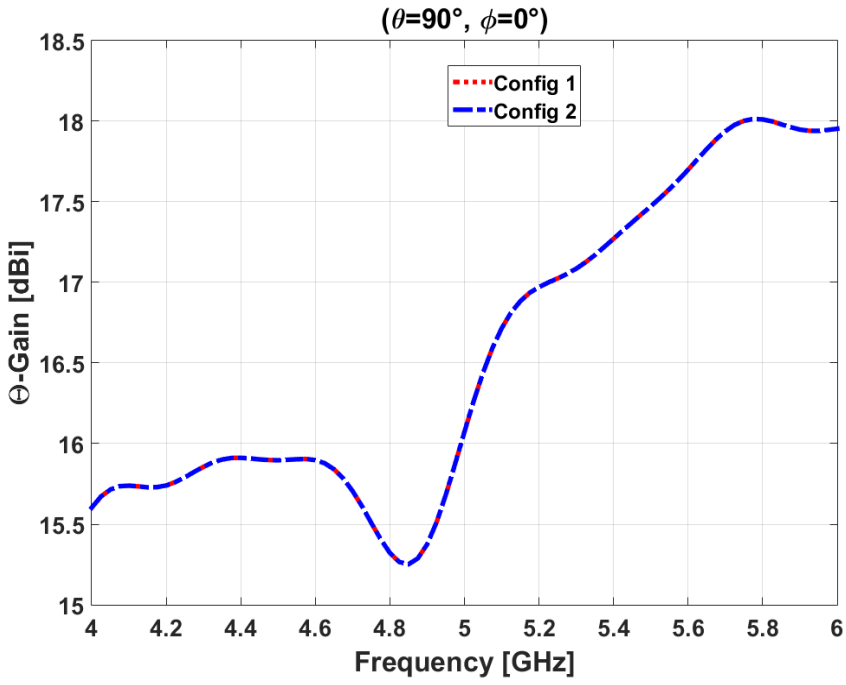

Figure 4. 22: Horn radiation (θ-gain) of the two configurations at (θ = 90°, ϕ = 0°) versus frequency

4.4.1.2. Diode polarization circuit

It is proposed here to design the polarization circuit of the beam lead PIN diode to provide a dynamic control of the slot radiation. We will also investigate the possibility to integrate this circuit on the already available antenna (cf. Figure 4.1).

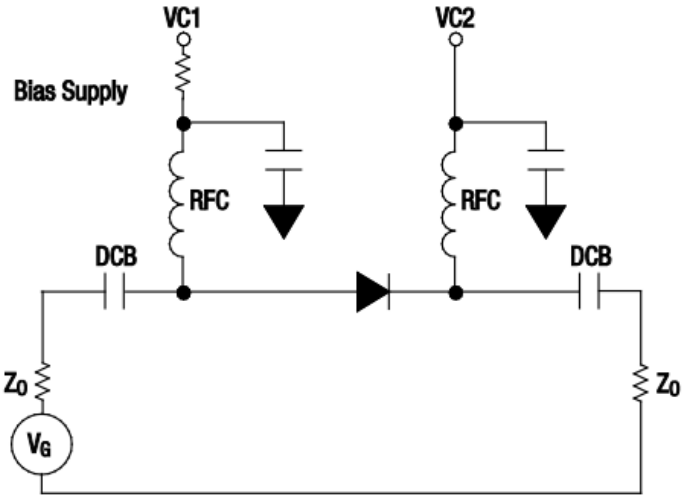

Figure 4. 23: Series connected PIN diode switch [2]

- **Circuit design**

Figure 4.23 depicts an equivalent circuit for a typical implementation of a series PIN diode switch [2]. A special polarization circuit is needed to isolate the DC bias current from the RF. This avoids the RF current to flow into the DC voltage source. In this figure, DCB (blocking capacitor) prevents the DC bias current from reaching the RF part, and RFC (RF choke) provides a path for the DC bias current while blocking the RF signal to reach the DC power supply.

In order to realize the polarization circuit based on series connected PIN diode (cf. Figure 4.23), we have designed an *H*-shaped circuit as depicted in Figure 4.24 which will be placed above the slot. The double-sided circuit was realized on 500 µm thick Rogers RO4003C substrate with ε_r = 3.38, tan δ = 0.0027, and copper thickness of 35 µm.
In this figure, the beam lead diode is located in the bottom face of the circuit, on the small portion (a) connecting the two metalized rectangles (R_l x R_w) forming the *H*-shape. Through two metallized via holes, the two ends of the diode are connected to the two RFC (in top face), which are obtained here by designing two thin $\lambda_g/4$ (9.68 mm at 5 GHz) transmission lines. The circuit also has four smaller pads (numbered from 1 to 4 in the figure) used to connect the $\lambda_g/4$ transmission lines to two 10 pF decoupling capacitors and also to connect the wires for applying the bias to the diode. The circuit was then placed on the waveguide using a 250 µm thick adhesive of permittivity ε_r = 6. Hence, by controlling the dimensions of the two rectangles (R_l x R_w) forming the *H* shape (and then the dimensions of the adhesive) we can adjust the capacitors formed between the waveguide and the bottom-metalized face of the polarization circuit corresponding to the two DCB. In the present

design, the rectangles have a dimension of 23.5 x 6 mm^2, which corresponds to 29.91 pF each. All the dimensions of the circuit are depicted in Appendix 4.

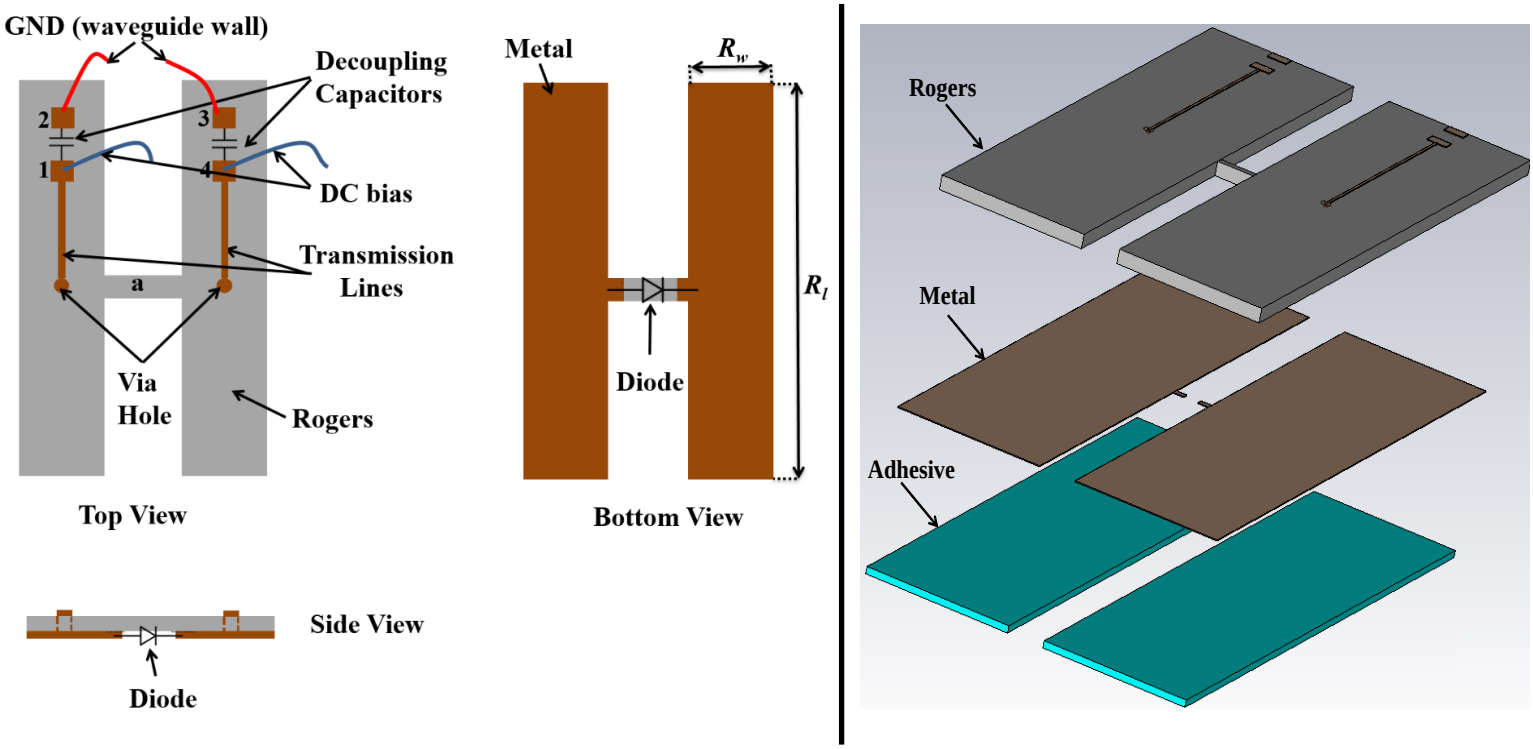

Figure 4. 24: Diode polarization circuit

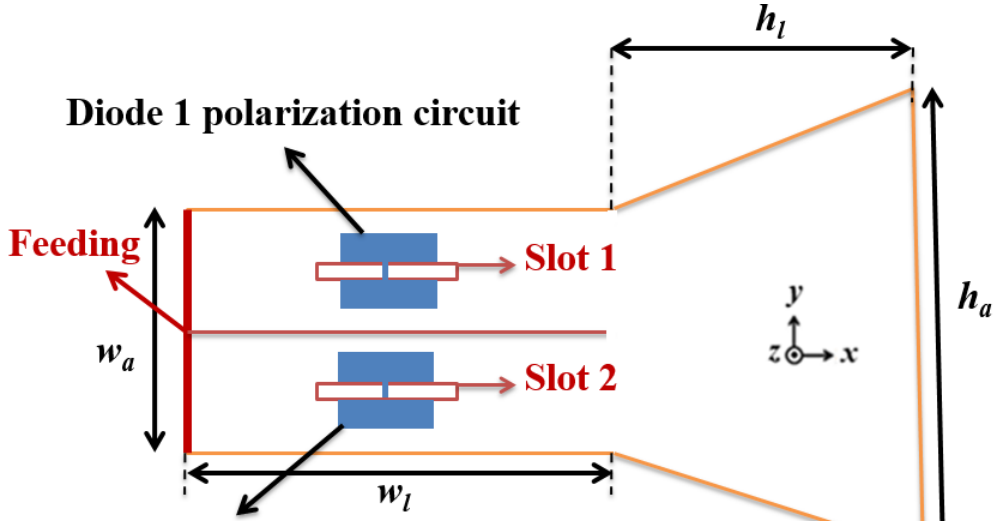

	Diode 1	Diode 2
Config 1	OFF	ON
Config 2	ON	OFF

Figure 4. 25: Configurations of the antenna system with two diode polarization circuits

- **Antenna performance**

We now investigate the impact of the polarization circuit on the antenna performance. As in section 4.4.1.1, in simulations, the diode will be replaced in the forward bias by its resistance (3.5 Ω) and in reverse bias by its capacitor (0.025 pF). Now, the two slots are each equipped with the polarization circuit. Hence the two opposite configurations considered for this study are presented in Figure 4.25. In configuration 1 diode 1 is in OFF mode (reverse biased) while diode 2 is ON (forward biased) and configuration 2 corresponds to the case where diode 1 is ON and diode 2 is OFF.

Figure 4.26 depicts the two configurations ϕ-gain at (θ = 0°, ϕ = 0°) versus frequency. For comparison purposes the ϕ-gain of ideal configuration 1 (without polarization circuit and slot 2 closed with PEC) is also given. As can be seen from this figure, the two configurations give exactly the same radiation pattern due to the symmetry is xOz plane. As already explained, the diode capacitor in OFF mode and the DCB capacitor produce a shift in the slot resonance frequency (4.7 GHz). The - 3 dB gain bandwidth of these slots is 435 MHz.

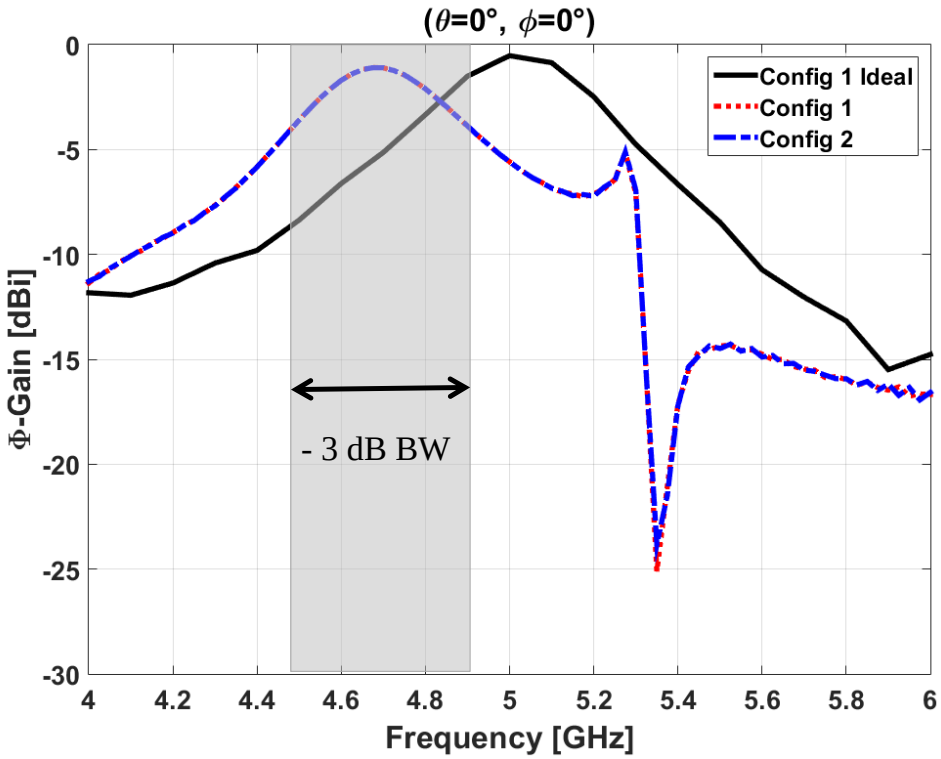

Figure 4. 26: ϕ-gain (slot radiation) of the two configurations versus frequency at (θ = 0°, ϕ = 0°)

Additionally, we also note a peak at 5.3 GHz. This can be explained by looking at the Figure 4.27. The results in this figure are obtained by considering only one slot in the feeding waveguide equipped with the diode polarization circuit (the other being closed with PEC). We note that when the diode is in ON mode, the peak at 5.3 GHz appears whereas in OFF mode it does not appear. This shows that the slot is not short circuited at this frequency by the diode. Thus, returning to the

case of Figure 4.26, where the two slots are equipped with diode polarization circuit (one in OFF mode and the second in OFF), we conclude that the peak at 5.3 GHz is linked to the contribution of the diode in ON mode. Definitely this is not a concern since the peak is outside the bandwidth. Furthermore, the gain drop between OFF and ON modes is 22.84 dB at the resonance frequency.

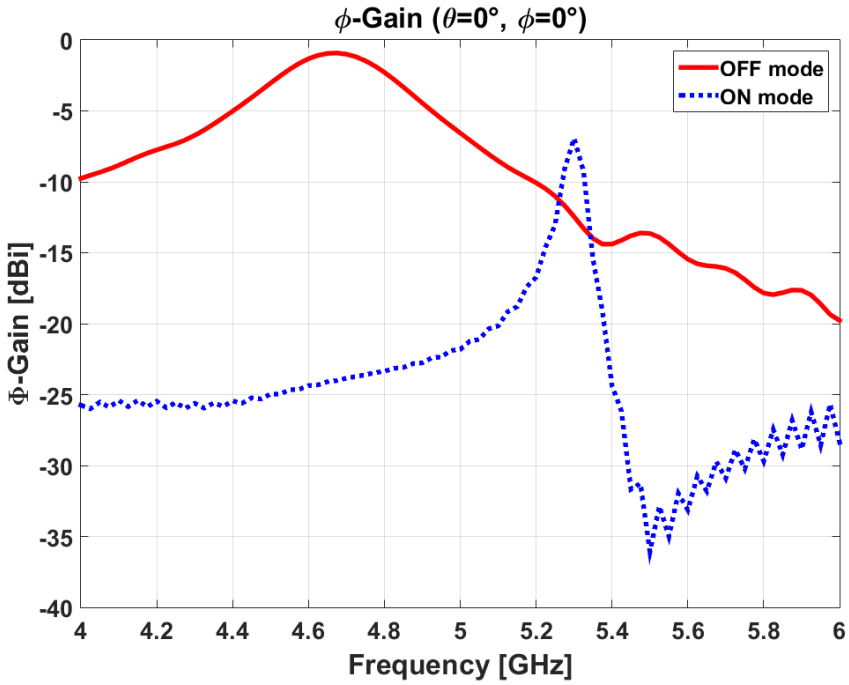

Figure 4. 27: Comparison between ON and OFF mode at (θ = 0°, ϕ = 0°) versus frequency using one polarization circuit

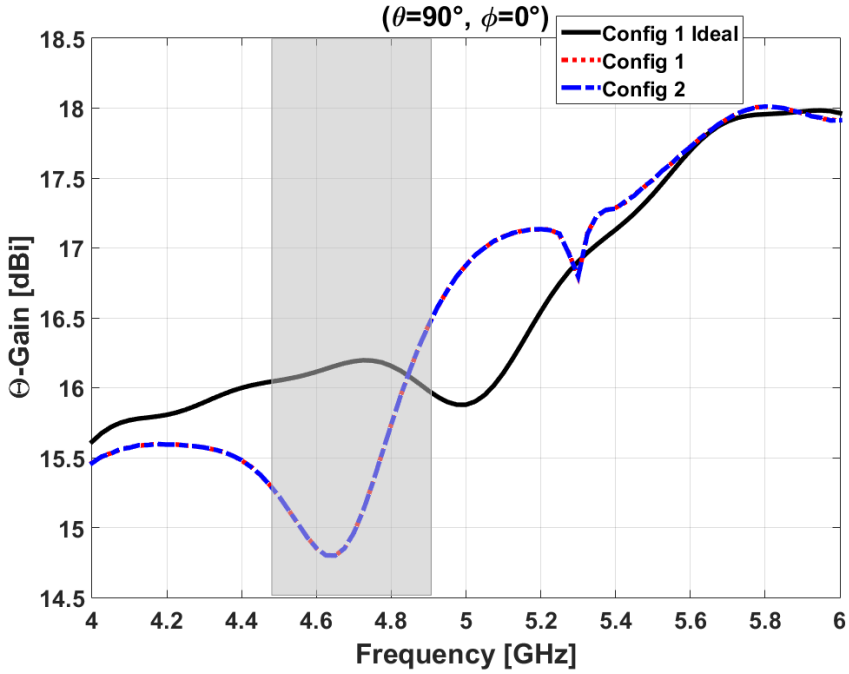

Figure 4. 28: θ-gain (horn radiation) of the two configurations versus frequency at (θ = 90°, ϕ = 0°)

Concerning θ-gain, Figure 4.28 depicts the horn gain in the main direction of the horn ($\theta = 90°$, $\phi = 0°$) versus frequency. As previously the gain is identical for the two configurations. Moreover, the gain drop in the two configurations (due to energy picked up by the slot) is also shifted in comparison to ideal configuration 1.

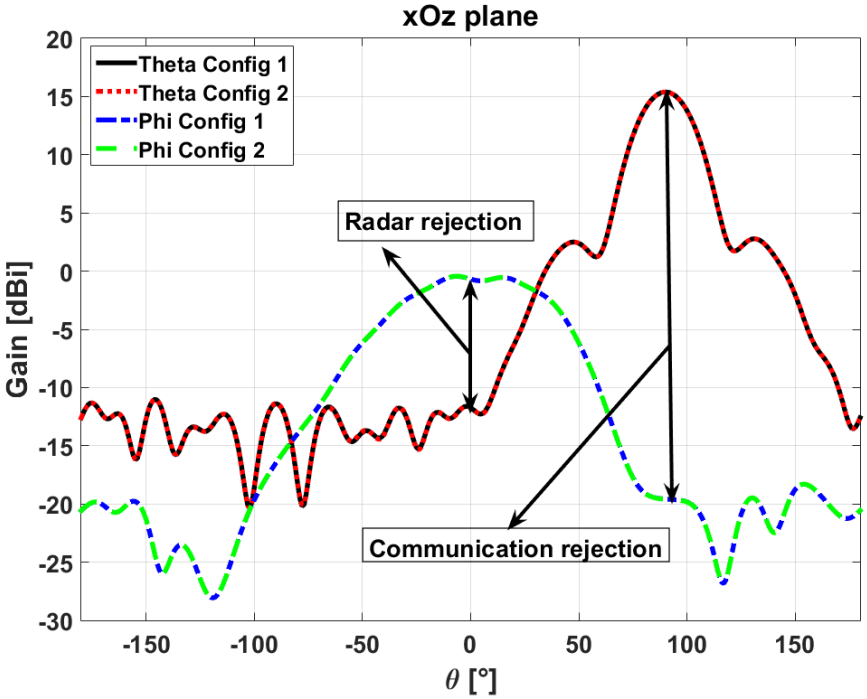

Figure 4. 29: Radiation pattern of the multifunction antenna at 4.7 GHz in xOz plane

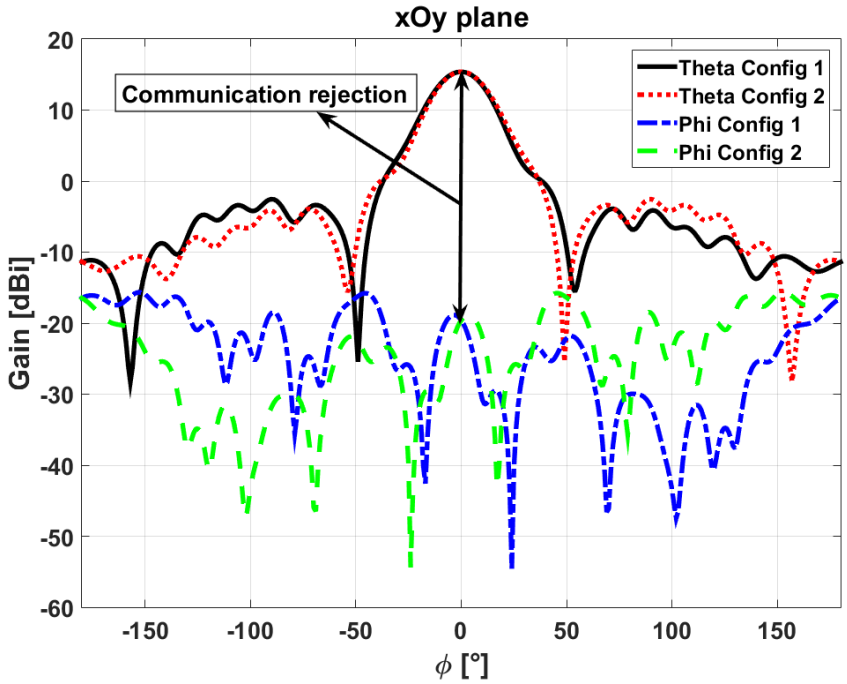

Figure 4. 30: Radiation pattern of the multifunction antenna at 4.7 GHz in xOy plane

The radiation patterns at 4.7 GHz of the two configurations in respectively xOz and xOy plane are given in Figure 4.29 and Figure 4.30.

In xOz plane, due to symmetry both configurations 1 and 2 give exactly the same radiation pattern which guarantees that the radar function (θ-gain at $\theta = 90°$) and the communication function (ϕ-gain at $\theta = 0°$) are not affected when switching the configurations.

In xOy plane, θ-gain is identical in the main direction of the horn. As in previous chapter the slots contribute to z-polarization resulting in the modification of the horn side lobes. Nevertheless, the SLL is -17.93 dB which is acceptable for radar applications.

We now study the rejections between the two functions as defined in Figure 4.29. Figure 4.31 (a) and (b) depict respectively the radar and communication rejections.

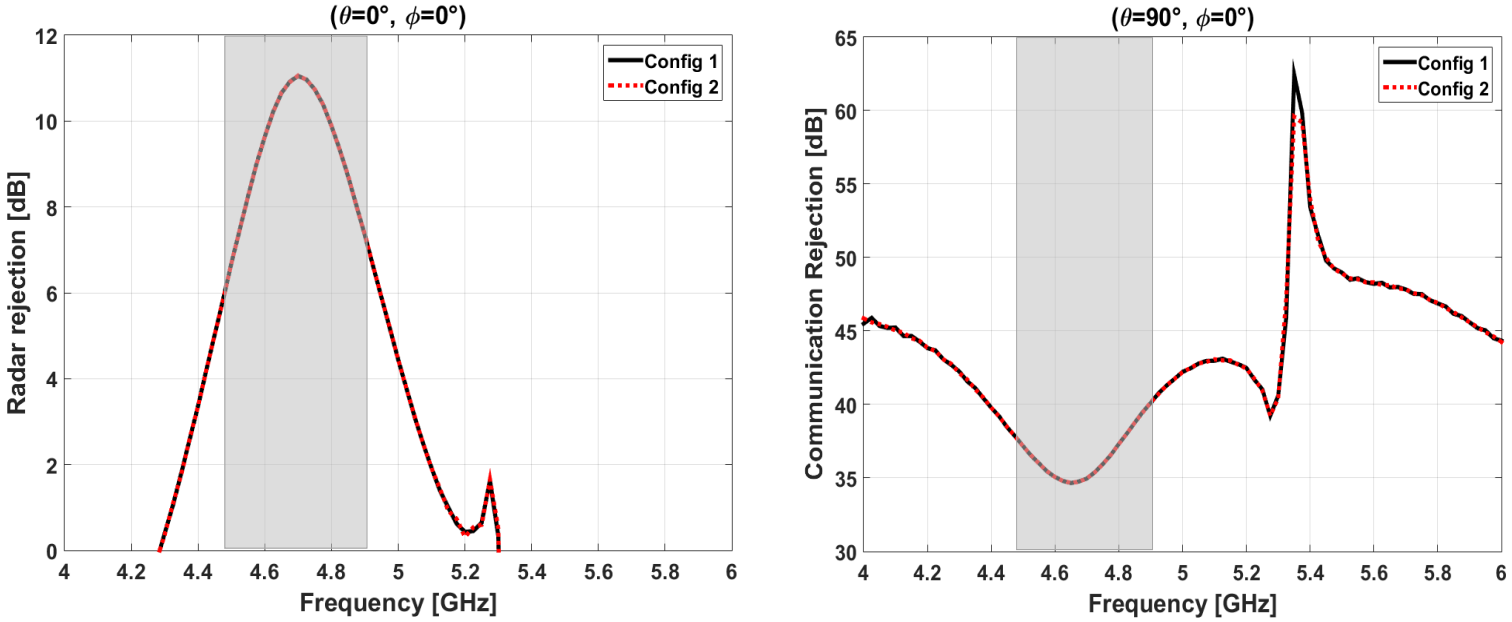

(a) (b)

Figure 4. 31: Radar rejection (a) and communication rejection (b) of the multifunction antenna versus frequency

At the resonant frequency of the slot (4.7 GHz), the radar rejection is 11.06 dB. However, when moving away from this frequency the rejection drops sharply showing a narrow band rejection in this direction.
Concerning the communication rejection it is at least 35 dB ensuring the isolation between the two functions in this direction.

The simulated reflection coefficient depicted in Figure 31 for the two configurations is below -16 dB from 4 to 6 GHz.

This first study using the beam lead PIN diode shows that it is possible, by loading the slot with the beam lead PIN diode resistance (in forward bias) and capacitor (in reverse bias), to control the communication function while keeping the same radiation patterns between the two configurations. In order to provide a dynamic control of the slots radiation, a polarization circuit is then built and integrated to the waveguide thanks to an adhesive. The diode capacitor in reverse bias and the DCB capacitor lead to a new resonance frequency of the slot at 4.7 GHz (instead of 5 GHz). At this resonance frequency, the gain difference between the OFF and ON modes of the diode is 22.84 dB validating the polarization circuit. The radar rejection of this antenna system is 11.06 dB at the resonance frequency and the communication rejection is at least 35 dB, showing a good isolation between the radar and communication functions.

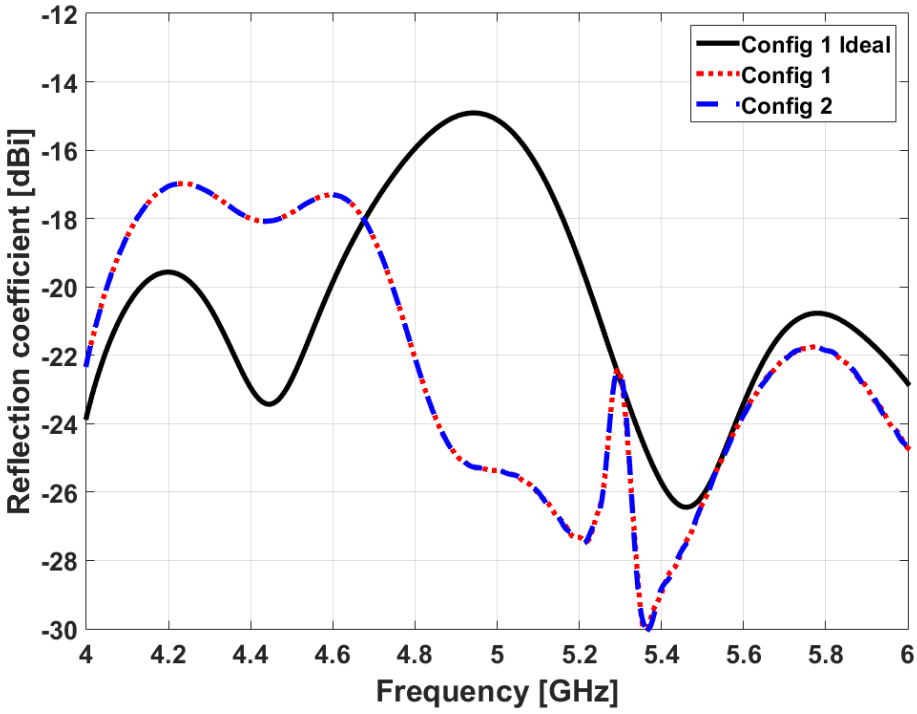

Figure 4. 32: Simulated reflection coefficient of the two configurations of the antenna system

For experimental validation of the antenna system and the polarization circuits, the *H*-shaped circuit was realized. But the very small size of the beam lead diode (0.89 mm long and 0.28 mm wide) requires very restrictive placement and soldering techniques to which we have been confronted without success. We then considered packaged PIN diodes (2.5 mm long and 1.25 mm wide) much simpler to handle than the beam lead PIN diodes. In the next section, we will show the results when using packaged PIN diodes.

4.4.2. Implementation using packaged PIN diode

For this study, we used the HSMP-381Z PIN (cf. Appendix 3) diode that was available in the laboratory. This diode was modeled as a 3Ω resistance when forward biased and a 0.135 pF capacitor when reverse biased. The expected performances are not optimal considering the characteristics of the diode, but the goal is to experimentally validate the concept. Because the value of the capacitor is much larger than the beam lead PIN diode one (0.025 pF), we checked in simulation that the packaged PIN diode could be used with the antenna system. To do so, we only considered one slot in the feeding waveguide loaded with the packaged PIN diode capacitor (reverse bias, corresponding to OFF mode). The other slot is closed with PEC.

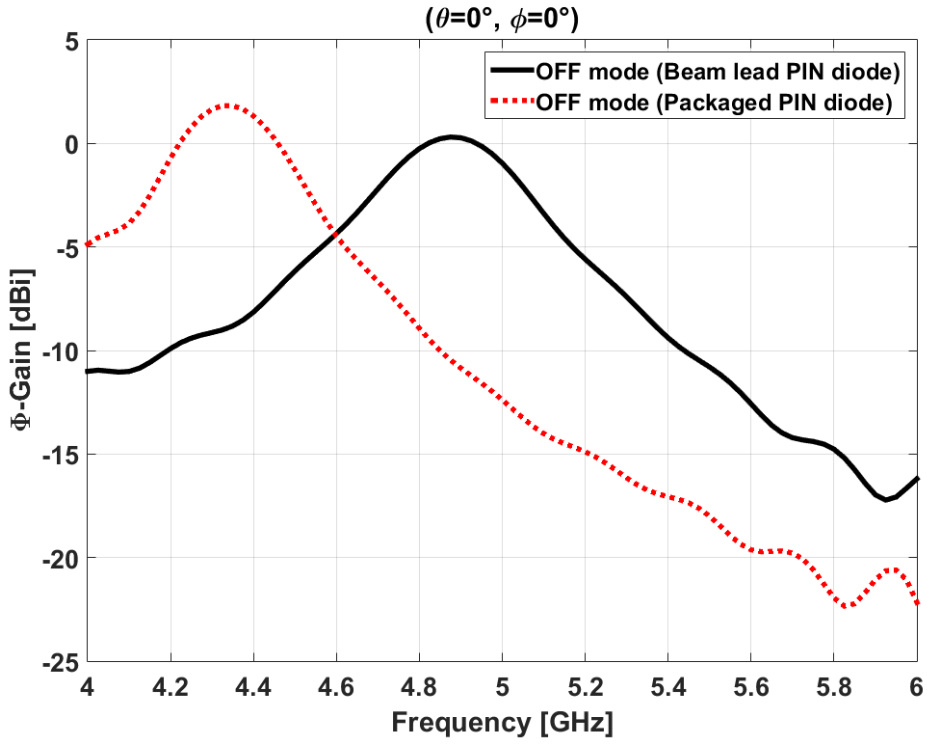

Figure 4. 33: Comparison between the OFF mode of beam lead PIN diode and packaged PIN diode at (θ = 0°, ϕ = 0°)

Figure 4.33 depicts the ϕ-gain of the antenna system at (θ = 0°, ϕ = 0°). As expected, the slot resonance frequency is shifted to 4.33 GHz. This frequency is still supported by the WR-187 waveguide (cut-off frequency of 3.15 GHz) used for this study.

To speed up the process, we now investigate the possibility to reuse the previous polarization circuit. Since the packaged diode is bigger than the beam lead one, we had to place it on the top face of the *H*-shaped circuit, just above the original position of the beam lead diode, cf. Figure 4.34.
For this study, we only considered one slot in the feeding waveguide equipped with the polarization circuit. The other one is closed with PEC.

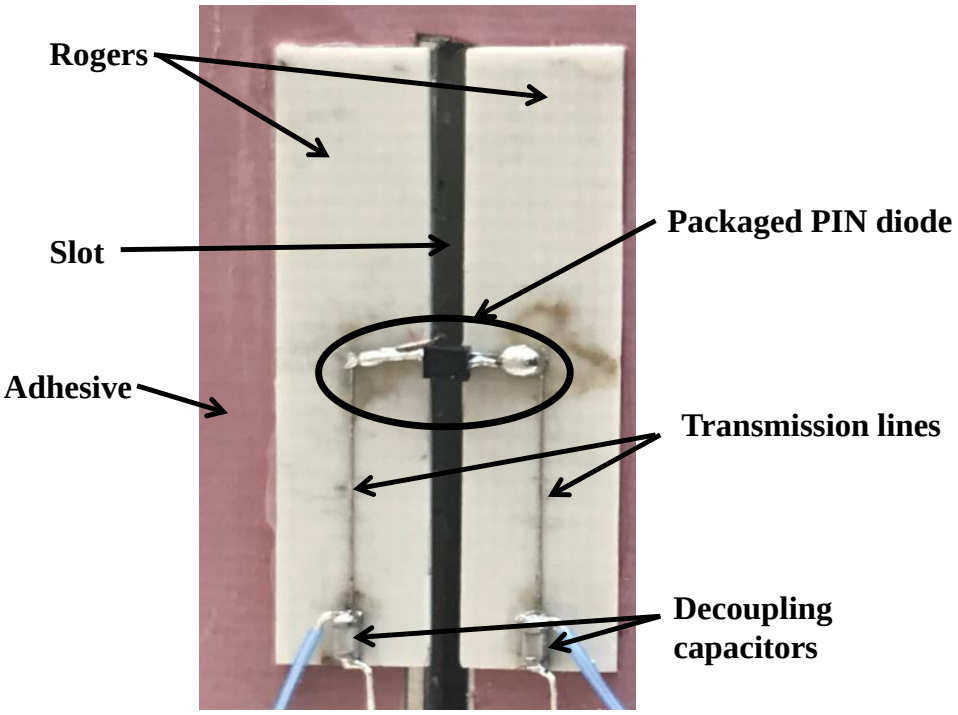

Figure 4. 34: Position of the packaged PIN diode in the polarization circuit

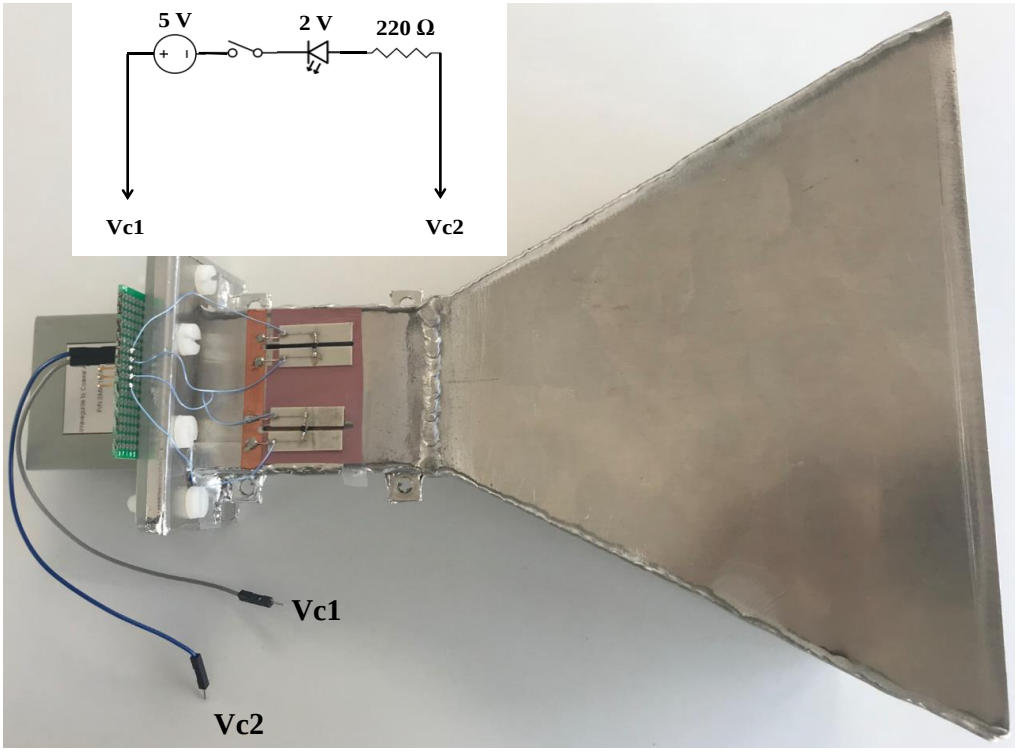

Figure 4. 35: Antenna prototype with packaged PIN diode

We then implemented the antenna system using the packaged PIN diode (cf. Figure 4.35). The feeding structure of the PIN diode is also depicted in Figure 4.35. A 5 V DC voltage source is used to feed the PIN diode along with an interrupter to switch the polarization of the diode. As can be

seen from this figure, a LED (2 V) is used to ensure that the PIN diode is properly operating. In order to control the current flowing through the PIN diode, a 220Ω resistance is added providing 10 mA to the diode. For the measurement, one of the slots is closed with cooper tape (inside of the waveguide).

The antenna was measured in the near field chamber, SATIMO STARGATE (working from 800 MHz to 6 GHz) at INSA Rennes (cf. Figure 4.36).

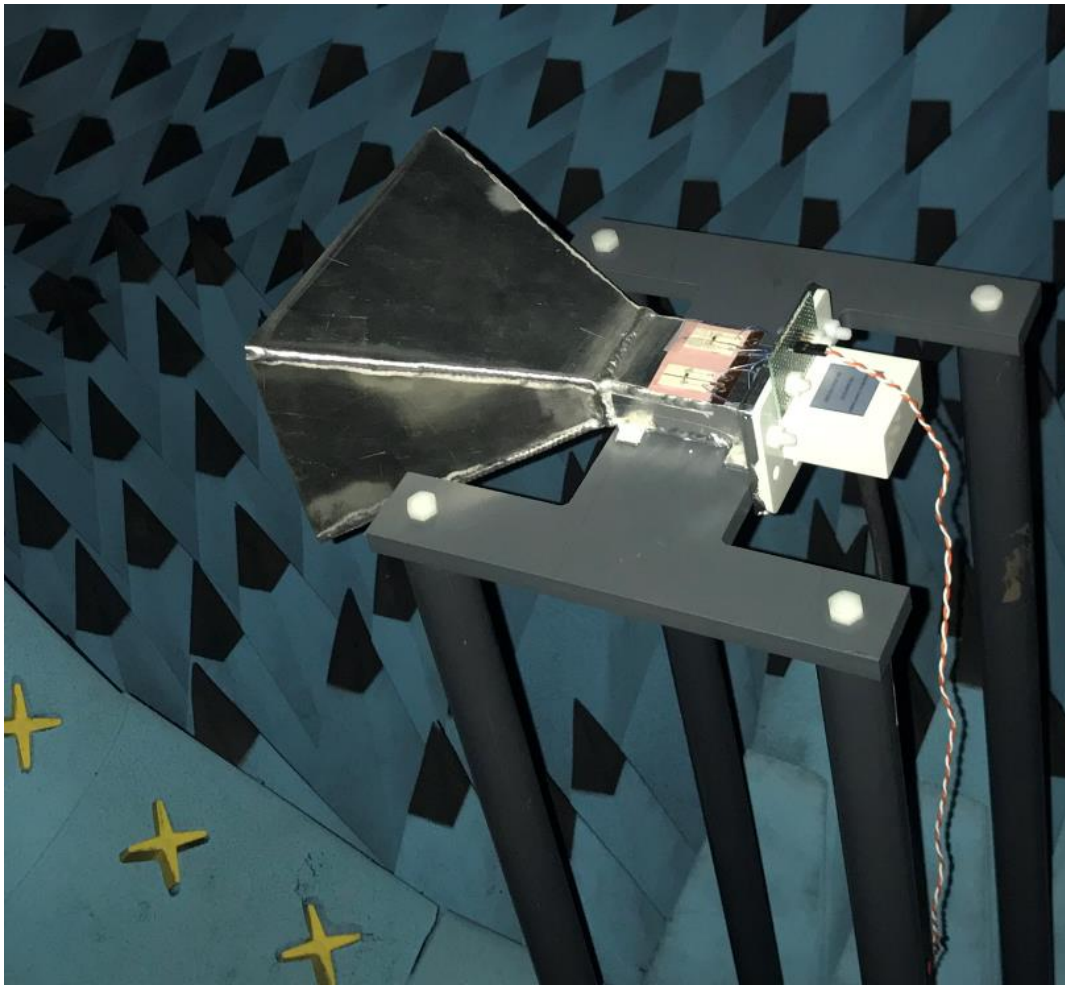

Figure 4. 36: Antenna under test in SATIMO STARGATE near field chamber at INSA Rennes

The results obtained at ($\theta = 0°$, $\phi = 0°$) in measurements and simulations are depicted in Figure 4.37 and are in good agreement. As expected, the polarization circuit produces an additional shift in the slot resonance frequency (4 GHz). We also remark 3.51 dB gain drop in the OFF mode in comparison to simulations results. This could be linked to the parasitic elements of the packaged PIN diode and to the polarization circuit. Nevertheless, the gain difference between OFF and ON modes in measurement is 15.18 dB at 4 GHz (21.65 dB in simulation).
We can see that even if the original circuit was designed for the beam lead PIN diode, simulations and measurements show that it is still efficient in the present implementation using packaged PIN diode.

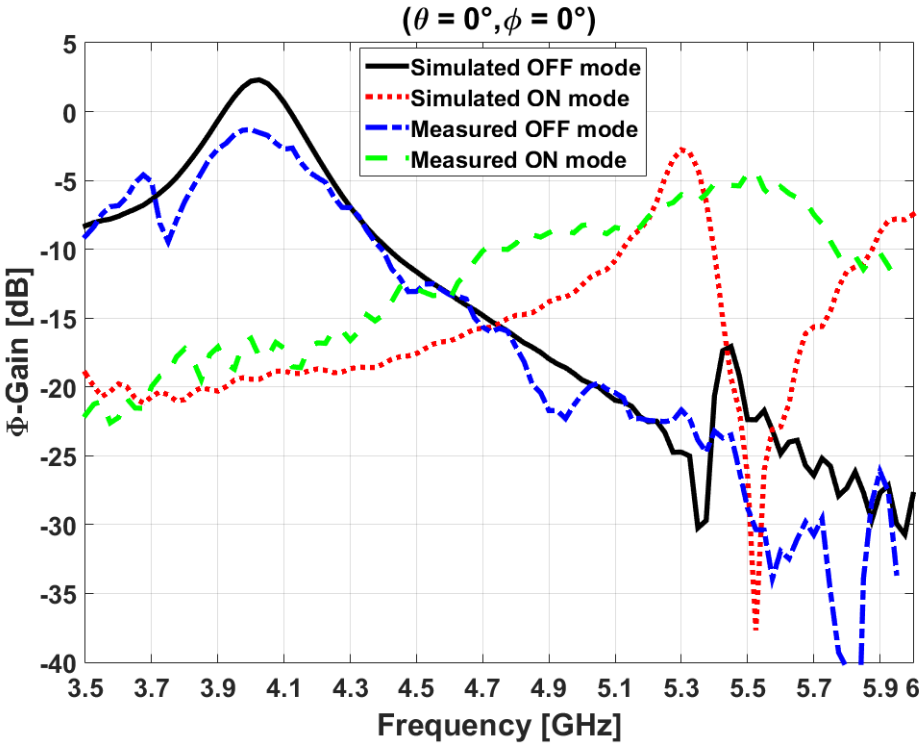

Figure 4. 37: Simulations and measurements results of the antenna system using packaged PIN diode

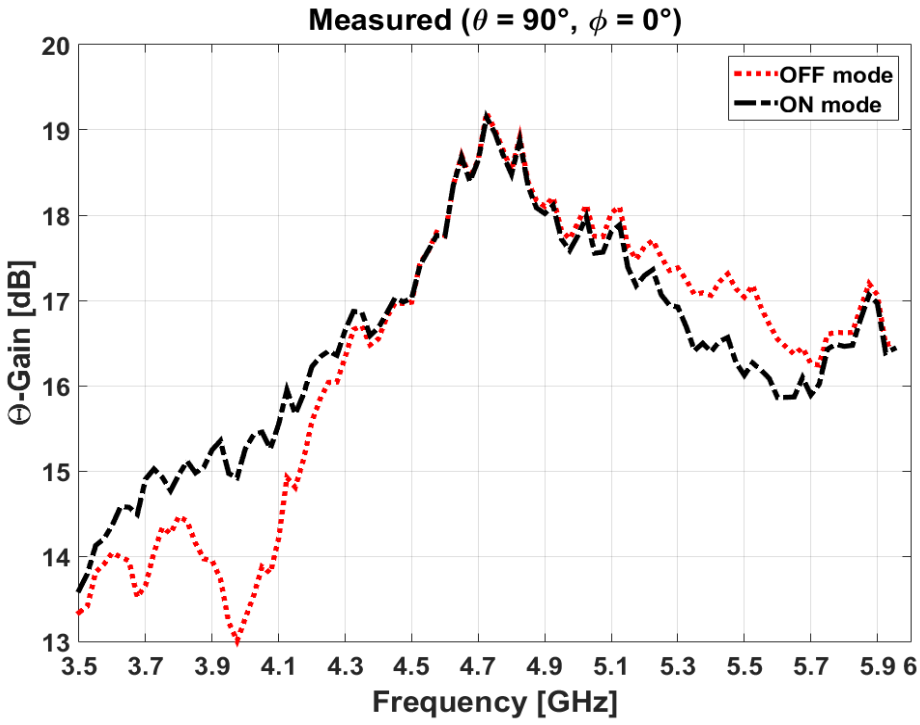

Figure 4. 38: Measured θ-gain (horn radiation) versus frequency in the main direction of the horn ($\theta = 90°$, $\phi = 0°$)

The gain in the main direction of the horn is depicted in Figure 4.38. From this figure we can see a 2 dB gain drop between OFF and ON modes at the resonance frequency of the slot (4 GHz) due to the energy picked up for communication function.

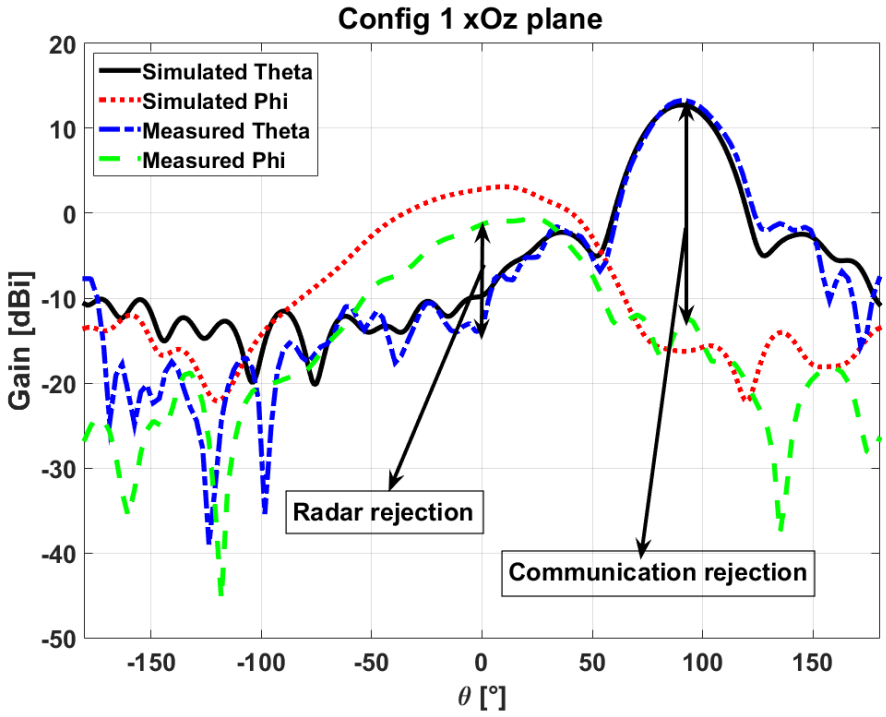

Figure 4. 39: Radiation pattern of configuration 1 at 4 GHz in xOz plane

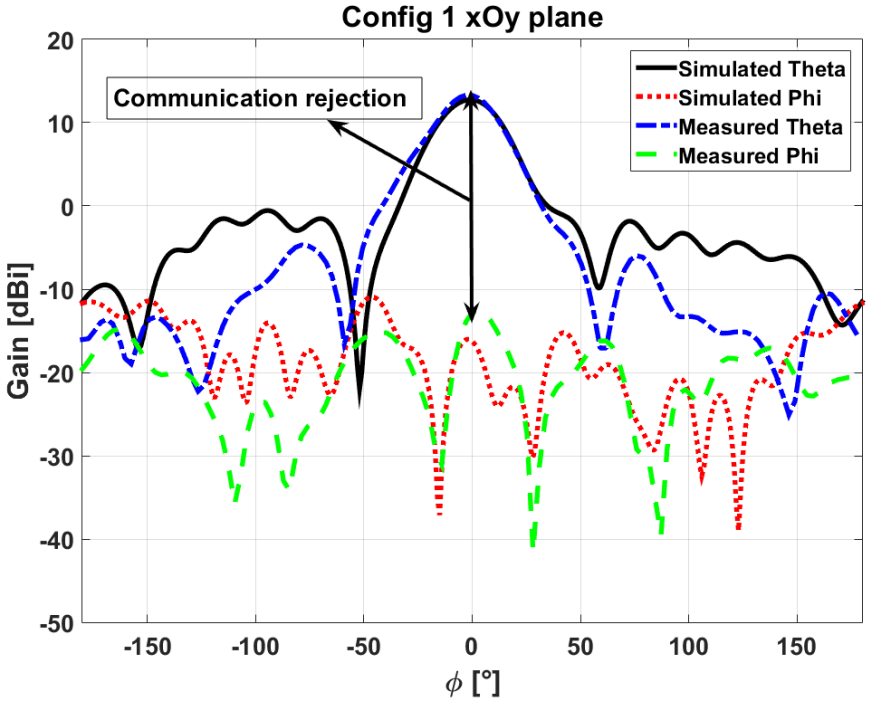

Figure 4. 40: Radiation pattern of configuration 1 at 4 GHz in xOy plane

The simulated and measured radiation patterns at 4 GHz of configuration 1 in respectively xOz and xOy plane are given in Figure 4.39 and Figure 4.40. As can be seen, the communication rejection is 26.1 dB in measurement (29 dB in simulation) and the radar rejection is 12.47 dB in measurement (12.58 dB in simulation) ensuring isolation between the two functions.

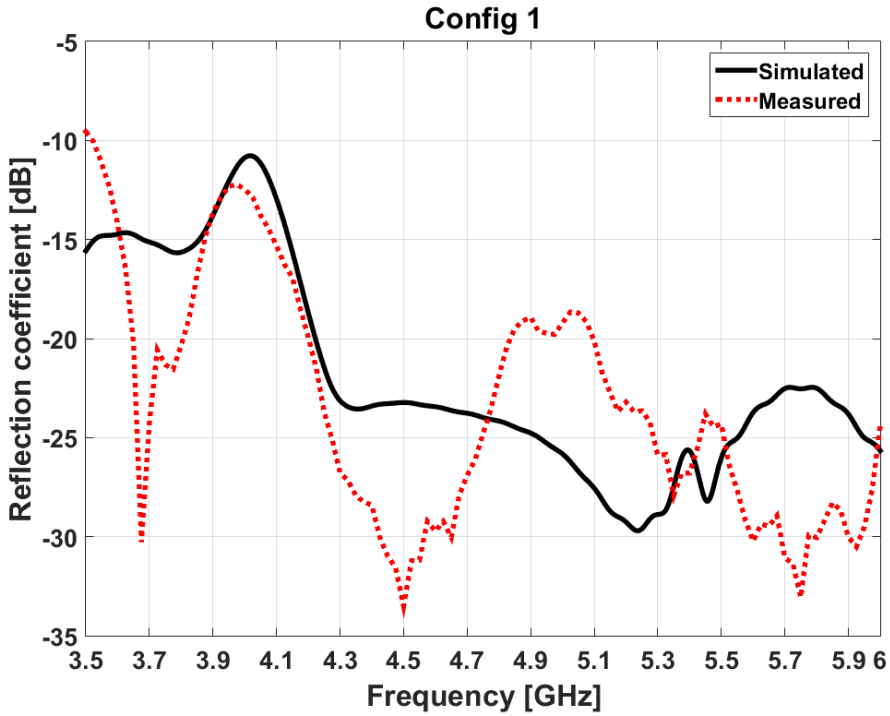

Figure 4. 41: Reflection coefficient of configuration 1

The simulated and measured reflection coefficients are depicted in Figure 4.41 and are below -10 dB from 3.5 GHz to 6 GHz.

4.4.3. Conclusion

This study has shown that it is possible, by loading to the slot a PIN diode, to control the communication function. In simulations, the PIN diode capacitor in reverse bias and the polarization circuits shifted the resonance frequency to 4.7 GHz when using the beam lead PIN diode and 4 GHz with the packaged one (instead of 5 GHz). At the new resonance frequency, the gain difference between the OFF and ON modes of the diode is 21.65 dB in the worst case, validating the polarization circuit. At worst, the radar rejection of this antenna system is 11.06 dB at the resonance frequency and the communication rejection is at least 29 dB, showing a good isolation between the radar and communication functions.
To experimentally validate the antenna system, a polarization circuit is mounted on the waveguide
The very small size of the beam lead PIN diode prevented us from successfully completing the circuit. We used instead the packaged PIN diode (giving a non-optimal configuration), which is much simpler to handle in order to experimentally validate the antenna concept. The measurements results are in good agreements with simulations and the gain difference between OFF and ON modes

is 15.18 dB. The measured radar and communication rejections are respectively 12.47 dB and 26.1 dB at 4 GHz ensuring the isolation between the two functions.

4.5. Conclusion of chapter 4

A full characterization of the multifunction antenna system providing simultaneously a radar function and a direct BPSK modulation has been carried out in this chapter. A first approach was to use frozen states, one of the slots being masked by a strip of copper tape. The results have shown quite good agreement between measurements and simulations. However, the measurement environment affects the radiation patterns, in particular the side lobes region, reducing the radar rejection at $\theta = 0°$ by 3.9 dB in comparison to simulation. The rejection in this direction can certainly be further increased by using a corrugated horn, which presents low side lobes. Nevertheless, when switching the activated slot, the two configurations give the same radiation patterns, ensuring that the two functions are not affected.

To dynamically control the slot activation and the BPSK modulation, the possibility to use beam lead PIN diodes have been studied. Hence, by loading the slot with the PIN diode, it is possible to control the communication function while keeping the same radiation patterns between the two configurations. In reverse bias, the diode capacitor and the diode polarization circuit shifted the frequency resonance to 4.7 GHz. At the resonance frequency, the gain difference between the OFF and ON modes of the diode is 22.84 dB validating the polarization circuit. The radar rejection of this antenna system is 11.06 dB at the resonance frequency and the communication rejection is at least 35 dB, showing a good isolation between the radar and communication functions.

For experimental validation of the antenna system, an *H*-shaped circuit was realized and mounted on the antenna prototype. Technical problems with the integration of the beam lead diode pushed us to use packaged PIN diode with poorer characteristics. Also, due to lack of time, the biasing circuit was not re-optimized as it should have been to fit the new diode properties. As a consequence, the obtained measured performance is not optimal and is only given to demonstrate the feasibility of the proposed solution. Nevertheless, simulations and measurements results are in good agreements and the gain difference between OFF and ON modes is 15.18 dB. For this new system the radar and communication rejections are respectively 12.47 dB and 26.1 dB at the resonance frequency, ensuring a good isolation between the two functions.

[1] Sarra Rebhi, Rim Barrak and Mourad Menif, “A Multistandard and Multiservice Radio over Fiber System for Next Generation Networks” 5th International Conference on Multimedia Computing and Systems (ICMCS), Marrakech, Morocco, 29 Sep - 01 Oct, 2016.

[2] http://www.skyworksinc.com/uploads/documents/Design_With_PIN_Diodes_200312D.pdf

[3] http://www.skyworksinc.com/uploads/documents/200823A.pdf

Chapter 5: Multifunction Antenna Consisting of SIW horn

5.1. Introduction

In the previous chapters, we have proposed and validated a multifunction antenna system for radar and communication applications with direct BPSK modulation consisting of a slotted waveguide feeding a horn antenna. However, the basic horn antenna and feeding waveguide suffer from its bulky size. These disadvantages could be overcome by using a planar technology such as substrate integrated waveguide (SIW) [1] which presents low profile and simple manufacturing. Due to the small substrate thickness, the SIW horn radiation is wide in the E-plane, which leads to a quite low directivity. Hence, in this chapter, we investigate the possibility to accommodate slots on the feeding waveguide of a SIW horn to achieve a multifunction antenna for applications that only require a moderate gain such as navigation/communication, communication/communication etc. In other words, radar will not be addressed here.

Section 5.2 will be dedicated to a brief state of the art of SIW to better understand its functioning and the techniques used to improve the impedance matching and radiation pattern. In section 5.3 and 5.4, we move to the transposition of the multifunction concept into planar technology using thin and thick substrates and we discuss the limitations and capabilities for our purposes.
In this chapter we did not implement a real switching mechanism, only the activated slot is present in simulations (the others being completely closed with PEC).

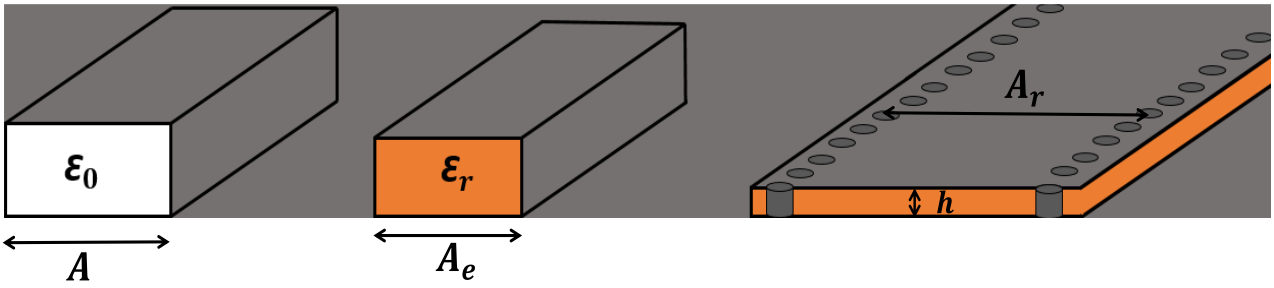

Figure 5. 1: From rectangular waveguide to SIW

5.2. SIW Technology

5.2.1. General overview

SIW technology was proposed in the last decades [1] [2] as a new concept for millimeter-wave integrated circuits and systems for the next generation. The purpose of this technology is to facilitate the integration of rectangular waveguide with planar circuits. Indeed, several studies of transitions between microstrip line and rectangular waveguide have been carried out [3]- [6]. These studies show that typical integration techniques from rectangular waveguide with planar structures are bulky and require a very precise manufacturing process, difficult to achieve at millimeter-wave frequencies. Hence, SIW is intended to replace traditional hybrid systems which are a combination of both waveguides and microstrip line. Due to its planar structure, low profile, simple

manufacturing and easy integration with other planar circuits using a standard printed circuit board or other planar processing techniques, SIW has received much attention [7]- [10]. In its simplest form, it is composed of two periodic rows of vias drilled through a dielectric substrate that connect two parallel metal plates (cf. Figure 5.1). To ease the via-hole metallization, the substrate thickness should be about 2.5 mm or lower [11]. SIW can then be viewed as a dielectric filled waveguide (DFW) where the vias replace the narrow walls of traditional rectangular waveguides then avoiding leakage.

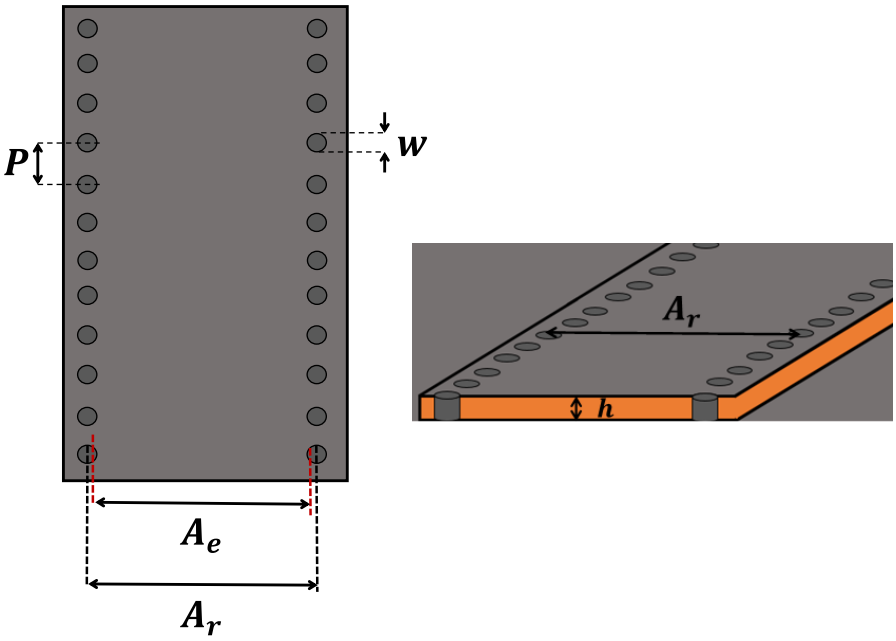

Figure 5. 2: Substrate integrated waveguide (SIW)

The gaps between metal vias prevent the propagation of TM modes in the SIW [9] offering then the same performance as conventional metallic waveguides with TE10 as dominant mode. SIW structures also preserve the advantages of conventional metallic waveguides such as high power handling capability, low losses and high quality factor [12] [13]. It is then a good candidate for feeding the surface wave or leaky wave antennas [14].

The key parameters for the SIW design are presented in Figure 5.2:

P: via holes spacing (also called pitch)
w: via diameter
A_r: central distance between via arrays
A_e: equivalent SIW width
ε_r: permittivity of the substrate
h: substrate thickness

The pitch *P* and diameter *w* control the leakage losses and return loss [8] [10] [15]. Then, for SIW design, the following two conditions are required:

$$w < \frac{\lambda_g}{5} \quad (1)$$

$$P \leq 2w \quad (2)$$

where λ_g, the guided wavelength of conventional rectangular waveguide of width A (cf. Figure 5.1 (a)) is defined by:

$$\lambda_g = \frac{2\pi}{\sqrt{\frac{\varepsilon_r (2\pi f)^2}{c^2} - \left(\frac{\pi}{A}\right)^2}} \quad (3)$$

c is the speed of light in vacuum, ε_r the relative dielectric permittivity, f the operating frequency and A the conventional rectangular waveguide width (cf. Figure 5.1 (a)).

The SIW width A_r, makes it possible to control the cut-off frequency of TE10 mode [16]. There is, however, an empirical relationship given in [12] [16] that allows us to move from a DFW to a SIW:

$$A_r = A_e + \frac{w^2}{0.95P} \quad (4)$$

where the equivalent width of SIW A_e, corresponding to the width of DFW with the same cut-off frequency (cf. Figure 5.1 (b)) is given by:

$$A_e = \frac{A}{\sqrt{\varepsilon_r}} \quad (5)$$

As for conventional rectangular waveguide, the SIW bandwidth is defined between $1.25f_c$ and $1.9f_c$. For TE10 mode, the cut-off frequency of a standard rectangular waveguide is given by:

$$f_c = \frac{c}{2A} \quad (6)$$

Hence by using equations (4), (5) and (6), the cut-off frequency f_c of the SIW can be determined once the geometrical dimensions are known by using the following relation [16]:

$$f_c = \frac{c}{2\sqrt{\varepsilon_r}} \left(A_r - \frac{w^2}{0.95P}\right)^{-1} \quad (7)$$

Then, the SIW dimensions must be chosen carefully to get the desired specifications.
In the next section a brief state of the art of SIW horn antenna will be presented.

5.2.2. SIW horn antenna

As mentioned in section 5.1, our goal is to transpose the developed multifunction concept for a horn antenna into SIW technology. For that reason, we consider a SIW horn antenna for the main function. The SIW horn antenna was proposed in [17] [18] because of its planar structure, simple fabrication and easy integration with other planar circuits. In general, due to the small substrate thickness, the SIW horn radiation pattern is wide without much directivity and the impedance matching is critical. In the literature [11] [18] - [23] we find that impedance matching techniques differ whether the thickness *h* is less than $\lambda_0/6$ (thin SIW horns) or more than $\lambda_0/6$ (thick SIW horns).

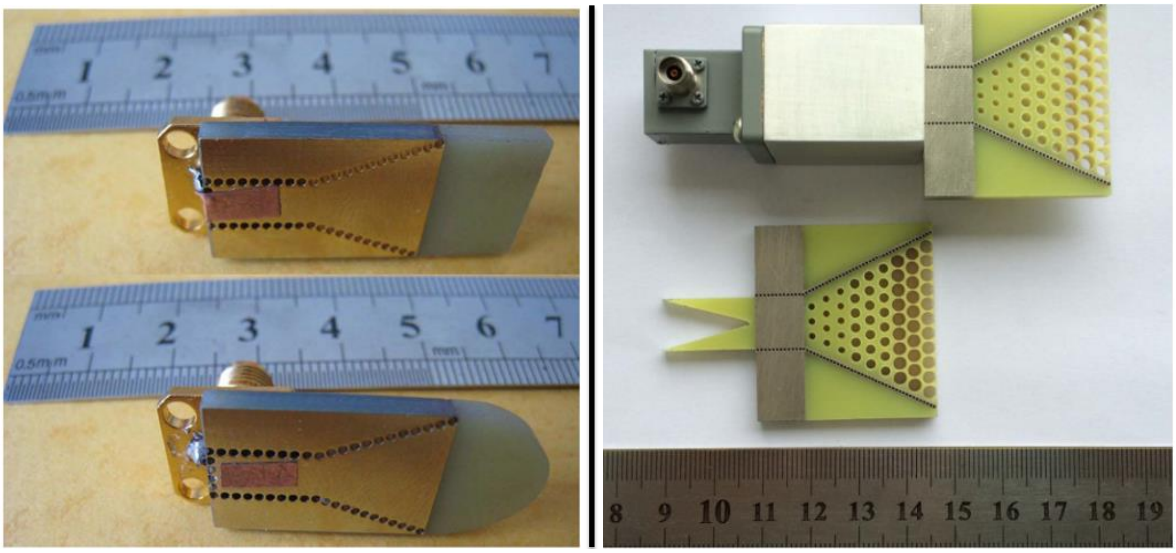

(a) (b)

Figure 5. 3: SIW horn: (a) with dielectric load [19] and (b) with perforating air-vias [20]

- **Thick SIW horns**

The techniques used to improve the impedance matching of thick SIW horns are based on loaded extensions at the horn aperture. Some of them require the use of non-planar elements [21] [22] resulting in bulky antenna and more complicated building procedure, whereas the extensions in [19] [20] share the same substrate as the horn.
In [19] the impedance mismatch and radiation pattern improvement are realized by extending the dielectric substrate. Sharing the same substrate with the horn (cf. Figure 5.3 (a)), the loading dielectric acts as an impedance transformer providing about 10% bandwidth. In [20] another impedance transformer based on [19] is achieved by removing the metal walls of the horn and by perforating the extended substrate improving the operating bandwidth up to 40%, cf. Figure 5.3 (b).

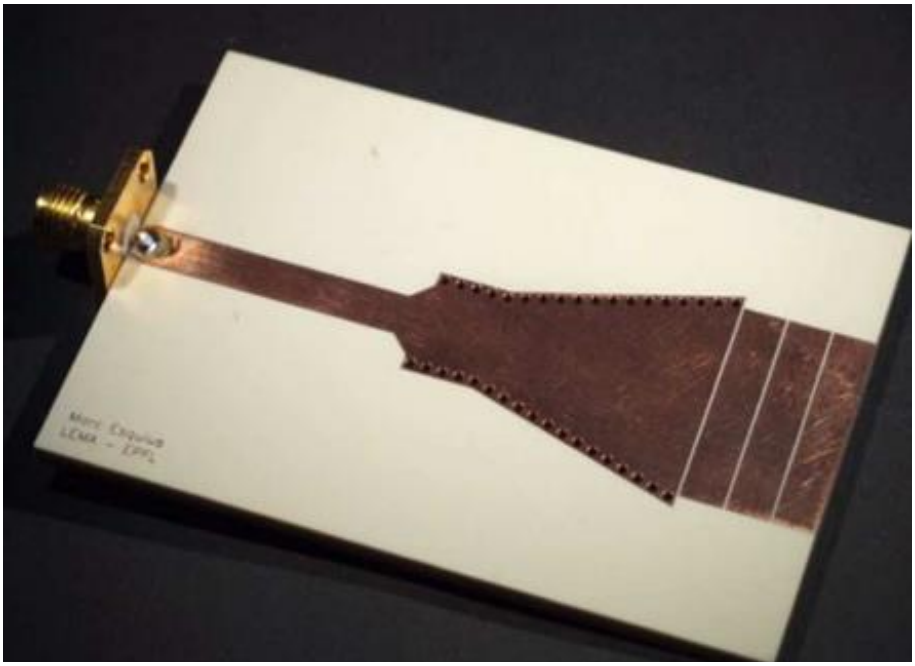

Figure 5. 4: SIW horn with parallel plate [23]

- **Thin SIW horns**

For thin SIW horn ($h < \lambda_0/6$), the dielectric extension technique cannot improve the antenna impedance matching because the effect of the dielectric extension would be negligible. On the other hand, the mismatch can be improved by loading several parallel plates on the extended dielectric as in [23], (cf. Figure 5.4). The coupling effects between the plates introduce capacitance effects, generating additional resonant frequencies making the antenna operate in wide bandwidth (16.7%).

As already explained, since the SIW horn radiation pattern is wide without much directivity, this prevents the use of this antenna for radar application. Hence, in this chapter we will work to enhance the performance of the SIW horn for other multifunction applications (navigation/communication, communication/communication …).

For this study we will consider thin substrate SIW horn. The design will be arbitrarily done in X-band (between 8 GHz and 12 GHz). By this way, the antenna could be built in commercial substrates, generally thinner than $\lambda_0/6$ and use appropriate feeding techniques to completely integrate the antenna with other elements printed in the same substrate [23].

5.3. Thin SIW horn antenna

This section is dedicated to the design of the multifunction antenna concept into thin SIW horn. The principle is the same as in the previous chapters: a small portion of the propagating power in the feeding SIW is picked up through slots to transmit a direct BPSK modulation at ($\theta = 0°$, $\phi = 0°$) for the second function without altering the main lobe of the horn (dedicated to the main function). Hence, as in previous chapters, the two complementary configurations are defined as (cf.

Figure 5.5): configuration 1, only slot 1 radiates while slot 2 is closed with PEC and configuration 2 corresponds to the reverse situation.

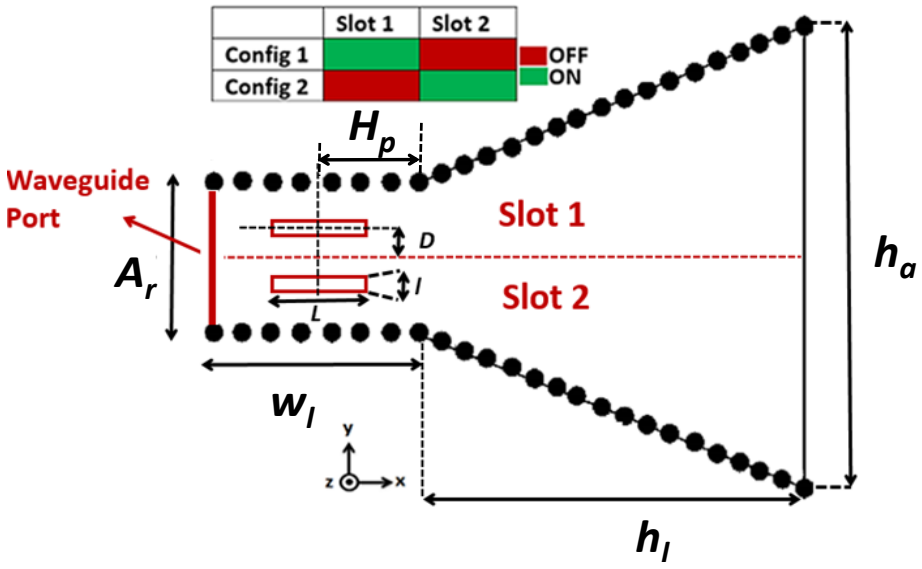

Figure 5. 5: Configurations of SIW horn antenna for the multifunction system

In the next section, the design of the SIW working in X-band that will be used to feed the horn antenna is presented.

Ar	15.36 mm
Ae	14.97 mm
P	4.95 mm
w	3.3 mm
f_c	6.4 GHz

Table 5. 1: Thin SIW dimensions and cut off frequency

5.3.1. SIW design

It is proposed in this section to design the multifunction antenna into thin SIW horn antenna allowing the design of the antenna in commercial substrates, generally thinner than $\lambda_0/6$. To realize the thin SIW horn antenna, we first start by designing the feeding SIW. The WR-90 is the standard X-band rectangular waveguide with dimensions: A = 22.86 mm and B = 10.16 mm that will be used in this case. A substrate of permittivity ε_r = 2.33, tan δ = 0.0013 (chosen arbitrarily) and h = 1.6 mm height is used for this study. By using (1), (2), (4), (5) and (7), the physicals characteristics of the X-band SIW and the theoretical cut-off frequency of the TE10 mode are presented in Table 5.1.

Based on the previous calculation, a SIW of length w_l = 76 mm is modeled in CST. The cut-off frequency of TE10 mode is 6.39 GHz. Then the results will be observed from 8 GHz to 12 GHz, corresponding to the SIW bandwidth (between 1.25f_c and 1.9f_c).

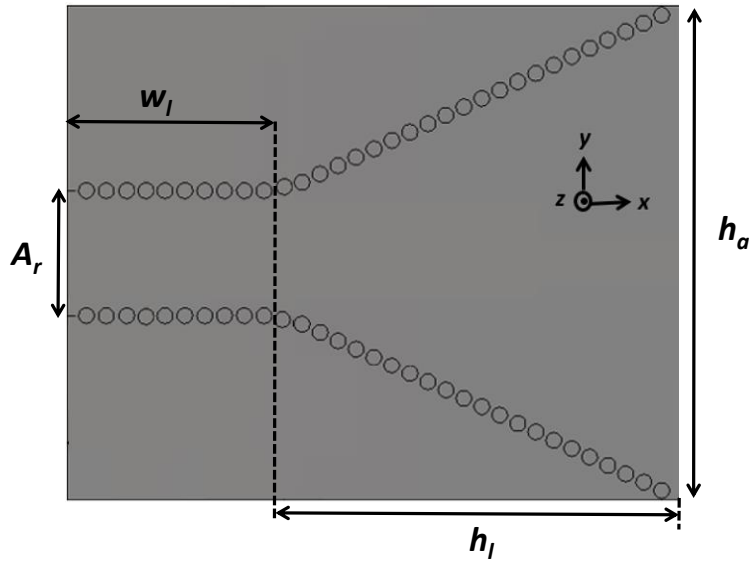

Figure 5. 6: SIW horn antenna (A_r = 15.36 mm; w_l = 76 mm; h_l = 50 mm and h_a = 64 mm)

5.3.2. SIW horn design

In this section we use the SIW designed in previous section to feed the horn antenna (cf. Figure 5.6). In this figure, h_a and h_l are respectively the horn aperture in xOy plane and the horn length. They are chosen to control the radiation pattern in this plane [17].

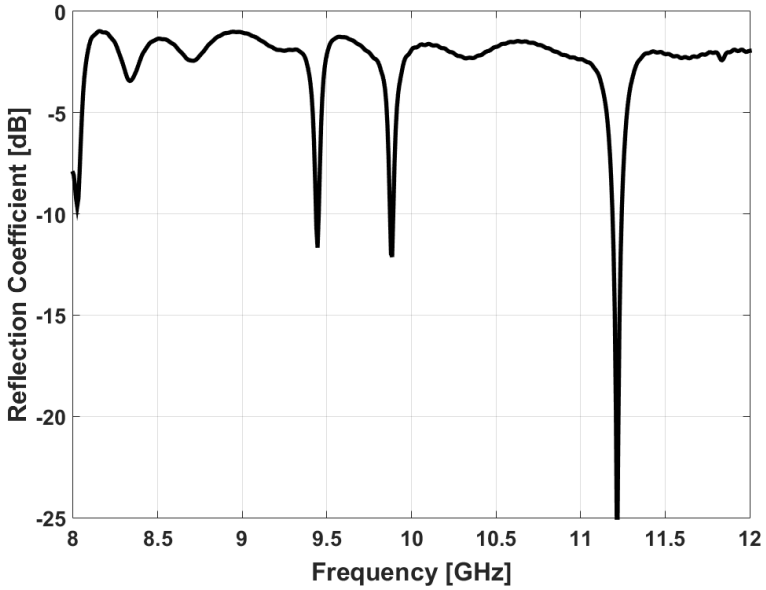

Figure 5. 7: Reflection coefficient of the thin SIW horn

Figure 5.7 depicts the reflection coefficient of the thin SIW horn antenna from 8 GHz to 12 GHz. As expected, due to the small substrate thickness (h = 1.6 mm), the mismatch between the horn aperture and free space is significant resulting in poor matching.

To improve the impedance matching of the thin SIW, in the next section, we investigate the possibility to add parallel plates at the horn aperture.

5.3.2.1. SIW horn with parallel plates

In this section, a parallel plate as the one presented in Figure 5.8 will be used to improve the impedance matching of the thin SIW horn antenna, more precisely at 10 GHz (center frequency).

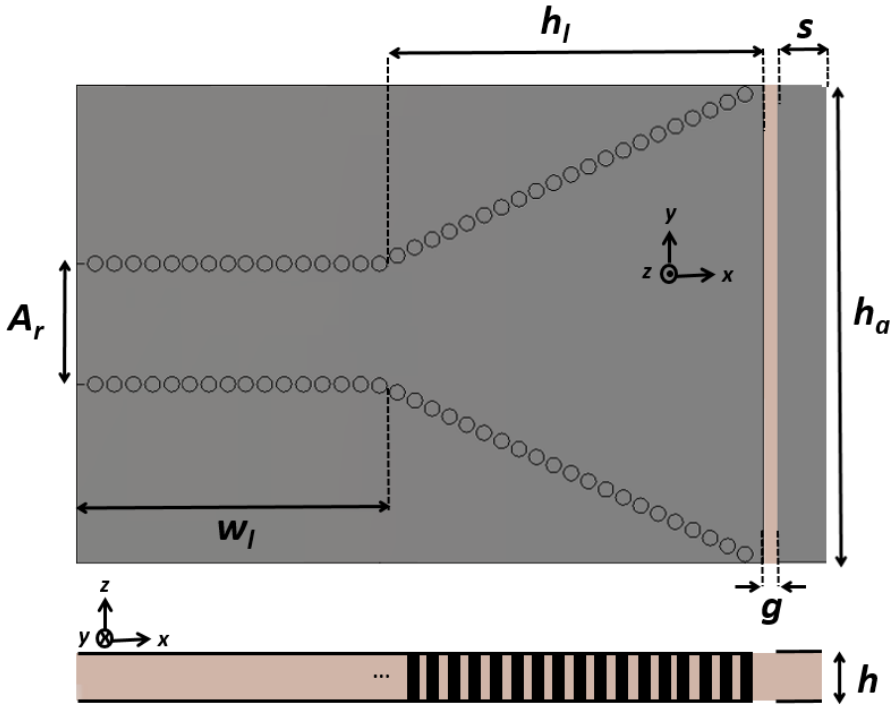

Figure 5. 8: SIW horn with parallel plate (A_r =15.36 mm; w_l = 76 mm; h_l = 50 mm; h_a = 64 mm, s = 8.36 mm, g = 0.3 mm and h = 1.6 mm)

It has been shown in [23] that such a plate introduces additional resonant frequency which improves the impedance matching of the antenna. The formulas for a proper design of the printed plate are also given in [23]:

$$s = \frac{0.4*\lambda_0}{\sqrt{\varepsilon_r}} \quad (8)$$

$$0.03 < \frac{g}{s} < 0.06 \quad (9)$$

$$0.03 < \frac{h}{s} < 0.06 \quad (10)$$

At 10 GHz, s = 8.36 mm and g = 0.3 mm.

Figure 5.9 presents the reflection coefficient of the antenna with one parallel plate. As expected a clear working band of 1 GHz is obtained from 9.6 to 10.6 GHz in comparison to the antenna without plate, allowing the SIW horn antenna to work properly.

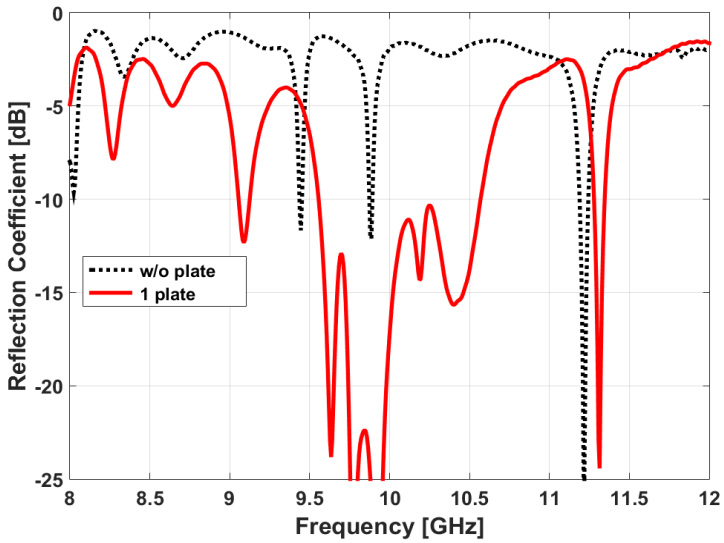

Figure 5. 9: Reflection coefficient of the SIW with and without parallel plate

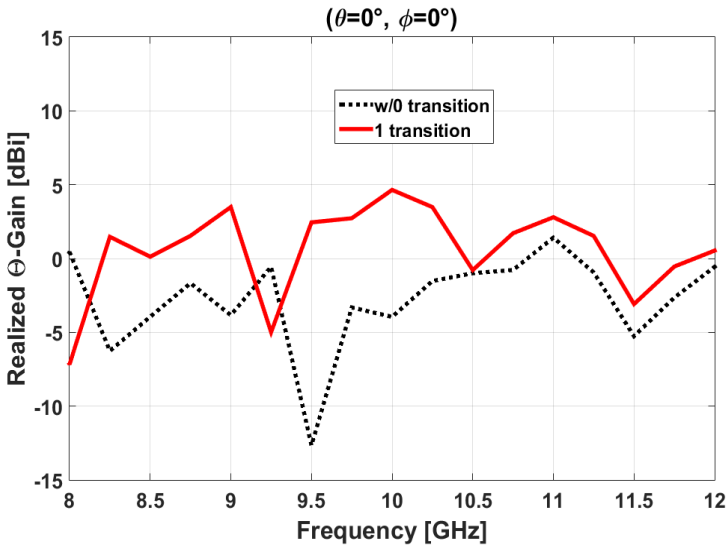

(a)

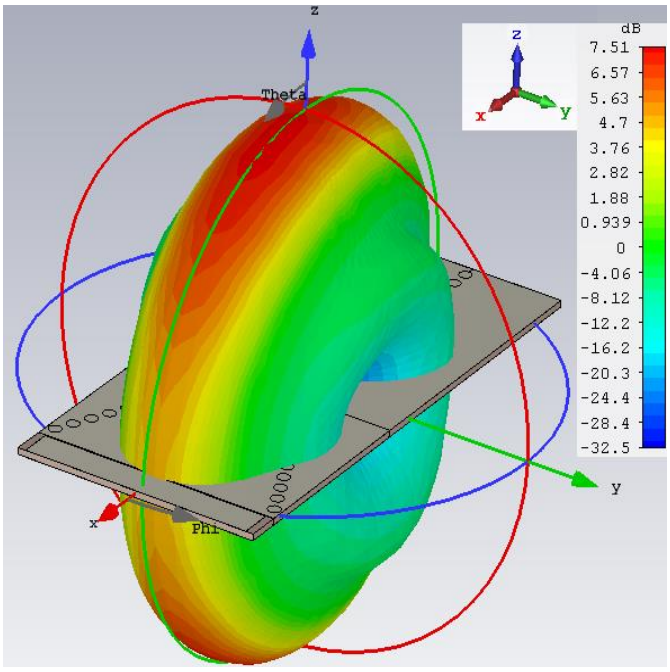

(b)

Figure 5. 10: (a) SIW θ-gain at (θ = 0°, ϕ = 0°) versus frequency and (b) 3D radiation pattern at 10 GHz

We now study the impact of this metallic strip on the radiated field. Figure 5.10 (a) and (b) depict θ-gain at ($\theta = 0°$, $\phi = 0°$) versus frequency and the 3D radiation pattern at 10 GHz. As can be seen from Figure 5.10 (a), the radiation at ($\theta = 0°$, $\phi = 0°$) has been increased in comparison to the SIW horn without plate. At 10 GHz, it has been increased by 8.6 dB. Indeed, the gap (g) between the horn aperture and the parallel plate acts as a slot antenna and contributes to horn radiation at ($\theta = 0°$, $\phi = 0°$). As expected, due to the small substrate thickness, the horn radiation is wide without much directivity (cf. Figure 5.10 (b)). Moreover, we can see that the gain in the main direction of the horn ($\theta = 90°$, $\phi = 0°$) is 4.64 dBi, which is 2.62 dB lower than the radiation at ($\theta = 0°$, $\phi = 0°$), cf. Figure 5.13 for the radiation pattern in xOz plane at 10 GHz. This means that the most of the energy is radiated by the gap (g) at the expense of the horn.

The purpose of the multifunction system being to transmit a direct BPSK modulation at ($\theta = 0°$, $\phi = 0°$), the horn radiation in this direction becomes problematic. In fact, the slot that will be etched in the feeding SIW (for the BPSK purposes) will have to take a lot of the energy propagating in the SIW at the expense of the gain in the main direction of the horn (which is already low) to transmit information and ensure a better isolation between the two functions in this direction.

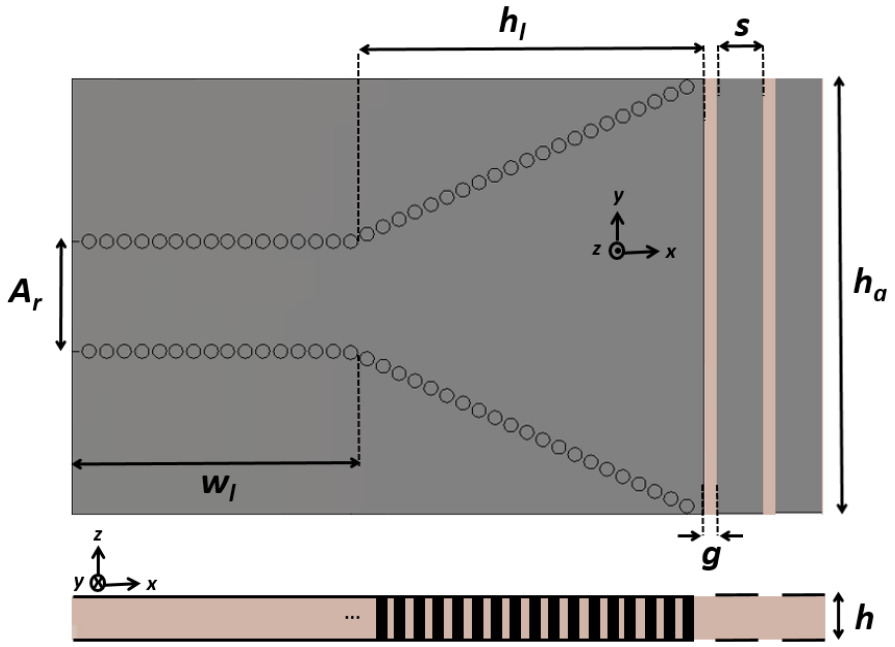

Figure 5. 11: SIW horn with two parallel plates (A_r =15.36 mm; w_l = 76 mm; h_l = 50 mm; h_a = 64 mm, s = mm, g = mm and h = mm)

To get rid of this problem, the idea here is to reduce the radiation brought by the parallel plate at ($\theta = 0°$, $\phi = 0°$) by using a second parallel plate (cf. Figure 5.11) so that the radiation of the two plates cancel out in this direction. The two parallel plates are designed following the same rules presented in [23] and the dimensions are now s = 8.9 mm and g = 0.2 mm.

We first investigate the reflection coefficient of the SIW horn with two parallel plates. Figure 5.12 depicts the reflection coefficient of the antenna with two plates. For comparison purposes the antenna with one plate is also given. As can be seen, the impedance bandwidth has been reduced by 600 MHz in comparison to the case with one plate. But, at 10 GHz it is below -20 dB.

Concerning the radiation characteristics, Figure 5.13 depicts the radiation patterns in xOz plane at 10 GHz with two plates. For comparison purposes the gain of the horn with one plate is also given. As can be seen, the use of two plates reduces the gain at ($\theta = 0°$, $\phi = 0°$) by 8 dB and further focuses the horn radiation in the main direction (2.8 dB more than the SIW horn with one plate). However, the front to back ratio (FTBR) is low (2.8 dB) in comparison to the horn with one plate.

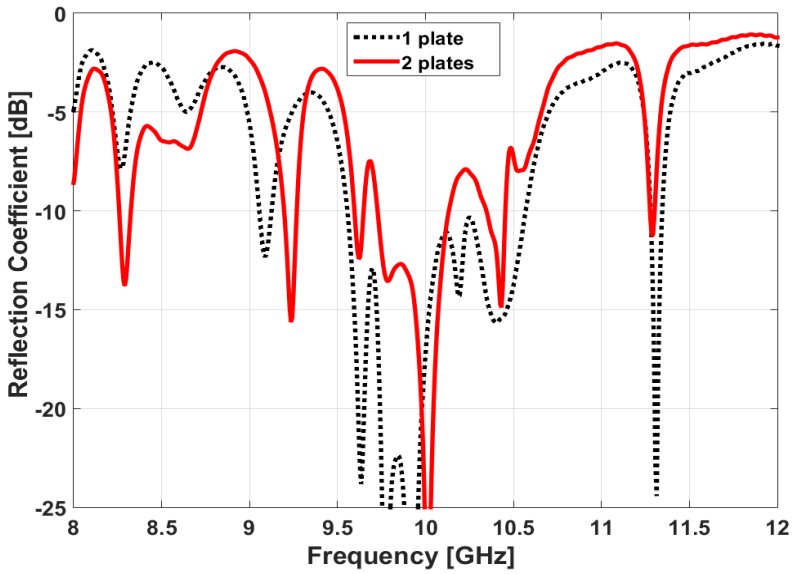

Figure 5. 12: Reflection coefficient of the SIW with one and two plates

Thus, the use of the two plates allowed us to further focus the horn radiation at ($\theta = 90°$, $\phi = 0°$) while reducing the radiation in ($\theta = 0°$, $\phi = 0°$) direction by 7.93 dB, cf. Table 5.2. The available impedance bandwidth is now 400 MHz.

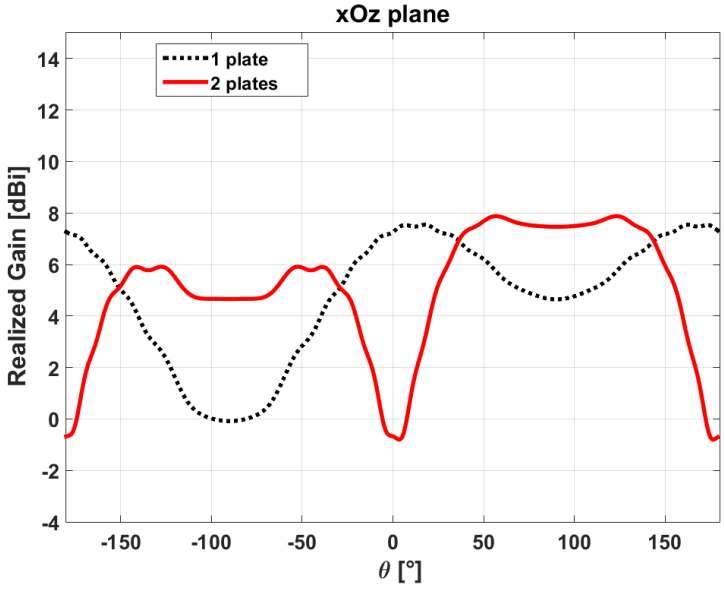

Figure 5. 13: Radiation pattern of SIW horn antenna with one and two plates in xOz plane at 10 GHz

After designing and discussing the performance of the SIW horn that will be used to perform the multifunction antenna, in the next section the slot design (at 10 GHz) in the feeding SIW will be studied.

	Impedance bandwidth	**Horn Gain (θ = 90°, ϕ = 0°)**	**Gain at (θ = 0°, ϕ = 0°)**
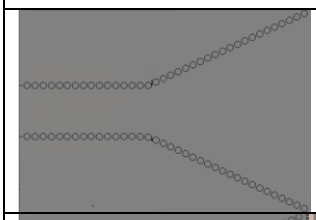	70 MHz	-3.01 dBi	-3.95 dBi
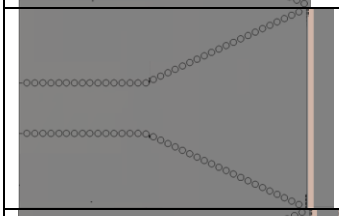	1 GHz	4.64 dBi	7.26 dBi
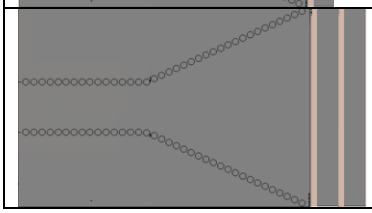	400 MHz	7.46 dBi	-0.67 dBi

Table 5. 2: Characteristics of the configurations studied

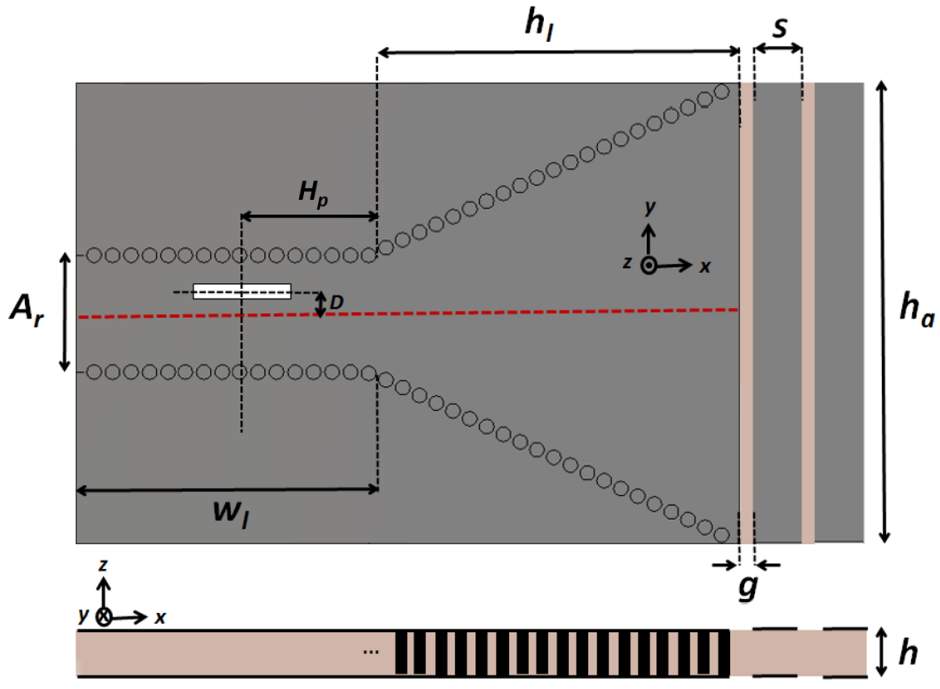

Figure 5. 14: Slot in the SIW horn with two plates (configuration 1) H_p = 38 mm

5.3.2.2. Slot design in the SIW

In this section it is proposed to design a slot in the feeding SIW working at 10 GHz for the multifunction antenna purposes. Through this chapter, we have seen that the SIW behaves like a conventional rectangular waveguide. Thus, all the studies carried out in chapter 2 concerning the slot width *l* and the offset to the waveguide centerline *D* also apply to the SIW [24].
Figure 5.14 presents the configuration 1 of the antenna used for this study. The slot length *L* is obtained by using equation (11) [24]. This formula has been adapted to take into account the dielectric substrate of the SIW. A parametric study is then necessary to find the resonant length of the slots while taking into account the effect of the horn.

$$L = \frac{\lambda_0}{\sqrt{2(\varepsilon_r+1)}} \qquad (11)$$

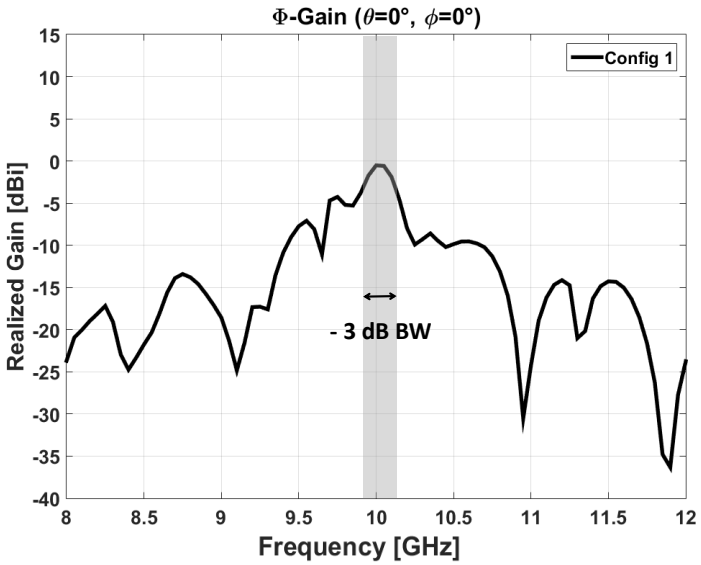

Figure 5. 15: ϕ-gain (slot radiation) versus frequency

Figure 5.15, shows ϕ-gain (slot radiation) versus frequency in the feeding SIW for a slot of length of *L* = 12 mm, width *l* = 0.2 mm, positioned at *D* = 0.6 mm from the SIW centerline. As can be seen from this figure, the peak gain (-0.5 dBi) is obtained at 10 GHz. This gain can be increased as already explained, by increasing the offset *D* (at the expense of the power available for the horn). We can also note that the slot radiation is narrow band (with 224 MHz -3 dB gain bandwidth) and could be improved by increasing the slot width *l* as shown in chapter 2.

Figure 5.16 depicts the reflection coefficient of the SIW horn configuration 1 (configuration 2 will give the same result). For comparison purposes the reflection coefficient of the antenna without slot is also given. As can be seen, the activation of the slot is responsible of some modifications in the reflection coefficient especially at 10 GHz, resonant frequency of the slot. Thus, the more the slot will radiate (a large offset), the more the degradation will be important. Nevertheless, from 9.7 GHz to 10.15 GHz the reflection coefficient is below -10 dB, providing 450 MHz impedance bandwidth.

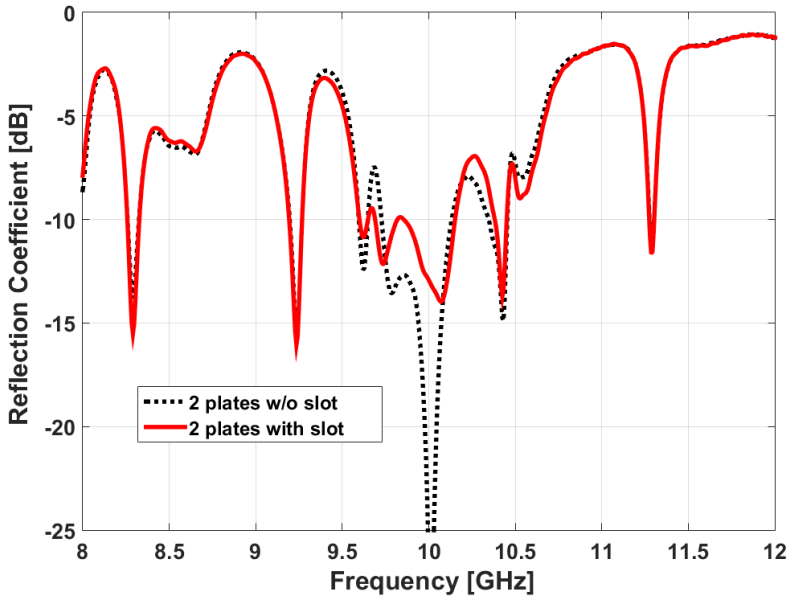

Figure 5. 16: Reflection coefficient of the SIW horn with two plates, with and without and slot

In the next section the performance of the antenna (radiation characteristics and rejections) due to slots will be studied.

5.3.3. Performance of the antenna system

In this section the performance of the antenna is studied. More precisely we will investigate the modification of the horn radiation due to the slots to make sur that the main function is not affected. The rejections between the two functions will also be discussed to evaluate the robustness of the system.
We recall that the configuration 1 used for this study is that of Figure 5.14. Configuration 2 corresponds to the reverse situation.

- **Radiation characteristics**

We first investigate the radiation pattern of the main function (SIW horn). Figure 5.17 and Figure 5.18 depict θ-gains in respectively xOz and xOy plane at 10 GHz. For comparison purposes the gain of the SIW horn without slot is also given.

In xOz plane, due to symmetry, both configuration 1 and 2 give exactly the same patterns, which guarantees the main function is not affected when switching the slots. In the main beam of the horn, 2.35 dB gain drop can be observed due to the energy picked up by the slot. Moreover, the FTBR is still low, it is 2.81 dB.

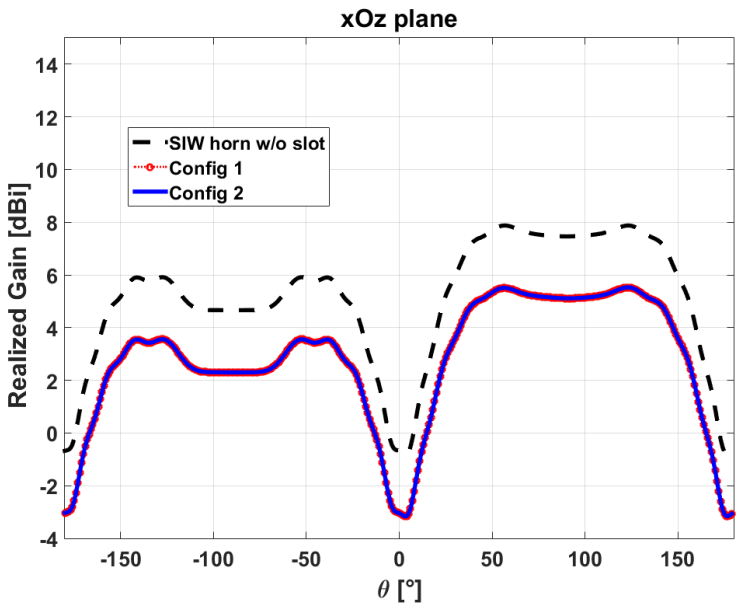

Figure 5. 17: Radiation patterns of the two configurations at 10 GHz in xOz plane

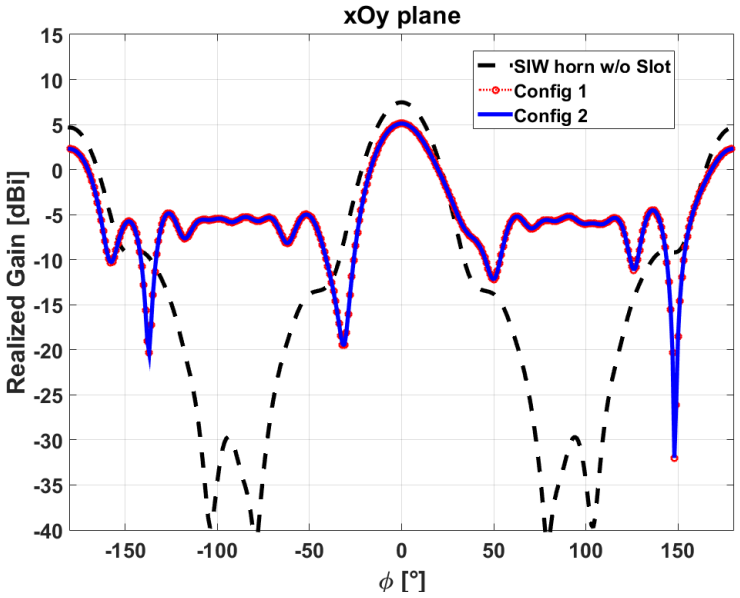

Figure 5. 18: Radiation patterns of the SIW horn (configuration 1) at 10 GHz in XOY plane

In xOy plane as expected, the slots contribute to *z*-polarization resulting in the modification of the horn side lobes at $\phi = \pm 90°$ and the SLL is now -9.64dB.

As already explained, all these results, in particular the low directivity of the SIW horn antenna prevents the use of this antenna for radar applications which require more directive radiation pattern.

We now investigate the slot radiation (secondary function). Figure 5.19 depicts ϕ-gain in xOz plane for the two configurations. As could be expected the gain is identical for the two configurations. The low value (-0.3 dBi) results from the use of non-directive radiating element and as stated

before, this value could be increased (by increasing the offset *D*) at the expense of the power available for the horn.

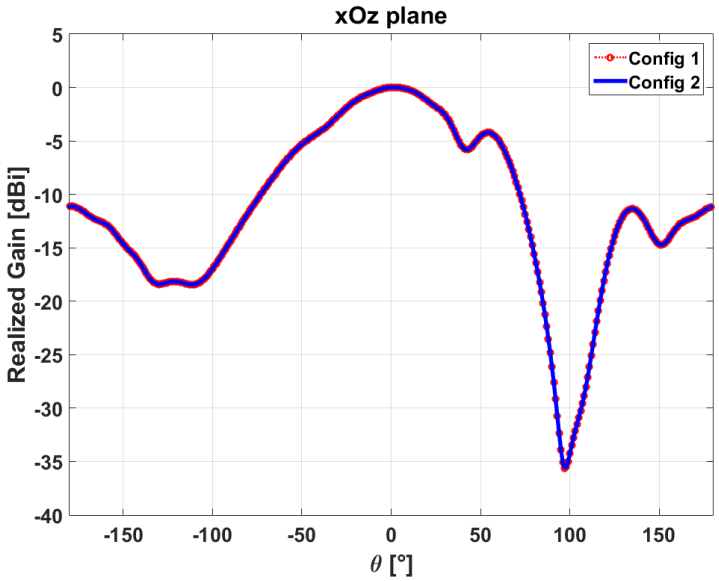

Figure 5. 19: Slot radiation (ϕ-gain) in xOz plane at 10 GHz

The BPSK characteristics for this antenna at 10 GHz are presented in Table 5.3.

Directions	Config	Phase (°)	Amp. (dBi)
$\theta = 0°$	1	0	-0.5
	2	180	-0.5

Table 5. 3: BPSK communication at $\theta = 0°$

- **Rejections between the functions**

We now investigate the rejection between the two functions. Figure 5.20 depicts the rejection at $\theta = 0°$ and $\theta = 90°$ (at 10 GHz) that will be considered for this study. We can see that at $\theta = 0°$ the slot radiation is slightly superior to that of the horn side lobes. Hence, the rejection in this direction is 3 dB (at 10 GHz) and could certainly be improved by providing more power to the slot either by increasing the slot offset *D* or by using slot array as in chapter 3. However, these solutions will lead to strong modification in the reflection coefficient as already explained (cf. Figure 5.16). Hence, a solution to further increase the rejection at $\theta = 0°$ by using SIW array will be studied in section 5.3.4.
Concerning the rejection at $\theta = 90°$ it is 38.5 dB at 10 GHz.

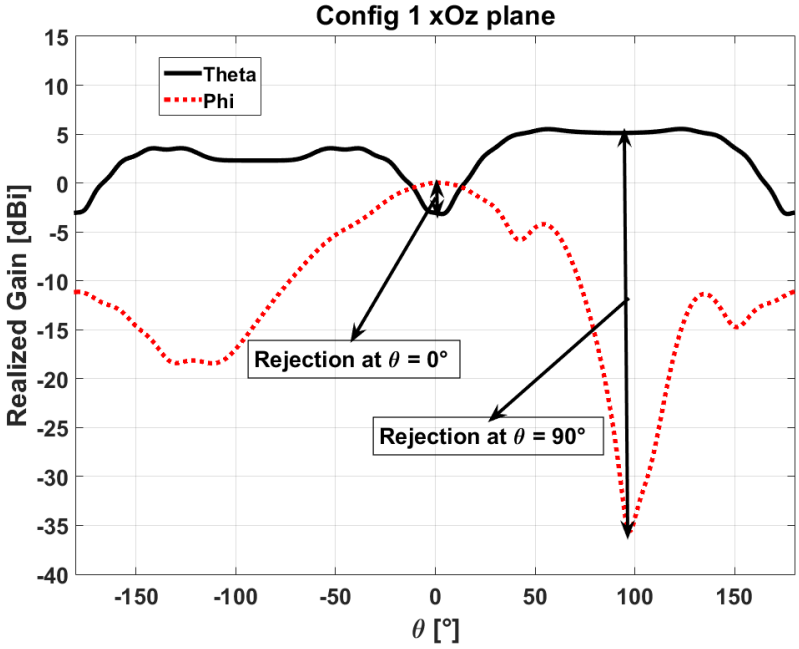

Figure 5. 20: Isolation between the two functions at 10 GHz

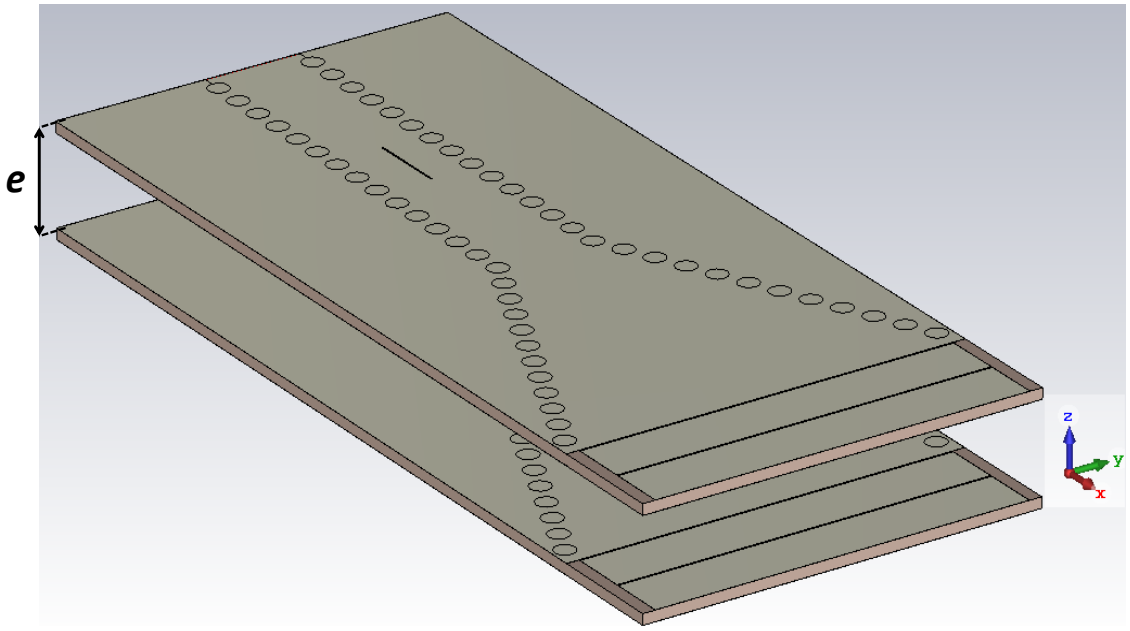

Figure 5. 21: SIW array (configuration 1): e = 15 mm

These first results on thin SIW horn show that we are limited in term of impedance matching (450 MHz bandwidth). This reduces our ability to improve the slot radiation which is -0.3 dBi at $\theta = 0°$ and then the rejection in this direction (3 dB). Furthermore, the radiation in the main direction of the horn is wide without much directivity (5.11 dBi).

To improve the horn radiation and the rejection at $\theta = 0°$, the SIW horn designed in this section will be used to realize a stacked array of SIW in the next section.

5.3.4. SIW stacked array

In this section, it is proposed to improve the horn radiation and the rejection at $\theta = 0°$. To do so, the SIW horn designed in previous section will be used to form an array of two SIW (fed in phase) and spaced by e along z-axis (cf. Figure 5.21). For the radiation at $\theta = 0°$, the slot is only located in the top SIW horn as shown in Figure 5.21 and corresponds to configuration 1 of the antenna system.

In order to improve the rejection at $\theta = 0°$, the two SIW are spaced by $e = \lambda_0/2$ (15 mm at 10 GHz) so that to create a null at $\theta = 0°$.

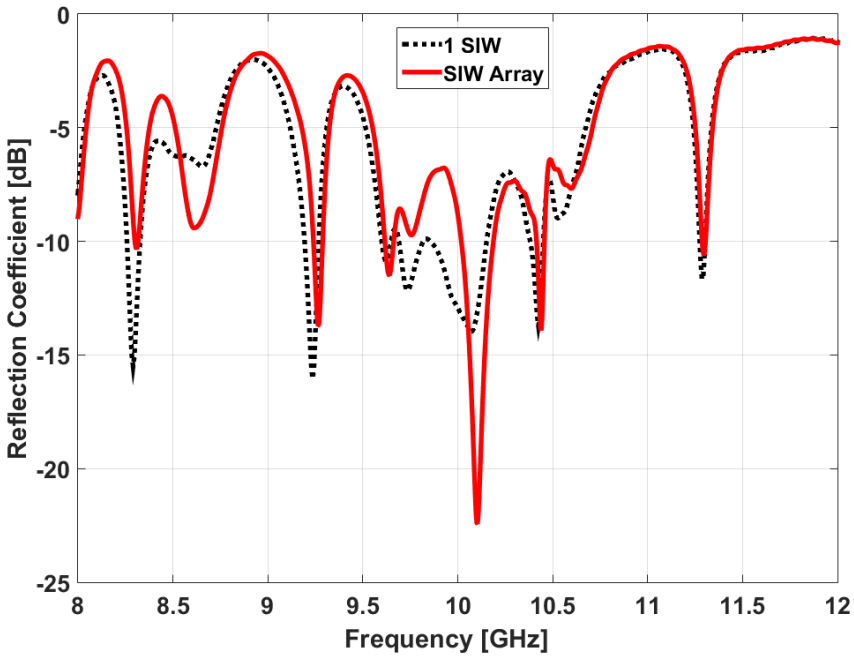

Figure 5. 22: Reflection coefficient of SIW array (configuration 1)

We first study the active reflection coefficient of this antenna array (cf. Figure 5.22). As can be seen, it is -8.81 dB at 10 GHz.

To improve the impedance matching, we extend the dielectric medium at the horn aperture ($s_l = 30$ mm) as in [19], cf. Figure 5.23. Given the small thickness of substrate considered ($h = 1.6$ mm), strong modifications are not expected. Furthermore, the plates dimensions have been retuned to take into account the dielectric extension: $s = 8.76$ mm and $g = 0.2$ mm.
Figure 5.24 depicts the active reflection coefficient of the antenna array (configuration 1) with dielectric extension. For comparison purposes the active reflection coefficient of the array without extension is also given. As can be seen, the impedance matching at 10 GHz has been improved (it is now below -10 dB) and the impedance bandwidth is 200 MHz around 10 GHz.

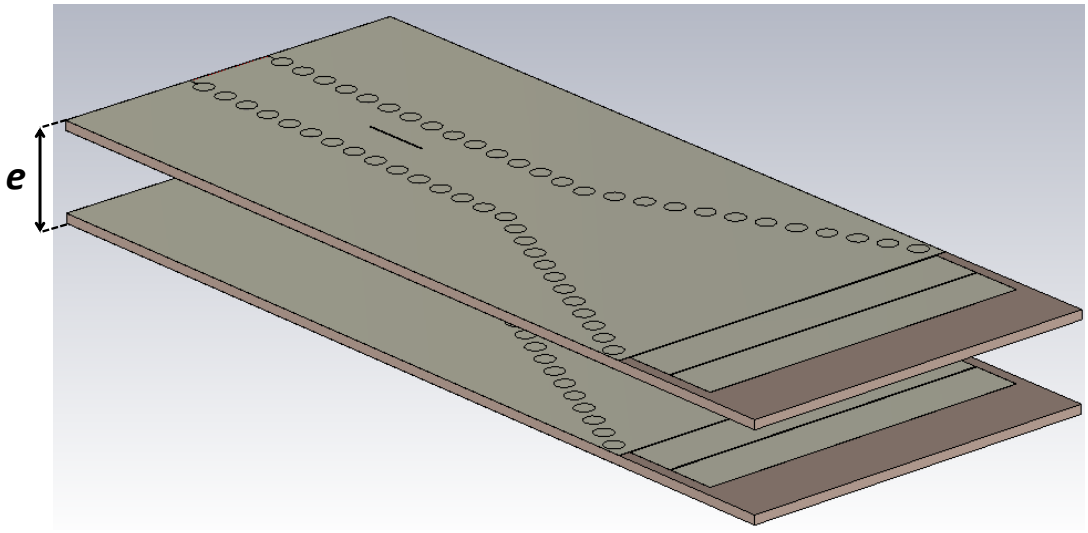

Figure 5. 23: SIW horn array with dielectric extension (configuration 1)

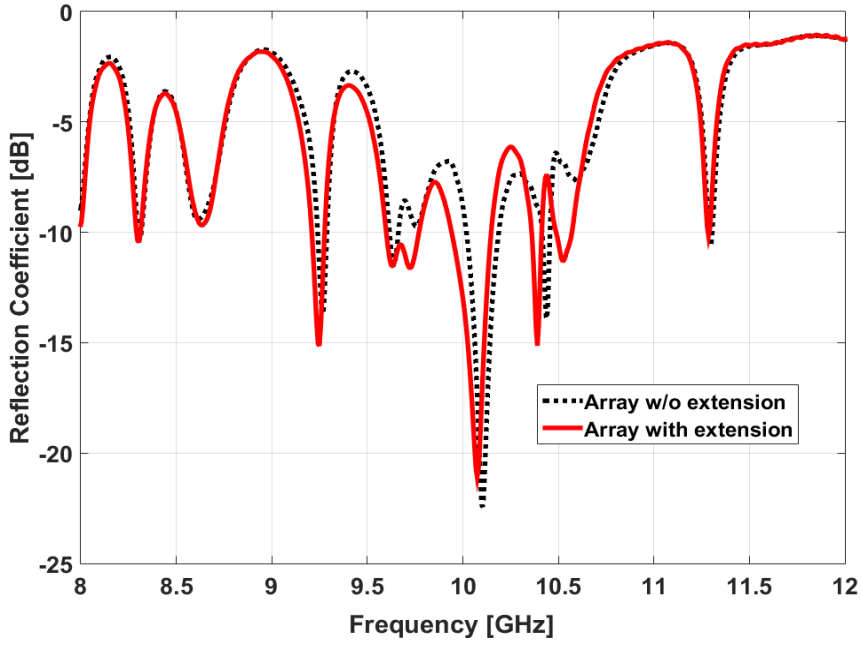

Figure 5. 24: Reflection coefficient of the SIW array (configuration 1) with and without extension

Concerning the radiation patterns, Figure 5.25 and Figure 5.26 depict the gains (ϕ and θ) in respectively xOz and xOy plane at 10 GHz. For comparison purposes the gain of the single thin SIW horn is also given. As expected, in the two planes, the horn radiation (θ-gain) is more directive (10.78 dBi) but, the FTBR is low still (2 dB).

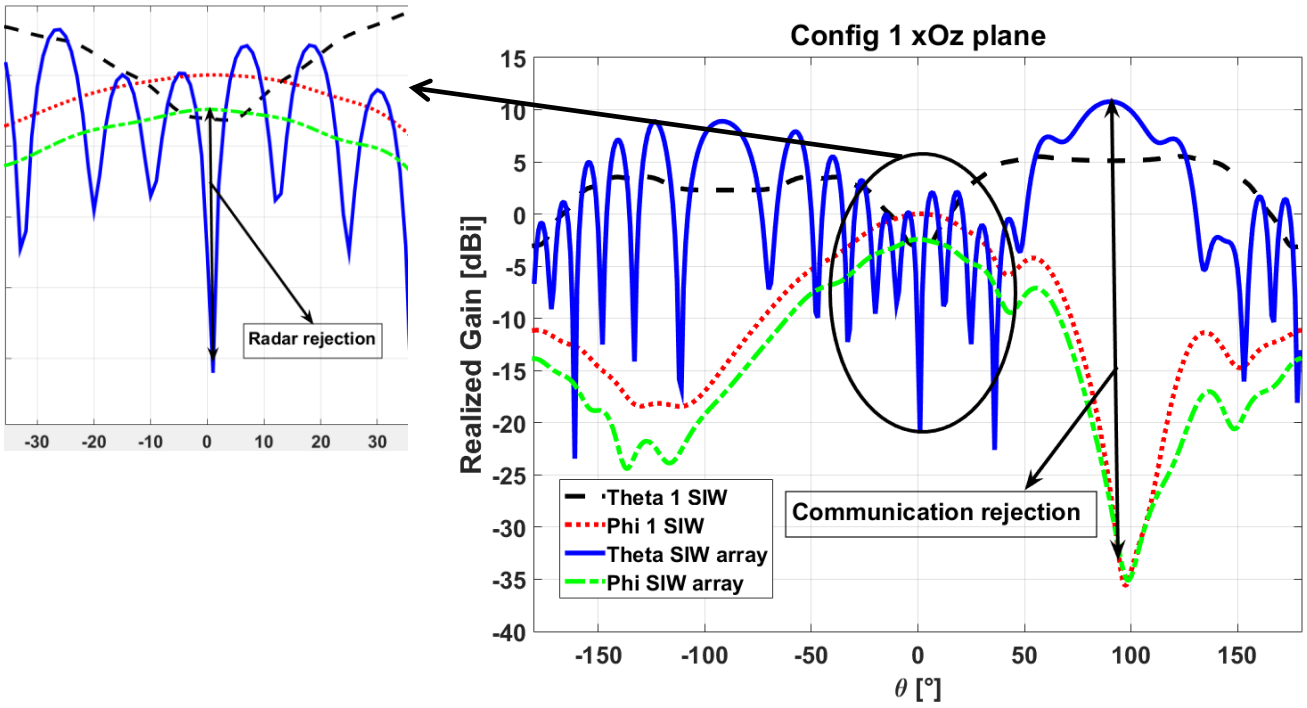

Figure 5. 25: Radiation patterns of configurations 1 in xOz plane: SIW array and one SIW at 10 GHz

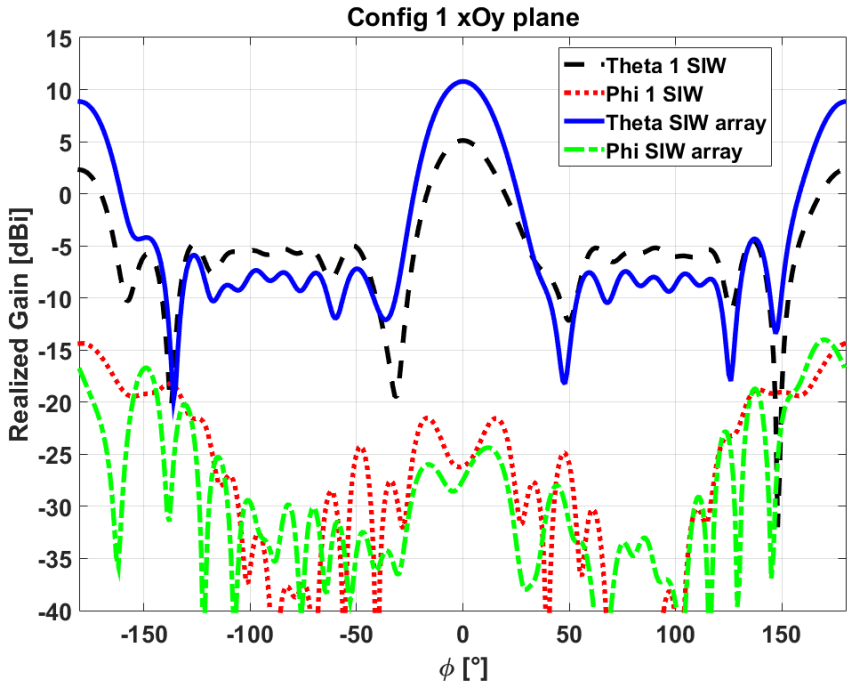

Figure 5. 26: Radiation patterns of configurations 1 in xOy plane: SIW array and one SIW at 10 GHz

In xOz plane, the rejection at $\theta = 0°$ was increased and it is now 10.27 dB. We can observe strong oscillations in the side lobes in which is embedded the slot radiation (at $\theta \neq 0°$). These oscillations are due to the proximity between the array elements.
Concerning the rejection at $\theta = 90°$ it is 38.25dB at 10 GHz ensuring a good isolation in this direction.

This study on thin SIW stacked array allows us to improve the horn radiation by 5.67 dB in comparison to the unique SIW horn (cf. Table 5.4). Moreover, the rejection at $\theta = 0°$ was also improved (10.27 dB). However, the use of such an array provides only 200 MHz impedance bandwidth.

	Impedance bandwidth	**Horn Gain (θ = 90°, ϕ = 0°)**	**Rejection at θ = 0°**	**Rejection at θ = 90°**
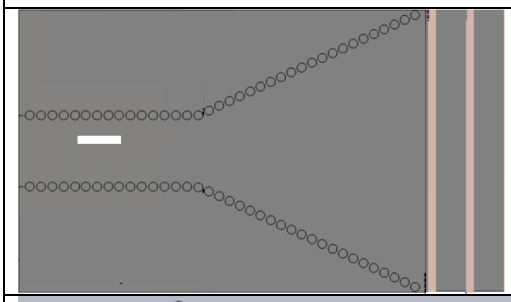	450 MHz	5.11 dBi	3 dB	38.5 dB
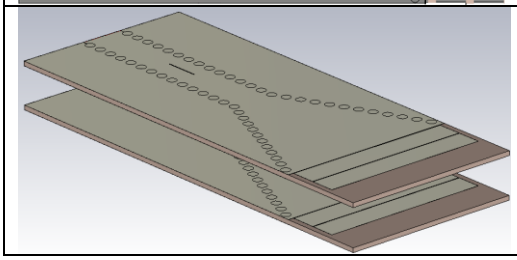	200 MHz	10.78 dBi	10.27 dB	38.25 dB

Table 5. 4: Performances of the SIW horns using thin substrates at 10 GHz

5.3.5. Conclusion

This study of thin SIW horn antennas shows that the SIW horns properties constitute a disadvantage in applying the multifunction concept. Indeed, the horn radiation is wide without much directivity (5.11 dBi). Furthermore, the impedance matching techniques increase the horn gain at $\theta = 0°$ (direction devoted to the second function), reducing the isolation between the two functions in this direction (3 dB at 10 GHz). Nevertheless, using an array of SIW provides much directivity to the horn (10.78 dBi), cf. Table 5.4. By spacing the array by $\lambda_0/2$ along *z*-axis, a null is created at $\theta = 0°$ increasing then the rejection in this direction (10.27 dB). However, stacking the antennas as in this section, could lead to complex integration issues.

In order to return to a more conventional solution and at the same time improve the performance of the SIW horn, in the next section, we will focus on the design of a thick SIW horn antenna.

5.4. Thick SIW horn antenna

It is proposed in this section to design a thick SIW horn antenna ($h > \lambda_0/6$). Indeed, as seen in previous section, the small substrate thickness of the SIW horn affects its radiation properties but also the impedance matching. Thus, to enhance the performance of the SIW horn, the substrate thickness will be increased. Additionally, due to physical constraints on the substrate thickness and to ease the via hole metallization [11], we decide to work at higher frequencies to gain even more electrical thickness. In this case, the Ka-band (between 20 GHz and 30 GHz) is arbitrarily choose for the study.

5.4.1. SIW design

To realize the thick SIW horn antenna, we first start by designing the feeding SIW. In Ka-Band, the WR-28 (standard Ka-band rectangular waveguide with dimensions: A = 7.11 mm and B = 3.56 mm) will be considered. The same substrate as the one used in previous section will be considered (ε_r = 2.33, tan δ = 0.0013) except that this time the substrate thickness is h = 3 mm. By using equations (1), (2), (4), (5) and (7), the starting dimensions needed for the SIW are presented in Table 5.5 below:

A_r	5.4 mm
A_e	4.7 mm
P	1 mm
w	0.8 mm

Table 5. 5: Ka-band SIW dimensions

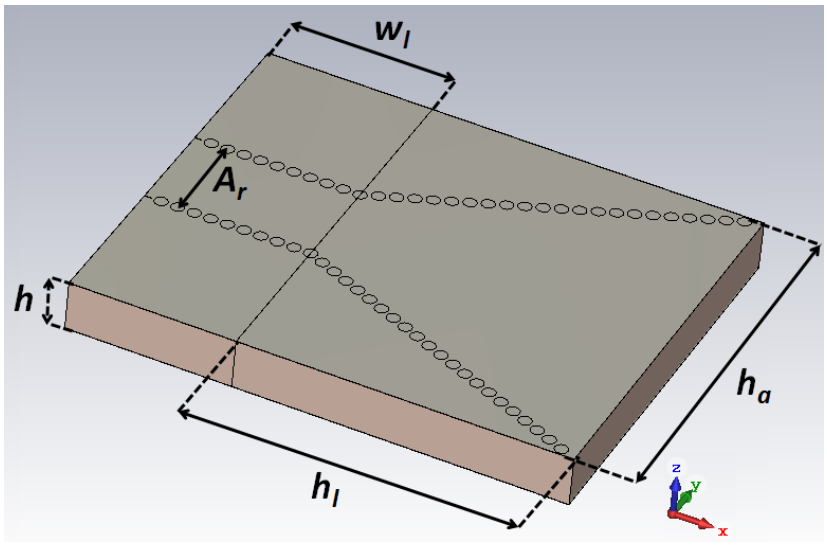

Figure 5. 27: Thick SIW horn antenna (h = 3 mm, A_r = 6.3 mm, wl = 10 mm, h_a = 25 mm and h_l = 20 mm)

However, to ensure that the second higher mode (in this case TE01) does not disrupt the fundamental mode, the parameter A_r has been refined to 6.3 mm, thus making it possible to

maintain a ratio of 2.1 between the SIW width and thickness (3 mm) as for conventional rectangular waveguide.
Hence, the theoretical SIW cut-off frequency for TE10 mode using (7) is f_c = 15.6 GHz.

Based on the previous calculation, a SIW of length w_l = 10 mm is modeled in CST. The cut-off frequency of TE10 mode is 15.64 GHz and 31.15 GHz for the second higher mode TE20. Then the results will be observed between 20 GHz and 30 GHz, corresponding to the SIW bandwidth (between 1.25f_c and 1.9f_c).

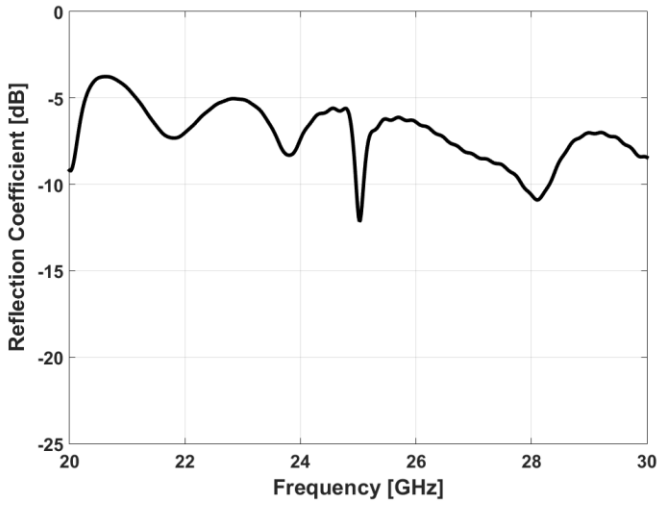

Figure 5. 28: Reflection coefficient of the thick SIW horn antenna

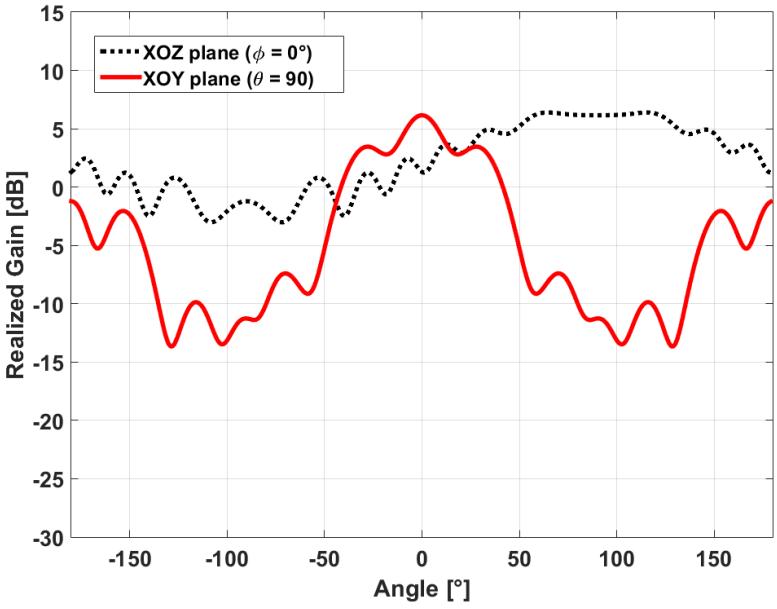

Figure 5. 29: SIW radiation patterns (θ-gain) in xOz and xOy planes at 28 GHz

5.4.2. SIW horn design

In this section the SIW presented previously will be used to feed the horn antenna (cf. Figure 5.27). In this figure, h_a and h_l are respectively the horn aperture in xOy plane and the horn length. They are chosen to control the radiation pattern in this plane [17].

We first study the reflection coefficient of this antenna. Figure 5.28 depicts the reflection coefficient of the SIW horn antenna. As expected, without the dielectric extension, the antenna matching is very critical. This is related to the field reflected on the horn aperture due to the impedance difference between the dielectric medium and free space. Nevertheless, there are two narrow bands with reflection coefficient below -10 dB, one at 25 GHz with 140 MHz bandwidth and the other at 28 GHz with 460 MHz bandwidth.

Concerning the radiation pattern, Figure 5.29 depicts θ-gain at 28 GHz in xOz and xOy plane. The realized gain in the main lobe is 6.15 dBi and the half power beamwidth (HPBW) is 132° and 84° in respectively xOz and xOy plane. Contrary to the previous chapters and as already explained, the SIW horn radiation pattern is wide without much directivity. Indeed, the large beamwidth in xOz plane is due to the small size of the horn aperture (cf. formulas (1) and (2) in [17]). Hence, as we will see later, to transmit information at ($\theta = 0°$, $\phi = 0°$), the slots will have to pick up more energy (at the expense of the power available for horn) in order to radiate more than the horn side lobes in this direction.

In the next section, the slot design (at 28.5 GHz) in the SIW horn is studied.

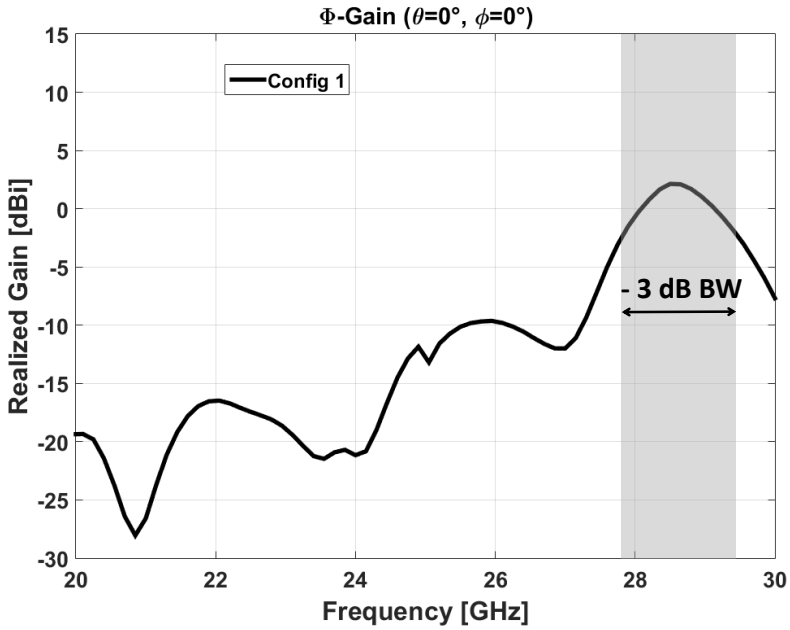

Figure 5. 30: Slot radiation (ϕ-gain) versus frequency at ($\theta = 0°$, $\phi = 0°$)

5.4.2.1. Slot design in the SIW

In this section we are interested in the design of a slot operating at 28.5 GHz in the feeding SIW. The slot length L is determined by using the formula (11). A parametric study is then necessary to find the resonant length of the slots while taking into account the effect of the horn.

Figure 5.30 presents the ϕ-gain of configuration 1 versus frequency obtained for a slot of length L = 3.8 mm, width l = 0.2 mm, positioned at D = 1.2 mm from the SIW centerline. As can be seen from this figure, the peak gain (2.13 dBi) is obtained at 28.5 GHz. As in the case of a rectangular waveguide, this gain value can be controlled by changing the offset D. The -3 dB gain bandwidth of the slot is 1.20 GHz.

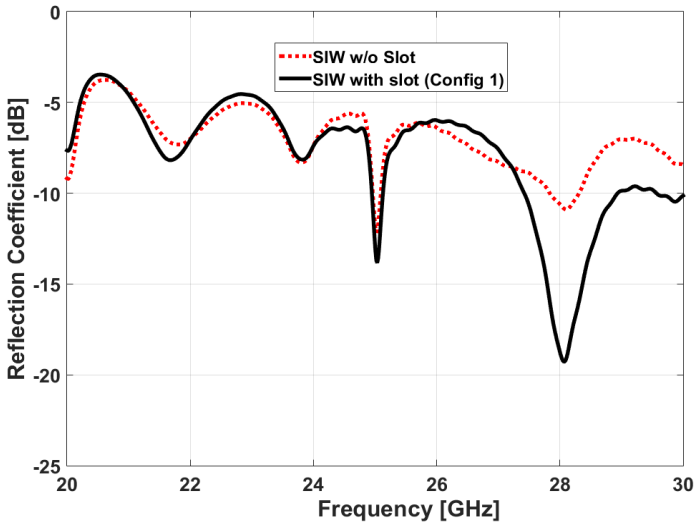

Figure 5. 31: Reflection coefficient of the SIW horn antenna with and without slot

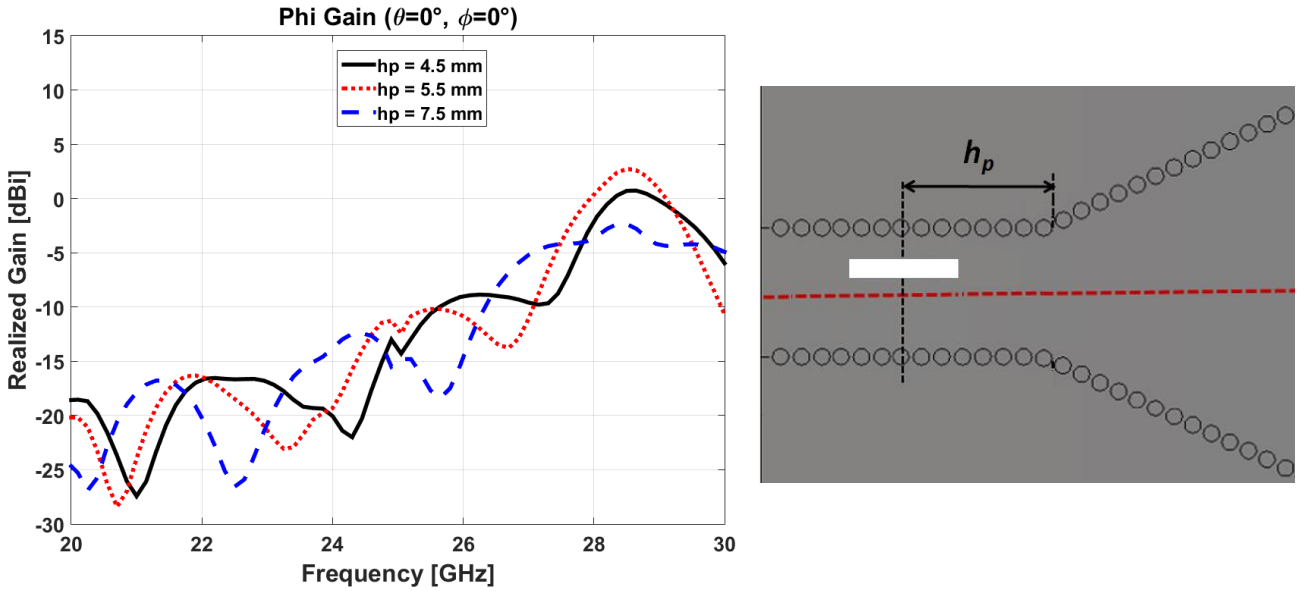

Figure 5. 32: Slot radiation (ϕ-gain) at different position (h_p) in the SIW

We now investigate the modification of the SIW horn reflection coefficient due to the slot. Figure 5.31 depicts the reflection coefficient of configuration 1 from 20 GHz to 30 GHz. For comparison purposes, the reflection coefficient of the SIW horn without slots is also given. As can be seen, the slot improves the impedance matching. A bandwidth of 1.5 GHz can be observed around 28 GHz. Indeed, as already explained, the poor matching is related to the field reflected at the horn aperture which goes back to the source. In the present case, the slot reduces the energy of the reflected field reaching the source, improving then the antenna impedance matching. Thus, by varying the slot dimensions and position, it is possible to shift the matching range of the system.

Moreover, if the slot is positioned in the SIW so that the incident wave in the slot is in phase with the reflected wave, this will provide much more energy to the slot for the radiation at (θ = 0°, ϕ = 0°). As an example, Figure 5.32 presents the slot radiation at different position from the aperture (H_p, cf. Figure 32). As can be seen from this figure the slot radiation is more or less important with H_p. For example, when H_p = 7.5 mm the peak gain is -2.3 dB while for H_p = 5.5 mm it is 2.64 dB.

Hence it is possible in our case to improve the impedance matching and the slot radiation by controlling the slot position in the feeding SIW.

Figure 5.33 shows θ-gain in the main direction of the horn versus frequency. As expected, at 28.5 GHz, due to the energy radiated by the slot, a 2.61 dB gain drop is observed in the main beam of the SIW horn in comparison to SIW horn without slots.

As for the SIW horn without slots, the radiation is wide without much directivity (-0.31 dBi peak gain in the main direction of the horn). To make the antenna more directive, in the next section, we investigate the possibility to increase the SIW horn gain by extending the dielectric substrate in the horn aperture.

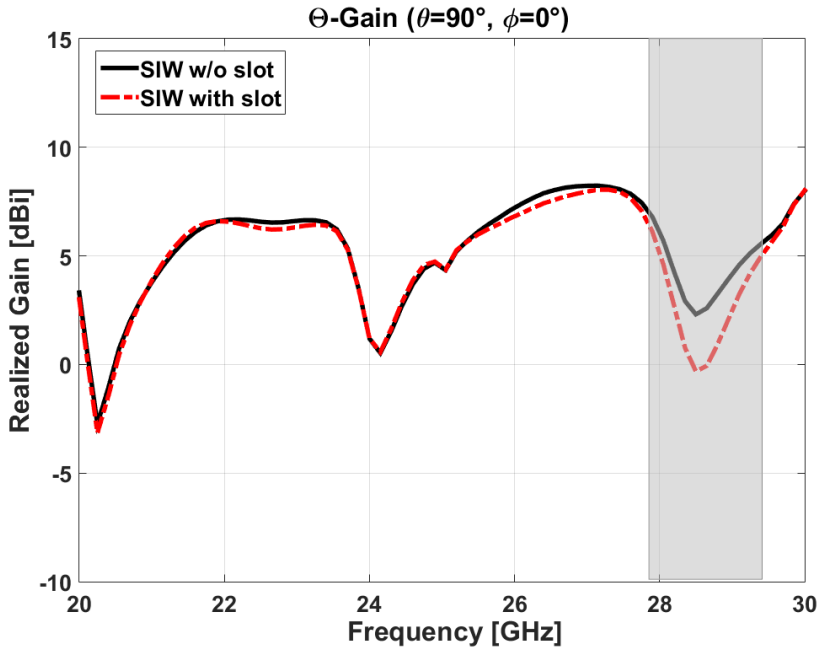

Figure 5. 33: SIW horn radiation with and without slot versus frequency at (θ = 90°, ϕ = 0°)

5.4.2.2. SIW horn with dielectric extension

In this section, we propose to extend the dielectric substrate at the horn aperture. Antenna configuration 1 as shown in Figure 5.34 will be used for this study.

It has been shown in [19] that such an extension improves the impedance matching and the directivity. This extension acts as a guiding structure at the interface between dielectric medium and free space resulting in a more directive radiation. As also shown in [18], the variation of the dielectric extension length (s_l, cf. Figure 5.34) makes it possible to control the gain in the main direction of the horn.

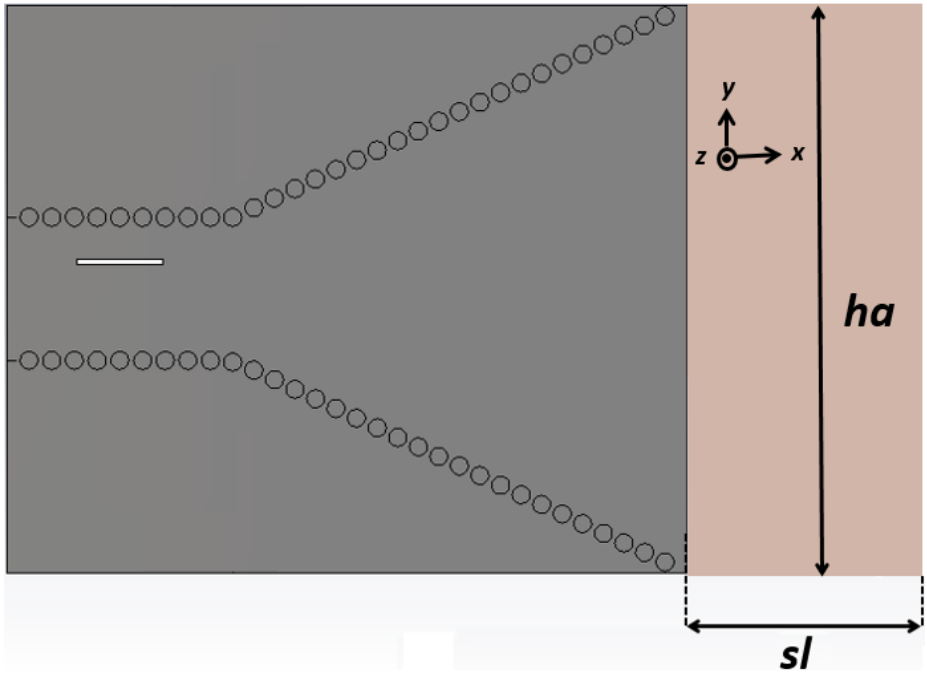

Figure 5. 34: Configuration 1 of the SIW horn antenna with dielectric extension (s_l = 18.5 mm)

In the present design, the length of the dielectric s_l is arbitrarily set to 18.5 mm. This corresponds to 7.9 dBi gain (at 28.5 GHz in the main direction of the horn). The gain appears to be low but in reality, it is also the consequence of the 2.73 dBi gain radiated by the slot. As a comparison, the gain of the same horn without slot is 10.69 dBi.

	Config 1 without extension	**Config 1 with extension**
Gain (horn main beam)	-0.31 dBi	7.9 dBi
HPBW xOz plane	137°	37°
HPBW xOy plane	78°	41°

Table 5. 6: Radiation characteristics of the antenna configurations 1 with and without slots at 28.5 GHz

Table 5.6 compares the results of antenna configuration 1 with and without dielectric extension at 28.5 GHz. As can be seen the gain has increased by 8.21 dB (in main direction of the horn) in comparison to the horn without dielectric extension.

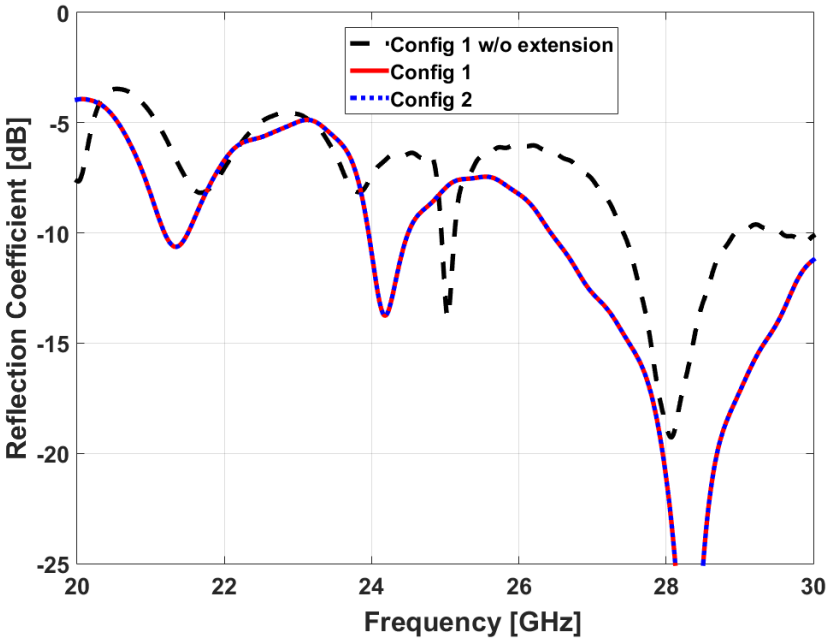

Figure 5. 35: Reflection coefficients of the configuration in comparison to SIW without extension

We now investigate the modification of the reflection coefficient due to the dielectric extension. Figure 5.35 depicts the reflection coefficient of the two configurations from 20 GHz to 30 GHz. For comparison purposes, the reflection coefficient of configuration 1 without extension is also given. As expected the dielectric extension improves considerably the antenna impedance bandwidth by 2.05 GHz in comparison to the case without extension.

This first study shows that the combination of the slot in the SIW and the dielectric extension (s_l = 18. 5 mm) has enabled us to considerably improve the impedance matching of the SIW horn (3.55 GHz bandwidth available), cf. Table 5.7. Moreover, thanks to the dielectric extension, the horn gain was increased by 8.21 dB compared to the case without extension. As already explained, all of these improvements are still possible and usable in our case because the antenna system requires always one slot active in the SIW.

	Impedance Bandwidth	Horn Gain	HPBW xOz plane	HPBW xOy plane
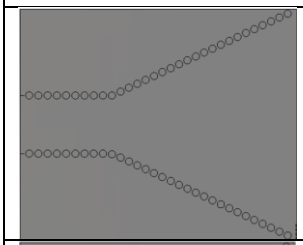	460 MHz	6.15 dBi	132°	84°
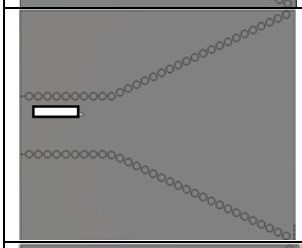	1.20 GHz	-0.31 dBi	137°	78°
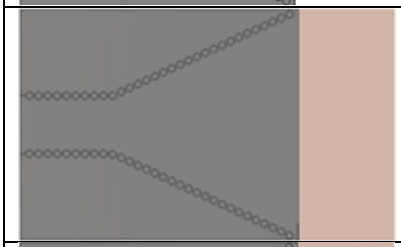	1.45 GHz	10.69 dBi	37.3°	47.15°
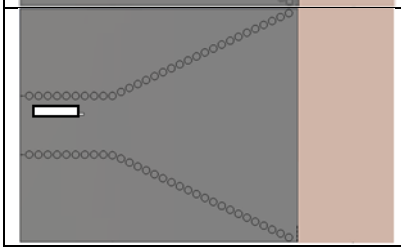	3.55 GHz	7.9 dBi	37°	41°

Table 5. 7: performances of the different types of antennas studied

In the next section this antenna with dielectric extension will be considered to evaluate the performances of the multifunction antenna system.

5.4.3. Antenna performances

In this part of the report, the simulated performances of the antenna in terms of radiation and rejection between the two functions are discussed. We recall that the configuration 1 used for this study is that of Figure 5.34. Configuration 2 corresponds to the reverse situation.

- **Radiation characteristics of the two functions**

The simulated performance of the main function and the secondary function are studied. More precisely, we investigate the impact of the slots on the antenna system.

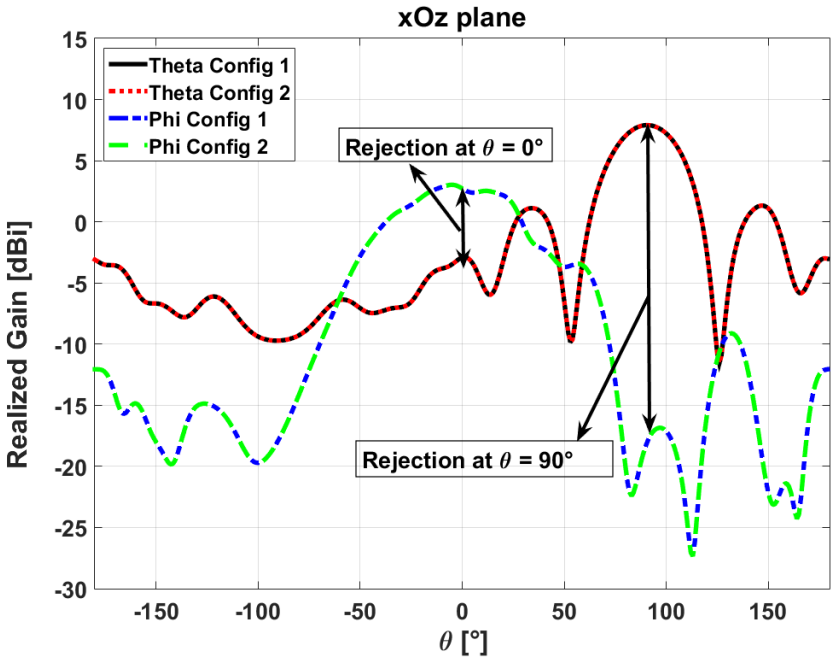

Figure 5. 36: radiation pattern of the multifunction antenna at 28.5 GHz in xOz plane

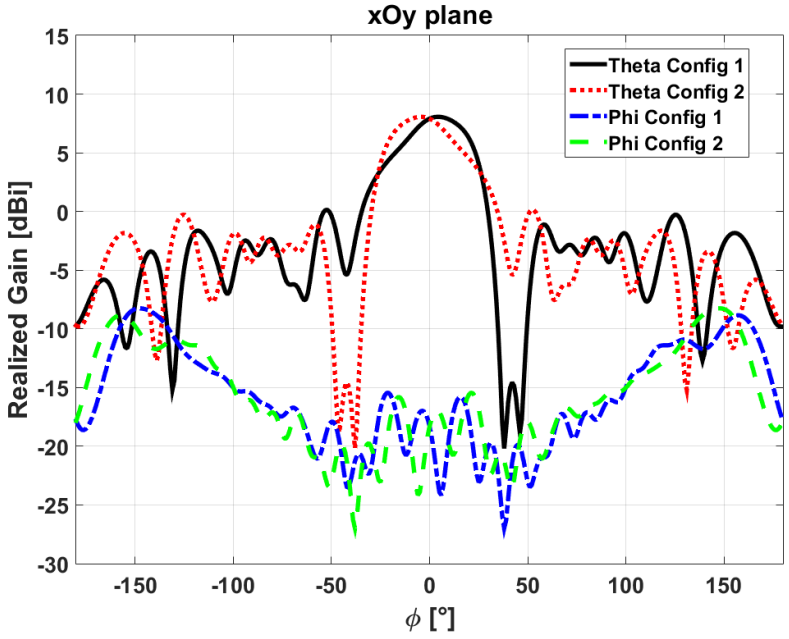

Figure 5. 37: radiation pattern of the multifunction antenna at 28.5 GHz in xOy plane

We first investigate the radiation pattern of the antenna system. Figure 5.36 and Figure 5.37 depict θ and ϕ-gain at 28.5 GHz in respectively xOz and xOy planes for configuration 1 and 2.

In xOz plane, as expected, due to symmetry, both configurations 1 and 2 give exactly the same patterns in ϕ and θ-gain, which guarantees that the two functions are not affected when switching configurations. The maximum gain is 7.9 dBi for θ-gain (at $\theta = 90°$) and 2.73 dBi for ϕ-gain (at $\theta = 0°$).

Directions	Config	Phase (°)	Amp. (dBi)
$\theta = 0°$	1	0	2.73
	2	180	2.73

Table 5. 8: BPSK communication at 28.5 GHz

A solution to further increase the slot directivity and then the rejection at $\theta = 0°$ by using slots array will be investigated in section 5.4.4.

Table 5.8 summarizes the characteristics obtained for the BPSK communication at ($\theta = 0°$, $\phi = 0°$).

In xOy plane, due to the dissymmetry brought by the activation of one of the two slots, the θ-gains of the two configurations present a mirror symmetry at $\phi = 0°$. This dissymmetry is more visible in this case because, contrary to previous chapters, the slots radiate much more power as explained in section 5.4.2. As we will see in section 5.4.4, using a slot array in the SIW can also further reduce this dissymmetry. Nevertheless, in the main direction of the horn ($\phi = 0°$) the two configurations are the same (7.9 dBi gain), which guarantees that the main function is not affected in this direction when switching configurations.
As for the SLL it is -7.77 dB, which is critical for radar applications.

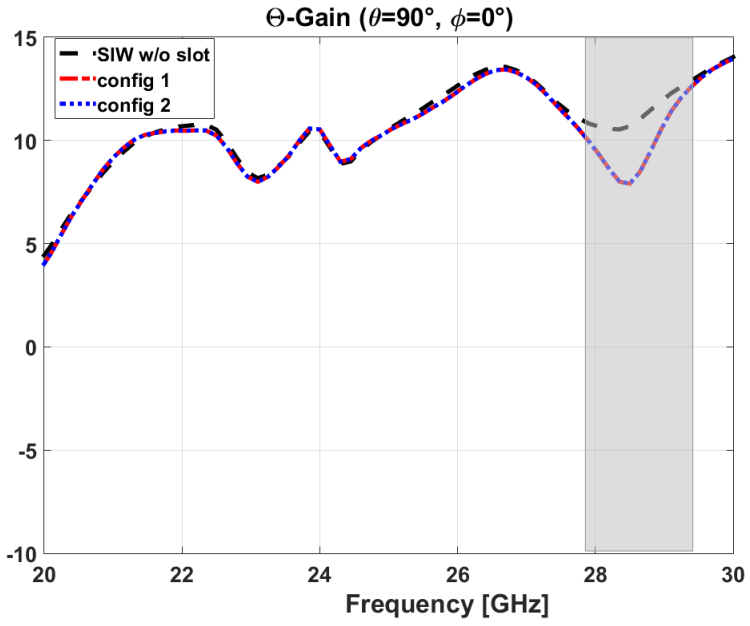

Figure 5. 38: SIW horn radiation at ($\theta = 90°$, $\phi = 0°$) versus frequency

Figure 5.38 depicts θ-gain in the main direction of the horn versus frequency for the two configurations in comparison to that of the horn without slot. As expected, the slot activation in the SIW causes a gain drop in the main direction of the horn. At 28.5 GHz (resonant frequency of the slot) the gain drop is 2.79 dB.

- **Study of the rejection between the functions**

We now investigate the rejections between the two functions as defined in Figure 5.36 versus frequency in order to evaluate the robustness of the solution.

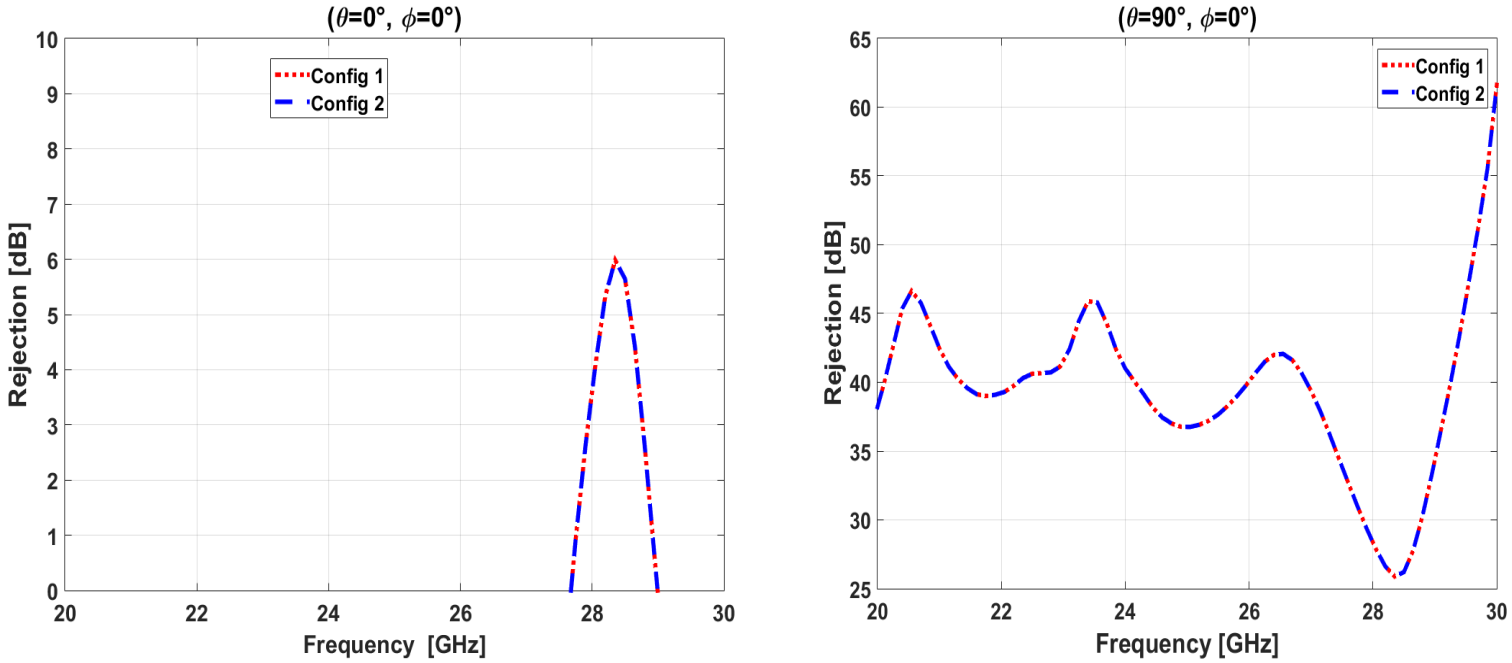

Figure 5. 39: Rejections of the multifunction antenna: (a) at θ = 0° and (b) θ = 90°

Figure 5.39 (a) and (b) present the variation of the two rejections versus frequency.
At the resonant frequency of the slot (28.5 GHz), the rejection at $\theta = 0°$ is 5.6 dB. However, when moving away from this frequency the rejection drops sharply showing a narrow band rejection at $\theta = 0°$. As already explained, a solution to further increase the rejection at $\theta = 0°$ through the use of slot array will be discussed in the next section.

Concerning the rejection at $\theta = 90°$ it is at least 26 dB from 20 GHz to 30 GHz ensuring the isolation between the two functions is this direction.

The transposition of the initial multifunction antenna concept into a SIW technology has been presented in this section. The direct BPSK modulation can be achieve at $\theta = 0°$ by switching the activated slot. However, the rejection level between the two functions particularly at $\theta = 0°$ is low (5.6 dB, at the resonant frequency of the slot) to ensure isolation between the functions in this direction and is narrow band. Furthermore, the gain in the main lobe of the horn is 7.9 dBi (only

5.17 dB higher than the slot radiation at ($\theta = 0°$, $\phi = 0°$)) with -7.77 dB SLL. As already explained, all of these characteristics prevent the use of this solution for a radar and communication applications which require high gain for the radar. A possible solution to increase the gain of the main function is to replace the horn by an antipodal linearly tapered slot antenna (ALTSA) array as in [25] which presents a more directional beam. Alternatively, this antenna may be used for navigation and communication applications for example.

In the next section, we investigate the possibility to increase the directivity at $\theta = 0°$ by using a slot array in the SIW while maintaining the BPSK modulation capabilities.

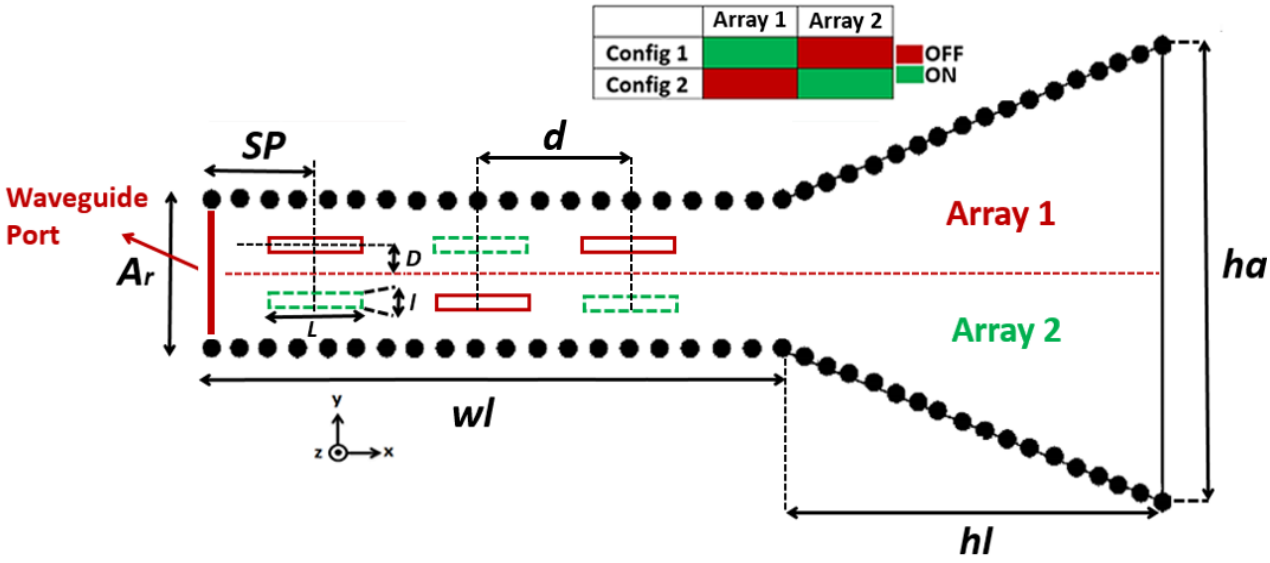

Figure 5. 40: SIW configurations with slots arrays (A_r = 6.3 mm, wl = 20 mm, h_a = 25 mm and h_l = 20 mm)

5.4.4. Slot array in the SIW

In this section the goal is to study the impact of a slot array on the previous SIW horn antenna. In doing so the directivity (and then the gain) at $\theta = 0°$ will be improved which might be of interest for some applications. Additionally, the impact of this array on the rejections will be discussed.

5.4.4.1. Antenna design

The same slots dimensions (L = 3.8 mm and l = 0.2 mm) as in the previous section are considered for the array design. The length of the dielectric extension in the horn aperture is still s_l = 18.5 mm

In order to increase the directivity at $\theta = 0°$, the array is here arbitrarily composed of three slots milled in the SIW (array 1, cf. Figure 5.40). To have consecutive elements in phase, the slots are spaced by $\lambda_g/2$ and offset on opposite sides of the centerline by D [24]. In order for the slots to not radiate a lot of the energy propagating in the SIW, in the present case the offset has been arbitrarily reduced to 0.8 mm (instead of 1.2 mm in the previous section).

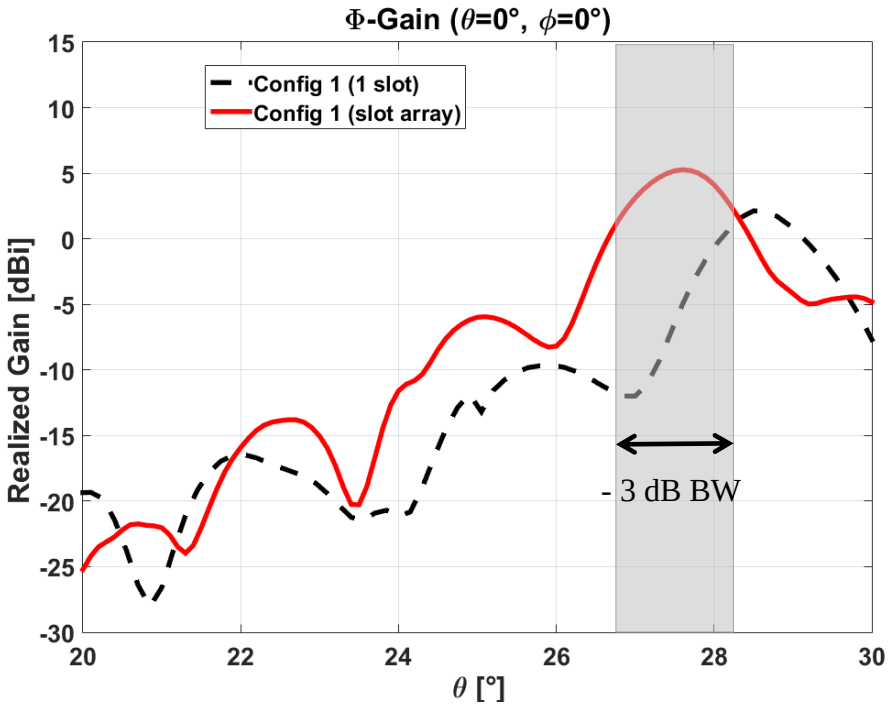

Figure 5. 41: Slots radiation (ϕ-gain) at (θ = 0°, ϕ = 0°) versus frequency

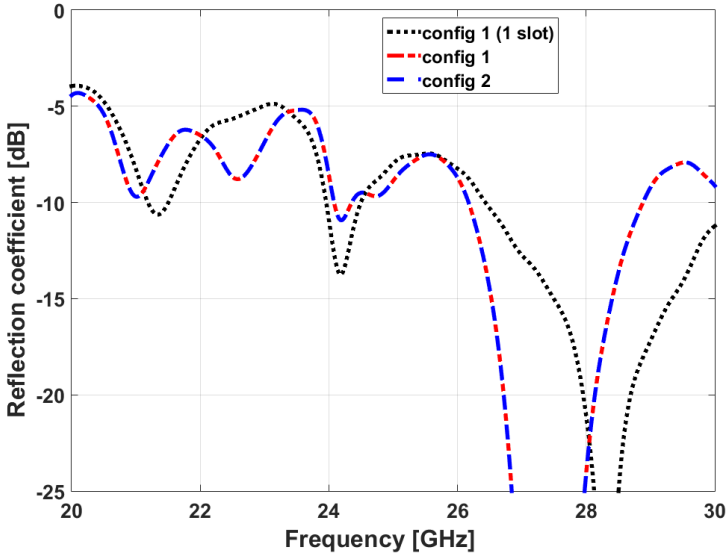

Figure 5. 42: Reflection coefficient of configurations 1 of the SIW horn with slots array and one slot

Figure 5.41 shows the ϕ-gain versus frequency of the array 1 (configuration 1). For comparison purposes, the gain of the SIW horn with one slot is also given. As shown in Figure 5.40, the mutual coupling between the slots causes a frequency shift in comparison to the case using one slot. The maximum gain (5.26 dBi) is obtained this time at 27.6 GHz. The gain improvement appears to be

low (only 2.53 dB higher than the case using one slot) because as explained before, the offset *D* has been reduced so that the slots do not radiate all the energy in the SIW at the expense of the SIW horn. The -3 dB gain bandwidth has been increased by 170 MHz (in comparison to the case using one slot) and it is now 1.37 GHz.

As previously, the radiation in $\theta = 0°$ direction corresponds to a direct BPSK modulation. For that reason a second array of three slots is placed symmetrically to the SIW centerline (array 2, cf. Figure 5.40) so as to generate a 180° phase shift in the radiated field each time the activated array is changed. This defines two complementary configurations (cf. Figure 5.40). In configuration 1, only the slots forming array 1 radiate while the other are closed. Configuration 2 corresponds to the reverse complementary situation.

We now investigate the modification of the reflection coefficient of this new antenna due to the slot array (cf. Figure 5.42). For comparison purposes the reflection coefficient of the SIW horn with one slot is also given. As expected, the interaction between the slots causes a frequency shift and the available impedance bandwidth is reduced by 910 MHz in comparison to SIW horn with one slot. It is 2.64 GHz (from 26.2 GHz and 28.9 GHz).

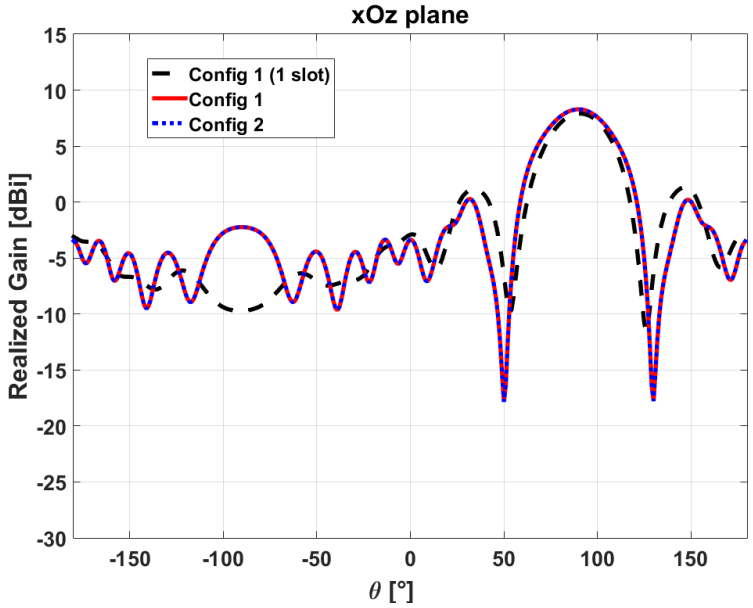

Figure 5. 43: Radiation pattern (θ-gain) in xOz plane at 27.6 GHz

5.4.4.2. Antenna performance

In this section, the performances (radiation patterns and isolations) of the antenna system due to the slot array are investigated.

- **The main function**

Here, we study the impact of the slot array on the main function.

Figure 5.43 and Figure 5.44 present θ-gain of the two configurations in respectively xOz and xOy plane at 27.6 GHz. For comparison purposes, the gain of the SIW horn with one slot at 28.5 GHz is also given.

In xOz plane, as expected, due to symmetry both configurations 1 and 2 give the same patterns which guarantees that the main function is not affected when switching the arrays. The maximum gain in the main beam is 8.28 dBi. We also notice a slight increase in the horn beamwidth (5.53°) due to the presence of slot array.

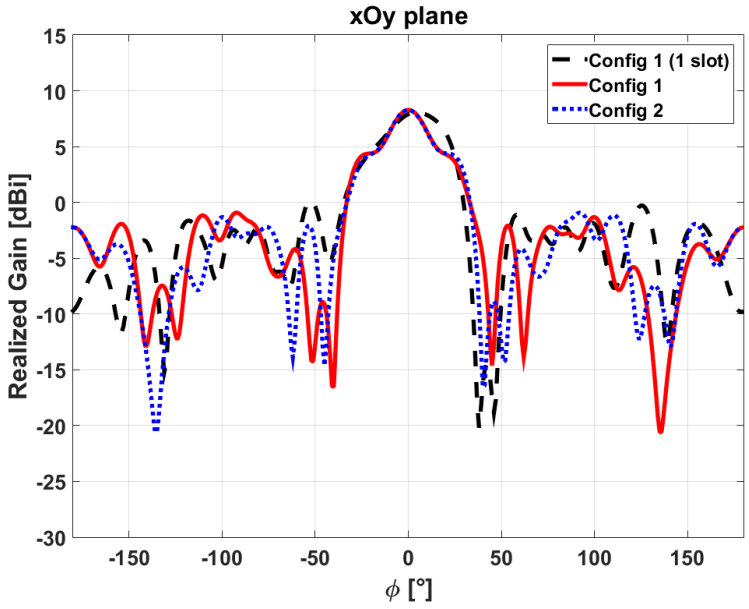

Figure 5. 44: Radiation pattern (θ-gain) in xOy plane at 27.6 GHz

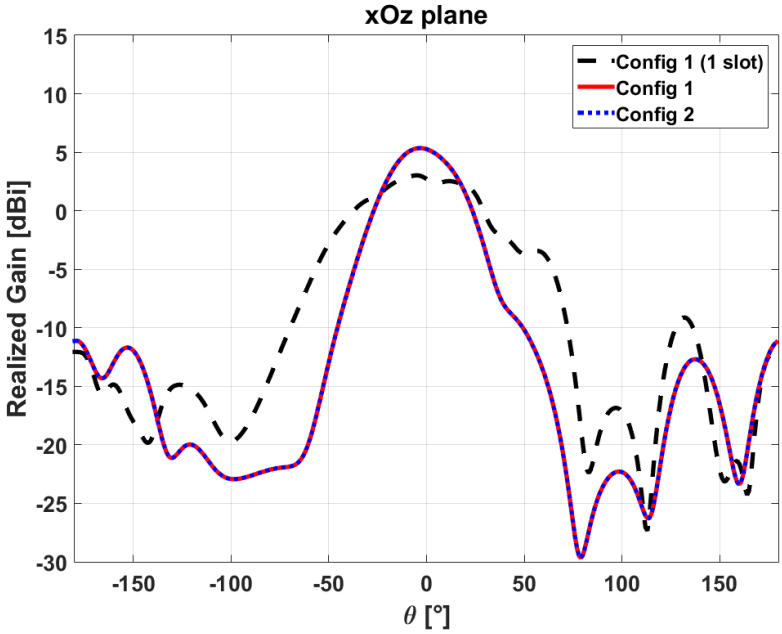

Figure 5. 45: Radiation pattern (ϕ-gain) xOz plane

In xOy plane, contrary to the case using one slot (cf. Figure 5.37) the slot array corrects the dissymmetry observed in the main beam between the two configurations. Indeed, the array leads to a radiation more located at (θ = 0°, ϕ = 0°) direction, reducing the impact of slots in other directions. The SLL is now -9.2 dB (instead of -7.77 dB).

- **Communication function**

We now analyze, the performance of the communication antenna (slot array).

Figure 5.45 depicts the ϕ-gain in xOz plane of the two configurations at 27.6 GHz. For comparison purposes, the gain of the SIW horn with one slot at 28.5 GHz is also given. As expected the slot radiation is more directive at θ = 0°.

Table 5.9 summarizes the results of the BPSK communication at θ = 0°.

Directions	Config	Phase (°)	Amp. (dBi)
$\theta = 0°$	1	0	5.26
	2	180	5.26

Table 5. 9: BPSK communication at 27.6 GHz

The rejections considered for this study are defined as in Figure 5.46.

	Impedance bandwidth	**Horn Gain**	**Slot Gain**	**Rejection at θ = 0°**	**Rejection at θ = 90°**
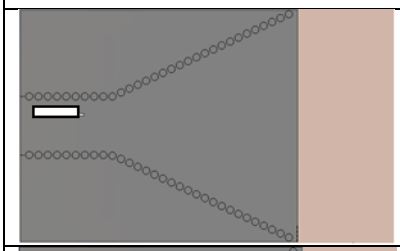	3.55 GHz	7.9 dBi	2.73 dBi	5.6 dB	26.19 dB
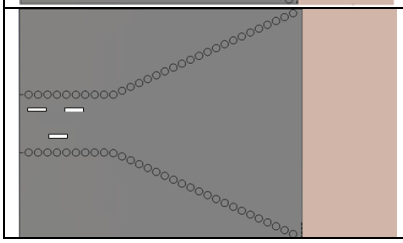	2.64 GHz	8.28 dBi	5.26 dBi	8.62 dB	32 dB

Table 5. 10: Performances of the antenna with one slot (28.5 GHz) and three slots array (27.6 GHz)

Table 5.10 compares the performances of the antennas configurations 1 with one slot (at 28.5 GHz) and three slots array (27.6 GHz). In comparison to the SIW horn with one slot, the use of the array allows us at the same time to increase the gain at $\theta = 0°$ by 2.53 dB and the rejection in this direction by 2.98 dB. These performances were achieved without affecting the horn gain.

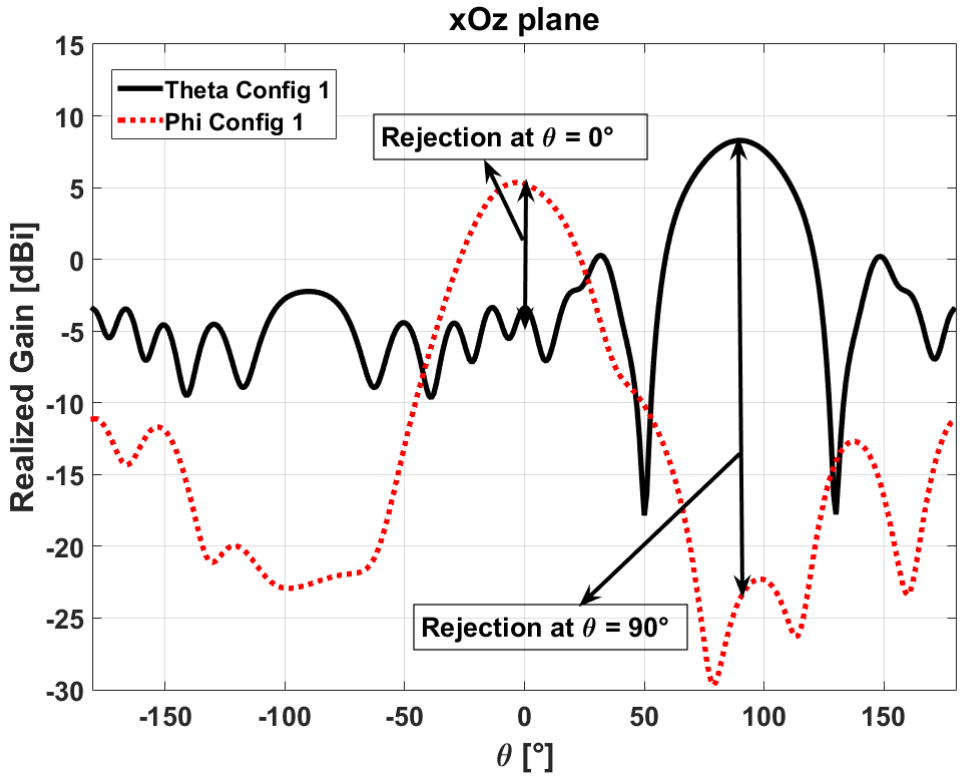

Figure 5. 46: Rejections of the antenna system at 27.6 GHz

- **Study of the rejection between the two functions**

We now investigate the rejection between the two functions of the antenna system versus frequency.

Figure 5.47 (a) and (b) present the variation of the rejections in respectively $\theta = 0°$ and $\theta = 90°$ versus frequency. The maximum rejection at $\theta = 0°$ (8.62 dB) is obtained at 27.6 GHz (resonant frequency of the array). We can also see that this rejection is narrow band.
As for the rejection at $\theta = 90°$, it is at least 32 dB from 20 GHz to 30 GHz ensuring the isolation in this direction.

The slots array allowed to improve the directivity at $\theta = 0°$ (5.26 dBi). Furthermore, the rejection at $\theta = 0°$ has been increased and is 8.62 dB, which ensures more isolation between the two functions at 27.6 GHz. In counterpart, the length of the SIW was doubled ($w_l = 20$ mm). The frequency study also demonstrated that the rejection at $\theta = 0°$ is narrow band while the rejection at $\theta = 90°$ is at least 32 dB.

5.4.5. Conclusion

In this first part, it has been shown that it is possible to transpose the multifunction antenna concept with direct BPSK modulation into thick SIW working in Ka-band. However, the rejection between the two functions is low, particularly at $\theta = 0°$ (5.64 dB), cf. Table 5.10. Moreover, the gain in the main beam of the horn is 7.9 dBi (only 5.17 dB higher than the slot radiation at $\theta = 0°$). These characteristics prevent the use of this solution for a radar and communication applications which require high gain for the radar. But this antenna may be used for other multifunction applications such as navigation/communication etc.
By using slots array in the feeding SIW, the directivity at $\theta = 0°$ has been improved and the rejections in this direction is now 8.62 dB (cf. Table 5.10), which ensures more isolation between the two functions. The frequency study also demonstrated that the impedance bandwidth was reduced by 910 MHz in comparison to the SIW with one slot (cf. Table 5.10). However, in the two cases (SIW with one slot and slot array), the rejection at $\theta = 0°$ is narrow band while the rejection at $\theta = 90°$ is at least 26 dB.

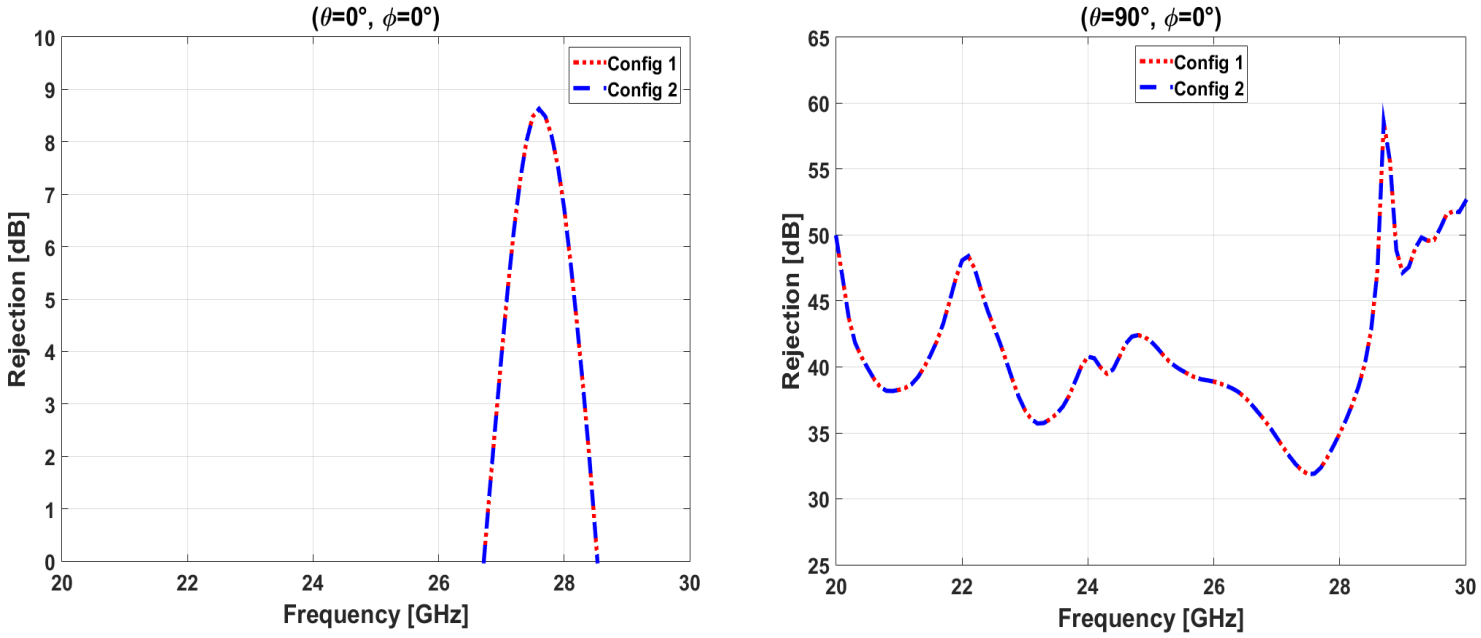

Figure 5. 47: Rejections of the multifunction antenna: (a) at θ = 0° and (b) θ = 90°

5.5. Conclusion of chapter 5

The possibility to transpose the multifunction antenna concept with direct BPSK modulation into SIW technology offering low profile and easy integration with planar circuits has been studied in this chapter. In order to realize the multifunction antenna on thin commercial substrate allowing the use of appropriate feeding techniques to completely integrate the antenna with other elements printed in the same substrate, the study of SIW horn in thin substrate has been carried out. The study has been done in X-band. As expected the thin SIW horn radiation is wide without much

directivity (5.11 dBi). Furthermore, the impedance matching techniques increase the horn gain at $\theta = 0°$ (direction devoted to the second function), reducing the isolation between the two functions in this direction (3 dB at 10 GHz). By using an array of thin SIW, the directivity of the horn has been increased (10.78 dBi). Additionally, the $\lambda_0/2$ spacing between the two thin SIW allows us to increase the rejection at $\theta = 0°$ (10.27 dB).
In order to return to a more conventional solution and at the same time improve the performance of the SIW horn, the substrate thickness has been increased (thick SIW horn). Due to physical constraints on the substrate thickness and to ease the via hole metallization, we work this time in Ka-band. However, the rejection between the two functions is still low, particularly at $\theta = 0°$ (5.64 dB). Moreover, the radiation of the horn is wide without much directivity (7.9 dBi) and is only 5.17 dB higher than the slot radiation at $\theta = 0°$. By using slots array in the feeding SIW, the directivity at $\theta = 0°$ has been improved (5.26 dBi) and then the rejections in this direction is now 8.62 dB. In counterpart, the use of such a slot array requires the use of a longer SIW. The frequency study also demonstrated that the impedance bandwidth was reduced by 910 MHz in comparison to the SIW with one slot. The rejection at $\theta = 0°$ is narrow band in the two cases (SIW with one slot and slot array) while the rejection at $\theta = 90°$ is at least 26 dB from 20 GHz to 30 GHz.

Hence, each of the approaches presented in this chapter have the disadvantage of having no directional radiation pattern and a low FBTR, preventing us from using this solution for radar and communication applications. Alternatively, these solutions can be used to perform a multifunction antenna for others applications which do not need a high directivity. In order to apply this solution to radar and communication applications, the SIW horn design and its radiation properties must first be treated to reflect the radiation characteristics of conventional horn antennas (directivity and FTBR). Another solution would be to replace the horn by an antipodal linearly tapered slot antenna (ALTSA) array as in [25] which presents a more directive beam.

[1] J. Hirokawa and M. Ando, "Single-layer feed waveguide consisting of posts for plane TEM wave excitation in parallel plates," IEEE Trans. Microwave Theory & Tech., vol. 46, no. 5, pp. 625-630, May 1998.

[2] F. Shigeki, “Waveguide line,” (in Japanese) Japan Patent 06-053 711, Feb. 25, 1994.

[3] B. N. Das, K. V. S. V. R. Prasad, and K. V. Seshagiri Rao, “Excitation of waveguide by stripline and microstrip-line-fed slots,” IEEE Trans. Microwave Theory Tech., vol. MTT-34, pp. 321–327, Mar. 1986.

[4] W. Grabherr, B. Huder, and W. Menzel, “Microstrip to waveguide transition compatible with MM-wave integrated circuits,” IEEE Trans. Microwave Theory Tech., vol. 42, pp. 1842–1843, Sept. 1994.

[5] T. Q. Ho and Y. Shih, “Spectral-domain analysis of E-plane waveguide to microstrip transitions,” IEEE Trans. Microwave Theory Tech., vol. 37, pp. 388–392, Feb. 1989.

[6] L. J. Lavedan, “Design of waveguide-to-microstrip transitions specially suited to millimeter-wave applications,” Electron. Lett., vol. 13, Sept. 1977.

[7] HIROSHI, U., TAKESHI, T., FUJII, M. “Development of a ‘laminated waveguide,” IEEE Trans. on Microwave Theory and Techniques. 1998, vol. 46, no. 12, pp. 2438–2443.

[8] DESLANDES, D., WU, K. “Single-substrate integration technique of planar circuits and waveguide filters”. IEEE Trans. on Microwave Theory and Techniques, 2003, vol. 51, no. 2, pp. 593 - 596.

[9] XU, F., WU, K. “Guided-wave and leakage characteristics of substrate integrated waveguide,” IEEE Trans. on Microwave Theory and Techniques, 2005, vol. 53, no. 1, pp. 66-73.

[10] DESLANDES, D., WU, K. “Accurate modeling, wave mechanisms, and design considerations of a substrate integrated waveguide,” IEEE Trans. on Microwave Theory and Techniques, 2006, vol. 54, no. 6, pp. 2516–2526.

[11] M. E. Morote, B. Fuchs, J. F. Zurcher, and J. R. Mosig, “Novel thin and compact H-plane SIW horn antenna,” IEEE Trans. Antennas Propag., vol. 61, no. 6, pp. 2911–2920, Jun. 2013.

[12] M. Bozzi, A. Georgiadis, K. Wu, “Review of substrate-integrated waveguide circuits and antennas”, Special Issue on RF/Microwave Communication Subsystems for Emerging Wireless Technologies”, doi: 10.1049/iet-map.2010.0463.

[13] M. Bozzi, L. Perregrini, K. Wu, P. Arcioni, “Current and Future Research Trends in Substrate Integrated Waveguide Technology,” Radioengineering, vol. 18 NO. 2, june 2009.

[14] R. E. Collin and F. J. Zucker, Antenna Theory, Part 2. New York: McGraw-Hill, 1969.

[15] Dominic Deslandes and Ke Wu, “Design Consideration and Performance Analysis of Substrate Integrated Waveguide Components”, Microwave Conference, 2002, 32nd European.

[16] Maurizio Bozzi, Feng Xu, Dominic Deslandes and Ke WU, “Modeling and Design Considerations for Substrate Integrated Waveguide Circuits and Components”, TELSIKS 2007, Serbia, Nis, September 26-28.

[17] Z. L. Li and K. Wu, “A new approach to integrated horn antenna,” in Proc. Int. Symp. on Antenna Technology and Applied Electromagnetics, Jul. 2004, pp. 535–538.

[18] W. Q. Che, B. Fu, P. Yao, Y. L. Chow, and E. K. N. Yung, “A compact substrate integrated waveguide H-plane horn antenna with dielectric arc lens: Research articles,” Int. J. RF Microw. Comput.-Aided Eng., vol. 17, Sep. 2007, pp. 473–479.

[19] H. Wang, D.-G. Fang, B. Zhang, and W.-Q. Che, “Dielectric loaded substrate integrated waveguide (SIW) H-plane horn antennas,” IEEE Trans. Antennas Propag., vol. 58, no. 3, pp. 640–647, Mar. 2010.

[20] Y. Cai, Z. P. Qian, Y. S. Zhang, J. Jin, and W. Q. Cao, “Bandwidth enhancement of SIW horn antenna loaded with air-via perforated dielectric slab,” IEEE Antennas Wireless Propag. Lett., vol. 13, pp. 571–574, Apr. 2014.

[21] Z. Li, X.-P. Chen, and K. Wu, “A surface mountable pyramidal horn antenna and transition to substrate integrated waveguide,” in Proc. Int. Symp. Signals, Systems and Electronics, Feb. 2007, pp. 607–610.

[22] M. Yousefbeiki, A. A. Domenech, J. R. Mosig, and C. A. Fernandes, “Ku-band dielectric-loaded SIW horn for vertically-polarized multisector antennas,” in Proc. 6th Eur. Conf. Antennas and Propagation (EUCAP), Mar. 2012, pp. 2367–2371.

[23] M. E. Morote, B. Fuchs, J. F. Zurcher, and J. R. Mosig, “A printed transition for matching improvement of SIW horn antennas,” IEEE Trans. Antennas Propag., vol. 61, no. 4, pp. 1923–1930, Apr. 2013.

[24] S. Moitra, A. K. Mukhopadhyay and A. K. Bhattacharjee, “Ku-Band Substrate Integrated Waveguide (SIW) Slot Array Antenna for Next Generation Networks,” Global Journal of Computer Science and Technology Network, Web & Security, vol. 13, 2013.

[25] Y. J. Cheng and Y. Fan, “Millimeter-wave miniaturized substrate integrated multibeam antenna,” IEEE Trans. Antennas Propag., vol. 59, no. 12, pp. 4840–4844, Dec. 2011.

Conclusion and perspectives

Conclusion

This thesis was dedicated to the development of a compact multifunction antenna for radar and communication applications. We have based our work on a standard horn antenna (for radar purposes), which has been modified to add a secondary function through the radiation from a slot or a series of slots etched into the feeding waveguide. The slots are designed so that the two functions use orthogonal polarizations and directions. By using a switching mechanism to activate one of the slots at a given time, a fraction of the power in the feeding waveguide is then radiated through the activated slot thus providing a unique communication link with direct BPSK modulation.

To validate the concept, a full characterization of the multifunction antenna has been carried out. To dynamically control the slot activation and the BPSK modulation, PIN diodes have been studied and mounted on the antenna prototype thanks to an *H*-shaped polarization circuit. At first, we considered beam lead PIN diode. Hence, by loading the slot with the beam lead diode, it is possible to control the communication function while preserving the main radar function. In reverse bias, the diode capacitor and the polarization circuit shifted the frequency resonance to 4.7 GHz instead of 5 GHz. At the new resonance frequency, the gain difference between the OFF and ON modes of the diode is 22.84 dB validating the polarization circuit. The rejection of cross-polarization for the communication function (i.e. difference between ϕ and θ gains, corresponding to radar rejection) is 11.06 dB in the directions devoted to communication. The rejection of cross-polarization for the radar function (i.e. difference between θ and ϕ gains, corresponding to communication rejection) is 35 dB in the radar direction, showing a good isolation between the two functions. However, technical problems with the integration of the beam lead diode pushed us to use packaged PIN diode with poorer characteristics. Also, due to lack of time, the biasing circuit was not re-optimized as it should have been to fit the new diode properties. The packaged PIN diode shifted the resonance frequency of the slot to 4 GHz and the measured gain difference between OFF and ON modes is 15.18 dB. For this new antenna using packaged PIN diode, the measured radar and communication rejections are respectively 12.47 dB and 26.1 dB at the resonance frequency, ensuring a good isolation between the two functions. To finish, this solution can be directly integrated to existing radar systems using a horn by only replacing the feeding waveguide.

In order to add more flexibility to the communication function, the possibility to extend the previous solution has been studied in simulations. Hence, by doubling the number of slots in the feeding waveguide, we obtained three additional communication directions with direct BPSK modulation. This new structure combines two different concepts: either the communication signal is transmitted in orthogonal polarization and direction to the radar system (as in the previous solution) or it uses phase-modulation of the radar side lobes to transmit the BPSK signal. In order to increase the slot directivity (communication function), while keeping the BPSK capabilities, 2 subarrays of 5 slots each was used in the feeding waveguide increasing the gain by 3.63 dB compared to the initial solution. Additionally, the radar rejection has been increased by 1.1 dB in comparison to the initial solution, improving the isolation between the two functions in the

communication direction. In counterpart, the use of such a slot array requires a longer feeding waveguide.
A QPSK modulation was also performed by changing the slots arrangement in the feeding waveguide. The constellation obtained in simulations is close to theory with 5.3° phase error. The error vector magnitude (EVM) was computed to evaluate the performance the modulation. The calculation gives 10%, which is acceptable for applications using QPSK modulation.

The antenna concept with direct BPSK modulation has been transposed into SIW horn technology offering low profile and easy integration with planar circuits. However, due to the small substrate thickness, the SIW horn radiation is wide in the E-plane, which leads to a quite low directivity. Hence, the SIW horn performances have been enhanced for other multifunction applications which do not require much directivity such as communication/communication, communication/navigation, etc. According to the techniques used to improve the SIW horns, two approaches were used: thin SIW horn working in X-band and thick SIW horn working in Ka-band. For thin SIW horn, the impedance matching techniques increase the horn gain in the direction devoted to the second function, reducing the rejection in this direction (3 dB at 10 GHz). This rejection has been increased by 7.27 dB by using an array of stacked SIW. Additionally, the directivity of the horn has been increased by 5.67 dB. In order to return to a more conventional solution and further enhance the performances, the substrate has been increased (thick SIW horn). By using slot array in the feeding SIW, the directivity of the second function has been improved and then the rejection in this direction is now 8.62 dB. In counterpart, the use of such a slot array requires a longer feeding SIW.

Perspectives

As we have seen in this thesis, the multifunction antenna developed allows to provide simultaneously radar and communication functions but in fixed directions. It would then be interesting to modify the characteristics of this antenna, in order to answer some applications requiring a steerable beam. This will offer more flexibility to the antenna system. In order to keep the compactness of the antenna without increasing the complexity accordingly, several tracks can be considered:

- Concerning the horn radiation dedicated to the radar function, the beam direction could be reconfigured by considering for example Huygens metasurface inside the horn. By this way, the radiation performance of the horn can be significantly enhanced, without increasing the size and compromising much the weight and the cost.

- As for the communication function, the slots in the waveguide could serve as sources to feed by coupling for example an array of elements in such a way to form a Fabry-Perot cavity. Thus, it would be possible to place an array of controllable element just above the slots to control the beam radiated for the communication function.

As potential application, the developed multifunction antenna could be used by drones. Indeed, the arms of drones being made of metal it could be possible to use them as a waveguide and to add slots. However, this will add mechanical constraints that will need to be considered in the design. Thus, we could consider a scenario where the slots in the arms could be used to transmit

information to the ground whereas the horn could be used to transmit information or detect the neighboring drones for example.

Concerning the SIW horn antenna presented in chapter 5, we have seen that the small substrate thickness affects the directivity of the antenna. This characteristic could be improved for radar applications by replacing the horn by an antipodal linearly tapered slot antenna (ALTSA) array, which is already a SIW antenna solution. In this way, the slots will always be etched in the feeding SIW for the secondary function purposes.

Appendices

Appendix 1:

EVM calculation for BPSK and QPSK modulation

In this appendix we present how to calculate the EVM for BPSK and QPSK modulation. In fact, EVM is used to determine the quality of a communication and expresses the difference between the expected symbol and the value of the actual symbol (cf. Figure A1.1). It is obtained by using the formula (1):

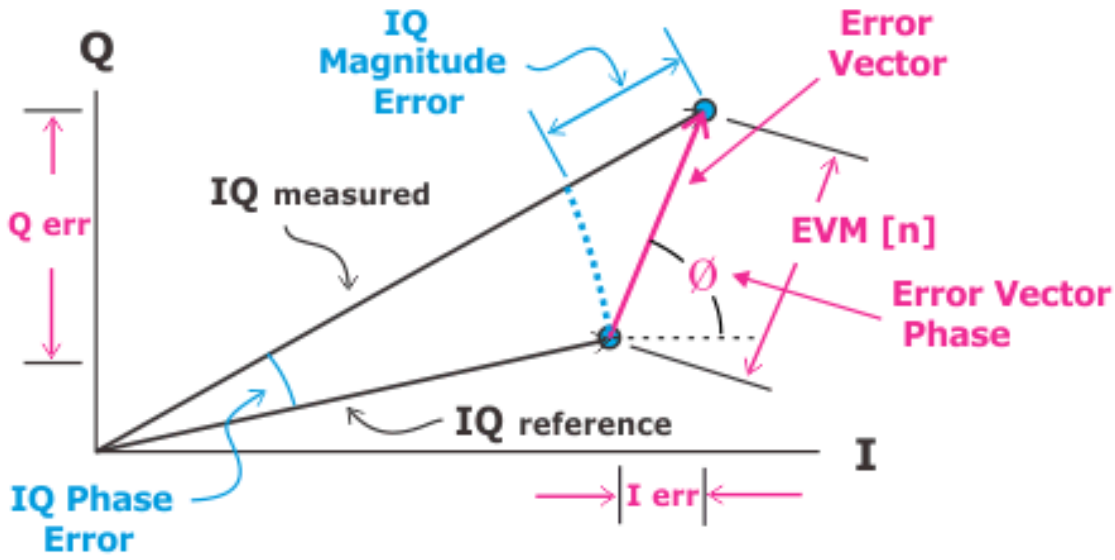

Figure A1. 1: EVM [1]

$$EVM(\%) = \frac{\sqrt{\frac{1}{N}\sum_{n=0}^{N-1}(I_{ideal}(n) - I_{meas}(n))^2 + (Q_{Ideal}(n) - Q_{meas}(n))^2}}{|P_0|} * 100\% \qquad (1)$$

where N is the number of symbols, $I_{ideal\ or\ meas}$ and $Q_{ideal\ or\ meas}$ are the normalized ideal (or measured) inphase and quadrature components. P_0 is the EVM normalization reference corresponding to the maximum magnitude of the ideal constellation.
We can go from the value in percentage to that in dB by using the formula (2):

$$EVM\ (\text{dB}) = 20 * \log(\frac{EVM\ (\%)}{100}) \qquad (2)$$

- **EVM for BPSK modulation**

You will find in Table A1.1 a copy of the Table 3.2 from chapter 3 (corresponding to BPSK modulation at $\phi = 90°$) in which we added the linearized values of the amplitude.

Directions	Config	Phase (°)	Amp. (dBi)	Amp. linear
$\phi = 90°$	1	0	-5.34	0.29
	3	180	-4.89	0.32

Table A1. 1: Linearized amplitude for BPSK modulation at $\phi = 0°$

For a BPSK modulation the number of symbols is $N = 2$ and $P_0 = 1$ (cf. Figure A1.2).

The characteristics of the ideal and simulated symbols are depicted in Table A1.2. Note that the simulated symbols presented in this table are normalized by dividing the amplitudes by the maximum value (0.32), cf. Table A1.1.

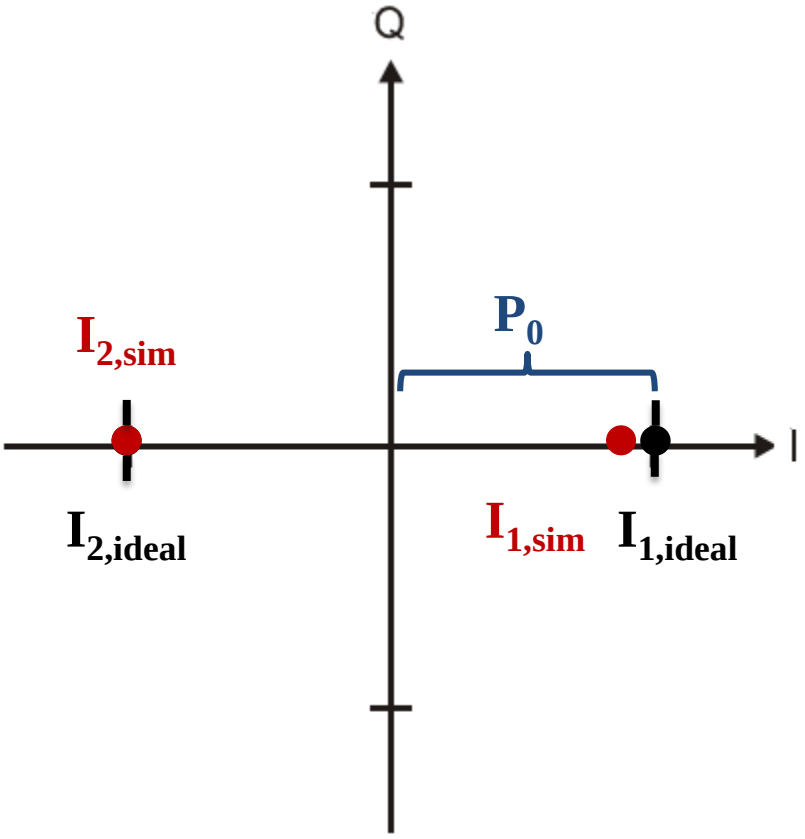

Figure A1. 2: Ideal and simulated BPSK symbols

Symbols	Ideal BPSK		Simulated BPSK	
	I	Q	I	Q
1	1	0	0.902	0
2	-1	0	-1	0

Table A1. 2: Ideal BPSK symbols and normalized values of simulated symbols

Hence using (1) and (2) we obtain respectively 6.92 % and -23.2 dB for the EVM.

- **EVM for QPSK modulation**

You will find in Table A1.3 a copy of the Table 3.5 from chapter 3 in which we added the linearized values of the amplitude.

Directions	Config	Simulation Phase (°)	Amp. (dBi)	Amp. linear
$\theta = 0°$	1	0	-0.3	0.93
	2	269.9	-0.87	0.81
	3	174.7	-0.79	0.83
	4	91.35	-0.63	0.86

Table A1. 3: Linearized amplitude for QPSK modulation at $\theta = 0°$

For a QPSK modulation the number of symbols is $N = 4$ and $P_0 = 1$ (cf. Figure A1.3).

The characteristics of the ideal and simulated symbols are depicted in Table A1.4. Note that the simulated symbols presented in this table are normalized to the maximum value (0.93), cf. Table A1.3.

Symbols	Ideal BPSK		Simulated BPSK	
	I	Q	I	Q
1	1	0	1	0
2	0	-1	-0.0015	-0.8770
3	-1	0	-0.889	0.0825
4	0	1	-0.0218	0.926

Table A1. 4: Ideal QPSK symbols and normalized values of simulated symbols

Hence using (1) and (2) we obtain respectively 10 % and -20 dB for the EVM.

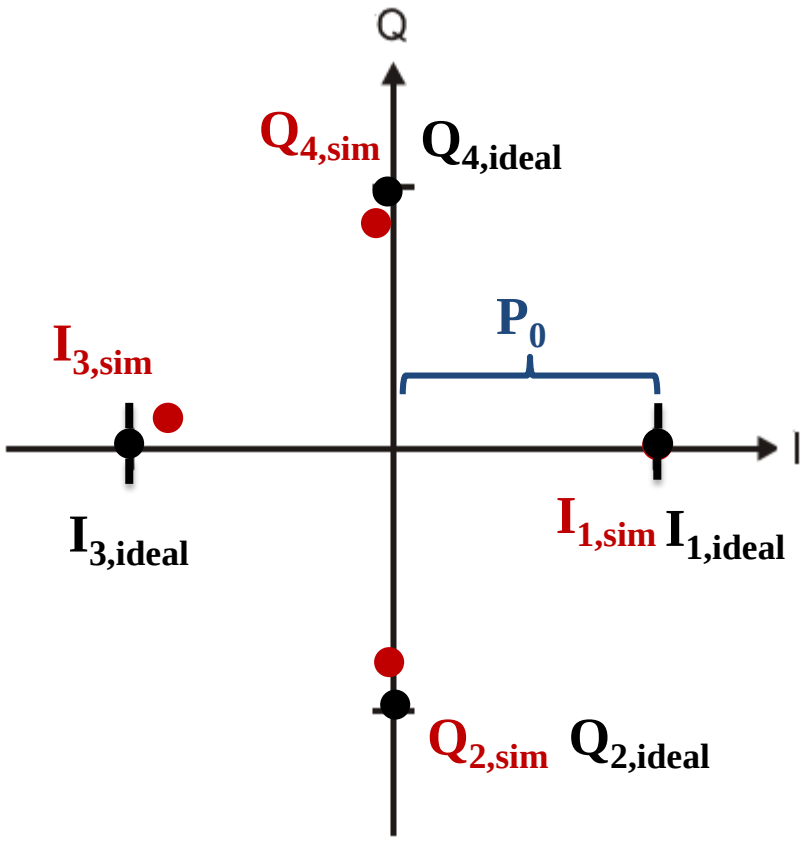

Figure A1. 3: Ideal and simulated QPSK symbols

[1] Downloaded from: (26/10/17)
http://rfmw.em.keysight.com/wireless/helpfiles/89600b/webhelp/Subsystems/digdemod/content/digdemod_symtblerrdata_evm.htm,

Appendix 2

WR-187 waveguide

PASTERNACK®
THE ENGINEER'S RF SOURCE

WR-187 CMR-187 Flange to N Female Waveguide to Coax Adapter Operating From 3.95 GHz to 5.85 GHz, C Band

Waveguide to Coax Adapters Technical Data Sheet PE9822

Features

- C Band, 3.95 to 5.85 GHz Frequency Range
- WR-187 Waveguide Interface with CMR-187 Flange
- N Female Coaxial Interface
- Comprehensive waveguide offerings also include E-Bends, H-Bends, Sections, Filters, Terminations, Couplers, and more.

Description

The PE9822 is a waveguide to coaxial adapter operating in the C band with a 3.95 to 5.85 GHz frequency range. This adapter offers a WR-187 waveguide interface size coupled with a precision tolerance CMR-187 flange. The PE9822 is constructed of aluminum to ensure durability and repeatable RF performance. The coaxial connector offered by this adapter uses a N type Female connector and the package is REACH and RoHS compliant.

Configuration

Waveguide Size	WR-187
Flange	CMR-187
RF Connector	N Female
Impedance	50 Ohms
Body Geometry	Right Angle

Electrical Specifications

Description	Minimum	Typical	Maximum	Units
Frequency Range	3.95		5.85	GHz
VSWR			1.3:1	
Input Power (Peak)			300	Watts

Mechanical Specifications

Size

Length	1.88 in [47.75 mm]
Width	2.78 in [70.61 mm]
Height	2.56 in [65.02 mm]
Weight	0.268 lbs [121.56 g]

RF Connector

Connector Type	N Female
Body Material and Plating	Stainless Steel

Waveguide Interface

Waveguide Type	WR-187
Flange Type	CMR-187
Body Material and Plating	Aluminum

Click the following link (or enter part number in "SEARCH" on website) to obtain additional part information including price, inventory and certifications: WR-187 CMR-187 Flange to N Female Waveguide to Coax Adapter Operating From 3.95 GHz to 5.85 GHz, C Band PE9822

Pasternack Enterprises, Inc. • P.O. Box 16759, Irvine, CA 92623
Phone: (866) 727-8376 or (949) 261-1920 • **Fax:** (949) 261-7451
Sales@Pasternack.com • Techsupport@Pasternack.com

ISO 9001 : 2008 Registered

WR-187 CMR-187 Flange to N Female Waveguide to Coax Adapter Operating From 3.95 GHz to 5.85 GHz, C Band

Environmental Specifications

Temperature

Operating Range	-40 to +85 deg C

Compliance Certifications (visit www.Pasternack.com for current document)

RoHS Compliant	
REACH Compliant	12/17/2015

Plotted and Other Data

Notes:

- Values at +25 °C, sea level unless stated otherwise

Typical Performance Data

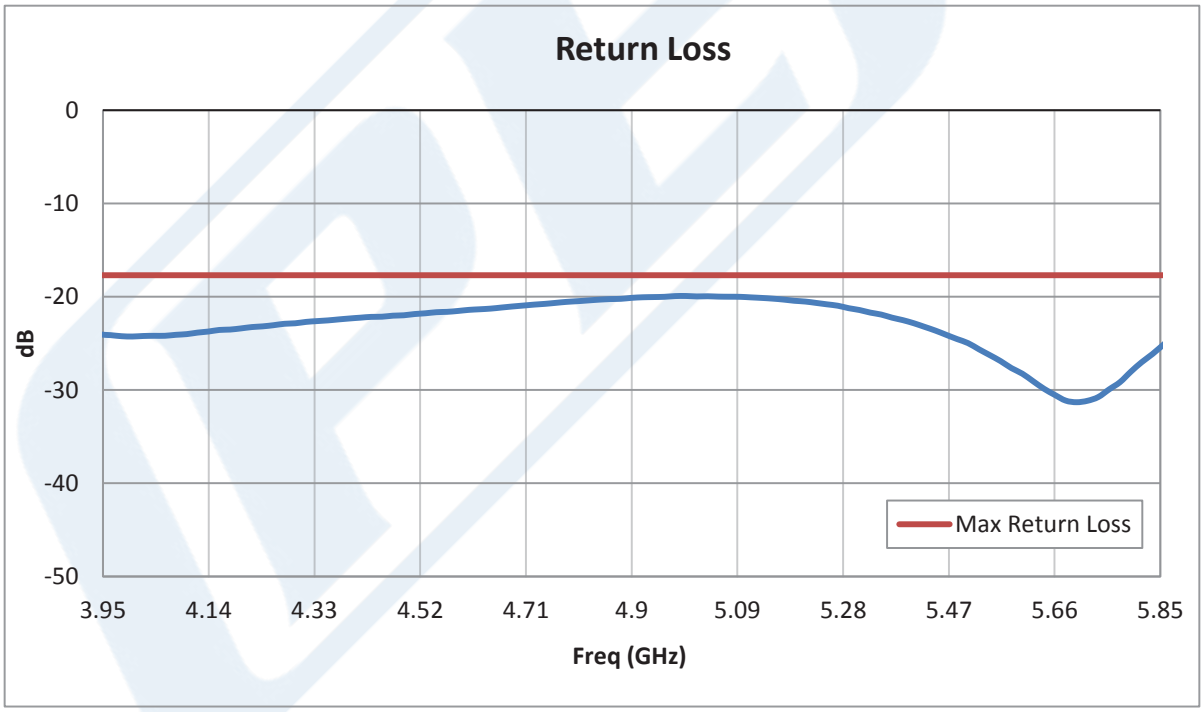

Click the following link (or enter part number in "SEARCH" on website) to obtain additional part information including price, inventory and certifications: WR-187 CMR-187 Flange to N Female Waveguide to Coax Adapter Operating From 3.95 GHz to 5.85 GHz, C Band PE9822

Pasternack Enterprises, Inc. • P.O. Box 16759, Irvine, CA 92623
Phone: (866) 727-8376 or (949) 261-1920 • **Fax:** (949) 261-7451
Sales@Pasternack.com • Techsupport@Pasternack.com

ISO 9001 : 2008 Registered

WR-187 CMR-187 Flange to N Female Waveguide to Coax Adapter Operating From 3.95 GHz to 5.85 GHz, C Band

Waveguide to Coax Adapters Technical Data Sheet PE9822

WR-187 CMR-187 Flange to N Female Waveguide to Coax Adapter Operating From 3.95 GHz to 5.85 GHz, C Band from Pasternack Enterprises has same day shipment for domestic and International orders. Our RF, microwave and millimeter wave products maintain a 99% availability and are part of the broadest selection in the industry.

Click the following link (or enter part number in "SEARCH" on website) to obtain additional part information including price, inventory and certifications: WR-187 CMR-187 Flange to N Female Waveguide to Coax Adapter Operating From 3.95 GHz to 5.85 GHz, C Band PE9822

URL: http://www.pasternack.com/wr-187-n-female-waveguide-coax-adapter-3.95-ghz-5.85-ghz-pe9822-p.aspx

Pasternack Enterprises, Inc. • P.O. Box 16759, Irvine, CA 92623
Phone: (866) 727-8376 or (949) 261-1920 • **Fax:** (949) 261-7451
Sales@Pasternack.com • Techsupport@Pasternack.com

PE9822 CAD Drawing

WR-187 CMR-187 Flange to N Female Waveguide to Coax
Adapter Operating From 3.95 GHz to 5.85 GHz, C Band

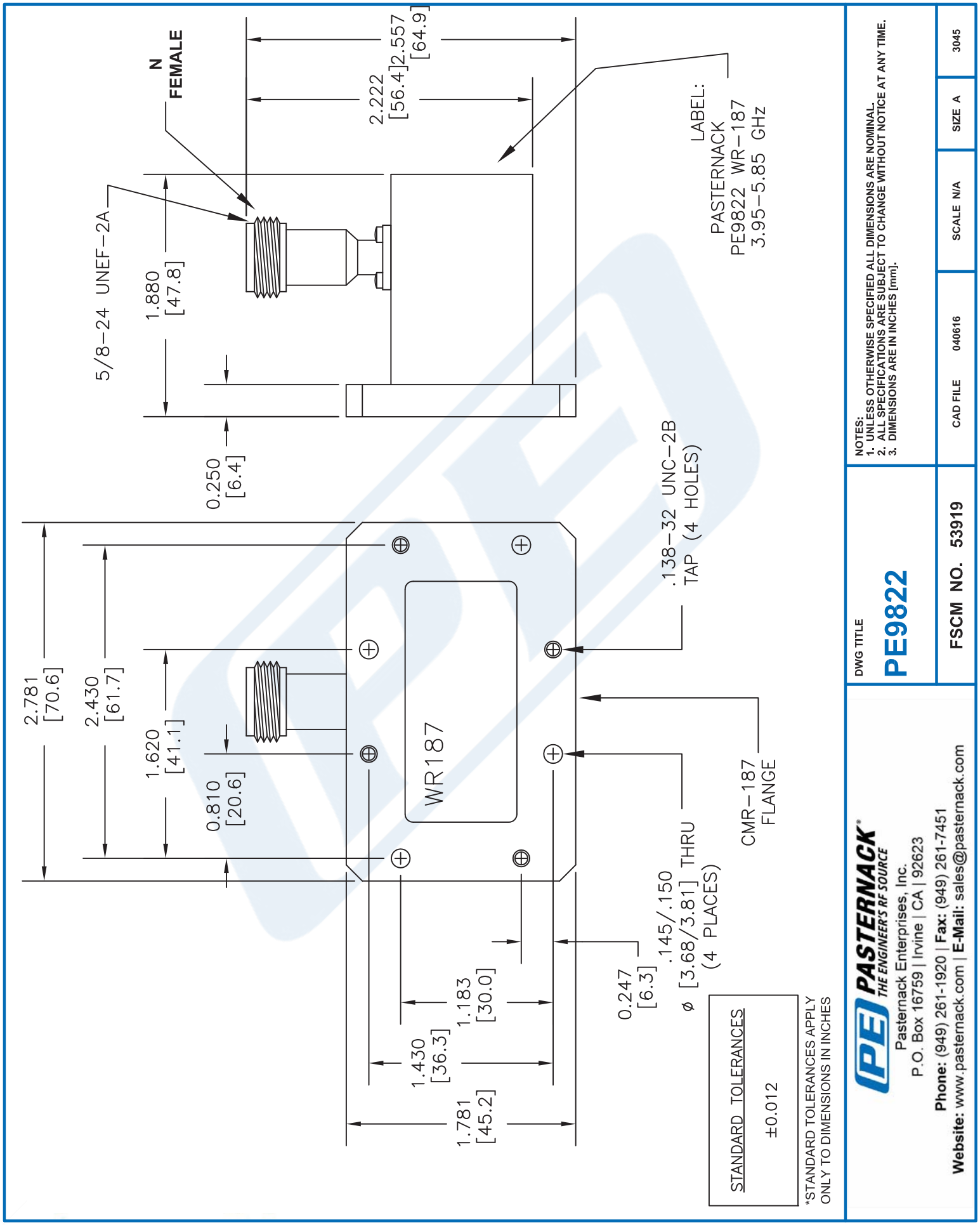

Appendix 3

Beam lead and packaged PIN diodes

DATA SHEET

DSM8100-000: Mesa Beam-Lead PIN Diode

Applications:

- Designed for switching applications

Features

- Low capacitance
- Low resistance
- Fast switching
- Oxide-nitride passivated
- Durable construction
- Lead (Pb)-free, RoHS-compliant, and Green™

Description

Skyworks Silicon Mesa Beam-Lead PIN diode is surrounded by a glass frame for superior strength and electrical performance that surpasses the standard beam-lead PINs. The DSM8100-000 is designed for low resistance, low capacitance and fast switching time. The oxide-nitride passivation layers provide reliable operation and stable junction parameters that provide complete sealing of the junction permitting use in assemblies with some degree of moisture sealing. A layer of glass provides increased mechanical strength.

The DSM8100 is designed for microstrip or stripline circuits and for circuits requiring high isolation from a series-mounted diode such as broadband multithrow switches, phase shifters, limiters, attenuators and modulators.

NEW

Skyworks Green™ products are RoHS (Restriction of Hazardous Substances)-compliant, conform to the EIA/EICTA/JEITA Joint Industry Guide (JIG) Level A guidelines, are halogen free according to IEC-61249-2-21, and contain <1,000 ppm antimony trioxide in polymeric materials.

Absolute Maximum Ratings

Characteristic	Value
Operating temperature	-65 °C to +150 °C
Storage temperature	-65 °C to +200 °C
Power dissipation (derate linearly to zero @ 175 °C)	250 mW
Typical lead strength	8 grams pull
Reverse voltage	60 V

Performance is guaranteed only under the conditions listed in the specifications table and is not guaranteed under the full range(s) described by the Absolute Maximum Ratings. Exceeding any of the absolute maximum/minimum specifications may result in permanent damage to the device and will void the warranty.

CAUTION: *Although these devices are designed to be robust, ESD (Electrostatic Discharge) can cause permanent damage. Static charges may easily produce potentials of several kilovolts on the human body or equipment, which can discharge without detection. Industry-standard ESD precautions must be employed at all times.*

Mesa Beam-Lead Diode Specifications

Part Number	Min. Voltage Rating[1] (V)	Max. Total Capacitance 10 V, 1 MHz (pF)	Max. Series Resistance 10 mA,100 MHz (Ω)	Typ. T_L I_F = 10 mA (ns)	Outline Drawing
DSM8100-000	60	0.025	3.5	25	389-003

1. Reverse current is specified at 10 µA maximum at the voltage rating. This voltage should not be exceeded.

Typical Performance Data

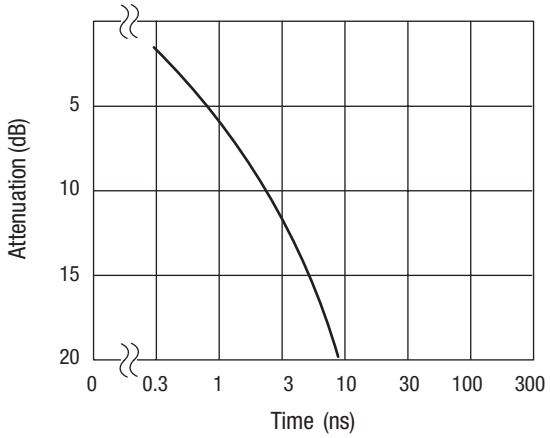

Switching Time Data

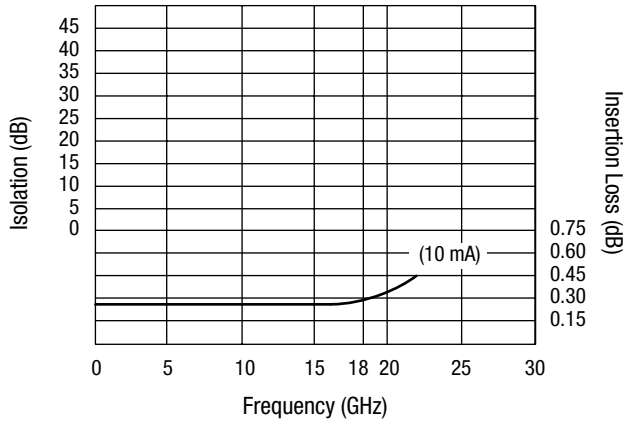

Typical Isolation and Insertion Loss Characteristics

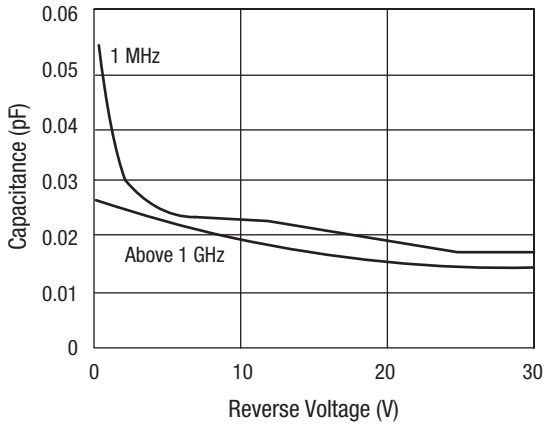

Typical Capacitance vs. Reverse Voltage

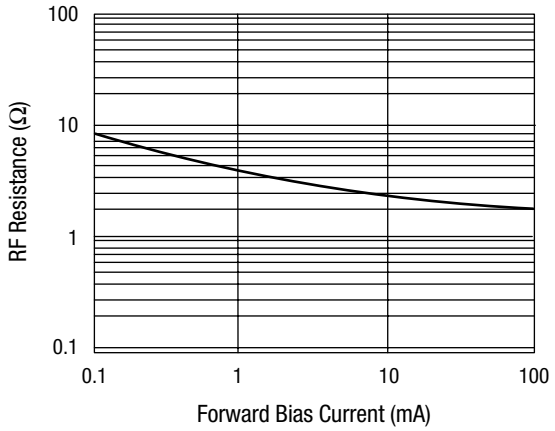

Typical RF Resistance vs. Forward Bias Current

Typical SPDT Circuit Arrangement

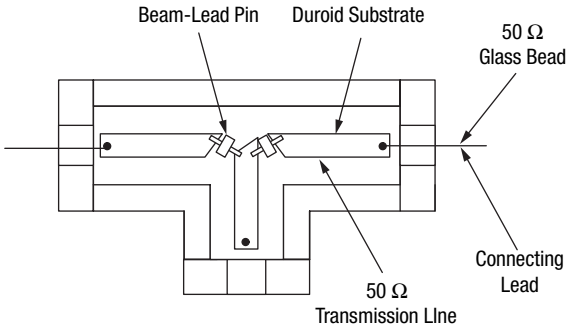

Typical Beam-Lead Mounting

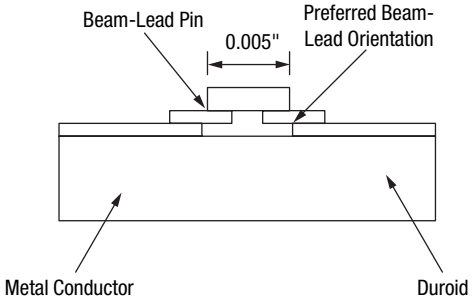

389-003

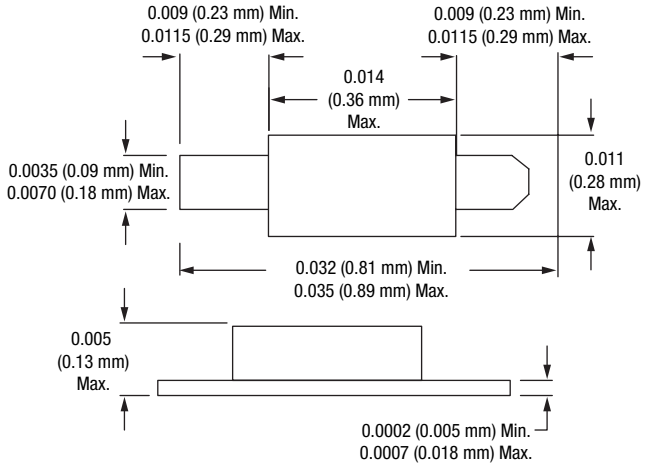

Beam-Lead Diodes

Handling

Due to their small size, beam-lead devices are fragile and should be handled with extreme care. The individual plastic packages should be handled and opened carefully, so that no undue mechanical strain is applied to the packaged device. It is recommended that the beam-lead devices be handled through use of a vacuum pencil using an appropriate size vacuum needle or a pointed wooden stick such as a sharpened Q-tip or match stick. The device will adhere to the point and can easily be removed from the container and positioned accurately for bonding without damage. Such handling should be done under a binocular microscope with magnification in the range of 20X to 30X.

Special handling precautions are also required to avoid electrical damage, such as static discharge.

Bonding

The DSM8100-000 can best be bonded to substrates by means of thermocompression bonding. Essentially this type of bonding involves pressing the gold beam of the device against the gold-plated metalized substrate under proper conditions of heat and pressure so that a metallurgical bond joint between the two occurs.

Procedure

The beam-lead devices to be bonded should be placed on a clean, hard surface such as a microscope slide. It is recommended that the beam side of the device be down so that this side will be toward the substrate when bonded. The device can be picked up by pressing lightly against one beam with the heated tip. The substrate can then be appropriately positioned under the tip and the device brought down against the substrate, with proper pressure applied by means of the weld head.

A bonding tip temperature in the 350 °C to 450 °C range is recommended along with a bonding force of 50 to 70 grams. The bonding time is in the range of 2 to 3 seconds. Optimum bonding conditions should be determined by trial and error to compensate for slight variations in the condition of the substrate, bonding tip, and the type of device being bonded.

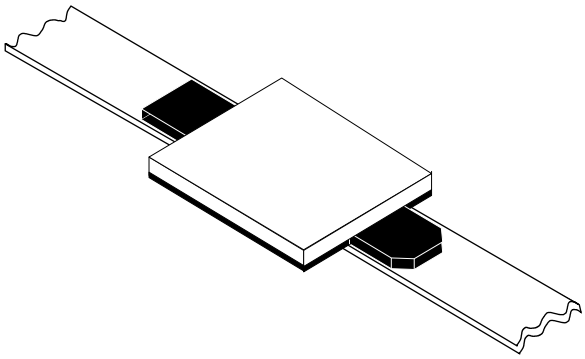

Equipment

The heat and pressure are obtained through use of a silicon carbide bonding tip with a radius of two to three mils. Such an item is available from several commercial sources. In order to supply the required tip-travel and apply proper pressure, a standard miniature weld head can be used. Also available is a heated wedge shank which is held by the weld head and in turn holds the tip and supplies heat to it. The wedge shank is heated by means of a simple AC power supply or a pulse-type heated tool.

Substrate

For optimum bonding, a gold-plated surface at least 100-microinches thick is necessary. Although it is possible to bond to relatively soft metalized substrate material such as epoxy-fiberglass, etc., optimum bonding occurs when a hard material such as ceramic can be used.

Quality

If a good bond has been obtained, it is impossible to separate the beam-lead device from the metalized substrate without damage. If the device is destructively removed, the beam will tear away, leaving the bonded portion attached to the substrate.

Beam-Lead Packaging

The DSM8100-000 is shipped in 2" x 2" black gel packs. The beam-leads are mounted on the gel, and the devices are covered with a piece of lint-free release paper, on top of which is placed a piece of conductive foam.

HSMP-381Z-BLKG

DATASHEET

View Part on Verical

Email Us

Sales: sales@verical.com
Support: support@verical.com
Suppliers: Visit our seller page

Company Address

Arrow Electronics, Inc
7459 S. Lima Street
Englewood, CO 80112-3879

HSMP-381Z

Low Distortion Attenuator RF PIN Diodes
In Surface Mount SOD-323 Package

Data Sheet

Description/Applications

Avago Technologies' HSMP-381Z is designed for low distortion attenuator applications. It is housed in a low cost, industrial standard surface mount package - SOD-323. This package offers customers who already use them in SOT-23 and SOT-323 packages, a logical transition to a smaller package outline to accommodate end product design with limited board space.

The HSMP-381Z has low distortion and high IP3 characteristics. The device can operate in microwave frequencies and suitable to be used as attenuating circuits in Infrastructure and CATV applications.

A SPICE model is not available for PIN diodes as SPICE does not provide for a key PIN diode characteristic -- carrier lifetime.

Package Marking and Pin Connections

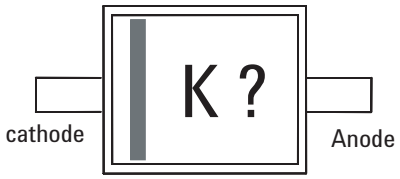

Note:
Package marking provides orientation and identification

"K" = Device Code

"?" = Month code indicates the month of manufacture

Features

- 2 Leads Surface Mount Package
- Low Distortion Attenuating
- Microwave Frequency Operation
- Tape and Reel Options Available
- Low Failure in Time (FIT) Rate
- MSL1 & Lead Free

Table 1. Absolute Maximum Ratings [1] at Tc = +25°C

Symbol	Parameter	Unit	Max Rating
I_f	Forward Current (1 µs Pulse)	Amp	1
P_{IV}	Peak Inverse Voltage	V	100
T_j	Junction Temperature	°C	150
T_{stg}	Storage Temperature	°C	-60 to 150
θ_{jb}	Thermal Resistance [2]	°C/W	135

Notes:
1. Operation in excess of any one of these conditions may result in permanent damage to the device.
2. Thermal Resistance is measured from junction to board using IR method.

Table 2. Electrical Specifications at Tc = +25°C

	Minimum Breakdown Voltage V_{BR} (V)	Maximum Total Capacitance C_T (pF)	Minimum Resistance at I_F = 0.01mA, R_H (Ω)	Maximum Resistance at I_F = 20mA, R_L (Ω)	Maximum Resistance at I_F = 100mA, R_T (Ω)	Resistance at I_F = 1mA, R_M (Ω)
	100	0.35	1500	10	3.0	48 to 70
Test Conditions	$V_R = V_{BR}$ Measure $I_R \leq$ 10uA	V_R = 50V f = 1MHz	I_F = 0.01mA f = 100MHz	I_F = 20mA f = 100MHz	I_F = 100mA f = 100MHz	IF = 1mA f = 100MHz

Note : Rs parameters are tested under AQL 1.0

Table 3. Typical Parameters at Tc = +25°C

	Carrier Lifetime τ (ns)	Reverse Recovery Time T_{rr} (ns)	Total Capacitance C_T (pF)
	1500	300	0.27
Test Conditions	I_F = 50mA I_R = 250mA	V_R = 10V I_F = 20mA 90% Recovery	V_R = 50V f = 1MHz

Typical Performance Curves at Tc = +25°C

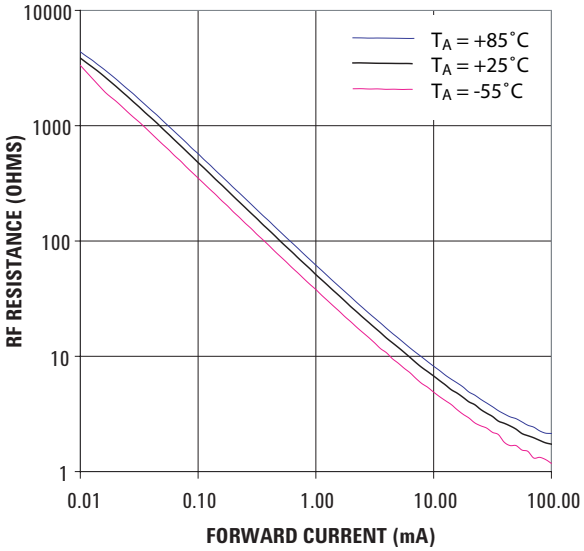

Figure 1. RF Resistance vs. Forward Bias Current

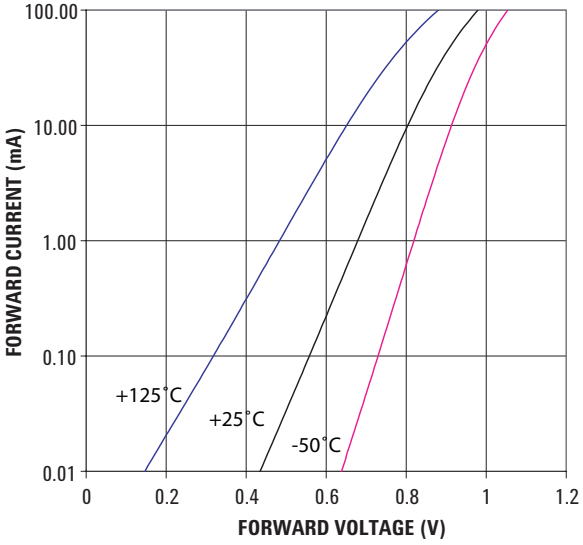

Figure 2. Forward Current vs. Forward Voltage

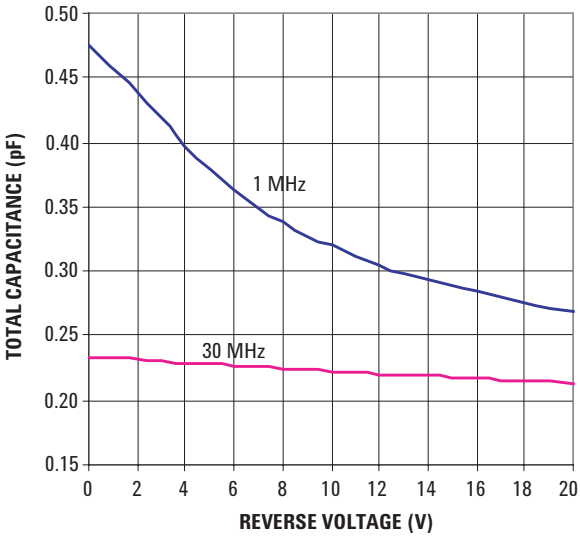

Figure 3. RF Capacitance vs. Reverse Bias

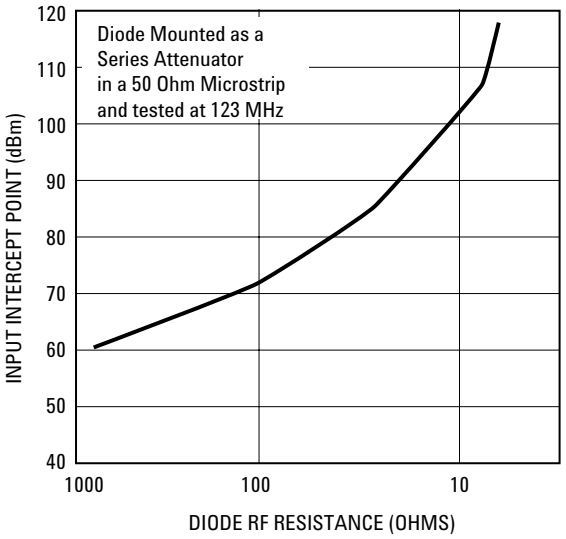

Figure 4. 2nd Harmonic Input Intercept Point vs. Diode RF Resistance

Note:

3. Typical values were derived using limited samples during initial product characterization and may not be representative of the overall distribution.

Package Outline and Dimension

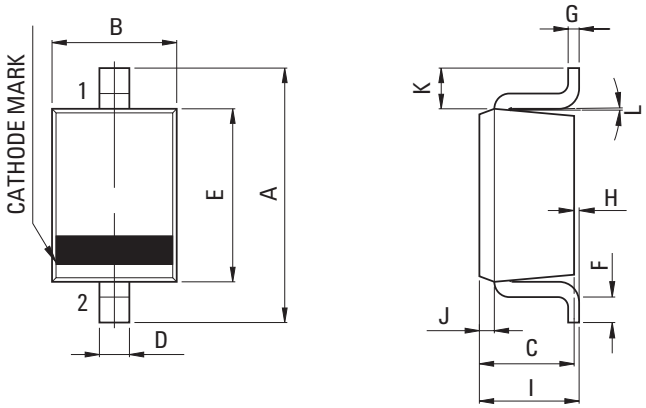

DIM	MILLIMETERS
A	2.50±0.2
B	1.25±0.05
C	0.90±0.05
D	0.30+0.06/-0.04
E	1.70±0.05
F	MIN 0.17
G	0.126±0.03
H	0~0.1
I	1.0 MAX
J	0.15±0.05
K	0.4
L	2°+4/-2
M4	~6°

PCB Footprint

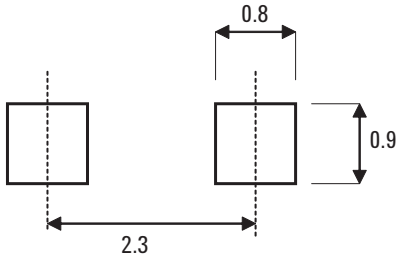

Dimension in mm

Device Orientation

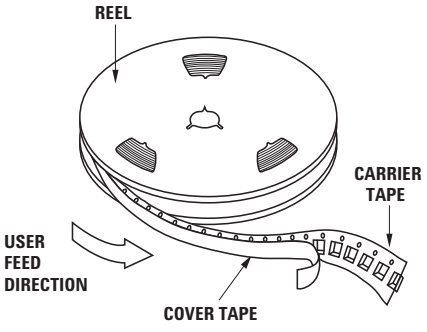

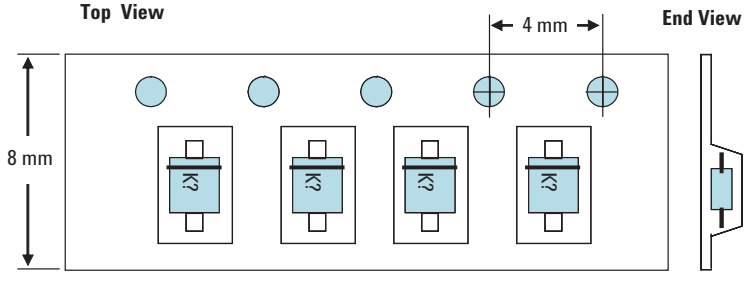

Note: "K" represents package marking code
"?" represents date code

Tape Dimensions

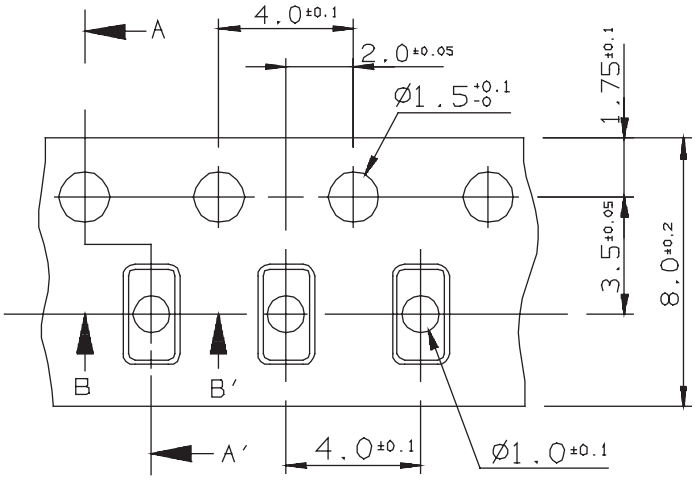

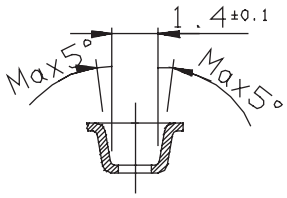

B - B′ SECTION

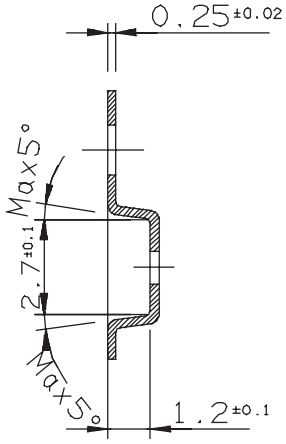

A - A′ SECTION

Specification < Unit: mm >

A. hole pitch : 50 Pitch Tolerance : 200 ± 0.3

Part Number Ordering Information

Part number	No. of Units	Container
HSMP-381Z-BLKG	100	Anti-static bag
HSMP-381Z-TR1G	3000	7″ reel

For product information and a complete list of distributors, please go to our web site: **www.avagotech.com**

AV02-0406 - July 31, 2007

Appendix 4

Diode polarization circuit (*H*-Shapped circuit)

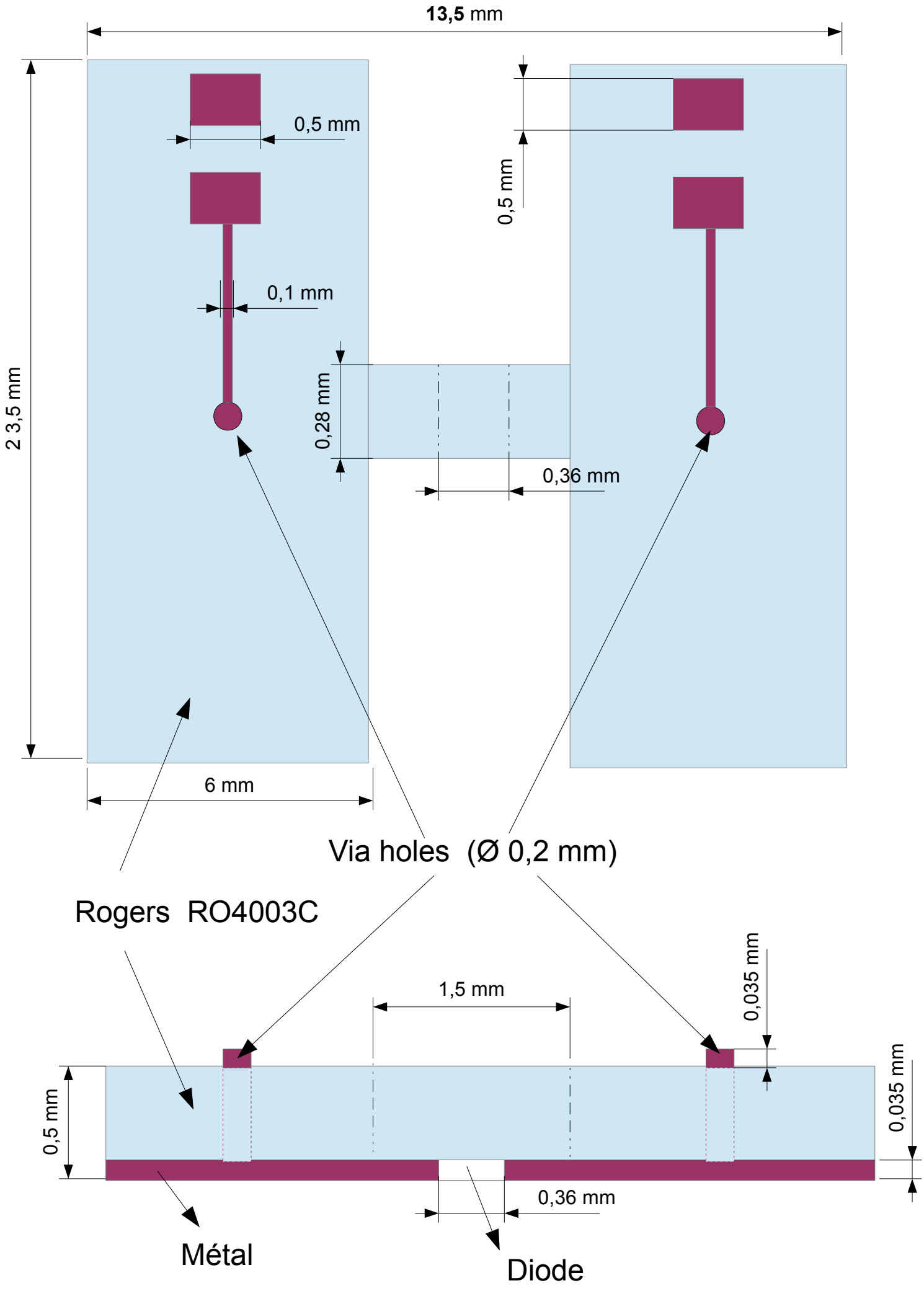
13,5 mm
0,5 mm
0,5 mm
0,1 mm
2 3,5 mm
0,28 mm
0,36 mm
6 mm
Via holes (Ø 0,2 mm)
Rogers RO4003C
1,5 mm
0,035 mm
0,5 mm
0,035 mm
0,36 mm
Métal
Diode

Publications

Journal

- S. Ouedraogo, I. Hinostroza, R. Guinvarc'h and R. Gillard, "Design and Experimental Validation of Multifunction Antenna with Direct Modulation for Radar and Communication", **submitted**.

Conferences

- S. Ouedraogo, I. Hinostroza, R. guinvarc'h and R. Gillard, "Antenna System for Simultaneous Radar and Communication Applications", 10th EuCAP, Davos, Switzerland, *Apr. 10-15, 2016.*

- S. Ouedraogo, I. Hinostroza, R. guinvarc'h and R. Gillard, "Large Bandwidth Analysis in Multifunction Antenna for Radar and Communication Applications", 6th IEEE International Symposium on Phased Array Systems and Technology, Waltham, MA, USA, *Oct. 18-21, 2016.*

- S. Ouedraogo, I. Hinostroza, R. Guinvarc'h and R. Gillard, "A Multifunction Antenna with Direct Modulation and Beam Agility", 11th EuCAP, Paris, France, *Mar. 19-24*, 2017.

- S. Ouedraogo, I. Hinostroza, R. Guinvarc'h and R. Gillard, "Antenne Multifunction à Modulation Directe et Agilité de faisceau", 20 ème, Journées Nationales Micro-Ondes (JNM), Saint-Malo, France, *16-19 Mai* 2017.

Titre : Antenne Multifonction pour Radar et Communication

Mots clés : Antenne multifonction, modulation directe, antenne cornet, guide à fentes

Résumé : Afin de répondre à la demande croissante de nouveaux services, les objets que nous utilisons au quotidien (les smartphones, les voitures, les avions, etc.) tendent à intégrer de plus en plus de systèmes radio tandis que l'espace disponible pour l'intégration de ces éléments est de plus en plus réduit. Ces systèmes radio nécessitent l'utilisation de plusieurs antennes devant répondre à des critères de compacité, d'isolation, de coût, etc. À titre d'illustration, un smartphone contient plusieurs antennes pour assurer des fonctions telles que la téléphonie, la navigation, la connexion à internet par WiFi, les liaisons Bluetooth, la technologie NFC (Near-Field Communications) et ce nombre tend à s'accroitre considérablement avec l'émergence de nouveaux services. Le même phénomène se retrouve également au niveau des plateformes aéroportées où des fonctions telles que la communication, la navigation, le radar, etc. sont utilisées. Cela conduit donc à la nécessité de réduire le nombre d'antennes en regroupant par exemple plusieurs fonctions au sein d'une même et unique antenne. Dans de précédents travaux de recherches, J. Euzière a démontré la possibilité de combiner une fonction radar et une seconde fonction (ici de communication) en utilisant un réseau de 16 monopoles initialement dédié au seul radar, grâce au Time Modulated Array (TMA). De cette façon, les deux fonctions utilisaient la même fréquence et étaient alimentées par une seule source.
L'objectif principal de cette thèse est de proposer une solution d'antenne multifonction pour radar et communication encore plus compacte (constituée d'une seule antenne). L'idée est de partir d'une solution antennaire déjà existante et d'y apporter les modifications nécessaires à l'ajout d'une seconde fonction, sans pour autant augmenter la surface de l'antenne ni la complexité du système.

Title : Multifunction Antenna for Radar and Communication

Keywords : Multifunction antenna, direct modulation, horn antenna, slotted waveguide

Abstract : In order to respond to the increasing of new services, the objects we use on a daily basis (mobile phones, cars, airplanes etc.), tend to integrate more and more radio systems while the space available is limited. These radio systems require the use of many antennas that must meet multiple requirements such as compactness, isolation, costs, etc. A smartphone, for example, contains several antennas for global navigation satellite system (GNSS), WiFi, Bluetooth, near-field communications (NFC) and the number is expected to increase as new systems are added. Another example is in airborne platforms where multiple functions such as communication, navigation, radar, electronic warfare are used. This leads to the need of reducing the number of associated antennas by regrouping several radio functions into a single antenna. During its Ph.D, J. Euzière demonstrated the possibility to combine a radar function and a secondary function from a 16-monopole array originally dedicated to radar operation by using Time Modulated Array (TMA) technique. By this way, the two functions were operating at the same frequency and the system was powered by a single source. The main objective of this thesis is to propose a more compact antenna (a single antenna) dedicated to radar and communication operations instead of using antenna array as J. Euzière did it. The idea is to start from an existing antenna solution and make the necessary modifications to add a second function without adding additional surface and complexity.

Université Paris-Saclay
Espace Technologique / Immeuble Discovery
Route de l'Orme aux Merisiers RD 128 / 91190 Saint-Aubin, France